II INTERNATIONAL WORKSHOP «SOLID STATE NUCLEAR TRACK DETECTORS AND THEIR APPLICATIONS»

Dubna 1993

ОБЪЕДИНЕННЫЙ ИНСТИТУТ ЯДЕРНЫХ ИССЛЕДОВАНИЙ

JINR - E3-93-61

II МЕЖДУНАРОДНОЕ РАБОЧЕЕ СОВЕЩАНИЕ «ТВЕРДОТЕЛЬНЫЕ ТРЕКОВЫЕ ДЕТЕКТОРЫ ЯДЕР И ИХ ПРИМЕНЕНИЯ»

Дубна, 24—26 марта 1992 г.

Сборник докладов

II INTERNATIONAL WORKSHOP «SOLID STATE NUCLEAR TRACK DETECTORS AND THEIR APPLICATIONS»

Dubna, 24—26 March 1992

Proceedings

Дубна 1993

Ответственный за выпуск сборника В.П.Перелыгин

CONTENTS

Introduction

Second International Workshop on Solid State Nuclear Track Detectors and Their Applications Dubna, 24–26 March 1992

The IInd International Workshop on Solid State Nuclear Track Detectors and Their Applications (SSNTD 92) was organized by the track detector scientists of Flerov Laboratory of Nuclear Reactions and Ingeneering Center of Applied Nuclear Physics of JINR.

The previous International workshop SSNTD 92 was held in Feburary 1990; the Proceedings of that workshop were published earlier in 1992 (ed. P.Yu.Apel, V.P.Perelygin, "Solid State Nuclear Track Detectors and Their Applications", Dubna, D13 90 479, pp. 1 184).

The IInd Dubna workshop on SSNTD was organized as an important step to prepare for the future, 17th International Conference on Nuclear Track in Solids, which will take place in August 1994 at Dubna.

More than 75 scientists from 20 countries of the Union of Independent States, members and nonmembers of JINR take part in the work of the Dubna meeting. At the 5th plenary and 3 poster sessions 62 reports were presented. The main topics of the sessions were:

1. New data on theoretical and experimental investigations of track formation, track stability and on a new kind of track detectors;

2. New important data on the investigations of cluster radioactivity, in the field of high and low energy nuclear physics, in cosmic ray physics;

3. The rather big number of reports in the field of ecology and especially the investigations of Chernobyl samples and hot particles.

   The new very sensitive method of ^{239}Pu exploration has been developed by Dubna scientist.

4. The investigations of track radiography of specimens and their applications in technology, geology and dosimetry.

5. The new results on further development of automatic devices for track counting and mapping.

We decide to publish the Proceedings "SSNTD-92" in English in order to inform the International Nuclear Track Society members about the last achievements in nuclear track detector study mainly in the countries of UIS (former USSR) and other countries.

Organizing Committee: V.P.Perelygin (Chairman), S.P.Tretyakova, P.Yu.Apel, S.A.Karamyan, S.G.Stetsenko.

THEORETICAL APPROACH FOR REGISTRATION OF MIXED CHARGED PARTICLES FLUX OF DIFFERENT TYPE BY SOLID STATE DETECTORS

Ditlov V.A.

Institute of Photo-Chemical Industry
Moscow, Leningradskij Pr., 47
Russia

The approach (Ditlov V.A. Theory of Spatial calculation... In: Proceeding of the X^{th} Int. Conf. of SSNTD, 1980, p.131-141) to the problem of electron detecting is based on assumptions:

1. Solid State detector consist of a very large number of sensitive microvolumes, similar, for example, to photographic emulsions of biological tissue.

2. Every sensitive microvolume can be only in two states "no" or "yes".

3. In order to describe the probability of appearance of local response (transition from state "no" to state "yes") it is necessary to use many-hit model.

4. The local responses are invoked by effective ionization acts inside sensitive microvolume, as a result of interactions of moving electrons with electron shells of atoms.

5. Because of very small sizes of sensitive microvolumes there takes place a very strong fluctuation of these interaction acts.

6. There is a strong multiple scattering of moving electrons and it is necessary to use the differential function of electrons distribution in phase space $f(\vec{r}, \vec{\Omega}, s)$ from the theory of multiple scattering $f(\vec{r}, \vec{\Omega}, s)$. Here $\vec{r}$ coordinate vector, $\vec{\Omega}$ direction of electron velocity and s residual range of electron.

At the base of this assumptions it is possible to built up expressions for a probability, that in a given point $\vec{r}$ after passing of electron flux $f(\vec{r}, \vec{\Omega}, s)$ we can observe response, sensitive microvolume in state "yes". These expressions can be used for calculation of local responses of sensitive microvolumes around track axis, formed by δ-electrons flow. Then it is possible to find any track parameters (Ditlov V., Upon Physical Grounds of Track Parameters Formation in SSNTD. In: Int.Workship "SSNTD and Their applications", Dubna, 1991, p.8-12).

Now let us remark, that when we established the relationship between the probabilities and differential distribution function of elec-

trons, we did not use any properties specific only for electrons. The expressions of P_ν^+ are applicable for particles of any nature. For different sorts of particles, it is just necessary to use different flux spatial functions $f(\vec{r}, \vec{\Omega}, s)$ and interaction cross-sections. For example, if we consider very heavy particles moving along straight lines without any scattering it is necessary to use distribution function expressed by δ-function.

So, the expressions P_ν^+ have more general meaning, than it was discussed before. More over, it is possible to do further generalization for the case of mixed flux containing particles of different nature.

Note, that this new goal does not make us to change the logical structure of our approach. We have only at the beginning to write down the mean effective acts number for one sensitive region as a sum of inputs from different flux fractions:

$$\xi = \sum_{i=1}^{N_1} \xi_{i,1} + \sum_{i=1}^{N_1} \xi_{i,2} + \ldots\ldots + \sum_{i=1}^{N_1} \xi_{i,m} . \qquad (1)$$

As a result we can built up the new expressions for P_ν^+:

$$P_1^+(\vec{r}) = 1 - e^{-\sum_{i=1}^{m} N_i \cdot \langle 1-e^{-\xi} \rangle_i} ; \qquad (2)$$

$$P_2^+(\vec{r}) = 1 - \{1 + \sum_{i=1}^{m} N_i \cdot \langle \xi e^{-\xi} \rangle_i\} \cdot e^{-\sum_{i=1}^{m} N_i \cdot \langle 1-e^{-\xi} \rangle_i} ; \qquad (3)$$

$$P_3^+(\vec{r}) = 1 - \left\{1 + \sum_{i=1}^{m} N_i \cdot \langle \xi e^{-\xi} \rangle_i + \right. \qquad (4)$$

$$\left. + \frac{1}{2} \left[\sum_{i=1}^{m} N_i \cdot \langle \xi^2 e^{-\xi} \rangle + \left(\sum_{i=1}^{m} N_i \cdot \langle \xi e^{-\xi} \rangle_i \right)^2 \right] \right\} \cdot e^{-\sum_{i=1}^{m} N_i \cdot \langle 1-e^{-\xi} \rangle_i} .$$

So, instead of $\langle \cdots \rangle$ we have sums $\sum_i \langle \cdots \rangle_i$.

Note, that the flux splitting into separate fractions can be rather arbitrary. For instance, the flux consisting of only electrons may be considered to be multicomponent according to their place and nature of origin or to their initial energies and original directions of ejection.

As an example we consider four private cases, shown on scheme of the Figure.

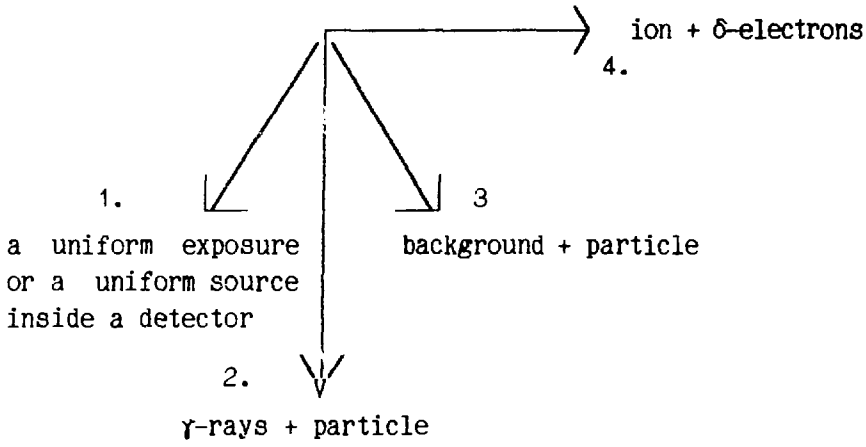

Four important cases of mixed charged particles flux

Case 1. If particle sources are uniformly distributed over the whole detector body, then we can rewrite:

$$P_1^+(\vec{r}) = 1 - e^{-\int N\langle 1-e^{-\xi}\rangle \, d\vec{r}}; \qquad (5)$$

$$P_2^+(\vec{r}) = 1 - \left\{1 + \int N\cdot\langle \xi e^{-\xi}\rangle d\vec{r}\right\}\cdot e^{-\int N\cdot\langle 1-e^{-\xi}\rangle d\vec{r}}; \qquad (6)$$

$$P_3^+(\vec{r}) = 1 - \left\{1 + \int N\cdot\langle \xi e^{-\xi}\rangle \, d\vec{r} + \right.$$

$$\left. + \frac{1}{2}\left[\int N\langle \xi^2 e^{-\xi}\rangle \, d\vec{r} + \left(\int N\cdot\langle \xi e^{-\xi}\rangle d\vec{r}\right)^2\right]\right\}\cdot e^{-\int N\cdot\langle 1-e^{-\xi}\rangle d\vec{r}}. \qquad (7)$$

Here we converted from summarization to integration by source coordinates over whole detector volume. Now it is possible to show, that if detector sensitive microvolumes have spherical form and their sizes are much less than the electron ranges, we can write:

$$P_1^+(\vec{r}) = 1 - e^{-2\pi N\int_0^a \rho\, d\rho \int_0^\infty f(s)(1-e^{-\xi})ds} \quad ; \tag{8}$$

$$P_2^+(\vec{r}) = 1 - \left\{1 + 2\pi N\int_0^a \rho d\rho \int_0^\infty f(s)\xi(\rho,s)e^{-\xi(\rho,s)}ds\right\}e^{-2\pi N\int_0^a \rho\, d\rho\int_0^\infty f(s)(1-e^{-\xi})ds} \quad ; \tag{9}$$

$$P_3^+(\vec{r}) = 1 - \left\{1 + 2\pi N\int_0^a \rho d\rho \int_0^\infty f(s)\xi(\rho,s)e^{-\xi(\rho,s)}ds + \right.$$
$$+ \left[2\pi N\int_0^a \rho d\rho \int_0^\infty f(s)\xi^2(\rho,s)e^{-\xi(\rho,s)}ds + \right. \tag{10}$$
$$\left.\left. + \left[2\pi N\int_0^a \rho d\rho \int_0^\infty f(s)\xi(\rho,s)e^{-\xi(\rho,s)}ds\right]^2\right]\right\} e^{-2\pi N\int_0^a \rho d\rho \int_0^\infty f(s)(1-e^{-\xi})ds} .$$

Thus we can formulate: *If detector sensitive region size is so small that the spatial distribution function doesn't vary much over the sensitive region volume and particle sources are uniformly distributed all over the detector's body then the integral result of such detector does not depend on any multiple scattering properties.* Being correct it makes the calculation of the response probabilities extremely simple. It is no need to use neither kinetic equation nor cross-section of interaction. There are only integrations along particle path.

Case 2. For example if you exposed the detector by γ-rays it is necessary to calculate the integrals only along trajectory of δ-electrons with appropriate energy spectrum f(E). It gives us a possibility to calculate a density of photographic emulsion exposed by γ-rays or to find the new etching body rate for any plastic after γ-exposure. If you want to calculate track parameter of any particle in detector also exposed by γ-rays you have to use expressions:

$$P_1^+(\vec{r}) = 1 - e^{-\left[N_\gamma\cdot\langle 1-e^{-\xi}\rangle_\gamma + \langle 1-e^{-\xi}\rangle_p\right]} \quad ; \tag{11}$$

$$P_2^+(\vec{r}) = 1 - \{1 + N_\gamma\cdot\langle\xi\cdot e^{-\xi}\rangle_\gamma + \langle\xi\cdot e^{-\xi}\rangle_p\}e^{-\left[N_\gamma\cdot\langle 1-e^{-\xi}\rangle_\gamma + \langle 1-e^{-\xi}\rangle_p\right]} \tag{12}$$

$$P_3^+(\vec{r}) = 1 - \left\{1 + N_\gamma \cdot \langle \xi \cdot e^{-\xi} \rangle_\gamma + \langle \xi \cdot e^{-\xi} \rangle_p + N_\gamma \cdot \langle \xi^2 e^{-\xi} \rangle_\gamma + \langle \xi^2 e^{-\xi} \rangle_p + \right.$$

$$\left. + \frac{1}{2} \left[N_\gamma \cdot \langle \xi^2 e^{-\xi} \rangle_\gamma + \langle \xi^2 e^{-\xi} \rangle_p + \left(N_\gamma \cdot \langle \xi \cdot e^{-\xi} \rangle_\gamma + \langle \xi \cdot e^{-\xi} \rangle_p \right)^2 \right] \right\} \cdot$$

$$\cdot e^{-\left[N_\gamma \cdot \langle 1 - e^{-\xi} \rangle_\gamma + \langle 1 - e^{-\xi} \rangle_p \right]} . \qquad (13)$$

Here the symbol $\langle \xi e^{-\xi} \rangle_\gamma$ means integral along the path of electrons, struck out by γ-quanta; and $\langle \xi e^{-\xi} \rangle_p$, integrals including $f(\vec{r}, \vec{\Omega}, s)$ of δ-electrons, struck-out by the particle.

Case 3. Similar it is possible to consider the fog, when some part of sensitive region goes spontaneously from the state "no" to the state "yes". Formally it may be assumed that these transitions are not spontaneous but caused by the action of a certain hypothetical background uniform irradiation from the outside, then:

$$\xi = \xi_{ion} + \xi_o \ . \qquad (14)$$

Where ξ_o may be understood as the average number of effective events per single sensitive region under the action of this radiation. Then it is possible to obtain:

$$P_1^+(\vec{r}) = 1 - e^{-\left[\xi_o + \langle 1 - e^{-\xi} \rangle \right]} \ ; \qquad (15)$$

$$P_2^+(\vec{r}) = 1 - \left\{1 + \xi_o + \langle \xi \cdot e^{-\xi} \rangle \right\} e^{-\left[\xi_o + \langle 1 - e^{-\xi} \rangle \right]} \ ; \qquad (16)$$

$$P_3^+(\vec{r}) = 1 - \left\{1 + \xi_o + \langle \xi \cdot e^{-\xi} \rangle + \right.$$

$$\left. + \frac{1}{2} \left[\langle \xi^2 e^{-\xi} \rangle + \left(\xi_o + \langle \xi \cdot e^{-\xi} \rangle \right)^2 \right] \right\} \cdot e^{-\left[\xi_o + \langle 1 - e^{-\xi} \rangle \right]} \ . \qquad (17)$$

If we have only fog, then

$$P_{1,sp}^+ = 1 - e^{-\xi_o} \ ; \qquad (18)$$

$$P_{2,sp}^+ = 1 - (1 + \xi_o) \cdot e^{-\xi_o} \ ; \qquad (19)$$

for $\nu = 1$ we can write

$$P_1^+ = P_{1,ion}^+ + P_{1,sp}^+ - P_{1,ion}^+ \cdot P_{1,sp}^+ , \qquad (20)$$

where $P^+_{1,ion} = 1 - e^{-\langle 1-e^{-\xi}\rangle}$. (21)

From the first expression it follows that for the total result P^+_1 will be somewhat less than the sum of $P^+_{1,ion}$ and $P^+_{1,sp}$. If we want to know $P^+_{1,ion}$ at the absence of fog we have to use:

$$P^+_{1,ion} = \frac{P^+_1 - P^+_{1,sp}}{1 - P^+_{1,sp}} . \quad (22)$$

Usually, for example for photographic emulsions, in order to find optical density in absence of fog one subtracts fog optical density D_o from experimental value D_{exp}. If emulsion is described by one-hit model it is more exactly to use:

$$D_{ion} = D_{max} \times \frac{D_{exp} - D_o}{D_{max} - D_o} . \quad (23) \qquad \left[\text{Here it was used } P^+ = \frac{D}{D_{max}}\right].$$

For a plastique it is possible that own body etching rate is defined by expression for $P^+_{\nu,sp}$.

In the case of $\nu>1$ it is impossible to receive equations like (22). It is necessary separately to find ξ_o and later to calculate any track parameters.

Case 4. And at last, when sensitive microvolume is on the path of moving nuclei effective ionization acts are produced both by the nuclei and by δ-electrons:

$$\xi = \xi_{nucl} + \xi_{\delta\text{-electron}} , \quad (24)$$

then: $$\Sigma N_i \langle \xi^\alpha e^{-\xi}\rangle_i = \langle \xi^\alpha e^{-\xi}\rangle_z + \int \frac{dn}{dw} dw \langle \xi^\alpha e^{-\xi}\rangle . \quad (25)$$

The first member may be calculated with the help of the δ-function instead of the differential function $f(\vec{r}, \vec{\Omega}, s)$, and the second member must be calculated with the help of the appropriate function of the theory of multiple scattering and of function dn/dw, describing initial spectrum of δ-electrons.

So, the general expressions (2,3) give us the rule to consider a complicated problem as a set of more simple tasks and sometimes we can produce a principal new result, as in cases 1 or 3.

HEAVY-ION INDUCED DAMAGE OF BINARY SEMICONDUCTORS GaP AND PbS

S.A.KARAMIAN*, V.N.BUGROV*, C.ASCHERON**, G.OTTO**,
S.YU.PLATONOV***, O.A.YUMINOV
* JINR-Dubna, POB 79, 101000 Moscow, Russia
** Universität Leipzig, Linnestr.5, O-7010 Leipzig, FRG
*** Moscow University, 119899, Moscow, Russia

Charged particle irradiation produces different extended defects in solid materials. The formation of the depleted zone, vacancy clusters and voids near the end of heavy-ion range is well known. Their appearance is dependent on material and ion species, temperature and ion fluence. The complicated mechanisms of a defect formation and evolution are discussed in literature but the basic idea is always that an atomic collision cascade is a fundamental reason of the damage. This concept is strongly supported by the location of disorder maximum near the maximum of the energy deposited into nuclear subsystem of the crystal.

Latent tracks generated by very heavy ions in insulators represent another class of the extended defect [1]. Their production correlates strongly with the electronic stopping power, and their profile reproduces the Bragg-maximum in stopping the energetic nucleus [2]. As known, latent tracks cannot be observed in all insulators. The nonobservation of tracks means that they are either not formed or not visualized. If the tracks are formed but not visualized, the crystal amorphization at low ionic fluences could indicate the extended defects formation. Thus the measurement of damaging rate gives a new experimental approach to investigations of the extended defects formation. It was used recently for studying the Xe-ion damage of a diamond [3] and semiconducting [4] crystals. Also a new process of tracks formation in some metallic alloys was revealed [5]. The interest in the investigation of the role of electronic and nuclear energy losses in the damage of semiconducting crystals is rather obvious.

In this paper we want to provide some information on the defects induced by swift heavy ions in GaP and PbS crystals. GaP crystal is a semiconductor whose properties are not far from insulators. Our sample grown by the Chohralski method had specific resistivity about 10^7 Ω·cm. It looks like a transparent orange colour glass. The electron spectrum-gap is about 2.25 eV, and the hardness is about 6 Moos units for the GaP. So it may be interesting to search for extended defects like latent tracks produced eventually in the GaP by very heavy ions. PbS crystal is another type of semiconductors, which has photoresistive and scintillating properties. The swift ion influence on optically active materials is not yet studied extensively.

The polished (111) oriented GaP wafers of about 0.5 mm thickness were irradiated along random directions at room or liquid nitrogen temperature by collimated heavy ion beams, which had the diameter of 1 mm, angular divergence $<0.5^\circ$, intensity $\leq 10^{10}$ s^{-1} and pulsed power ≤1 W. The fluences ranged from 10^{13} to 10^{16} cm^{-2}. Glass plates were used as track detectors for the registration of the elastically scattered projectiles and recoils. The active layer thickness of the

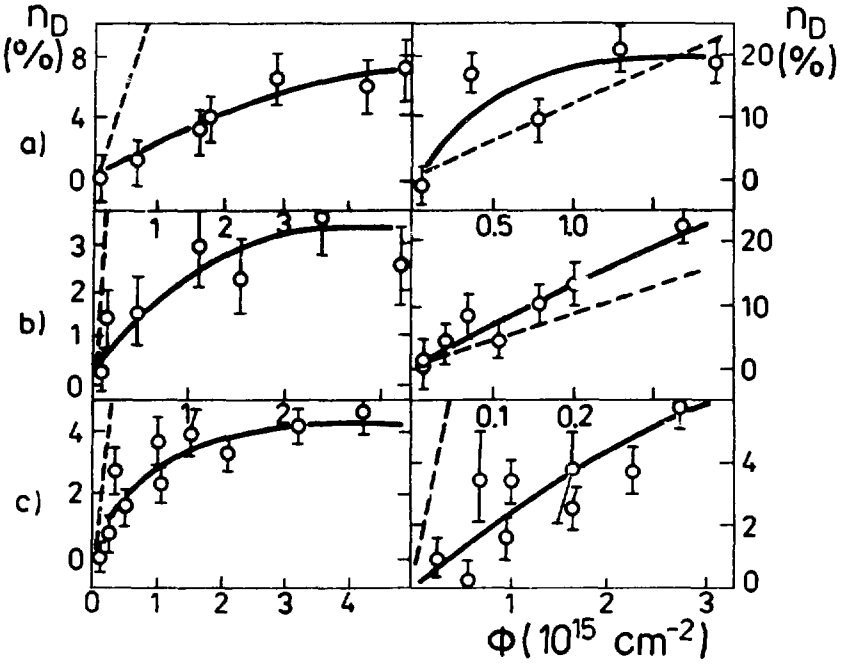

Fig.1. Defect concentration as a function of Xe-ion fluence for semiconducting crystals Si(a), Ge(b) and GaP(c) measured at room (left-hand side) or liquid nitrogen (right-hand side) temperatures. Solid line is a guide over experimental points, dashed one refers to the calculated concentration of displaced atoms

target is restricted in the range of 0.5-2.0 μm by the scattered products energy-losses. The blocking reflection patterns were recorded in-situ during the crystal exposures to heavy ions and visualized after the chemical development of the tracks. The blocking minimum yield as a function of the ion fluence $\chi_{min}(\Phi)$ was measured by counting the track density using an optical microscope. The defect concentration values $n_D(\Phi)$ were extracted by the quantitative treatment of the $\chi_{min}(\Phi)$ function using mathematical formulation from ref.[6]. The defect concentrations induced by Xe-ions in GaP are compared in fig.1 with those for Si and Ge crystals. For all the crystals it can be seen that at the room temperature defect concentrations are saturated at the level of about 3-4% when the fluence of the 1 MeV/u Xe-ions is increased up to $5 \cdot 10^{15}$ cm^{-2}. Hence, one can assume neither the latent track formation nor the usual damage due to nuclear scattering. If the first process is realized, the crystal has to be amorphized at fluence values of about 10^{12} cm^{-2}, the second

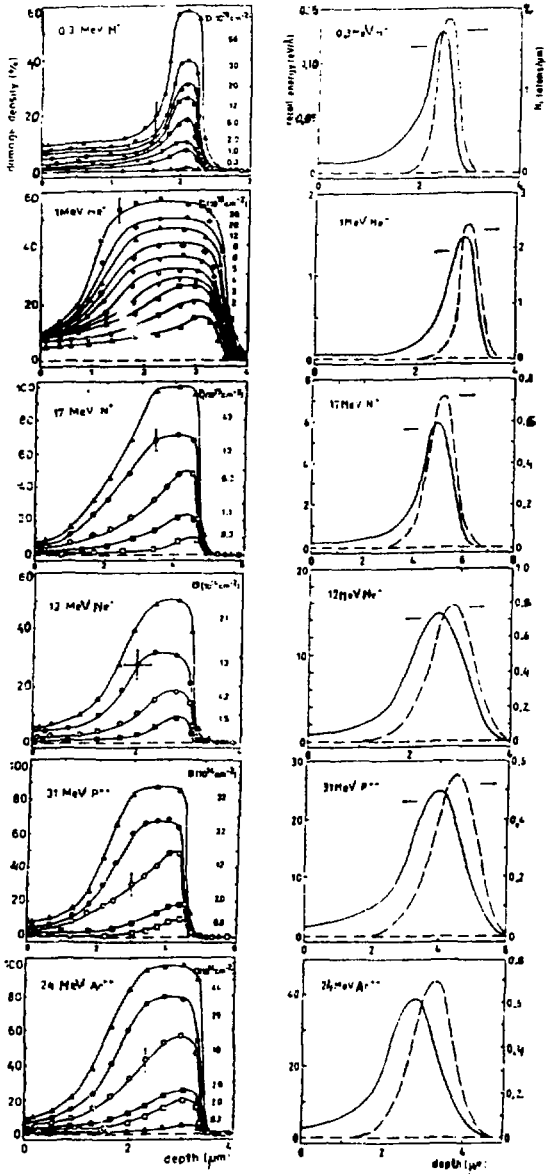

Fig.2. Experimental depth profiles (left-hand side) of the GaP damage in comparison with calculated profiles (right-hand side) of recoil energy - solid line, and stopped ions - dashed line. The experimental points are connected by guide line, ion species and fluence values are presented in fig

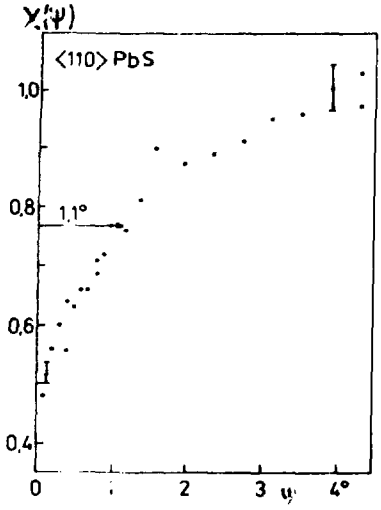

Fig.3.Blocking minimum measured for fission fragments emitted from the PbS crystal in the bombardment with 105 MeV ^{12}C ions

one leads to the amorphization at the fluences of about 10^{14} cm^{-2}. So we have to propose active recrystallization processes in the Xe-ion track surrounding which are stimulated by the energy deposited into the electronic subsystem of the crystal. This interpretation does not contradict to the damage increase at lower crystal temperature and lower ion energy (see fig.1).

It was important to study the question, whether the recrystallization processes are also active in the cases of lighter ions and lower energies incident on GaP? For this purpose depth profiles of radiation damage were measured using Rutherford backscattering spectra of 1 MeV protons treated on the basis of the multiple scattering model. The proton beam was directed along the normal to the crystal surface while heavy ion beam at 60° to the normal.The experimental data obtained are compared in fig.2 with the recoil energy and the implanted atom profiles calculated using the programme [7]. In principle, the measured profile is reproduced satisfactorily by the calculated recoil energy profile, however there is some excess (about 30%) of the measured value above the calculated one at the nearsurface region. This excess can be explained as the contribution of electronic energy-deposit into the crystal damage. Thus, at the GaP bombardment with ions from H to Ar no recrystallization process is stimulated by the energy deposited into the electron subsystem.

However low damage induced by Xe ions in semiconducting crystals gives the possibility to assume the threshold activation of the recrystallization process in condition $-(dE/dx) \geq 9$ KeV/nm. The conclusion that electronic energy losses could be active not only for crystal damage but also for crystal annealing has to be discussed.

The damage of the PbS crystal was studied using the crystal-blocking technique like the one described above. Single crystalline (100) oriented PbS was bombarded with 9 MeV/u ^{12}C and ^{20}Ne ions. Fission fragments emitted from the crystal target were detected by the glass detector. The blocking minimum observed in this case is shown in fig.3. The increase of the minimum yield $\chi_{min}(\Phi)$ as a function of the

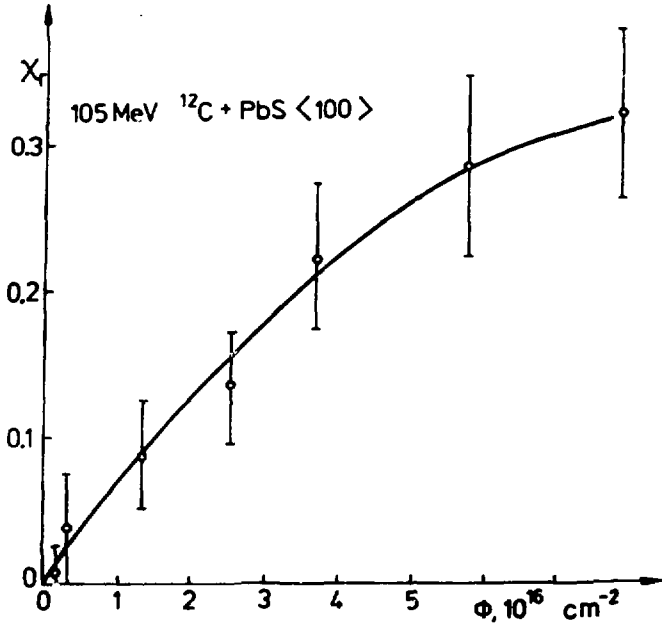

Fig.4. Radiation damage component of the PbS blocking minimum yield as a function of ^{12}C-ions fluence

fluence was measured, and radiation-damage contribution into the minimum yield $\chi_r(\Phi)$ was extracted using the expression:

$$\chi_r(\Phi) = 1 - [1-\chi_{min}(\Phi)]\,[1-\chi_{min}(0)]^{-1}, \qquad (1)$$

where $\chi_{min}(0)$ corresponds to the virgin crystal. The function $\chi_r(\Phi)$ is shown in fig.4, and it is clear that the long-range order in the PbS lattice still remains at the fluence of up 10^{17} ions/cm^2. Thus, the high radiation resistance of the lattice is revealed at heavy-ion irradiations of semiconductors while their electric properties (for instance, carriers concentration), as known, is much more sensitive to the charge particle fluences.

The nonobservation of the latent tracks in the diamond [3] and in many other insulators, the Xe-ion induced recrystallization of semiconductors revealed in ref.[4] and in this work, and the track formation in some metallic alloys [5] lead to conclusion that the idea about direct correlation between latent track formation and insulating properties of the medium can be excluded.

After ion passage in solid material the energy dissipation process can be going by different ways. What scenario realized, it is dependent on medium properties and the ion specy. Thoughtable scheme of the processes is present in the table with rough time scale coordinate. The primary energy deposit is universal phenomenon but the secondary process of the fast electron dissipation is already pluralistic one and it determines the following stages of the evolution. Some crucial role plays probably the capability of the medium to accept the electrons, which promotes the volume charge stabilization. There is another universal stage of the particle track evolution - the thermal spike formation. Following developments are

Table. Post ion-tracing phenomena in solids

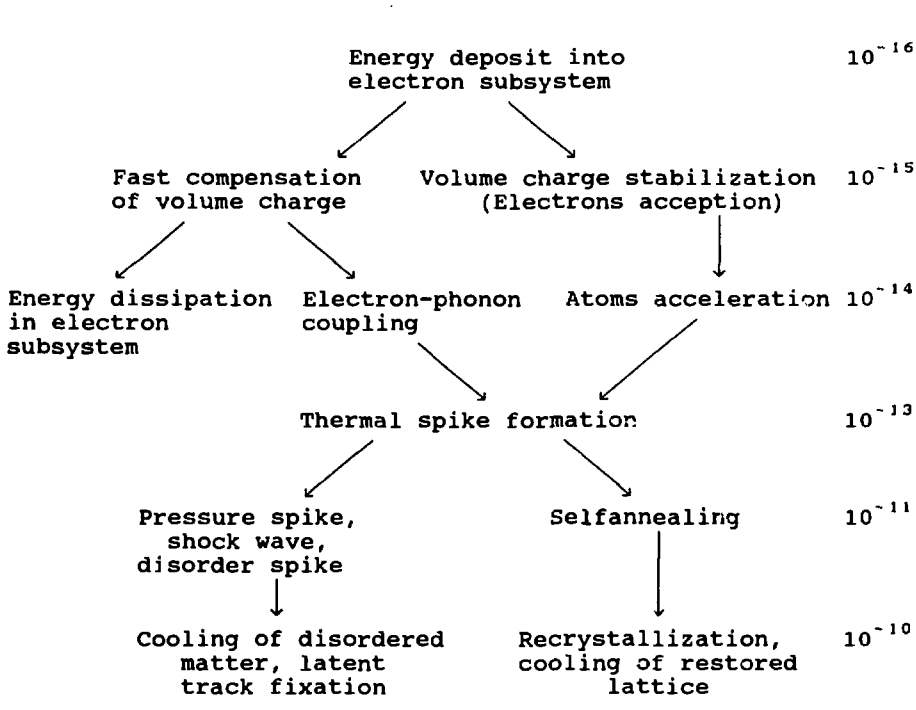

governed by such parameters of the spike as maximum temperature and profile and also macroscopic thermodynamical properties of the medium.

The heavy-ion induced damage of monocrystalline binary semiconductors GaP and PbS is studied using the blocking and channeling technique and the conclusion is made about the nontrivial role of the electronic stopping power, which can be active either for the lattice damage or for the recrystallization or can be passive dependending on the concrete conditions of irradiations. Some scheme of the processes developed in solid matter after ion passage is proposed.

References

[1] R.L.Fleischer, P.B.Price, R.M.Walker Nuclear Tracks in Solids (1975) Univ.Calif.Press.Berkeley.
[2] V.P.Perelygin, S.G.Stetsenko, G.Yu.Starodub, W.Birkholz, R.I.Petrova, G.G.Bankova Isotopenpraxis 23 (1987) 117.
[3] A.Yu.Didyk, A.M.Zaitsev, S.A.Karamyan JINR Rapid Commun. 4(37) (1989) 44.
[4] S.A.Karamyan Nucl.Tracks Rad.Meas. 18 (1991) 365.
[5] A.Barbu, A.Dunlop, D.Lesueur, R.S.Averback Europhys. Lett. 15 (1991) 37.
[6] J.F.Ziegler J.Appl.Phys. 43 (1972) 2973.
[7] J.F.Ziegler, J.P.Biersack, U.Littmark The Stopping and Range of Ions in Solids (1985) Pergamon.

On Mechanism of Tracks Formation in Alumophosphate Glasses

V.K. Lyapidevsky

Moscow Engineering Physics Institute, Moscow

Russia

Alumophosphate glasses are widely applied as thermoluminescent detectors /I/. The measurement of tracks number simultaneously with thermoluminescence yield irradiated by heavy ions in such detectors allows to determine spatial distribution of absorbed energy by detector cross-section, energy thermoluminescence yield referred to one track, absorbed energy distribution along track /2/.

At the same time simultaneous registration of two effects enables to obtain additional information about thermoluminescence and track formation mechanism. The spatial distribution of electrons and ions with the following electrons capture into deep traps is the necessary condition for track formation as well as for the light sum accumulation. Upon detector heating the electrons escape from traps recombine with the ions and excite the luminescence centres. The experiments described below showed that at the same time heavy ion tracks remained. Detectors on the basis of alumophosphate glasses IS-7 /2/ were irradiated by xenon ions with the energy of I MeV per nucleon on the U-300 accelerator and by nickel ions with the energies of 7 MeV per nucleon on the U-400 JINR accelerator. Thermoluminescence was investigated on the "Hashaw-2000" set-up. To determine track numbers the detectors were etched in hydrofluoric acid during 4 hours at room temperature. The ion flux density was 2.10^7 ions per cm^2. The tracks were observed under the optimal microscope.

The tracks conservation after thermoluminescence indicates that tracks annealing is connected not with a positive charge neutralization but with a thermal destruction of structure defects.

The analogous data were obtained in the work /3/ while investigating crystals thermoluminescence of aluminium and yttrium composite oxides /4/. Crystals heating up to the temperature of 800 K does not influence on characteristics of etched tracks. Tracks thermal destruction is observed at the temperature of more than I000--II00 K whereas thermoluminescence occurs in the range of 300-750 K.

These results are in agreement with the experiments on detectors irradiation by fast electrons and gamma-quanta after exposure in heavy ion beam. Two equal detectors of alumophosphate glass were irradiated by xenon ions then one of the detectors was irradiated by gamma-quanta Co^{60} of $I0^6$ rad dose. Then track parameters were compared during etching. It turned out that gamma-quanta irradiation carried out after heavy ion irradiation does not change track parameters. If one of the detectors is irradiated by gamma--quanta prior heavy ion irradiation then this will lead to track parameters change, track length decreases with etching rate decreasing in track.

The experiment showed that in the alumophosphate glass detectors preliminarily irradiated by gamma-radiation of $I0^6$ rad dose xenon ion tracks had the lower length and diameter than in unexposed detectors by etching at the same conditions.

This effect can be explained from the point of view of the Coulomb explosion model /5/. After heavy ion passing through detector the ionization takes place, electrons elapse from ions and are captured by traps. The ions due to electrostatic repulsion form structure defects which manifest themselves upon etching. Preliminary alumophosphate glasses irradiation by gamma-quanta produces a great number of electrons in traps. It impedes the electrons capture produced in heavy ion track. Therefore the probability of produced electrons and ions recombination increases that leads to the decrease of space charge, diameter and track length. Analogous effects have to be observed on admixture insertion being electron donors into detector. In the work /3/ the investigation of xenon ion track parameters versus activator concentration in crystals of aluminium and cerium composite oxides was carried out. Crystals were irradiated by xenon ions with the energy of I MeV per nucleon at an angle of 45° to crystal surface. The etching is performed in orthophosphoric acid at the temperature of 490 K. The experiments showed that with increasing of activating admixture of CeO_2 concentration the etching rate along track and therefore stable defects density decrease. The etching rate of crystal surface unexposed by ions does not depend on cerium admixture concentration.

The decrease of a number of formed stable radiative defects on increasing of admixture concentration being electrons donor can be explained by partial neutralization of a positive charge in track by admixture electrons for a period of time compared with the time of ion shift. The observable decrease of track etching rate in the described experiments can be explained by the fact that with increasing of the activator concentration and irradiation dose by gamma-quanta in detector volume the electron number capable to recombine with the positive ions increases that leads to space charge neutralization and ion shift prevention.

Thus to introduce admixtures into the basic material or to clean it one can change characteristics of track detector. The admixture introduction being electron donors (or filling the existing traps by electrons) leads to track density decrease. The admixture introduction capturing electrons during thermalization after heavy ion passing leads to track density increase. Purification of material from the admixtures capturing electrons leads to the increase of electrons recombination probability with the ions and to the decrease or loss of a positive charge until ion shift occurs. From this point of view one can explain the track absence in bubble chambers filled by pure xenon /6/.

On the grounds of above-stated one can assert that there is a primary multipurpose mechanism of tracks formation in condensed media. After penetration of a charged particle through medium the produced electrons elapse from ions during thermalization. In order that ions are shifted and track is formed one should execute the condition

$$\tau_{sh.} < \tau_{rel.}$$

where $\tau_{sh.}$ is ion shift time; $\tau_{rel.}$, relaxation time during which a positive charge compensation takes place that can be characterized by the mean lifetime of positive charges. Then the probability of elementary event of defect creation has a view:

$$W = \exp\left(\frac{\tau_{sh.}}{\tau_{rel.}}\right).$$

The efficiency of track formation process is determined by a value

$$\Delta = E_{Coul.} - E_{sh.},$$

where $E_{Coul.}$ is the Coulomb repulsion energy; and $E_{sh.}$, the energy required for creation of long-lived defects. The less is the distance between ions the more is the value Δ. Therefore the tracks formation in condensed medium is available only at sufficiently high density of space charge.

The mean lifetime of positive charges increases within the decreasing of free electrons number. Free electrons number can be decreased by admixtures introducing which are electron traps. By decreasing the detector temperature the electrons lifetime in traps increases. Therefore materials which do not register tracks at room temperature can detect heavy ion tracks. After charge separation the following heating and electron release will not lead to tracks destruction as seen in the work /2/.

The discussed mechanism of heavy ion track formation has to work in all cases when electrons produced by ionization escape from the detector. Therefore a heavy ion passing at a distance from matter surface of hot electron range order has to produce a track in any matter including metals on condition that $\tau_{sh.} < \tau_{rel.}$

References

1. Bochvar I.A., Gimadova T.I., Keirim-Markus I.B., Kushnerov A.Ya., Yakubik V.V. Dosimetry method IKS. M.: Atomizdat, 1977, p.224
2. Zverev S.A., Lyapidevsky V.K., Svetlichny M.I., Khokhlov N.B. Izv. of Acad. of Sciences, Ser. Phys. v.50 №3, 1986, p.542-543
3. Averkiev V.V., Lyapidevsky V.K., Khokhlov N.B., Izv. Ac. of Scien. Ser. Phys. v.50, №3, 1986, p.568-570
4. Averkiev V.V., Valbis Ya.A., Grigoryan A.Kh. et al, In: Luminescence receivers and ionizing radiation converters. Novosibirsk: Nauka, 1985, p.30
5. Fleisher R.L., Price P.B., Walker R.M., J.Appl.Phys., 1965, v.36, p.3645-3652
6. Brown J., Glaser D., Perl M., Phys.Rev., 102,586 (1956).

ENERGY LOSS AND MEAN RANGES OF ^{129}Xe AND ^{209}Bi IN ALUMINIUM AND KAPTON

K.K. Dwivedi*, P. Vater and R. Brandt

Kernchemie, FB 14, Philipps Universität

D-3550, MARBURG, Germany

Abstract: *The energy loss and mean ranges of 13.0 MeV/u ^{129}Xe and ^{209}Bi have been measured in aluminium and Kapton polyimide using a nuclear track technique. Calibrated CR-39 and ZnP-glass detectors were used to determine degraded energy of the heavy ions transmitted through the stair-case type stacks of Al and Kapton. The experimental results are discussed and compared with the theoretical values obtained from three different computer codes in order to verify their applicability.*

1. INTRODUCTION

The application of solid state nuclear track detectors has been well established in measuring energy-loss and mean ranges of heavy ions in both elemental and complex media[1-6]. In last few years, the heavy ion research involving track detectors has shown great potential in several fields like nuclear reactions[7-8], particle identification[9-10], fusion-fission and α-evaporation[11], multifragmentation reactions[12], cosmology[13], radiation biology[13,14], health physics[13] and in the development of microfilters and single-pore membrane[15-16]. It is important to note that these studies require reliable and accurate data on heavy ion ranges and energy loss in several commonly used elemental and complex materials. Both CR-39 and ZnP-glass detectors have high sensitivity for particle detection and good energy resolution and hence offer a very characteristic range-energy dependence for heavy ions. Thus, after appropriate calibrations, these detectors may be employed for measuring the energy, mean ranges and energy-loss rate of any heavy ion in any media.

---

* Visiting senior scientist under a fellowship from Commission of the European Communities.
Permanent address : Department of Chemistry, North-Eastern Hill University, Shillong - 793 003, India.

Among elemental materials our choice has restricted to aluminium because it has been extensively used as degrader foils and backings in many nuclear physics experiments. On the other hand the Kapton polyimide was chosen due to its growing application in nuclear research[17] and in production of nuclear track microfilters[18] on account of the high tensile strength and good thermal and chemical resistivity of the plastic.

In this paper we describe the experimental procedure for obtaining energy loss and mean ranges of ^{129}Xe and ^{209}Bi ions in Al and Kapton. The results are discussed and intercompared with the corresponding theoretical values computed from computer codes (a) RANGE[19] (b) TRIM[20] and (c) Benton's code[21].

2. EXPERIMENTAL

2.1 Preparation of Targets and Detectors

Thin foils of aluminium and Kapton were used to prepare stair-case type targets with effective thickness ranging from 21.2 μm to 127.3 μm for Al and 36.5 μm to 182.5 μm for Kapton respectively. The target thickness was measured by weighing method as well as by using Heidenhain depth measuring device. CR-39 and ZnP glass plates were used as track detectors. The target-detector assembly is shown in Fig 1(a).

2.2 The Irradiation Geometry

The target detector assemblies [Fig.1(a)] were mounted on glass-plates and then these were exposed to 13.0 MeV/u ^{129}Xe and ^{209}Bi ions at UNILAC, GSI Darmstadt. The irradiations were done at 45° using an ion fluence of about $5x10^4$ cm^{-2}. Fig.1(b) shows the irradiation geometry used in the present work.

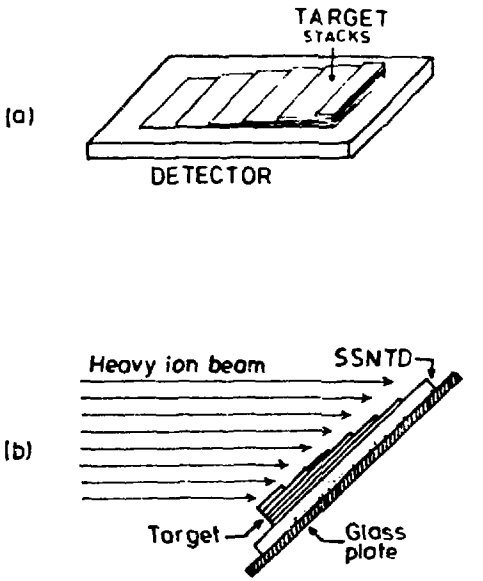

Fig. 1 .

Diagram showing
(a) target-detector assembly
and (b) the irradiation geometry

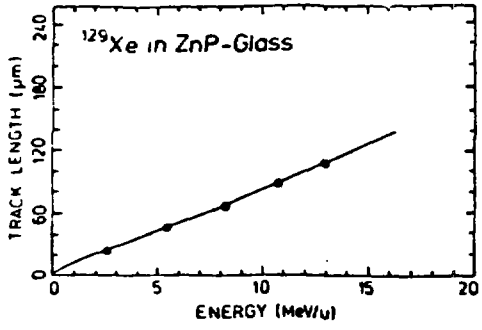

Fig. 2 . A calibration curve between the energy of ^{129}Xe ions and the measured track length in ZnP-glass detector up to 13.0 MeV/u

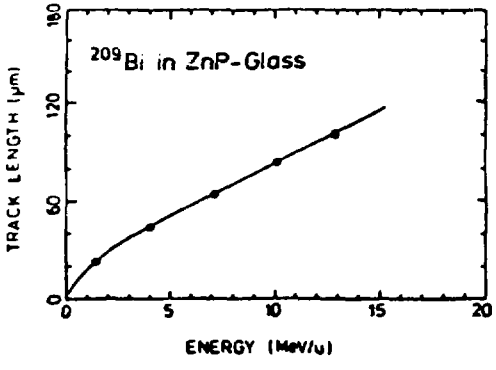

Fig. 3 . A calibration curve between the energy of ^{209}Bi ions and the measured track length in ZnP-glass detector up to 13.0 MeV/u

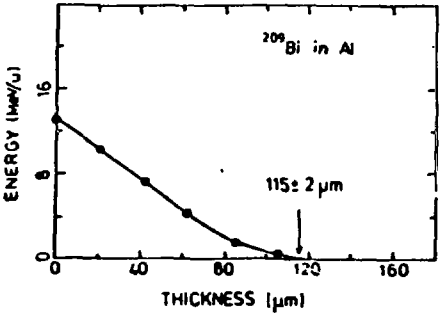

Fig. 4 . The energy-loss curve for 13.0 MeV/u ^{209}Bi in aluminium

2.3 Chemical Etching and Measurement of Nuclear Tracks

The latent tracks caused due to trasmitted ions in CR-39 and ZnP-glass detectors were etched in 6N NaOH at 60°C. While CR-39 was etched for a period of 1-3 hours, the ZnP-glass detectors were etched for a shorter time ranging from 15-20 minutes. The etched detectors were then marked at the edges into equi-energy zones. Nearly 100 fully etched tracks from each zone were measured and the most probable true track lengths were obtained from the length distribution curves.

2.4 *Experimental errors*

The accuracy of ion beam energy of UNILAC is ± 0.1% and the degraded energies from calibration curves are accurate within ± 0.5 MeV/u. The variation in target thickness was estimated to be < 5%. The track lengths were measured within a typical accuracy of ≈ 1.5 μm. From these, the error in the measurements of mean ranges was found to vary between 5-10%, except for the ion energies below 2 MeV/u at which it ranged upto 15%.

3. RESULTS AND DISCUSSION

The calibration curves for ^{129}Xe and ^{209}Bi in CR-39 and ZnP-glass have been constructed. Fig.2 and Fig.3 show such calibrations in ZnP-glass for both ^{129}Xe and ^{209}Bi upto 13.0 MeV/u. With the help of these calibration curves and the measured track lengths in the detectors, we have obtained the values of energy lost by projectiles after transmitting through targets of thickness x. From these data the energy-loss curves for ^{209}Bi in Al and ^{129}Xe in Kapton were constructed and shown in Fig. 4 and Fig. 5 respectively. It has been found that the thickness of Al (R_i) required to stop 13.0 MeV/u ^{209}Bi ions completely is equal to 115 ± 2 μm. The corresponding thickness of Kapton for 13.0 MeV/u ^{129}Xe was found to be 168 ± 3 μm. Using energy-loss curve and the values for R_i, the mean ranges of ^{129}Xe in Kapton and ^{209}Bi in Al at several energies have been determined. The range-energy plots for these ions in Al and Kapton are shown in Fig.6 and Fig. 7. The theoretical ranges from three different computer codes (a) RANGE[19] (b) TRIM[20] and (c) code of Henke and Benton[21] are also plotted in these figures. It may be observed (in Fig.6) that the theoretical ranges of ^{209}Bi in Al from all the above codes are fairly comparable with the experimental values while comparing the experimental ranges of ^{129}Xe in Kapton with theoretical values (Fig. 7), we have observed that the values from codes RANGE[19] and TRIM[20] are in good agreement whereas the ranges obtained from computer program of Henke and Benton[21] seem to have been underestimated by about 8% above 10 MeV/u. The present investigation provides a simple and accurate method for measuring heavy ion energy-loss and mean ranges in elemental and complex media. It has further supported the earlier views[1-6] that computer codes TRIM[20] and RANGE[19] predict quite reliable values of heavy ion ranges in elemental and composite solids.

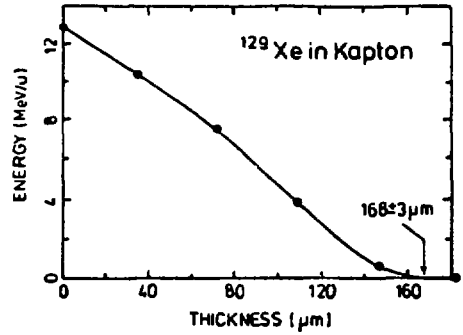

Fig. 5 . The energy-loss curve for 13.0 MeV/u ^{129}Xe in Kapton

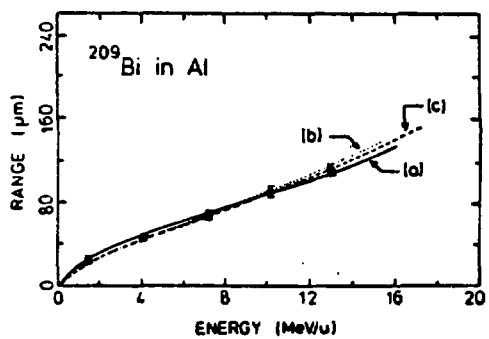

Fig. 6 . Experimental mean ranges as a function of ion energy for ^{209}Bi in Al, alongwith theoretical values obtained from (a) code RANGE[19], (b) code TRIM[20] and (c) the code of Henke and Benton[21].

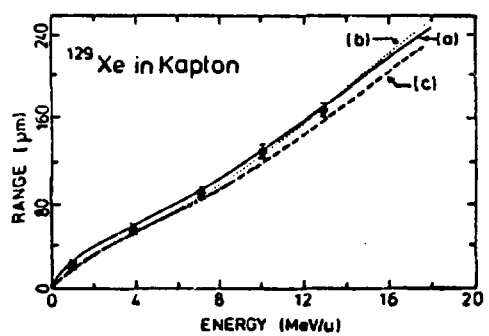

Fig. 7 . Experimental mean ranges as a function of ion energy for ^{129}Xe in kapton, alongwith theoretical values obtained from (a) code RANGE[19], (b) code TRIM[20] and (c) the code of Henke and Benton[21]

Acknowledgements - We wish to thank Dr. R. Spohr, Dr. J. Vetter and other staff of UNILAC, GSI Damstadt for rendering heavy ion irradiations. A senior visiting fellowship to KKD by CEC, Brussels and DST, Govt. of India is gratefully acknowledged.

REFERENCES

1. K.K. Dwivedi, Nucl. Tracks. Rad. Meas., 19 (1991) 71.
2. A. Saxena and K.K. Dwivedi, Nucl. Tracks. Rad. Meas., 17 (1990) 447.
3. S. Ghosh, A. Saxena and K.K. Dwivedi, Rad. Effects and Defects in Solids, 112 (1990) 149.
4. A. Saxena, K.K. Dwivedi, R.K. Poddar and G. Fiedler, Pramana J. Phys., 29 (1987) 485.
5. A. Saxena, K.K. Dwivedi, E. Reichwein and G. Fiedler, Nucl. Instrum. Meth. in Phys. Res., B36 (1989) 276.
6. A. Saxena and K.K. Dwivedi, J. Phys. D : Appl. Phys., 23 (1990) 476.
7. P. Vater, H.J. Becker and R. Brandt, Nucl. Instrum. Meth., 147 (1977) 271.
8. R. Haag, G. Fiedler, R. Ulbrich, G. Breitbach and P.A. Gottschalk, Z. Physik. A., 316 (1984) 183.
9. D.O. Sullivan, P.B. Price, E.K. Shirk, P.H. Fowler, J.M. Kidd, E.J. Kobetich and R. Thorne, Phys. Rev. Lett., 26 (1972) 416.
10. R. Beaujean and W. Enge, Z. Phys. 256 (1972) 416.
11. K.K. Dwivedi and G. Fiedler, Nucl. Tracks Rad. Meas., 15 (1988) 353.
12. C. Brechtmann and W. Heinrich, Phys. Rev. C39 (1989) 2222 (and references therein).
13. R.L. Fleischer, P.B. Price and R.M. Walker, 'Nuclear Tracks in Solids : Principles and Applications', Univ. of California Press (1975).
14. G. Kraft, Nucl. Science Appl.3 (1987) 1.
15. P. Vater, Nucl. Tracks Rad. Meas., 15 (1988) 743.
16. R. Spohr, 'Ion Tracks and Microtechnology : Principles and Applications' (1990), Vieweg, Braunschweig.
17. F. Foroughi, B. Vuilleumier and E. Bovets, Nucl. Instrum. Meth., 159 (1979) 513.
18. Zhu Tian-Cheng, R. Brandt, P. Vater and J. Vetter, Nucl. Tracks Rad. Meas., 15 (1988) 799.
19. K.K. Dwivedi, Nucl. Tracks Rad. Meas., 15 (1988) 345.
20. J.P. Biersack and L.G. Haggmark, Nucl. Instrum. Meth., 174 (1980) 257.
21. R.P. Henke and E.V. Benton, USNRDL-TR-67-122 (1967).

INVESTIGATION OF LATENT ION TRACKS IN SSNTD WITH SMALL ANGLE NEUTRON SCATTERING

W. Birkholz*, F. Häußler**, S.G. Stetsenko***

* University of Technology Leipzig, Germany
** University of Technology Leipzig, Germany
Joint Institute of Nuclear Research, Dubna
*** Joint Institute of Nuclear Research, Dubna

1. Introduction

Passing the SSNTD (solid state nuclear track detector) charged particles (protons and heavier) form latent tracks. The parameters of these tracks vary with the atomic number and the energy of particles. It is nearly impossible to observe and to analyze latent tracks. We hope that by using the small angle neutron scattering (SANS) it is possible to get information about the diameter of the latent tracks after analysing the signals of collective effects of a big number of tracks. This work is the first attempt to get information about latent tracks by SANS on MURN-TEXT facility of JINR. Essentially the study of the influence of partial annealing and of other environmental conditions on the storage of irradiated detectors over a long period requires the analysis of the latent tracks.

2. Some Remarks about the Small-Angle Neutron Scattering Method

Small-angle neutron scattering (SANS) is useful as a technique to characterize matrix inhomogeneities in a variety of materials [1]. SANS gives average information for an ensemble of scattering

objects. The inversion of scattering pattern to real space cannot yield specific data of individual scattering centers like a direct imaging method [2]. Certain models for an interpretation of experimental results are needed too.

Two regions of the scattering curve are discussed by Pearson et al. [3]. In the following they are used for the analysis of the scattering data. At low scattering angles the Guinier approximation holds [4].

$$\frac{d\Sigma}{d\Omega}(Q) \propto \text{volume concentration} \times \text{contrast} \times V(a_i) \times \exp[-Q^2 R_g^2 / 3] \quad (1)$$

and

$$Q = 4\pi/\lambda \sin(\beta/2), \quad (2)$$

Thereby β is the scattering angle, λ denotes the neutron wavelength and Q the scattering vector. R_g is the radius of gyration of a scattering particle of type (i) with a volume $V(a_i)$. The radius of gyration is the mean squared distance of all points within the particle seen from the particle center. On the spectrometer MURN-TEXT the macroscopic differential cross section $d\Sigma/d\Omega(Q)$ can be measured in a straightforward procedure and contains all scattering information about the sample.

3. Experimental

3.1. SANS-Experiments on the Spectrometer MURN-TEXT

The spectrometer MURN-TEXT (Fig. 1a) is located on the beam-line 4 at the pulse reactor IBR-2 ' of the Joint Institute for Nuclear Research, Dubna. By using the TOF-method a wide variety of incident wavelengths (from 0.07 nm to 1.5 nm) is available for measuring inhomogeneities on a length scale of approximately from 1 nm to 30 nm. A momentum transfer from 0.07 nm^{-1} to 7 nm^{-1} is detectable. At sample position a neutron flux from (6 10^6 to 3.7 10^7) $cm^{-2}sec^{-1}$ exists [5,6]. A detailed description of the SANS-spectrometer MURN-TEXT is given in [7,8]. By means of a vanadium scatterer placed into the direct neutron beam the macroscopic cross section $d\Sigma/d\Omega$ (Q) is measurable.

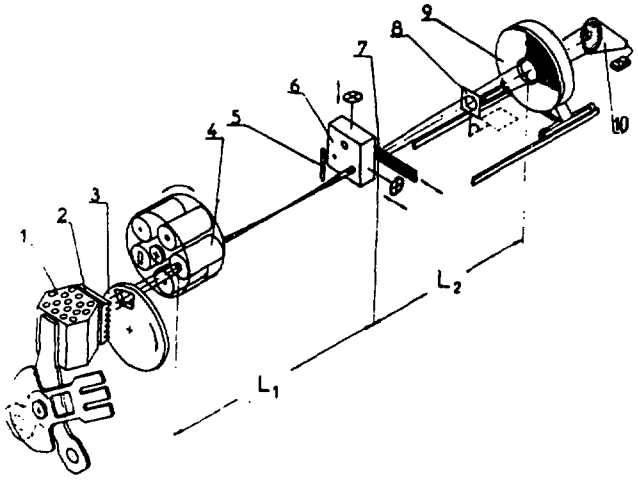

Fig. 1.

Layout of the spectrometer MURN. The numbers denote: 1 - active core of IBR-2; 2 - grooved moderator; 3 - slow rotating beam chopper; 4 - first variable aperture collimator; 5 - monitor counter; 6 - 2nd variable aperture collimator; 7 - cartridge with samples; 8 - internal scattering standard; 9 - one of two assemblies of scattering detectors; 10 - direct beam detector

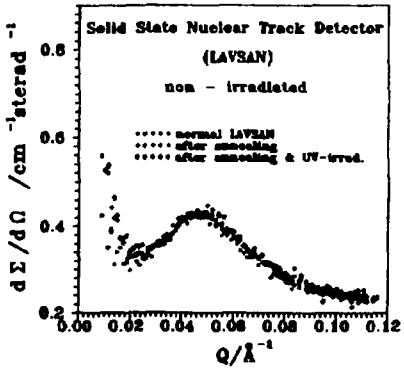

Fig. 2.
Guinier-plot of non-irradiated SSNTD against air.
The procedures "annealing" and "UV-irradiation" show no changes in the structure of the material

All samples were put into a sample holder which consisted of six circular hollows. The scattering signal of one irradiated foil (thickness of about 62 μm) is too low for analysis. Therefore we used a stack of 15 SSNTD (total thickness of about 0.93 mm). The diameter of the samples is 40 mm. At sample position the neutron beam cross section is of about 1.5 cm^2.

3.2 Heavy Ion Irradiation of SSNTD and Measuring with SANS

For the first attempt it was investigated the possibility of analysing latent tracks in SSNTD. We used polyethylenterephtalate (PETP) foils (Lavsan) and operated with two parts of foils from the same party, (i) irradiated with Ti ions perpendicularly to its surface, (ii) non-irradiated to get background signals. Their radiations took place at the U-400 heavy ion accelerator in the Laboratory of Nuclear Reaction of JINR. The energy of the Ti-48 ions was 5.5 MeV/nucleon. The track density shall be as high as possible, but the tracks shouldn't overlap each other. From this reason the latent track density shall be of about 10^{11} cm^{-2}. After a first SANS measurement all detectors were annealed at 160 degrees Centigrade) during 30 minutes and were measured once more by SANS. Next step was irradiation of the foils by ultraviolet (UV) ligth during three hours and measuring by SANS.

3.3. Experimental Results

Fig. 2 represents the results of the neutron scattering data of non-irradiated with heavy ions SSNTD. There is no difference between the three steps of procedure: (i) usual foils, (ii) annealed foils and (iii) annealing plus UV-irradiation. The peak of the curves depends of the structure of Lavsan. The peak doesn't change by the procedures of annealing and UV-irradiation.

The very big difference of the scattering signal between the detector irradiated with heavy ions and non irradiated one is

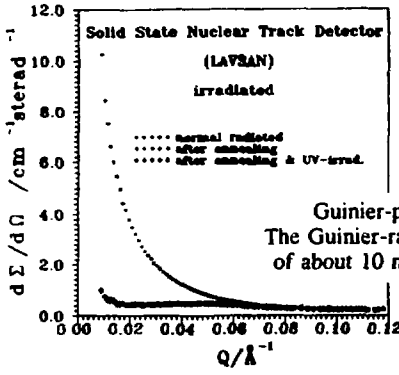

Fig. 3.
Guinier-plot of Ti-48 irradiated PETP against air.
The Guinier-radius $R_g \approx 8$ nm corresponds with a diameter of about 10 nm for a cylidrical model of the latent tracks

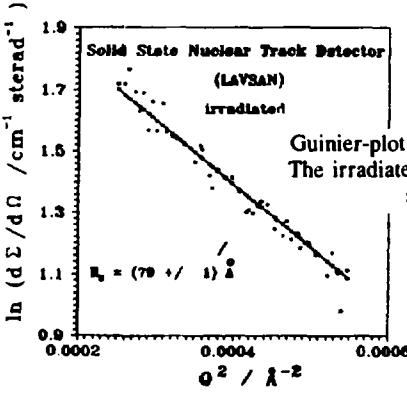

Fig. 4.
Guinier-plot of irradiated and annealed Lavsan against air.
The irradiated and annealed detector shows nearly the same signal like non-irradiated material

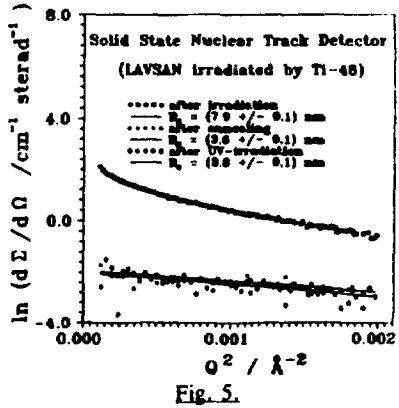

Fig. 5.
Guinier-plot of irradiated and annealed detectors against non-irradiated material.
After annealing result structures with a Guinier-radius with a half of those of latent tracks.

demonstrated in fig. 3. The procedure of annealing and UV-irradiation was repeated with the detector containing latent tracks. Fig. 4 shows the scattering curves. The scattering signal of annealed detectors strongly decreases. There is not any influence of UV radiation after annealing of latent tracks at that conditions evident.

The calculated radii of gyration are shown in fig.5. The background measurements (Fig. 2) for this calculations are used. The radius of gyration is of about 8 nm for normal radiated foils and about 4 nm for foils with annealed latent tracks.

For the further interpretation of the scattering data via modeling additional data about the latent tracks are necessary (form of latent track; i.e. the density distribution parallel and perpendicular to the track axis, exact track density of the irradiated region, i.e. homogeneity of the track distribution, etc.).

Acknowledgements

The authors wish to acknowledge Prof. Yu. M. Ostanevich, Dr. V.P. Perelygin from LNP and LNR of JINR and Prof.H. Baumbach of UT Leipzig for their permanent interest, the fruitful discussions and the support for the work. Beyond it we thank the colleagues of the SANS-group, especially A. I. Kuklin, for their helpful discussions and support by realization of the SANS-experiments.

References

[1] H. Walther, P. Pizzi, Small Angle Neutron Scattering for Non-destructive Testing. In: Research Techs. for NDT 4, ed. by M. S. Sharp, London: Academic Press, 1980, Chap. 10, p.341

[2] G. Kostorz, Small-Angle Scattering and its Application to Materials Science. In:Treatise on Materials Science and Technology, ed. by G. Kostorz, London: Academic Press, 1979, Vol. 15, p. 227

[3] D. Pearson et al., J. Mat. Si. 18(1983) 430

[4] A. Guinier and G. Fournet, Small-Angle Scattering of X-Rays, New York: John Wiley & Sons Inc. 1955

[5] Yu. M. Ostanevich, Time-of-Flight Small-Angle Scattering Spectrometers on Pulsed Neutron Sources, Makromol. Chem., Macromol. Symp. 15 (1988) 91

[6] User Guide, Neutron Experimental Facilities at JINR, Dubna, USSR 1991

[7] Yu. M. Ostanevich, Time-of-Flight Small-Angle Scattering Spectrometers on Pulsed Neutron Sources JINR-preprint, P 13 - 87 - 407, Dubna 1987

[8] V. Yu. Bezzabotnov, Yu. M. Ostanevich, Solution of Some Experimental Problems Met in the Time-of-Flight Small Angle Neutron Scattering, Physica B 156 & 157 (1989) 595

THE DEVELOPMENT OF A NEW TECHNOLOGY FOR PREPARING AgCL(Cd)-DETECTORS

Bradnova V., Kulikova S., Nevzorova N.

Joint Institute for Nuclear Research, Dubna

The development of the technology for preparing AgCl (Cd) - detectors by means of fusion leak [1,2] was accompanied by some experiment based on pressing.

High chemical activity of silver and mechanical properties of silver chloride have defined both the shape of press moulds (PM) and its protection by means of some thin film. As a result, the classical PM has been replaced by a PM composed of six separate blocks placed inside a rigid frame. Fig.1 shows the PM seen from above. It is manufactured from a steel prone to tempering up to 50-55 units with a high quality (7th class) mechanical processing of its surface. The best protection film has been made by vacuum deposition of titanium trinitride. As a result, the finished surfaces have no corrosion traces after 50 cycles of repeated usage.

Plates have been manufactured by means of the DP-36 pressing machine with a maximum pressure of 500 KP/cm^2. The plates have a 6x35 mm^2 size. The thickness of 0.8 and 1.2 mm is due to initial raw material portions of 1.5 and 2.5 g, respectively. The raw material is a silver chloride doped by 0.05 M% of Cd in the form of powder and grains.

The plates have been subjected to a standard sintering procedure. By means of a cold rolling there has been manufactured a foil 0.15-0.2 mm thick.

Radiation testing of the detectors has been realized with ^{210}Po α - particles. The process of development consists in visualizing particle tracks by the light with 405 nm wavelength (the light source is a KGM-30 lamp) with a light source - detector distance of 15 cm and the development time of 30 min for both sides of the detector.

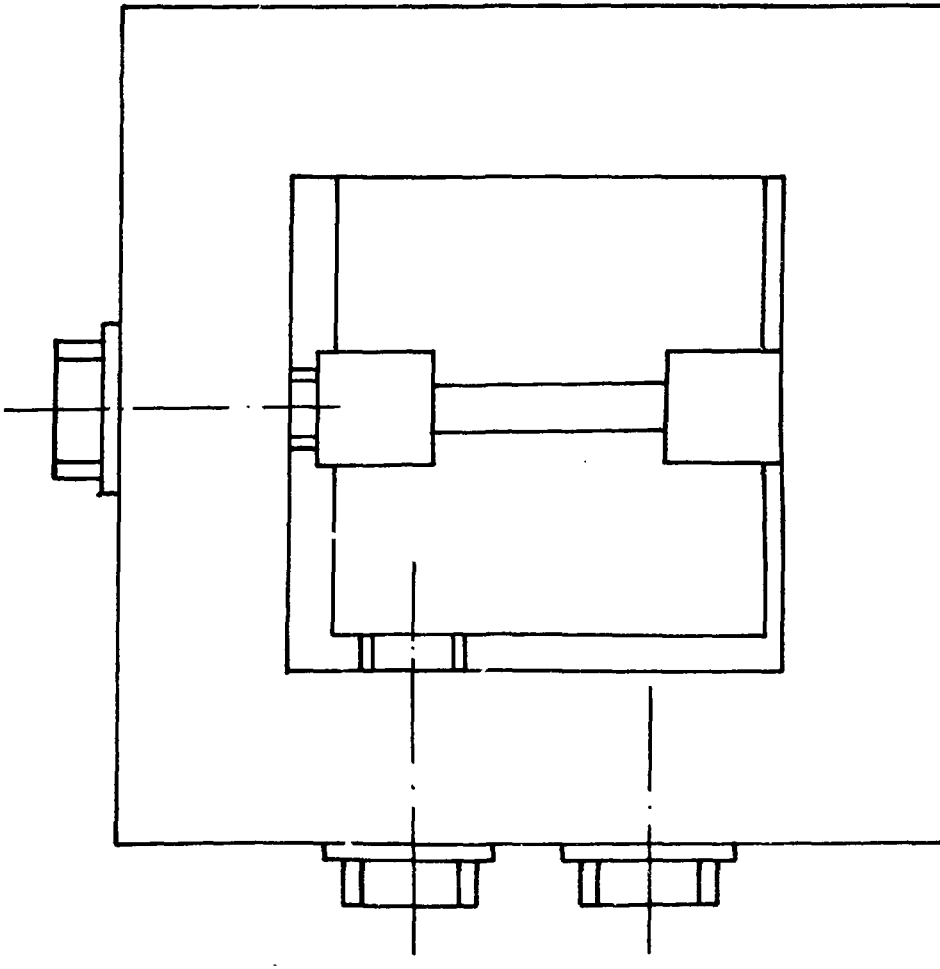

Fig.1. Press moulds from above

The powder - made detectors produce no tracks, while the grain - made ones exhibit black noninterrupted tracks on both sides.

References

1.Брадна и др. Препринт ОИЯИ, Р13-83-419, Дубна, 1983.
2.Kiradhiefova R. - Cs.Cas.Fys.,1963, p.333.

LOW REGRESSION NUCLEAR EMULSION FOR ν-EXPERIMENTS

Maleev A.M., Myltseva V.A. (NIIKFP)
Egorov O.K., Kolganova E.D., Pozharova E.A., Smirnitsky V.A. (ITEP)

Neutrino experiments require several months exposure [1,2,3] to get reasonable statistics for physical aims. But for new experiments, for example CERN WA 95 experiment for search neutrino oscilations ($\nu_\mu \Leftrightarrow \nu_\tau$), the emulsion must conserve the main quality during one two years [4].

In NIIKEP under leadership of V.A.Myltseva the modified fotoemulsion gels were synthesized. Nuclear emulsion from each one had regression time more than one yea. [5]. Regression time means the time, when grain density becomes 20 grains/100 mkm. (Our definition).

At first, it is necessary to understand how to estimate a time, using accelerated regression test, during which it is possible to use fabricated nuclear emulsion.

Standard NIIKFP emulsion BR-2 samples have been tested to estimate the fading effects for time intervals in real time and compare it with fading effect under conditions accelerated regression test NIIKFP (Point 7 on Table 1; Point 6 shows residual sensitivity after one year).

Table 1

NN	time interval between exposure and developing (days)	residual grain density (grains/100 mkm)	%
1	0	32.7±0.4	100.0
2	30	31.2±0.4	95.4
3	120	29.6±0.4	90.8
4	180	24.8±0.4	75.8
5	365	16.9±0.3	51.7
6	0	29.9±0.4	91.4
7	3	22.0±0.5	67.2

Table 2

conditions		grain density (grains/100 mkm) (s1)	(s2)
emulsion processing just after exposure		38.3±0.7 (100%)	38.4±0.7 (100%)
emulsion keeping after exposure before processing under conditions of NIIKFP (T=20°C, 100% RH)	for 3 days	36.5±0.7 (95.3%)	36.3±0.7 (94.5%)
-"-	for 6 days	32.3±0.6 (84.3%)	29.3±0.6 (76.3%)
-"-	for 9 days	11.8±0.4 (30.8%)	12.5±0.4 (32.6%)
emulsion keeping after exposure before processing under conditions of Fuji (T=45°C, 70% RH)	for 2 days	36.0±0.7 (94.0%)	38.9±0.7 (101.3%)

The emulsion samples were exposed by negative pions with momentum 1.8 GeV/c in ITEP accelerator. The thickness of the pellicles were 600 mkm, and all samples were kept under temperature 5 -10°C. It is possible to see, the accelerated test coincide, approximately, 40 weeks regression in real time.

Table 2 shows the improvement of the stability of BR-2 emulsion [5]. The thickness of that samples was 100 mkm.

It is possible to propose, that the samples s1 and s2 can conserve the image of the event more than one year.

We thank V.A.Ditlov, K.Hosino, K.Niu, M.Sakai, and V.V.Shamanov for useful discussion.

References

1. W.Smart e.a. Acta Physica Polonica, V.B17 (1986) p.41.
2. N.Ushida e.a. Nucl. Instr. and Meth., v.224 (1984) p.50.
3. Ю.Алешин и др. Препринт ФИАН N3, М., 1991.
4. Preprint CERN-SPSC/90-42 SPSC P254.
5. В.Мыльцева, Доклад на Всесоюзном совещании по фотоэмульсиям, Дубна, февраль 1992.

TRACK PARAMETERS OF MULTICHARGED PARTICLES IN CRYSTALLINE DETECTORS

V.A.Ditlov[1)], V.P.Perelygin[2)], S.G.Stetsenko[2)]

[1)] *Gosniichimfotoproject, Moscow, Russian Federation*

[2)] *Joint Institute for Nuclear Research, 141980, Dubna*

In the present paper one of the possibilities of our theoretical approach to application [1,2] for experimental track analysis of heavy nuclei search in meteorites is considered. In application of this approach there are the following difficulties. First, olivine meteorite substance parameters should be found. These parameters include — sensitive region size - Q_o; characteristic energetic value ΔE_o or $(dE/ds)_o$; parameters ν-hit and m-target model of sensitive region response [1]. Second, the information on a spatial distribution of the local response by the track volume or on surfaces of equal response probabilities does not permit to obtain immediately a geometric form of the etched track or simply its length, as for this additional calculations of material etching kinetics is required. In the present paper the determination method for the etched track length relation to the atomic number of the nucleus is proposed except etching kinetics consideration. For this purpose a certain effective value of the track section similar to biocell inactivation section is introduced [3]:

$$\sigma_{\nu m}(R) = 2\pi \int_o^\infty (P_\nu^+(\rho, R))^m \rho \, d\rho, \qquad (1)$$

here: R is the residual path of the recorded nucleus; $(P_\nu^+(\rho))^m$ is the probability of the local response appearance at ρ distance from the track axis in the ν-hit and m-target model in a cross section of the point R.

The relation energy–nucleus path as well as the energy losses were calculated by Spencer algorithms [4]. The energy distribution of δ-electrons was taken from paper [5], but in the application it was re-normalized so that the total energy of a δ-electron current would coincide with the energy spent by nucleus on collisions with atomic shell electrons according to Steward [5]. For determination of four olivine parameters σo, $(dE/ds)_o$, ν and m the experimental data on the etched track lengths of the following nuclei were used: Z = 24; 26; 28; 32; 36, for which the lengths are equal to $L_{24} = 8.5$; $L_{26} = 13.5$; $L_{28} = 21.0$; $L_{32} = 37.0$ and $L_{36} = 68.0$ μm. The material etching process determines the necessity to introduce additional parameters. The critical parameter σo will be additional parameter to four parameters. Assume that the track will be etched only in case if the track effective section value exceeds this critical parameter σo. In this case only the section of the nucleus track between two equal track sections will be etched:

$$\sigma_{\nu m}(R_1) = \sigma_{\nu m}\ (R_2), L = R_2 - R_1. \qquad (2)$$

The search for olivine parameters was made in the following way. First, the coefficients of the quantity $< \xi^n e^{-\xi} >$ expansion in terms of Legendre polynomials as a function on the angle Θo of electron emission for discrete energy spectrum were calculated and recorded in the data bank. These calculations were made for seven values of the sensitivity characteristic value $(dE/ds)_o$ and for models with ν = 1,2,3 and 4 (the values $(dE/ds)_o$ from 4.8 to 26.15 keV/μm). Each subsequent value is twice as large as the previous one. For the sensitive

region radius four values αo=5., 10., 15., 20. Å were taken. Then the values $\sigma_{\nu m}$ were calculated and recorded in the data bank. The parameter "m" was changed from 1 to 12. Thus, for calculation of the values $\sigma_{\nu m}$ 1344 combinations of the detector parameters were considered.

The idea to select the most probable set of detector parameters was connected with the search for a functional minimum:

$$F(\alpha o, (\frac{dE}{ds})_o, \nu, m) = \sum_{j_1 j_2} \left(\frac{\sigma o_{j_1} - \sigma o_{j_2}}{\sigma o_{j_1} + \sigma o_{j_2}} \right)^2, \qquad (3)$$

here, indices j_1, j_2, numerate calibration nuclei. The values σo_j are determined for each j-track separately. If values for different tracks with given set $(\alpha o, (dE/ds)_o, \nu, m)$ are more consistent, then the functional value (3) is lower and this parameters value combination is more probable.

A few words about the search for σo_j values. First, by known values L_j such points of the nucleus trajetory were found at which the equation is valid:

$$(dE/ds)_{R=S_1} = (dE/ds)_{R=S_1+L} \qquad (4)$$

Then for effective values calculation (1) the following six cross sections of the track were chosen:

$$R_1 = S_1, R_2 = S_{max}/2, R_3 = S_{max}, R_4 = \frac{S_1 + S_2}{2}, R_5 = L, R_6 = S_1 + L, \qquad (5)$$

where S_{max} is the point at which the nucleus energy losses are maximum.

After determination of the values at these points by linear interpolation such points of trajectory were searched for at which equation (2) was valid. The values σo(R) at these points were taken as σo for a given set of detector parameters of the j-th nucleus. After sampling of all the calibration tracks the value of functional (3) was found.

The calculations made according to this scheme have shown that the minimum value of the functional is obtained with the following set of parameters:

$$Q_o = 15Å; (dE/ds)_o = 9.6keV/\mu m; \nu = 4; m = 1. \qquad (6)$$

Here, the critical value of the track cross section appeared to be $\sigma o = 0.0002693\ \mu m^2$, that gives for the critical radius of an effective cross section at the etched track ends $\rho_{eff} = 92.6$Å.

The functional (3) behavior along the sections of space $(Q_o(dE/ds)_o, \nu, m)$ passing through the found point (5), is shown in Fig.1. As it follows from the presented curves, the functional (3) minimum is peaked for all the parameters except for parameters αo on the side of its low values.

In Fig.2 the dependence for xenon nucleus Z=54 is presented. The etched part of a xenon nucleus track designated by the dashed line is L=242 μm. Note that points of the nucleus trajectory with equal energy losses do not coincide with those of equal track section. For example, for nucleus Z=36 the track points with specific losses dE/ds = 0.1077×10^5 kev/μm being 68 μm apart, have coordinates S = 7.528 μm and S = 75.7 μm while the points being the same distance apart, equal to the etched track length value, and with equal σo lie in the points S_1 = 12.7 μm and S_2 = 70.7 μm.

In Fig.3 the dependence of the estimated lengths of etched tracks on the atomic number Z is presented for all the atoms of the Mendeleev table and also for nuclei near the stability island Z=114.

It is necessary to note that the search method of the etched track lengths L by criterion σo yields the largest error in the region of high Z, though this region is important for superheavy

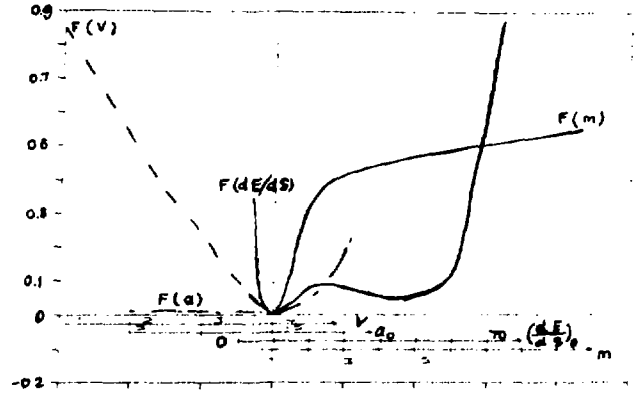

Fig. 1. Behavior of functional (3) over parametric sections of space (Q_o), $(dE/ds)_o, \nu, m)$ passing through the obtained point (5).
— — — – dependence of the minimized functional on ν;
– – – – – – dependence of the functional on the sensitive region radius Q_o;
———— – dependence of the functional on parameter $(dE/ds)_o$;
———— – dependence of the functional on parameter m

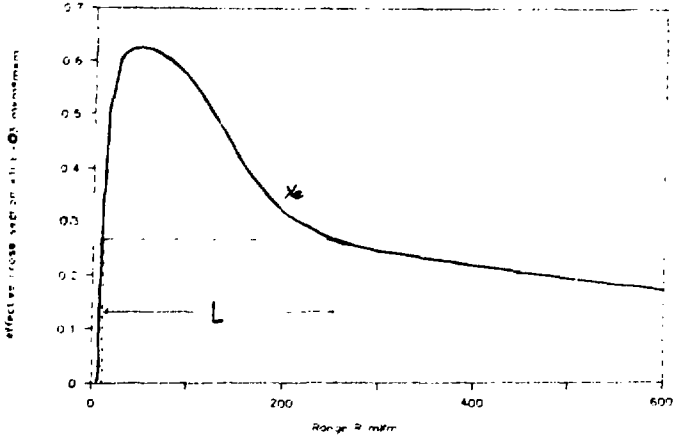

Fig. 2. The dependence $\sigma(R)$ for a xenon nucleus Z = 54.
The estimated length of the etched track $L_{54} = 242\ \mu m$

nuclei identification. This error results from the fact that for high Z the dependence σo(R) is very weak and little mistakes in σo value may lead to large mistakes for etched track length L. To determine L(Z) dependence in this region of Z more accurately it is necessary to supplement calibration calculations by calculations of olivine etching kinetics.

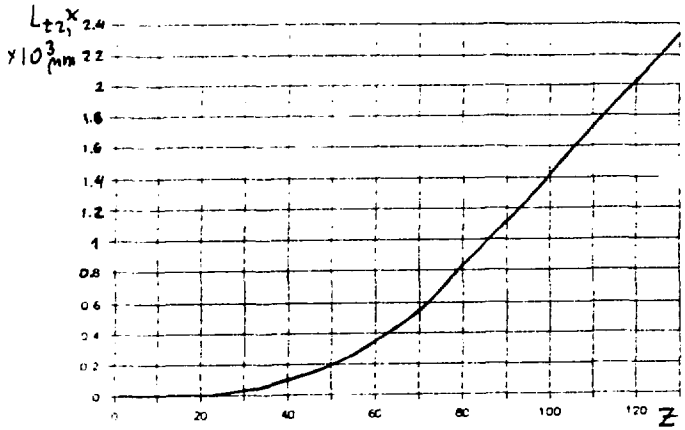

Fig. 3. The estimated dependence of etchable track length L on atomic number Z

References

[1] Ditlov V.A. Theory of Spatial calculation of primary action of δ–electrons in track detectors with account of multiple scattering. – In: Solid St. Nucl. Track Detectors, 1980, Pergamon Press, Ltd, p.131–141.

[2] Ditlov V.A. Theory for detecting fast nuclei by Solid State Detectors and Problems of Theory of Multiple Electrons Scattering. (The first paper).

[3] Katz R. Track Structure Theory in Radio-biology and in Radiation Detectors. – In: Solid St. Nucl. Tr. Detectors. 1978, Pergamon Press, Ltd, v.1, p.27–86.

[4] Steward P.G. Stopping power and range for any nucleus in the specific energy interval 0.01–500 MeV/amu in any nongaseous material. – In: Ph.D.Thesis. 1968. UCRL–18127–130 p.

[5] Bradt H.L. and Peters B. Investigation of the Primary Cosmic Radiation with Nuclear Photographic Emulsions. – Phys. Rev. 1948, v.74, n.12, p.1828–1837.

REGISTRATION CHARACTERISTICS OF THE NEW "CZ"-TYPE NUCLEAR TRACK DETECTOR

L.L.Kashkarov(x), S.V.Stovbun(xx), V.P.Perelygin(xxx)

(x) Institute of Geochemistry and Analytical Chemistry, RAS, Moscow, Russia. (xx) Institute of Chemical Physic, RAS, Moscow, Russia. (xxx) Joint Institute for Nuclear Research, Dubna

The registration characteristics of the new "CZ"-type SSTD has been studied using α-particle track parameters. The "CZ"-plates about 1 mm thick were irradiated with α-particles from ^{239}Pu source with E_{max}= 5,16 MeV. The more smaller (up to 0.5 MeV) energy α-particles were obtained at the corresponding air distances. The volume formation of the track cone was traced by means of the step-etching procedure in the 6N NaOH solution at the temperature $T=(65\pm1)^{o}C$. For this the exposed detector plates were etched in the same conditions during from 1 to 9 hours. In the first etching step (after 1 hour) only very small (diameter $D \lesssim 1$ μm) pits were observed on the plate surface, irradiated by the 0.5-1.0 MeV α-particles. In Fig.1 D-values, obtained for the normal oriented α-tracks are shown as a function of a total etching time. As is seen after 9 hours D-values for the α-particles with $E \lesssim 3$ MeV lie in the interval (15 ± 1) μm. Approximately half of this value equals a surface layer of thicness Δh, removed during total track development time, that gives about $(\Delta h)=(0.75\pm0.05)$ μm/hour.

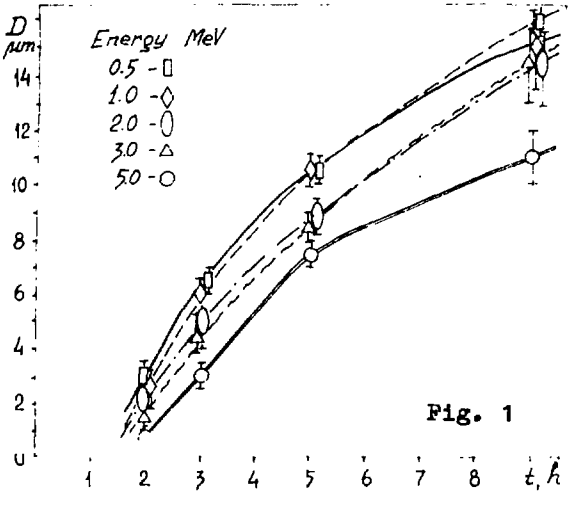

Fig. 1

Measuring of the basic geometry parameters [1] for the tracks inclinated to the exposed surface under different angles, gives possibility to calculate the true track length L for particles with different

energy. The preliminary data give the maximal L values for the α-particles with 3 and 5 MeV egual to 13 and 18 μm, respectively.

The observed smallest track-surface inclination angle was about 10 degrees, that characterised "CZ"-type material as one of the high-effective plastic track detector.

One of the main characteristics of the solid state track detectors (SSTD) is the relation between V_T corrosion velocity along the track length and V_G general dissolution velocity of detector surface (bulk etching). In the first approximation, when V_T and V_G are the constant along the track, its formed shape would be near conical and the opening half-angle is $\theta = \arcsin V_G/V_T$ [2].

The mostly exact measuring of the V_T/V_G-relationship can be obtained by means of the being as possible long tracks which can be formed by the high-energy charged h· y ions. With this aim we have used the accelerated (E=9.1 MeV/nucleon) ^{20}Ne ions. Irradiation was performed in the Joint Institute for Nuclear Research Heavy Ion Accelerator. The step-like chemical etching of the tracks inclined under 30° angle to the irradiated SSTD plate surface was performed in the same condition. The results of measuring of some geometry parameters (see Fig.2) for the ^{20}Ne tracks are shown in the Table.

Table. The parameters for the ^{20}Ne accelerated ion tracks in "CZ" SSTD

Etching time, min	Track diameter (μm) D	d	Track length (μm)
120	2- 4	<1	80- 85
240	5- 6	1	130-140
360	8-10	2	150-170
540	13-15	6	185-190

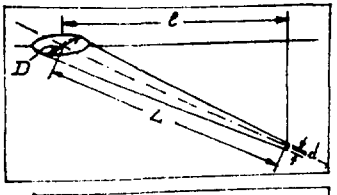

Fig.2

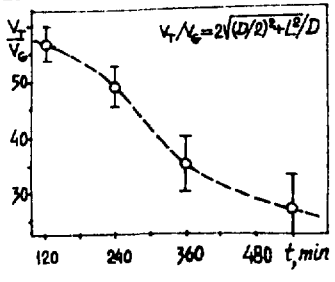

Fig.3

The obtained results indicate that in the "CZ"-type SSTD the total observed track length for the used ^{20}Ne ions L_{max} = 190 μm that was achieved after ~540 min of etching time. V_T/V_G relation during etching procedure decreases from 55 to 27 as it is indicated in Fig.3.

References: 1. Hence R.P., and Benton E.V. 1971, Nucl. Instrum. Methods 97, 483. 2. Fleischer R L., Price P.B., Walker R.M., 1975, "Nuclear Tracks in Solids", Berkeley Univ. of Calif. Press, 605 p.

FISSION TRACK DATING AND THERMAL HISTORY ANALYSIS: RECENT ADVANCES USING SURFACE TRACKS

M. Rebetez, A. Chambaudet and M. Grivet

Université de Franche-Comté, U.F.R. des Sciences et des Techniques,
Laboratoire de Microanalyses Nucléaires, 16 route de Gray, F-25030 Besançon Cedex
France

ABSTRACT

Fission track dating is already commonly used to retrace the thermal history of rocks. A rock's thermal history can be traced by first determining the fission track age and then by measuring the track lengths. Major advances have been made on the study of confined track lengths. For this reason, we wished to fine-tune the method by reinvestigating surface track lengths, which seem to provide additional information on thermal history.
A new tool for length measurements and a more up-to-date analysis of length distributions are presented. This information helped us to devise an original age correction method and a new instrument for chrono-thermometric investigations.

INTRODUCTION

Many geochronological methods can be used to retrace the thermal history of a rock. Each of them has its own chronometer which is set off at a given temperature. These methods include mainly U-Pb, Rb-Sr and K-Ar, which use the natural radioactive elements of minerals.
In fact, there is a continuous series of chronometers which can be combined to retrace the complete history of rocks. The time interval between the ages of two chronometers reveals the cooling rate which the rock has experienced since its geological setting. This characteristic has been largely developed to come up with a cooling curve, by using either the fission track method with another method, or several fission track chronometers with closing temperatures that are different enough from each other.
Apatites, sphenes and zircons are the three main fission track chronometers.
But the final cooling period, for temperatures below 150°C can only be described by conducting a fission track study on apatite.
Moreover, for minerals with a complex thermal history, traditional chronometers do not provide any thorough information on the cooling history (Rebetez, 1987).

In actual fact, a detailed study of only one chronometer such as the apatite-fission track couple can provide very precise information which enables two different complex thermal histories to be differentiated.

FISSION TRACK DATING

Uranium 238 contained in minerals can fission spontaneously, thus creating damages called 'latent tracks' in crystallographic structure. To determine the concentration of uranium, the sample may be irradiated by a known fluence of thermal neutrons which induce the fission of a finite number of uranium 235 atoms. Therefore, the fission track dating method is based on the ratio of a density of fossil tracks over a density of induced tracks. This ratio is a measure of age because the decay constant of uranium is quite clear.

Induced and fossil tracks are usually etched on a polished surface cut through mounted grains of the mineral being examined. Only tracks crossing the polished surface will be etched and optically counted. Various environmental factors, but mainly temperature, can affect the stability of fossil tracks over geological time, leading to a reduction of the mean etchable length and thus to a lower fossil track density.

This is why the apparent fission track age, determined in this way, only means something in geological terms when there is no length reduction. Experimentally, this is the case in volcanic rocks which have experienced a very brief cooling period and have not undergone consecutive reheating.

But a more general case of interest corresponds to the study of rocks having experienced partial heating after their setting. In petroleum exploration, the temperature zone of production and maturation of hydrocarbons is located between 60 and 120°C and corresponds exactly to the closing temperature of fission tracks in apatite. Fossil track fading is, then, a very good indicator in studying the thermal history of sedimentary basins. The entire fission track length distribution--not just the fission track age--must be studied because all tracks carry a complete baggage of thermal information dating back to when they were formed.

CONFINED AND SURFACE TRACKS - BIAS OF CHEMICAL ETCHING

Fossil tracks due to damage caused by uranium fission fragments are produced in the bulk of a mineral. But it is impossible to directly obtain the latent etchable length of a track. To be observed with an optical microscope, the minerals are polished so that an internal surface is obtained. This surface generates a population of latent tracks having a distribution of lengths displayed from 0 to the maximum. These latent tracks are called surface tracks and are measured after undergoing chemical etching to provide a semi-track length distribution. The measurement of the projection of these tracks on the polished surface can easily be obtained through experimentation. The theoretical distribution

has a triangular shape (Dakowski, 1978), but chemical etching disrupts this ideal distribution. It has been shown (Chambaudet et al., 1986) that the etching time and the choice of the concentration of the etchant greatly influence the shape of the distributions. This explains why the operator cannot observe shorter tracks and shows the complicated distributions for overetching conditions.

Another observation technique is related to the measurements of confined tracks. The lengths are only measured into the bulk of the mineral on horizontal tracks for which the etchant operates by way of a previously etched surface track or by a crack in the crystallographic structure. If optimal etching conditions are used (Rebetez et al., 1988), the confined track length distribution is directly representative of the bulk latent track distribution. Ideal in the beginning, this technique is unfortunately restricted to samples having a sufficient uranium concentration so that the confined track counting provides good statistics.

This is why much credit has been given to the studies of surface track length distributions. Among the advantages of this method is the fact that it can be applied to a wider range of track densities using fewer samples and without having to use overetching conditions.

Nevertheless, care must be taken in interpreting surface track length distributions in order to differentiate between the bias introduced by polishing and etching and the real value of thermal annealing.

MATHEMATICAL SIMULATION AND CHRONOTHERMOMETRIC INTERPRETATIONS

A mathematical model was suggested in order to gather thermal information from the Projected Track Length Distribution, or PTLD (Grivet et al., 1992a). The basic idea of this model is that the fission track population in an apatite is composed of several sub-populations of tracks with different etchable lengths.

The mathematical expression of a PTLD of all samples is given, with respect to the triangular frequency distribution of a single population of tracks shown by Dakowski (1978). Consequently, any difference in the PTLD between the fossil track population and the induced track population can be expressed in terms of annealing.

Unlike other age correction methods, this theoretical approach may be applied to samples which have experienced a variety of thermal histories. Rather than giving one corrected fission track age, with this method, the age function can be drawn. This graph provides:

- the type of thermal history,
- the time of entry into the partial annealing zone, around 120°C for apatite,
- the time of entry into the total track length stability zone, around 60°C,
- the actual reduction rate.

Different simulations have been made to correlate the shape of the age function with several distinctive thermal histories:

- a slow cooling in the partial annealing zone,
- different reheating up to the 120°C limit,
- a thermal event.

The calculations show that any thermal step can be differentiated in the graph and enable the time-temperature relation to be quantified.

This concept was then applied to geological samples, first on standard material then on geological samples whose thermal history was already determined.

In Durango apatite, the theoretical age function was found to fit the data for ~ 5% annealing, leading to a corrected fission track age of 33±4 Ma, in good agreement with the literature (Jonckheere et al., 1992).

In a second sample of the Durango apatite, a bimodal track population was artificially generated by a partial annealing of the fossil tracks in addition to neutron irradiation, generating an induced unannealed population of tracks. The calculated PTLD is also in good agreement with the experimental distributions.

Other experiments (Grivet et al.,1992b) have resulted in another potential standard material. The apatite 88-5 was first distributed for the 1988 interlaboratory experiment. It is a fragment of a single crystal from a pegmatite of the late Precambrian Grenvillian structure in southeastern Canada. The age function derived from the PTLD shows a convex trend, which is typical of a single population of tracks, with an annealing rate of ~ 15%. The corrected age is consistent with the value of 184±15 Ma proposed by Van den Haute and Chambaudet (1990).

Presently, the PTLD and the age function concept are the only way of obtaining information on the thermal history of rocks after the sample has last been cooled at ~ 120°C. The method is limited, however, due to its lack of precision in the measurements. For this reason, a minimum of 1000 fossil and induced tracks has to be measured to obtain reliable results.

ATOM: A SOFTWARE PROGRAM DEVELOPED TO ANALYSE TRACK CHARACTERISTICS

From an equipment standpoint, only automatic systems developed specifically for fission track analysis have the precision and can count a large number of tracks needed to provide reliable results. This is precisely why we developed ATOM, a software program for performing input operations of data such as track densities, lengths and orientations of tracks (Rebetez et al., 1991). The system consists of a microscope equipped with a drawing tube, connected to an IBM compatible computer by a digitizer. The resolution of the system is good enough to analyze track lengths within half a micron.

The software program was written in Turbo Pascal (a Borland, Inc. trademark) and is compiled in an execution file requiring 200Kb to work. Much care went into the design of ATOM to make it user-friendly and ergonomical, thus reducing eye strain and measurement time. The computer monitor is broken down into three sections. The first section is the menu which lists the various available options. The second section is an information line and a window which display information on the current measurement being taken. The last section shows the grid of the occular with all track input indicated. A cursor moves simultaneously with the bitpad mouse, which enables the user to perform any function, whether it is measuring a track, counting, erasing, or selecting an option in the menu.

The main menu of the software includes a few utility options. The "Bitpad" option is used to correlate the screen grid with that of the microscope. The "Calibration" option is used to input the calibration coefficient from the keyboard or by measurements with the bitpad by using a micrometric grid.

The main three options, however, are the "Lengths and Angles Study", "External Detector Method" and "Population Method"; these last two options are dating methods.

For each option, no data input can be plugged in before entering the measurement characteristics. Tracks are then drawn on the screen of the computer but may be erased at any time just by clicking on them after having chosen the "Erase" option in the menu.

When measuring lengths and orientations, a statistical menu is available which displays the track length distribution between two modifiable limits. The graph of orientations can also be obtained in this way, and statistical data such as the mean value, standard deviation and number of tracks counted are given.

When dating by the external detector method, each grain of the mineral is analyzed individually. To save time in the recognition of their exact images in the detector, we added a module to the software for automatic positioning of the motorized stage of the microscope. A sequence option allows the programming of successive positions of the stage to date a series of selected grains, so the microscope stage moves automatically between the mount and the detector. Finally the fission track age is calculated and the plot of individual grain ages is displayed or may be printed out.

In every case, all data are registered in files which may be read on IBM compatible or Macintosh (Apple) computers so that any further statistical analysis is possible using commercially-available standard software programs such as Excel (Microsoft).

CONCLUSION

Major advances have been made in the fission track dating and thermal history analysis of surface tracks.

A very low-cost semi-automatic measuring system using the ATOM software program quickly takes a large number of reproducible measurements.

When interpreting fission track analysis data in apatite, the age function concept, based on the mathematical model of the Projected Track Length Distribution (PTLD), provides very useful information on the type of thermal history the mineral has undergone. This information enables the reduction rates and the date of entry in the partial annealing zone, and more generally the time-temperature function, to be quantified at temperatures below ~ 120°C.

The surface track analysis method, used in addition to the confined track analysis method, is a reliable means of calculating the final cooling temperature of a rock.

REFERENCES

Chambaudet A., Mars M., Rebetez M. and Theobald F. (1986), *"Chemical Etching and Length Distribution of Fission Tracks: a Model"*, Int. J. Radiat. Appl. Instrum., Part D, Nuclear Tracks 12 (1-6), 855-8.

Dakowski M. (1978), *"Length Distributions of Fission Tracks in Thick Crystals"*, Nucl. Track Detection, 2, 181-190.

Grivet M., Rebetez M., Ben Ghouma N., Chambaudet A., Jonckheere R. and Mars M. (1992a), *"Apatite Fission Track Age Correction and Thermal History Analysis from Projected Track Length Distributions"*, Chemical Geology (Isotope Geoscience section), 108.

Grivet M., Rebetez M., Ben Ghouma N. and Chambaudet A. (1992b), *"The Use of the Projected Track Length Distributions of Fssion Tracks in Apatite for Thermal History Analysis"*, submitted to Nuclear Tracks Radiat. Meas..

Jonckheere R., Mars M., Van den Haute P., Rebetez M. and Chambaudet A. (1992), *"L'apatite de Durango: analyse d'un minéral standard pour la datation par traces de fission"*, to be published in Chemical Geology.

Rebetez M. (1987), *"Modélisation des distributions de longueurs de traces de fission de l'uranium dans le but de retracer l'histoire chrono-thermométrique de minéraux"*, Thèse de Doctorat de l'Université de Franche-Comté Besançon, n°40, 283 p..

Rebetez M., Chambaudet A. and Mars M. (1988), *"Theoretical Etching Effects on 'Track in Track' and 'Track in Cleavage' Length Distributions"*, Int. J. Radiat. Appl. Instrum., Part D, Nuclear Tracks Radiat. Meas. 15 (1-4), 69-72.

Rebetez M., Zoppis B., Rebrab A., Grillon P., Gentina E. and Chambaudet A. (1991), *"Atom: A Semi-Automatic Measuring System for the Analysis of Fission Track Characteristics in Anisotropic Minerals"*, Int. J. Radiat. Appl. Instrum., Part D, Nuclear Tracks Radiat. Meas. 19 (3-4), 255-60.

Van den Haute P. and Chambaudet A. (1990),*"Results of an Interlaboratory Experiment for the 1988 Fission Track Workshop on a Putative Apatite Standard for Internal Calibration"*, Int. J. Radiat. Appl. Instrum., Part D, Nuclear Tracks Radiat. Meas. 17 (3), 247-252.

CLUSTER EMISSION OF ^{114}Ba

Tretyakova S.P., Oganessian Yu.Ts., Lazarev Yu.A., Mikheev V.L., Utenkov V.K., Shirokovsky I.V.

Laboratory of Nuclear Reactions, JINR, Dubna

Introduction

The first theoretical predictions of cluster decay probabilities in new region near nuclear shells Z=50, N=50 were made in the work *[1]*. The most favourable variant according to these estimates is $^{114}Ba \rightarrow {}^{12}C$ (Q=18-19 MeV). However, the value of relative probability of cluster decay ($\sim 10^{-9}$) required excessively much time (years) for its studying on accelerators because of low production cross-sections of neutron-deficient nucleus ^{114}Ba. Theoretical calculations of cluster decay probability of ^{114}Ba performed in the work *[2]* give values of this probability of 6-7 orders higher than *[1,3]* using the same nuclei masses. The results of calculations of α-decay probability performed in these works coincide. The estimations accuracy is small because of great indefiniteness in nuclei mass predictions in this region. Other source of calculation uncertainty is the absence of correct data on life-time of ^{114}Ba relatively to α and β-decay. Extrapolation of different literature data showed that the total halflife ^{114}Ba is about 0.1-1 s.

There are two methods of its production:

1. in spallation reactions with proton beams (a system of the ISOLDE-type);
2. in nuclear reactions induced by heavy ions.

The reaction $^{58}Ni(^{58}Ni,2n)^{114}Ba$ was chosen for this purpose. The cross section calculations of this reaction give the value of $\sim 10^{-30}$ cm^2. In this paper there will be presented the first experimental data observation by dielectric detector on searching for cluster radioactive decay of ^{114}Ba.

Experiment

a. Irradiation. Internal ^{58}Ni beam of the U-400 accelerator for effective use of the maximal intensity of ion beams was used. The experimental arrangement designed for the investigation of [illegible]nd nuclei decay is shown schematically in Fig.1 (4). The ^{58}Ni beam was incident tangentially upon the lateral face of a hollow cylinder placed vertically, which was rotated with angular velocity of 10 rev/s. The lateral face was covered by 3 mg/cm^2 of ^{nat}Ni deposited electrochemically. This layer served as the target and recoil catcher simultaneously. As the angle between the beam direction and the cylinder surface is very small, the Ni layer is thick target in which the reaciton excitation function is integrated from the Coulomb barrier to E_{max}. The maximum energy of

the internal ^{58}Ni beam was chosen to be equal to 280 MeV. The integral ion flux on the target was about $4.5 \cdot 10^{17}$ ions. At a distance of 2 mm the rotating target was surrounded by dielectric detectors.

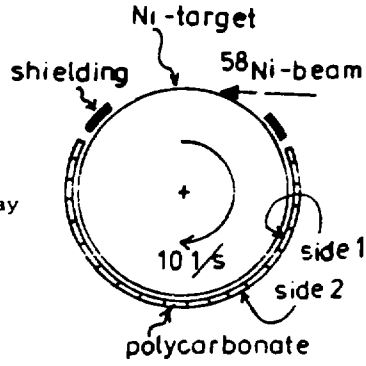

Fig. 1. Schematic view of the experimental device for detecting short-lived cluster decay

The time of one cycle of rotating target was chosen equal to 0.1 s in accordance with estimate of partial period of β-decay ^{114}Ba (~0.1 s) which evidently is the main decay channel of this nucleus.

b. Detector. Different products are formed as a result of the ^{114}Ba decay:

$$^{114}Ba \rightarrow \begin{matrix} ^{12}C + ^{102}Sn \\ ^{4}He + ^{110}Xe \\ \beta^{-} + ^{114}Cs \end{matrix}$$

For registration of ^{12}C clusters there were used polycarbonate detectors (Makrofol, Bayer) of 185 μm thickness.

Preliminary the detector calibration was performed by extracted beam of the ^{12}C ions with the energy of 7-24 MeV at different angles to detector surface and by alpha-particles of ^{233}U source using different absorbers for their energy change.

It was established that this detector registers the ^{12}C ions starting with the energy of about 0.1 MeV and higher but alpha-particles only with the energy less than 2 MeV. The detector etching was being performed in 20% NaOH at 70°C during 2 hours.

The alpha-particle tracks look like a point background. The other background source could be the recoil nuclei tracks producing by the scattering of α-particles and fast neutrons from the ion beam on light nuclei of detector material.

The number and length of etched nuclear recoil tracks were determined in special calibration experiments. One part of detectors irradiated by ^{12}C ions was exposed in 2π geometry by alpha-particle flux of about 10^{8} cm^{-2} and with energy about 4 MeV. The other part of such detectors was irradiated by fast

neutrons at an angle of 15° to the ^{4}He beam accelerated on the U-200 cyclotron to 9 MeV/amu (total ^{4}He flux ~ $7 \cdot 10^{18}$) and stopped in Al target. The fast neutron flux was measured by the ^{238}U calibrated target in contact with dielectric detector (Mellnex-0) located close the polycarbonate detectors.

After the etching the number of nuclear recoil tracks was counted by microscopic scanning. The density of such tracks after alpha-particle irradiation was about 2 cm^{-2} with length ≤4 μm; after neutron irradiation there were observed less than 10 tracks/cm^2 with length ≤9 μm.

In experiment ^{nat}Ni + ^{58}Ni (280 MeV) a background of etched nuclear recoil tracks (number and length) connected with fast neutrons was measured after the etching on the back detector side.

Results

The results of irradiation are presented in Fig. 2. For three days of irradiation there were obtained ~10 tracks the length of which was in the expected range for cluster decay of ^{114}Ba. Neutron spectrum on the beam of ^{58}Ni turned out to be essentially more hard one than that in the background experiments which were carried out on the beam of ^{4}He with the energy of 9 MeV/n. In time interval of ~0.1 s they uniformly distributed within the statistics. In terms of calculated cross-section of the reaction $^{58}Ni(^{58}Ni, 2n)^{114}Ba$ is $\sim 10^{-30}$ cm^2, target thickness is 3 mg/cm^2 and integral ion flux with the energy of 280 MeV is $4.5 \cdot 10^{17}$, the total number of obtained nuclei ^{114}Ba is $\sim 10^{7}$. Taking into account of cluster registration efficiency ~8% (from 4π geometry) it follows from our data that $\lambda_{Cl}/\lambda_{total} \leq 10^{-5}$. It is necessary to note that experimental results presented here are preliminary ones.

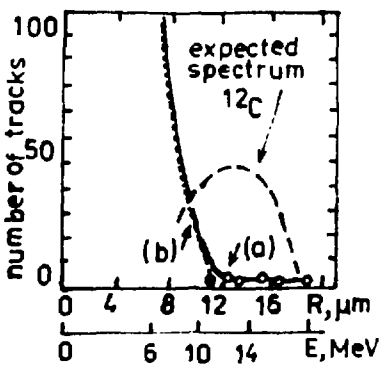

Fig. 2. The etch track length distribution obtained on detector side 1 (solid curve) and detector side 2 (dashed curve) (fig. 1)

In future experiments one should improve the effect-background ratio at registration of ^{12}C clusters. On the internal beam it can be done due to maximum possible energy decrease of bombarding ions. This will lead to neutron yield decrease and energy spectrum softening. The experiments on extracted beam could be a radical solution. In this case, one could provide the production of thin layers of ^{114}Ba due to their stopping in gas and the following collection by - helim-jet, electrostatic method or absorption. Consequenly, we will have the narrow energy spectrum of ^{12}C near 17-18 MeV. However, the effective cross-section for cluster yield ($\simeq 10^{-35}$ cm^2) makes high demands to the beam extraction efficiency.

References

1. *Greiner W. et al. In: Treatise on Heavy Ion Science (Plenum Press, New York, ed. Bromley, v.8, p.641, 1989).*
2. *Kadmenskl S.G. et al. In: Proc. Int. Meeting on Nuclear Spectroscopy and Nuclear Structure, Alma-Ata, 1992, Abstract, SPB, Nauka, p.173.*
3. *Poenaru D.N. et al. ADNDT, v.48, p.231, 1991.*
4. *Oganessian Yu.Ts. In: Proc. Int. School-Seminar on Heavy Ion Physics (Alushta, USSR, 1983) D7-83-644, Dubna, JINR, p.55, 1983.*

MEASUREMENTS ON CARBON AND OXYGEN RADIOACTIVITIES OF HEAVY NUCLEI WITH NUCLEAR TRACK DETECTORS

R.Bonetti, C.Chiesa, A.Guglielmetti, R.Matheoud and C.Migliorino
Istituto di Fisica Generale Applicata dell'Universita' di Milano and
INFN, Sezione di Milano, Italy

ABSTRACT

We present results obtained with phosphate glass nuclear track detectors on recently measured exotic decay modes of ^{228}Th and ^{225}Ac via ^{20}O and ^{14}C emission respectively.

I - INTRODUCTION

The recent outburst of experimental results on exotic (cluster) radioactivity is certainly mainly due to the availability to the nuclear physics community of detectors such as those celebrated in the present conference, SSNDTs.
All but two of the 22 cases of cluster decay of heavy nuclei investigated up to now (1) have been studied by means of properly chosen plastic or glass detectors. In fact it is easy to optimize their response to the particular ion being searched for (in the Z range 6-14), while keeping a threshold high enough to reject the background of α particles emitted together with heavy clusters 10^{10}-10^{16} times more frequently.

In our laboratory in Milano we started to investigate heavy cluster radioactivity since 1988 by using mainly the following types of SSNDTs:

1 - the polyethylene terephtalate MELINEX
2 - the phosphate glass PSK-50
3 - the phosphate glass BP-1

We used Melinex film for a long-time, large area experiment with a ^{232}Th source at Gran Sasso underground Laboratory to detect spontaneous fission and Neon radioactivity, which is still in progress; PSK-50 phosphate glass was used in two experiments on ^{232}U (2) and one on ^{233}U (3), while BP-1 glass in the two experiments we will discuss in the present paper, i.e. on ^{228}Th and ^{225}Ac.

BP-1 detector is the glass having the highest sensitivity now available (4). Its response is similar to that of a polycarbonate, being capable of registering tracks due to ^{14}C ions with E $\simeq$ 2 MeV/n.
In respect to polycarbonates it has several advantages such as better transparency after etching, homogeneity and higher tolerability of α background (of the order of 10^{12} α/cm^2).

These features make it an attractive detector in cluster decay experiments. Moreover the above qualities allow, in favourable cases, an image analyzer system to be used for the automated scan of the exposed plates.

II - THE EXPERIMENT $^{228}Th \longrightarrow {}^{20}O + {}^{208}Pb$

This experiment was aimed at filling a gap between Carbon and Neon emissions, which have been observed in several experiments in the last few years (1). When looking at a compilation of cluster radioactivity half lives such as the one of ref. 5, one sees that the most favourable oxygen emitters are thorium isotopes, and, between them, ^{228}Th, which leads, after ^{20}O emission, to the tightly bound ^{208}Pb. The Q value is 44.72 MeV.

Using as a starting point the theoretical estimate (4) for the branching ratio $B = \lambda_{cluster}/\lambda_{\alpha} = 10^{-14}$ we set up an experiment to collect at least a few ^{20}O events.

We obtained a (1.84 ± 0.09) mCi ^{228}Th source from the Chemistry Division of Harwell Laboratories, UK, and covered it with an hemispherical array of BP-1 glass detectors with a radius of 9.75 cm.

We kept the system under vacuum for 134 days.

At the end of the irradiation, the detector received a dose of 2×10^{12} α/cm^2, which previous tests, based on accelerator simulations (4), indicated to be at the upper limit of tolerability of BP-1. We etched the plates in HBF_4, 48%, at 65°C for 40 hours. This etching time was chosen because it allows ^{20}O tracks to develope till the end of the range of the corresponding ions, while being largely insufficient to make ^{14}C tracks (from ^{224}Ra in equilibrium) visible at the same magnification (200 X) used to scan the plates.

Manual scan of the etched plates gave 27 events, which were all attributed to ^{20}O after comparison with a calibration curve obtained with heavy ion beams provided with a Tandem accelerator (Fig. 1).

By considering that the global efficiency was 64% of 2π, we obtained

$$B_{\alpha} = (1.13 \pm 0.20) \times 10^{-13}.$$

This result compares well with the theoretical prediction of the cluster model of Buck and Merchant (6) and reasonably well with that given by the superfluid tunneling model of Barranco and Broglia (7). The cluster model of Blendowske and Walliser (8) and the superasymmetric fission model of Poenaru (5) do worse, although an order of magnitude should be considered a still reasonable error for the present day models. Table I summarizes the above comparisons.

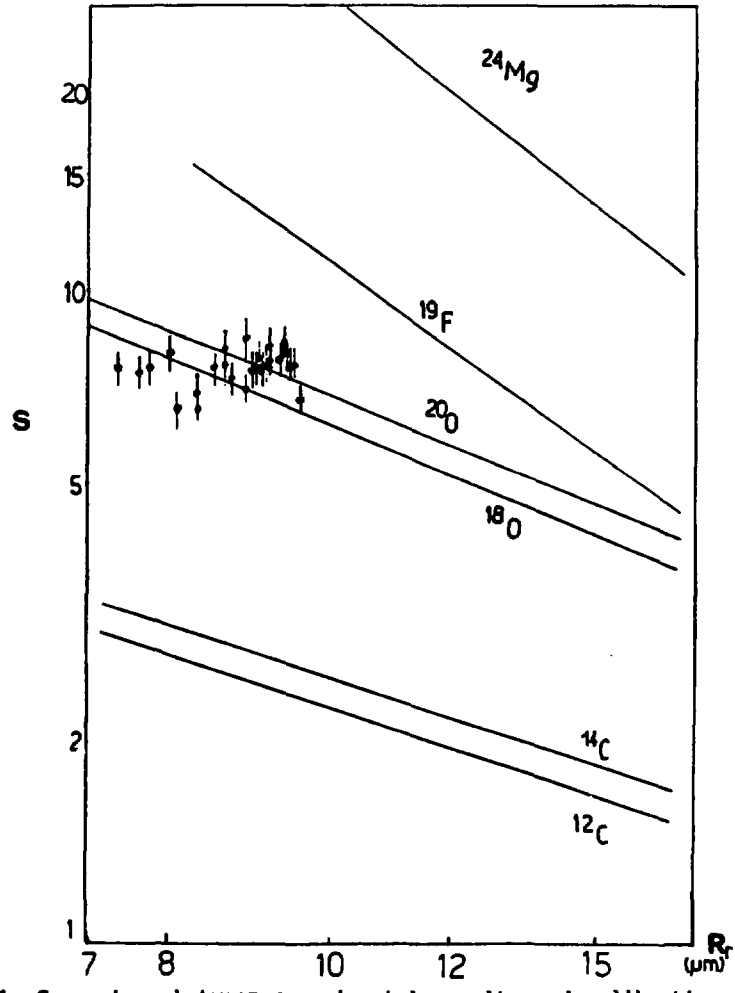

FIGURE 1. Comparison between experimental results and calibration curves for the $^{228}Th \longrightarrow {}^{20}O + {}^{208}Pb$ measurement

TABLE I. Comparison between experimental result and theoretical predictions for the $^{228}Th \longrightarrow {}^{20}O + {}^{208}Pb$ measurement

Present experiment		$(1.1 \pm 0.2) \times 10^{-13}$
ASAFM Poenaru, Sandulescu, Greiner	(5)	1×10^{-14}
Barranco, Broglia, Bertsch, Vigezzi	(7)	1.7×10^{-14}
Blendowske Walliser	(8)	9.0×10^{-15}
Buck Merchant Perez	(6)	6.5×10^{-14}

III - THE EXPERIMENT $^{225}Ac \longrightarrow {}^{14}C + {}^{211}Bi$

All of the four parent nuclei which have been found, up to now, to emit ^{14}C are Radium isotopes (1). In order to study the effect of the odd proton in the initial and final states involved in the radioactive transition, we decided to search for ^{14}C emission in the exotic decay of ^{225}Ac.

The choice of such isotope was motivated by the fact that contrary to the other neighbour and short lived Ac isotopes, which are also predicted to be good Carbon emitters (5), ^{225}Ac can be readily obtained by β decay of its ^{225}Ra and ^{225}Fr isobars. These nuclei are, on turn, easily produced with high intensities at a facility such as Isolde (CERN).

We therefore produced a ^{225}(Fr + Ra) beam of (2.1 ± 0.4) x 10^9 atoms/sec by means of spallation reactions induced by the 600 MeV proton beam of the synchrocyclotron of Cern on a thick ThC_2 target.

After diffusion, ionization and extraction, the Fr + Ra beam was magnetically separated into its isotopic components. After 66.6 hours of irradiation we collected (5 ± 1) x 10^{14} atoms of A = 225 in the focal plane of the magnetic separator of Isolde-2.

We then waited 26.4 days before starting the irradiation of our hemisphere of BP-1 detectors. The above waiting time was chosen from one hand to optimize the build-up of ^{225}Ac from ^{225}Ra and ^{225}Fr, and from the other to minimize a possible contamination of the source by adjacent masses, particularly ^{224}Ra, which could have been collected because of the finite resolution of the separator. We calculated that, during the 26.4 day waiting time, a ^{224}Ra impurity of the (pessimistic) order of 1/100 would have decreased to a such low level, due to its relatively short half life (3.66 days), that it would have given at worst one ^{14}C track in the subsequent irradiation, no matter the exposure time.

The BP-1 plates were covered with 19 ± 1 μm Makrofol foils acting as absorber to improve the signal/noise ratio.

The irradiation, performed in two steps with an interval of 43 days after the first 21 days of exposure, lasted 86 days.

We followed the decay of (1.7 ± 0.3) x 10^{14} ^{225}Ac atoms. The α fluence was 5.9 x 10^{11} α/cm^2. We etched the plates in HBF_4, 48%, at 65°C for 48 hours.

Scanning was accomplished automatically by means of our image analyzer manufactured by Elbek, Siegen (Germany), which was previously calibrated and optimized by using samples irradiated with the same α fluence and with ^{13}C ions delivered by a Tandem accelerator.

In 319.4 cm^2 of the irradiated detectors, we found 305 tracks attributed to ^{14}C. Comparison with calibration is shown in Fig.2.

The resulting branching ratio is $B_\alpha = (7.2 \pm 1.6) \times 10^{-12}$.
This result is compared with theoretical predictions in Table II.

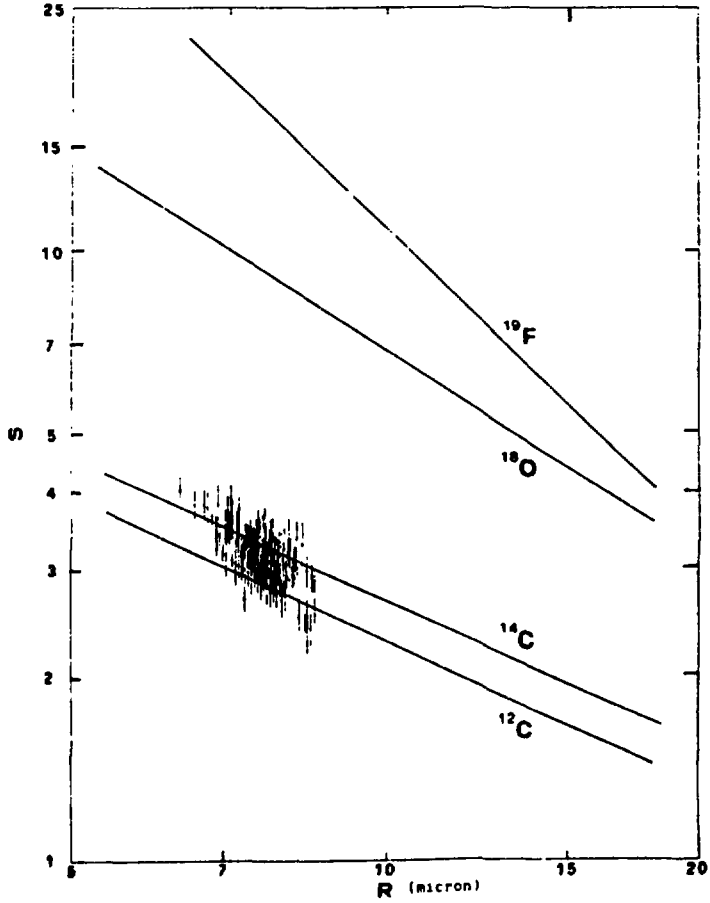

FIGURE 2. Comparison between experimental results and calibration curves for the $^{225}Ac \longrightarrow {}^{14}C + {}^{211}Bi$ measurement

TABLE II. Comparison between experimental result and theoretical predictions for the $^{225}Ac \longrightarrow {}^{14}C + {}^{211}Bi$ measurement

Present experiment		$(7.2 \pm 1.6) \times 10^{-12}$
ASAFM Poenaru, Sandulescu, Greiner	(5)	1.4×10^{-12}
Barranco, Broglia, Bertsch, Vigezzi	(7)	1.7×10^{-12}
Blendowske Walliser	(8)	2.4×10^{-13}
Buck Merchant Perez	(6)	2.3×10^{-13}

The systematic underestimate given by all models can be understood in the frame of nuclear structure effects related to the unpaired odd proton in ^{225}Ac and in ^{211}Bi.

It is found, in short, that Nilsson levels of the odd proton in the ground states of ^{211}Bi and ^{225}Ac are the same due to their different deformations.

This gives rise to a favourite decay to the ground state of the daughter nucleus, a situation which is quite unusual both in α decay and in cluster decay of odd emitters.

The above discussion leads therefore to the conclusion that ^{14}C decay of ^{225}Ac is not "hindered" and should be treated in the same way as transitions from even nuclei, which are always "favoured" by definition.

When the above interpretation is implemented in a model such as the cluster model of Ref.8, one obtains $B_\alpha = 4.5 \times 10^{-12}$ in very good agreement with our result.

IV - EXPERIMENTS IN PROGRESS

We have briefly discussed in Section I the ^{232}Th experiment at Gran Sasso.

Another experiment in progress is the one on ^{231}Pa, aimed at detecting ^{23}F. This experiment was designed in order to reach one order of magnitude higher sensitivity in respect of that of Tretyakova et al.(9), which gave 252 events of ^{24}Ne and a null result for ^{23}F.

Again, BP-1 glass is used under vacuum in hemispherical geometry.

We hope to report soon some interesting results.

REFERENCES

1 - P.B.Price *Ann. Rev. Nucl. Part. Sci. 39* (1989), 19

2 - I - R.Bonetti et al. *Phys. Lett. B 241* (1990), 179
II - R.Bonetti et al. *Phys. Rev. C 44* (1991), 888

3 - P.B.Price et al. *Phys. Rev. C 43* (1991), 1781

4 - R.Bonetti et al. *Nucl.Tracks. Radiat. Meas. 18* (1991), 325

5 - D.N.Poenaru et al. *Publ. NP-54-86* (1986)

6 - B.Buck et al. *Nucl. Phys. A 512* (1990), 483

7 - F.Barranco et al. *Nucl. Phys. A 512* (1990), 253

8 - R.Blendowske et al. *Phys. Rev. Lett. 61* (1988), 1930

9 - S.P.Tretyakova et al. *Proceedings of the 6th International Conference on Nuclear reaction mechanism, Varenna* (1991)

CR-39 CHARGE RESOLUTION AND RELATIVE YIELDS OF NUCLEAR FRAGMENTS PRODUCED IN INTERACTIONS OF 77.1 MeV/NUCLEON ^{20}Ne BEAM WITH WATER

A. Golovchenko, S. Tretyakova, R. Anne, C. Tostain*, G. Tousset*, R. Bimbot**, F. Clapier**, B. Kubica** and C. Borcea****

JINR, Laboratory of Nuclear Reactions, 141980 Dubna
*GANIL, BP 5027, F-14021 Caen, FRANCE
**IPN, BP no. 1, F-91406 Orsay, FRANCE
***IFA, R-76900 Magurele-Bucharest, P.O.Box MG-6, ROMANIA

INTRODUCTION

Recently, special attention is paid to the possible applications of heavy-ion beams for the treatment of cancer (see, for instance, Bimbot, 1991). There are at least two basic advantages of the heavy charged particles use: a superior concentration of the dose deposition and increased relative biological efficiency at a depth of the tumor location (Bimbot, 1991; Kraft et al., 1991). In previous experiments the depth dose profiles were measured and it was found that a definite part of the dose is deposited beyond the Bragg peak of primary particles (Lawrence Berkley Lab., 1977; 1980). This effect associates with the production of nuclear fragments which are lighter and of the same energy per nucleon that as the original particles. At the same energy per nucleon the ions of lower atomic numbers have a greater range in matter and produce a tail of residual ionization beyond the end of the primary beam particles range.

The present study is a part of the research being carried out at the IPN (Orsay, France) and GANIL (Caen, France) aimed at the application of heavy ion beams for radiotherapy of cancer. The solid state nuclear track detector, CR-39, was used to estimate the relative fragment yields due to interactions of 77.1 MeV/nucleon ^{20}Ne GANIL beam with 9.5-mm-thick water (taken as a tissue-equivalent material). By means of chemical etching and semiautomated image analyzer the track diameter spectra at the surfaces of all the plastic sheets were obtained. The detector charge resolution as well as preliminary results on relative yields of fragments with atomic numbers from 3 to 9 beyond the Bragg peak of ^{20}Ne-ions are obtained in this work.

EXPERIMENTAL

The stack composed of 9.5-mm-water-target followed by 750-μm- and 400-μm-thick CR-39 (TASTRAK) plastic sheets interleaved with 100-μm-thick CN-

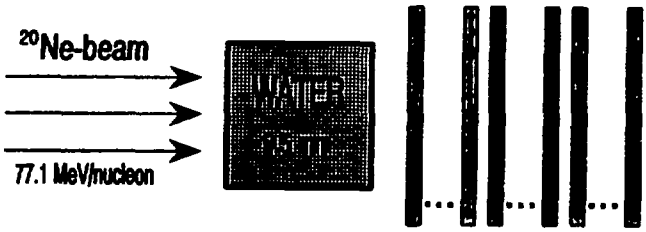

Fig. 1. Beam-target-detector setup

85 (KODAK) sheets was exposed to a 77.1 MeV/nucleon ^{20}Ne GANIL beam at a density of about 7.5×10^3 particles per cm^2 at normal incidence (see Fig. 1). After exposure the CR-39 and CN-85 sheets were etched in 6N NaOH solution for 20 and 30 h at 70°C, and 2 h at 50°C, respectively. A semiautomated image analyzer, MOP-Videoplan (Austria), was employed to measure track diameters at the surfaces of the plastic sheets.

RESULTS

The track diameter spectra at the top surfaces of CR-39 sheets number 1, 2 and 3 along with detector set (see Fig. 1) are presented in Fig. 2(a,b,c) as examples. Similar distributions were obtained for all other sheets of CR-39.

As was mentioned above, the fragment energy per nucleon is about the same as that of the primaries. It leads to a monotonic function between the track diameter and the fragment charge (Price and He, 1991). Moreover, there is a linear relation between the track diameter and the charge for light fragments (in our case, $Z \leq 6$). For heavier fragments (^7N, ^8O, ^9F) the charge resolution is worse because of few reasons. First, there is a nonlinear relation between the track diameter and the fragment charge, as a consequence of which the charge resolution decreases with the increasing charge (Price and He, 1991). Next, we achieved the insufficient statistics in this measurement, especially for ^7N, and the peaks corresponding to ^7N, ^8O and ^9F are superimposed and broadened due to fragment short distances to the range end. Fig. 3(a,b) shows the track diameter spectrum for ^3Li, ^4B, ^5B and ^6C as a result of three measurements (in three different sheets) per track, and the corresponding function of the track diameter versus the fragment charge. It should be noted that the spectra were summed up for the sheets at which the fragment ionization and the respective track diameter are changed insignificantly. The Gaussian fitting procedure, employed to peaks indicated in Fig. 3(a), gives the parameters which lead to a good detector charge resolution (see the Table).

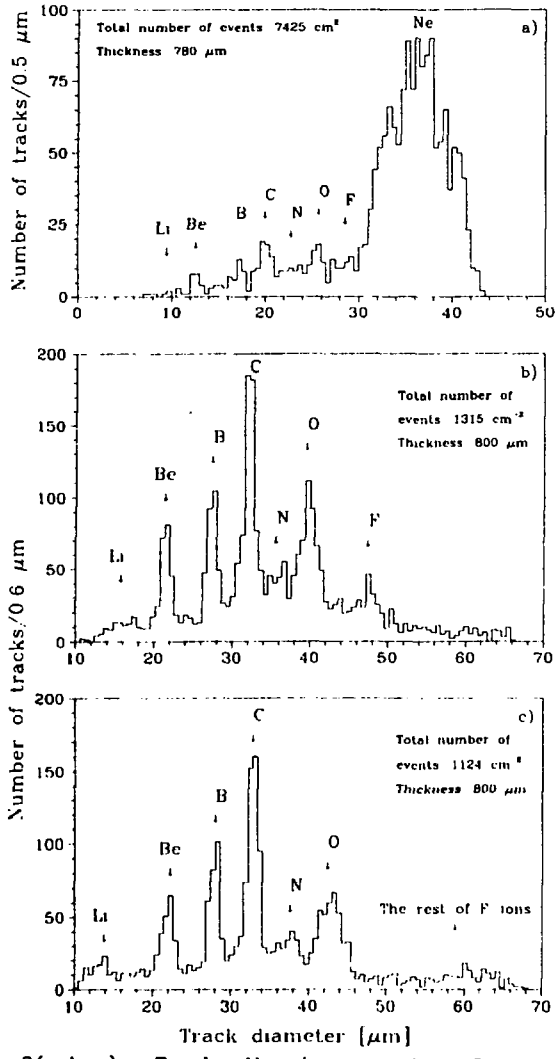

Fig.2(a,b,c). Track diameter spectra for CR-39 sheets number 1(a), 2(b) and 3(c). Sheet number 1 was etched for 20 h in order to avoid the overlapping of large ^{20}Ne etch-pits. Other sheets were etched for 30 h. The total number of measured events and thickness of the sheets is given in the legends. Arrows indicate the fragment charge state.

Thus, one can estimate the relative fragment yields after interactions of ^{20}Ne beam with 9.5-mm-thick water. We used the following expression:

$$Y = \frac{N_F}{N_P},$$

where N_F and N_P are the numbers of fragments of the given charge and of

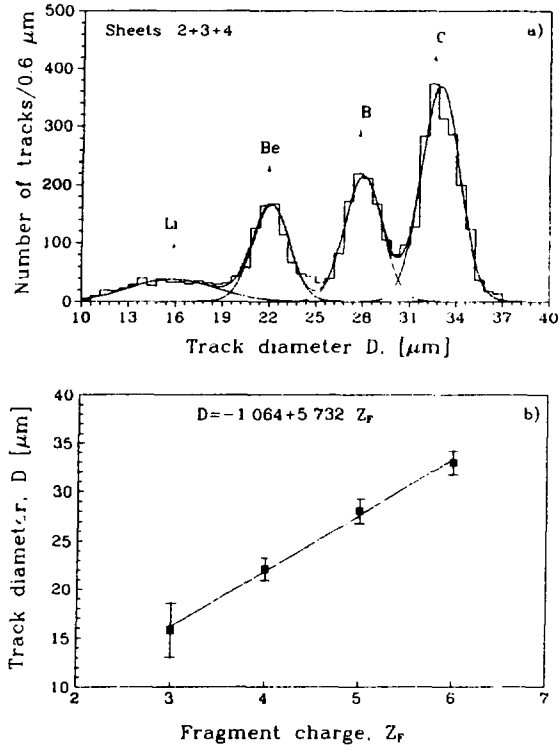

Fig. 3(a, b). The summed up track diameter spectrum (a) and the corresponding function of the track diameter versus the fragment charge (b)

Table. Gaussian fitting parameters and fragment charge resolution

Parameters	Z=3	Z=4	Z=5	Z=6
mean track diameter, D, μm	15.82	22.11	28.04	32.95
standard deviation of track diameter, σ_D, μm	2.75	1.18	1.11	1.23
σ_D/D	0.174	0.053	0.043	0.037
σ_Z	0.48	0.21	0.21	0.21

surviving neon nuclei. Fig. 4 illustrates the relation between the relative yield, Y, and the fragment charge, Z_F. The maximal Y-values are observed for the fragment charge equal to 6 and 8.

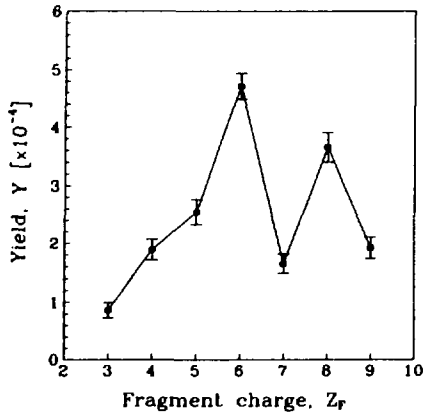

Fig. 4. The relation between the fragment yield and the fragment charge

CONCLUSIONS

The obtained results show the possibility to use a solid state nuclear track detector, namely CR-39, for measuring relative fragment yields and, therefore the absorbed dose due to both primaries and secondaries. We plan further experiments in order to improve the results obtained in this work and to measure ^{20}Ne beam and its secondaries depth dose profile in tissue-equivalent materials. The new irradiation, at skew geometry, with ^{20}Ne-ions of the same energy has been performed at GANIL, using plexiglas and CR-39 itself as the targets.

REFERENCES

Bimbot R. (1991) Biomedical applications of radioactive nuclear beams. Report IPNO-DRE-91-27.

Kraft G., Becher W., Blasche K., Böhne D., Fischer B., Gademann G., Geissel H., Haberer Th., Klabune J., Kraft-Weyrather W., Langenbeck B., Münzenberg G., Ritter S., Rösch W., Schardt D., Stelzer H. and Schwab Th. (1991) The heavy ion therapy project at GSI. Nucl. Tracks 19, 911-914.

Lawrence Berkely Laboratory (1977) Biological and medical research with accelerated heavy ions at the Bevalac 1974-1977. Report 5610.

Lawrence Berkely Laboratory (1980) Biological and medical research with accelerated heavy ions at the Bevalac 1977-1980. Report 11220.

Price P.B. and He Y.D. (1991) Behaviour of nuclear projectile fragments produced in collisions of 14.5 *A* GeV ^{28}Si with Pb and Cu targets. Phys. Rev. C 43, 835-848.

Application of SSNTD for Investigations of Anomalous Cosmic Rays

Grigorov N. L., Zhuravlev D. A., Kondratyeva M. A.,
Panasyuk M. Y., Tretyakova Ch. A., and Tretyakova S. P.*

Research Institute for Nuclear Physics MSU, Moscow
*Joint Institute for Nuclear Research, Dubna

The results of systematic measurements of 4 - 20 MeV/nucleon CNO - group ion fluxes with dielectric solid detectors in the near-earth space during period of Solar minimum activity are presented. From 1985 to 1988 the average composition energy spectra and angular distributions of $Z \geq 6$ ions were measured appximately 10 times per year using small cellulose nitrate detector stacks exposed on COSMOS satellite flights [1]. These three-axis stabilized spacecrafts were placed in nearly circular orbits of 62 - 82 inclination at altitudes from 200 to 400 km. The energy of nuclei was found from the range - energy curves for cellulose nitrate, the procedure of charge identification was a standard one, by L - R technique (see fig. 1). The dip angle and asimuth angle specify a particle's arrival direction in the detector coordinate system. The duration of flights ($\sim$14 days) provides the possibility of discrimination between exposures made in solar quiet periods and those which took place during solar flares.

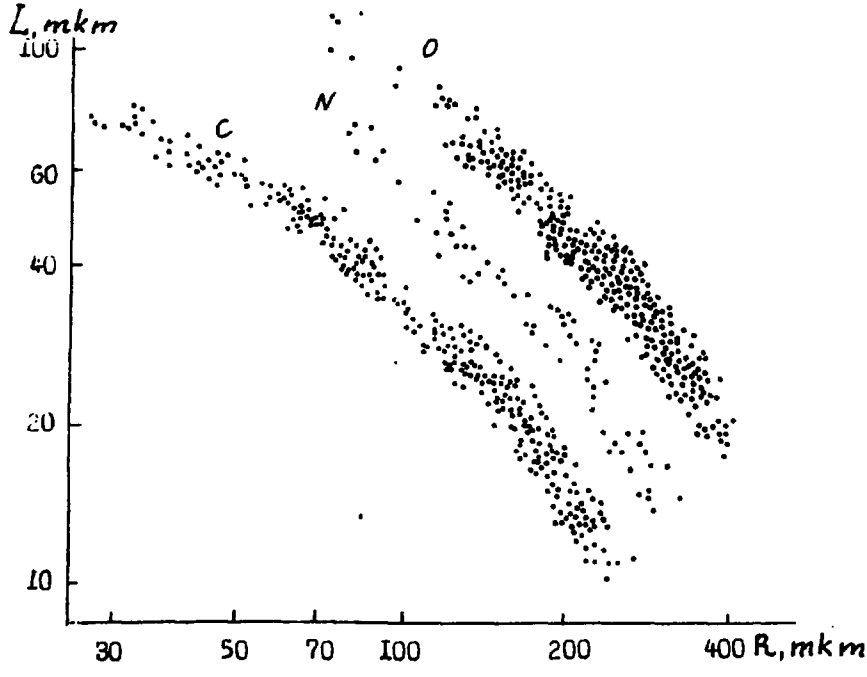

FIG. 1. L - R DEPENDENCE for CNO NUCLEI in CELLULOSE NITRATE

The temporal variation of 10 MeV/nucleon ion flux obtained in 1985 - 1988 is shown in fig. 2 (points), the curve represents the galactic cosmic ray (GCR) intensity variation according to neutron monitor data. [2] From fig. 2 one can see that the temporal variation of ion flux is similar to solar modulation of GCR. But striring difference between ion flux and GCR flux in charge composition and spectral forms made us think that ions belong to anomalous component (AC) of cosmic rays. [3] The latter was discovered in 1973 during previous minimum of solar activity. According to theory for origin of AC [4] anomalous ions are partly ionized atoms and the most clear test to confirm the theory is determination of the charge state Q of anoma-

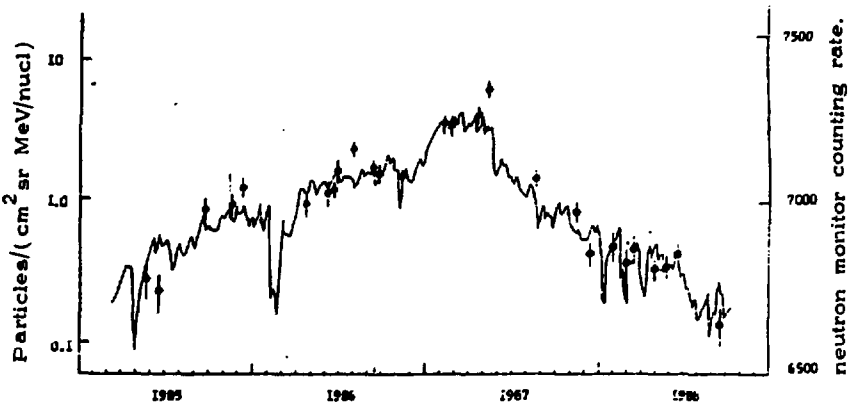

FIG. 2. TEMPORAL VARIATION of ION FLUX DURING SOLAR QUIET PERIODS

lous ions. Up to data, there are no direct measurements of ionic charge states because of technical difficulties. That's why there have been numerous attempts to determine Q by indirect methods, particularly, to infer Q from the transmission of the AC through the Earth's magnetic field. The idea based on the difference in rigidities of ions, which have the same energy per nucleon, but different charge state (rigitity $\xi = pc/Q$ where p - impuls of a particle and Q - its sharge). We used our experimental data to determine the anomalous oxygen charge state. In fig. 3 the intensity of anomalous oxygen ions measured in interplanetary space on board of American spacecraft IMP - 8 [5] during solar quiet period are shown. The intensity of oxygen ions obtained in Cosmos exposures during the same period and recalculated outside magnetosphere using a grid of cut off rigidities for Q = +8 are shown in fig. 3 too (points and crosses respectively). It is seen from fig. 3 that the ion intensity measured in interplanetary space is consistent with that one recalculated from Cosmos data if the charge state of oxygen ions is equil to +1.

When determing the charge state we used not all the particles registered by detectors but only those ones arrived from around the zenith directions and marked by hatch in fig. 4a. In the figure the angular distribution is highly anisotropic while the corresponding angular distribution of solar ions (ordinary, not anomalous ions)

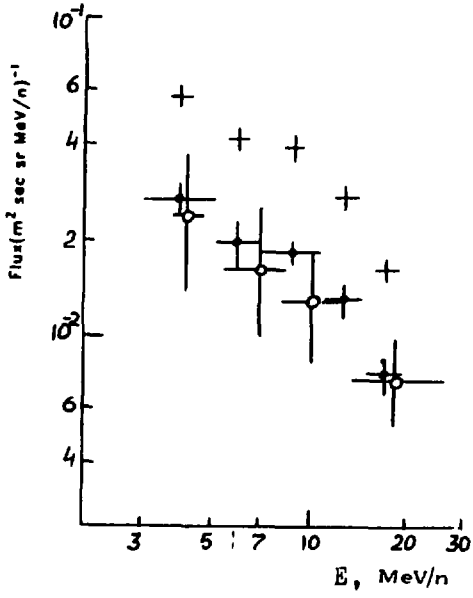

FIG. 3. OXYGEN ION INTENSITY OUTSIDE the MAGNITOSPHERE in JUNE - SEPT. 1986

○ I M P - 8 DATA

• O^{+1}

: O^{+8} } COSMOS DATA

is quite isotropic (see fig. 4a). An anisotropy of angular distribution is a characteristic feature of anomalous ions. It can be explained if one takes into account that anomalous ions are singly ionized and can be trapped by geomagnetic field [6]. From analysis of Cosmos data we have drawn a conclusion that only a small part of detected ions arrives directly from interplanetary space, the rest ions

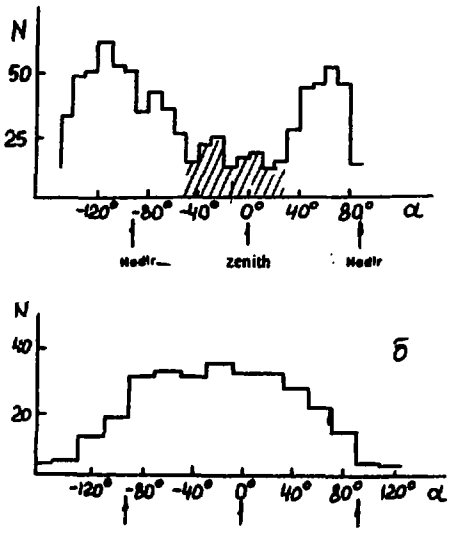

FIG. 4. ANGULAR DISTRIBUTIONS of ANOMALOUS IONS (a) and SOLAR PARTICLES (b)

(particles from directions near horison in fig. 4a) fall onto detectors from magnitosphere being trapped by Earth's magnetic field [7]. Monte - Carlo simulations of ion angular distributions in Cosmos experiments made by american colleagues [8] confirm our suggestion that trapped anomalous ions are registered near mirror points in the South Atlantic Anomaly [9].

REFERENCES

[1]. Grigorov N. L. et al, Proc. 21st ICRC, 1990, 6, 176-179 .

[2]. Solar Geoph. Data

[3]. Grigorov N. L., et al, 1988, MSU Preprint 88 - 48/69.

[4]. Fisk L. A. et al, 1974 ApY, 190, L35.

[5]. Cummings A. C. et al, Proc. 20th ICRC, 1987, 3, 421.

[6]. Blake J. B. et al, Proc. 15th ICRC, 1977, 2, 341.

[7]. Grigorov N. L., et al, Geomag. ang Aeron., 1989, 29, 1018.

[8]. Grigorov N. L., et al, Geoph. Res., 1991, 18, 1959.

[9] Grigorov N. L., et al, Proc. 21st ICRC, 1990, 6, 176.

PRELIMINARY RESULTS FOR THE ULTRA HEAVY COSMIC RAY EXPERIMENT ON THE LDEF MISSION

R.Keegan, D. O'Sullivan, A.Thompson and J.Bosch
Dublin Institute for Advanced Studies (DIAS), Ireland
Phone: +353-1-774321, Fax: +353-1-682603

K.-P. Wenzel and F. Jansen
Space Science Dept of ESA, ESTEC, Noordwijk, The Netherlands
Phone:+31-1719-83573, Fax: +31-1719-84698

C. Domingo
Universitat Autònoma de Barcelona, Spain
Phone: +34-3-581-1530, Fax: +34-3-581-2155

ABSTRACT

The Ultra Heavy Cosmic Ray Experiment (UHCRE) is based on a modular array of 192 side-viewing solid state nuclear track detector stacks. These stacks were mounted in sets of four in 48 pressure vessels employing sixteen peripheral LDEF trays. The extended duration of the LDEF mission has resulted in a greatly enhanced scientific yield from the UHCRE. The geometry factor for high energy cosmic ray nuclei, allowing for Earth shadowing, was 30 m^2sr, giving a total exposure factor of 170 m^2sr y at an orbital inclination of 28.4 degrees. Scanning results indicate that about 3000 cosmic ray nuclei in the charge region with Z >65 have been collected. This sample is more than ten times the current world data in the field (taken to be the data set from the HEAO-3 mission plus that from the Ariel-6 mission) and is sufficient to provide the world's first statistically significant sample of actinide (Z > 88) cosmic rays.

Results to date are presented including details of a sample of ultra heavy cosmic ray nuclei, analysis of pre-flight and post-flight calibration events and details of track response in the context of detector temperature history. The integrated effect of all temperature and age related latent track variations cause a maximum charge shift of ±0.8e for uranium and ± 0.6e for the platinum-lead group. The precision of charge assignment as a function of energy is derived and evidence for remarkably good charge resolution achieved in the UHCRE is considered. Astrophysical implications of the UHCRE charge spectrum are discussed.

INTRODUCTION

Prior to LDEF there were only two spacecraft which carried experiments dedicated to the investigation of ultra heavy nuclei. HEAO-3 and Ariel 6 were launched in 1979 and employed electronic detectors of geometric factors 5 m^2sr and 2 m^2sr respectively. The combined sample from both missions with $Z \geq 65$ comprises approximately 300 events, and the entire sample of actinides ($Z \geq 88$) is only 3.

The experiment on LDEF which was dedicated to the study of ultra heavy (UH) nuclei consists of an extensive array of primarily lexan polycarbonate solid state nuclear track detectors, of geometric factor 30 m^2sr, which were mounted within cylindrical aluminium pressure vessels in 16 LDEF experiment trays.

DESCRIPTION OF UHCRE

Since the primary objective of the UHCRE experiment was to study ultra heavy cosmic ray nuclei of $Z > 65$ and the geomagnetic cut-off was $\sim$ 1 GeV/N, the main detector material chosen was lexan polycarbonate.

Each stack consists of a sandwich of many layers of lexan (approx 70 plates) together with several sheets of lead interleaved. The lead sheets act both as electron strippers and velocity degraders and were chosen because of their low cross section for nuclear interactions.

The stacks are 20.5 cm × 26.0 cm in area and are approximately 5 g cm^{-2} thick. All 192 stacks were mounted in sets of four within cylindrical Eccofoam moulds which were then inserted into aluminium pressure vessels (48 in total).

All cylinders, except one, were pressurised to 1.0 bar with a dry oxygen-nitrogen-helium mixture in the ratio of 20:70:10. Three pressurised vessels were mounted on each experiment tray which in turn was mounted on the LDEF framework.

PRESENT UHCRE STATUS

Following an initial scan using wide field Nikon zoom scanning microscopes, it was decided to employ the ammonia scanning technique for event location. This technique, which involves long term etching (of up to 21 days) in 6.25N NaOH at 40°C was undertaken on 2 plates situated approximately at $\frac{1}{3}$ and $\frac{2}{3}$ of a stack depth and correlations between the etched cylinders were sought.

Current scanning gives approximately 15 cosmic ray events per stack bringing the expected number of cosmic ray nuclei recorded to approximately 2800 nuclei.

Having located the UH candidates alternate plates from a set of 20 plates at the top of each stack and a similar set from the bottom of each stack were etched for 5 days at 40°C. The remaining plates in each set were kept for further analysis if required.

Etch cone measurements are carried out on Leitz Ortholux microscopes which have 10x and 12.5x eyepieces and 100x oil immersion objectives. From these cone measurements, both track etch rate (V_t) and bulk etch rate (V_g) are calculated and the reduced etch rate $\left(S = \frac{V_t}{V_g}\right)$ is then determined.

To date approximately 65 cosmic ray events have been measured and processed. Charge identification is based upon the determination of the fractional etch rate gradient, (Fowler et al., 1976), defined as

$$G = \frac{1}{S}\frac{dS}{dx},$$

where S is the reduced etch rate and x is the path length, and on the effective reduced etch rate (S_{eff}). The relevant data for a given event is reduced to one point which may be plotted on an $S_{eff} - G$ plot as shown in Fig. 1. All cosmic ray events to date are shown in Fig. 1, together with the location of the Z =80, 72, and 62 preliminary calibration curves which are based on the assumed relation

$$S = g(REL)^h,$$

where REL is the restricted energy loss rate and g and h are determined from calibration data. The preliminary UHCRE status report (O'Sullivan et al., 1991) was

based on calibration using U nuclei. The present work includes calibration with 1150 MeV/N Au nuclei also. Calibration studies will be extended over the next few months.

CONCLUSIONS AND DISCUSSION

A post flight thermal analysis on the UHCRE was published in March 1992 by Lockheed Engineering and Sciences Co. The results of the thermal analysis showed that the tray located at position C6 had the widest temperature cycle of 28.8°C with a maximum of −2.3°C and a minimum of −31.1°C. The tray position E10 had the smallest temperature cycle of 11.9°C with a temperature range of −26.0°C to −14.2°C. The analysis also showed that the maximum detector stack thermal gradient was 0.15°C per stack. Hence we expect virtually no difference in sensitivity between the top and bottom of a given stack.

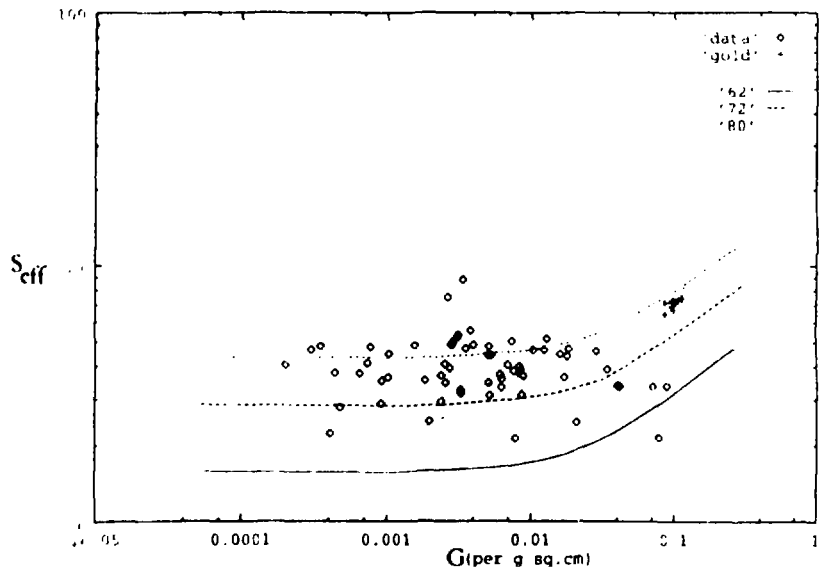

Fig. An S_{eff} versus G plot showing all cosmic ray events to date together with some gold calibration events. The preliminary locations of the calibration curves are shown for charges Z = 80, 72 and 62

Uranium calibration work indicates that the UHCRE detectors have undergone virtually no change in sensitivity or loss of charge resolution over the 5.8 year exposure period. The initial observations (see Fig.) show a dramatic decrease in flux at approximately charge 83 with most of the events falling into the region $70 \leq Z \leq 83$. The distribution of points indicates a concentration of events in the platinum–lead region. It is also apparent that two actinide cosmic ray nuclei have been located at this stage of the analysis.

Further measuring and analysis is continuing and it is hoped that a set of data equivalent in size to the present world sample will be available by the end of 1993. In view of the excellent quality of the UHCRE data it is hoped that we will be able to distinguish between different cosmic ray source and propagation models when a sufficient sample of nuclei has been analysed. For instance, attempts to describe the abundances of actinides and anti-protons in the cosmic radiation by means of the Leaky Box model have not been satisfactory. Eventually, results from the Dublin–ESTEC experiment will be compared with the predictions of a diffusion model which will be developed to examine the propagation of these particles.

ACKNOWLEDGEMENTS

The authors wish to express their thanks to the LDEF Office Project Staff, in particular J.L. Jones and W.H. Kinard, for their excellent managerial support since LDEF experiment selection. Furthermore they wish to acknowledge the support of many colleagues in ESTEC during hardware development, testing, integration and during de-integration activities. They are indebted to the LBL Bevalac staff, in particular H. Crawford, for continued technical support and assistance with numerous heavy ion exposures for UHCRE calibration and detector development. They wish to express their appreciation to Geraldine Broderick, Gerry Daly, Eileen Flood, Anne Grace, Susan Ledwidge and Hilary O'Donnell for SSNTD processing, measurement and data reduction. Part of this work was supported by the Spanish CICYT.

REFERENCES

1. Thompson, A., D. O'Sullivan, K.-P. Wenzel, V. Domingo, C. Domingo, J. Daly, A. Smit. Proc. 21st ICRC (1990) 4, 441, Adelaide.

2. Binns W.R., T.L. Garrard, P.S. Gibner, M.H. Israel, M.P. Kertzmann, J. Klarmann, P.J. Newport, E.C. Stone and C.J. Waddington. The Astrophysical Journal, (1989) **346**, 997-1009

3. Fowler P.H., R.N.F. Walker, M.R.W. Masheder, R.T. Moses, A. Worley and A.M. Gay. The Astrophysical Journal, (1987) **314**, 739-746.

4. Sampair T.R., W.M. Berrios. Post Flight Thermal Analysis, (1992) A0178-UHCRE

5. O'Sullivan D., A. Thompson, K.-P. Wenzel, C. Domingo, J. Bosch, R. Keegan and A. Smit. LDEF–69 Months in Space, First Post-Retrieval Symposium, (1991), 367-375.

6. Fowler P.H., C. Alexander, V.M. Clapham, D.C. Henshaw, C O'Ceallaigh, D. O'Sullivan, A. Thompson. High Resolution Study of Nucleonic Cosmic Rays with Z >31. Proc. 9th Int. Conf. on SSNTD, Munich, 1976, 1007.

ENERGY SPECTRA OF LOW-ENERGY HEAVY NUCLEI INSIDE THE EARTH'S MAGNETOSPHERE ON THE ORBITAL STATIONS

Yu.F.Gagarin, V.A.Dergachev

A.F.Ioffe Physico-Technical Institute, Russian Academy of Sciences, 194021 St.Petersburg, Russia

New data on energy spectra of light and heavy nuclei at energy of ~ 10-200 MeV/nucleon inside the Earth's magnetosphere were obtained in recent times. An interpretation of the results in this energy range is complicated by some factors: a presence of different nuclear sources (solar flares, galactic cosmic rays(GCR), anomalous components, trapped particles et al.), intensity changes of nucleus sources during the solar cycle or cycles, energy spectrum deformation in geomagnetic field. At the same time these factors allow us to obtain an additional information about analysed nuclei. For example, geomagnetic field separates particles at different ionization states. In such case, the comparison of proton and nucleus fluxes inside and outside the Earth's magnetosphere at various perturbations of geomagnetic field permits to make some new qualitative and, may be, quantitative conclusions.

During some years we detected low-energy heavy nuclei with charges $z \geq 20$-28 in lavsan (polyethyleneterepthalate) chambers on the outer surface of orbital stations. Exposure time is for one or two years. Counting area of detector is ~ 300-600 cm^2. As a result, there is possibility to obtain a large statistics for GCR and detect single low-energy nuclei with charges from 30 to 90. It should be noted that all solar nuclear flares are integrated in such prolonged experiments. But the most intense flares (one or two during the solar cycle) are able to generate about ~ 80-95% of common nucleus flux at minimal energies in exposition and they may be analysed.

A nuclear charge was determined by LR-technique. In *Fig.* 1 LR-diagrams are given at different track angles of inclinations with respect to layer plane: a) θ = 52-57° and b) θ = 20-23°. The nucleus charge was estimated according to formula [1]:

$$z(LR) = 1.325 \cdot (\theta^\circ)^{0.1} \cdot 1/N \cdot \sum_{i=1}^{N} L_i^{0.159} \cdot R_i^{0.302},$$

where N is a number of track cones and angle correction for cone length after ultraviolet irradiation of layers takes into account.

Fig. 1.

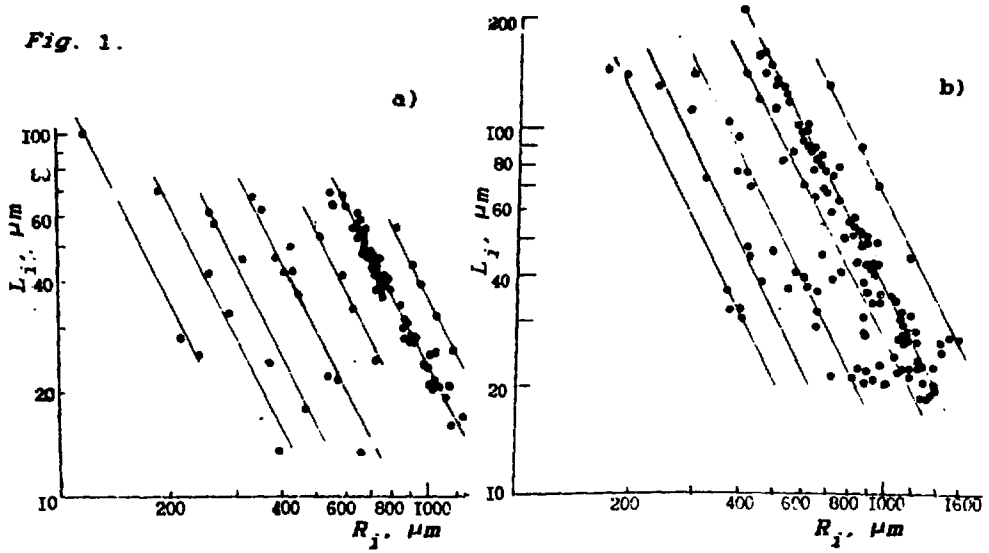

Fig. 2 shows preliminary estimates of the integral flux densities of nuclei with charge ⩾ 20 in three exposures at altitudes of ~ 300–350 km and orbital inclination of ~ 51.6° with respect to the equatorial plane: 1 – Salyut-6, 29 July 1978 to 15 August 1989; 2 – Salyut-7, 8 August 1984 to 4 August 1985; 3 – Mir, 26 February 1988 to 11 January 1990. The thermal shields on the chambers had thicknesses ~ 27, ~ 6 and ~ 8.5 mg·cm^{-2} in exposures 1, 2 and 3, respectively.

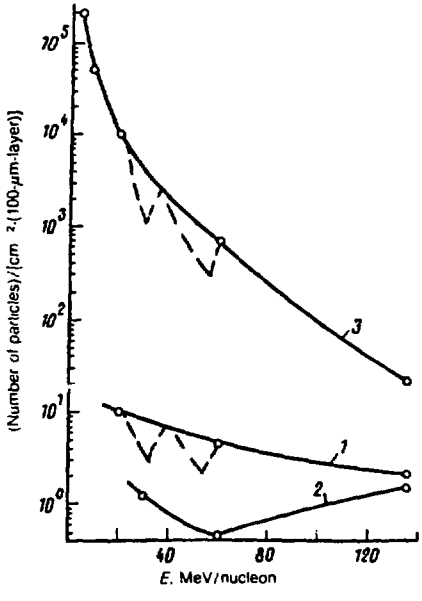

Fig. 2.

Detailed study of spectrum in the first exposition in the energy range of ~ 100–200 MeV/nucleon shows the fluxes of Sc – Cr nuclei are compatible with those of iron. The ratio (Sc–Cr)/Fe is ~ 0.7–0.9 [2]. This value agrees with that ~ 1 in energy range ~ 30 – 280 MeV/nucleon inside the magnetosphere [3] and differs from that ~ 0.4–0.5 outside the magnetosphere [4]. This difference may take place when the effective charge q (q is ratio of an ion charge to a nucleus charge) of (Sc – Cr)'s group $q_{Sc-Cr} < q_{Fe}$. (Up till now it was suggested for GCR $q_{GCR} \equiv 1$, that is GCR are

completely ionized). In this case Sc - Cr nuclei will penetrate to station orbit in the greater range of high latitudes than Fe-nuclei. As a result, relation (Sc-Cr)/Fe which was measured inside magnetosphere must increase.

Observations of heavy nuclei due to the solar flares in the energy range 5-50 MeV/nucleon (below geomagnetic threshold of ~ 50 MeV/nucleon) at the orbit in our experiments (*Fig.* 2) show that solar particles at low energies are not fully ionized. Therefore there is an opportunity to detect solar particle events at the stations with the orbital inclination of ~ 52° and to study the most powerful solar events in three expositions: 23 August 1978, 24 April 1985, 29 September 1989 and 19-26 October 1989.

Comparison of energy spectra in our second experiment and in Space Shuttle Mission flight on 1984, October 5-13 in a 57° inclination orbit [5] shows an agreement of GCR fluxes at energy of ~ 100-200 MeV/nucleon. Simultaneously, in paper [5] a minimum in energy spectrum is observed at the lesser energy in comparison with our data. This effect is due to the greater orbit inclination of the Shuttle - ~ 57°.

The analysis of the observed solar proton fluxes on the orbit allows to come to some interesting conclusions for expected nucleus energy spectra. Indeed, protons at energy range of 39-82 MeV (it corresponded to energy of ~ 20-40 MeV/nuclen for nuclei) from solar event on 1989, September 29 below geomagnetic threshold (curve 2, *Fig.*3) were not detected on the Mir orbit [6] for quiet gecmagnetic conditions. Change of radiation doze (curve 1, *Fig.* 3) is insignificant. And protons from solar flare on 1989, October 19

Fig. 3

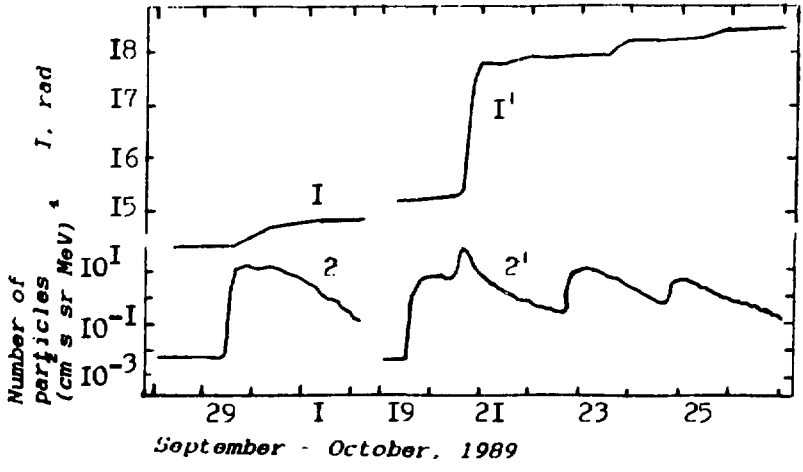

(curve 2', *Fig.* 3) were effectively detected only a day after solar event's onset (curve 1', *Fig.* 3) at the moment of great geomagnetic storm. Therefore, we have possibility to observe a fine structure in detailed energy spectra of heavy nuclei in experiment. Namely, one or two humps corresponding to one or two thresholds in different geomagnetic conditions. These humps suggested are shown in *Fig.* 2 (dashed curves) for the first and third expositions. In the second experiment the threshold in energy spectrum of 50-60 MeV/nucleon is observed.

Conclusion. Studies of charge and energy spectra of heavy nuclei at low energy in long duration experiments inside the magnetosphere and comparison with nucleus fluxes outside the magnetosphere will permit to establish charge states of solar and Galaxy heavy particles at energies of 10-200 MeV/nucleon and determine real geomagnetic thresholds for nuclei in different conditions.

REFERENCES

1. Gagarin Yu.F, Dvoryanchikov Ya. V., Lyagushin V.I. et al., Preprint PTI AN SSSR - 1430, Leningrad, 1990.

2. Gagarin Yu.F, Dvoryanchikov Ya. V., Lyagushin V.I. et al., 1990, 21 ICRC, Conf.Papers, Adelaide, 3, 11.

Gagarin Yu.F, Dvoryanchikov Ya. V., Dergachev V.A. et al., 1992, Pis'ma Zh. Eksp.Teor. Fiz., 55, 95.

3. Biswas S., Durgaprasad N., Mitra B. et al., 1990, Ap.J., 359, L5.

4. Fernando P., Lal N., Mc Donald F.B., Webber W.C., 1990, 21 ICRC, Conf. Papers, 3, 40

5. Adams J.N.,Jr., Beahm L.P., Tylka A.J., 1991, Ap. J., 377, 292.

6. Tverskaya L.V., Telttsov M.V., Shumshurov V.I., 1991, Geomagnetizm i Aeronomia, 31, 928.

PARAMETERS AND RETAINTION OF VH-NUCLEI TRACKS DUE TO PRE-ACCRETION IRRADIATION IN THE ORDINARY CHONDRITE OLIVINE CRYSTALS

L.L.Kashkarov

Vernadsky Institute of Geochemistry and Analytical Chemistry, Russian Academy of Sciences, Moscow

Fossil track investigation of the silicate minerals of the ordinary chondrites (OC), enriched no in the solar type inert gases [1], indicates in the great part of meteorite samples under investigation the presence of a small portion (up to some per cent) of crystals, track characteristics for which can be explained only from the position of their irradiation by the low-energy ($E \leq 100$ MeV/nucleon) VH - nuclei group ($24 < Z < 28$) of cosmic rays that was occurred at the conditions of a weak shielding [2]. In these cases two basic quantitative criteria must be taken into consideration: the presence of the crystals with the specific track density gradient ($\Delta\rho/\Delta X$) and crystals with the comparatively high track density (ρ) the value of which essentially exceeds the contribution from the galactic cosmic ray VH-nucley [3]. However the number of mineral grains of the investigated OC samples revealed that marked $\Delta\rho/\Delta X$-values are extremely low. From the other side the different parts of the individual crystals have the ρ-values that are not ten-fold higher than the galactic cosmic rays VH-nuclei track densities [4]. At the same time the numerous track investigations of the lunar regolith matter [5] indicated that for the more complete knowledge of the radiation history and for estimation of the effective exposure degree it is very useful to measure the statistical track density distribution for all the crystals of each sample under investigation. Corresponding parameters ρ_{MED}, ρ_a, ρ_{MIN}, ρ_{MAX}, N_H/N, etc., are measured in these instances.

With a view to further more detailed investigation of the pre-accretion radiation history of the OC matter it was particularly important to measure the track parameters in the olivine grains separated from the micro-porphiritic chondrules of these meteorites. The main attention was given to elucidation of the two questions: (1) whether or not there exist the difference between the ρ -values for the crystals representing each individual chondrule and (2) measurement and obtaining of the quantitative statistical track parameters for these objects as it is possible for any chondrules.

Chondrules of the used type with micro-porphiritic structure as it was obtained from the model experiments [6], can be formed in the high-temperature, short-time processes which are not accompanied by the total melting of the initial matter inoluding silicate crystals. In these cases the total track annealing in the olivine grains was not necessarily occurred that gives the possibility to retain the trace of the pre-accretion cosmic ray irradiation of the individual crystals.

We have studied the track parameters in the olivine grains separated from the chondrules of the nonequilibrated OC Tieschitz H3.6. Grains (sizes of 50-100 μm) were mounted in epoxide resin, polished and etched in the boiling WN solution [7] during 6-24 hours. The observation and measurements of the traok parameters were performed by an optical mioroscope technique. Induced by the spontanous fission fragments of ^{252}Cf tracks and special annea-

ling treatments were used for the identification and checking of the observed fossil tracks.

The results of the track parameters measurements in six chondrules, representing all typical cases of the characteristic ρ-distribution observed in individual chondrules (see the Figure), are given in the Table.

Table. Track parameters in the olivine grains of the micro-porphyritic chondrules of the OC Tieschitz H3.6

Chondrule N	Number of search crystal	Track densities, $\times 10^6$ cm^{-2} ρ_{MIN}	ρ_{MAX}	$\bar{\rho}$
1	6	2.2+-0.4	4.5+-0.7	3.3+-0.2
2	5	1.5 0.3	4.3 0.6	2.8 0.2
3	6	0.8 0.3	3.8 0.4	2.3 0.2
4	5	0.7 0.2	1.4 0.3	1.0 0.1
5	5	1.0 0.3	6.1 0.8	3.5 0.2
6	7	0.9 0.2	5.8 0.6	1.7 0.1

Based on these data we can register: (1) In chondrite sample under investigation the chondrules were observed with very different track density distribution characteristics. (2) The difference of ρ_{MIN} and ρ_{MAX} values in individual hondrules is beyond the scope of the measured statistical errors. (3) The mean values $\bar{\rho}$ obtained for each chondrule, also vary in the interval, which exceeds the standard error deviation. (4) At least six (A...F, see fig.) specific cases for the track density distri-

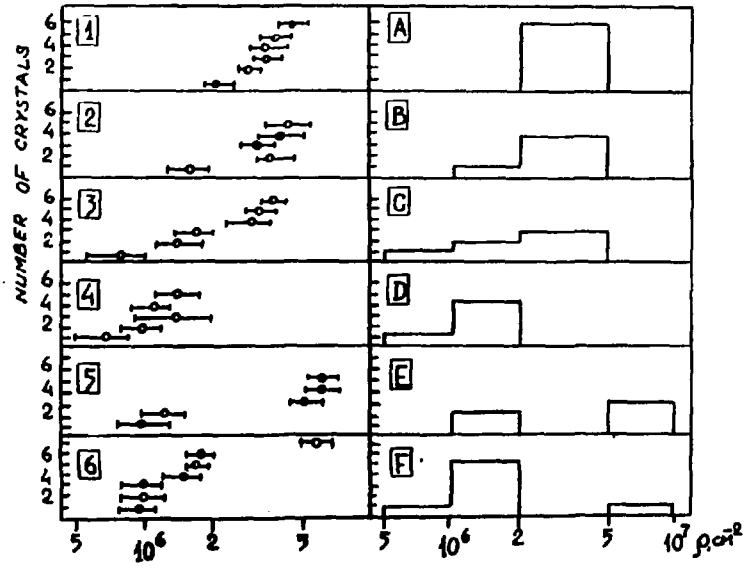

Fig. Track density distribution of the olivine crystals of the individual chondrules of the Tieschits H3.6 meteorite

bution can be indicated: the olivine crystals incoming in the individual chondrules, conserved almost completely (groups A and B) or partially (groups C, E and F) the pre-compaction exposure traces of VH-nuclei cosmic ray. At that time the crystals in group D of chondrules either underment more intensive thermal track annealing or these chondrules consist of nonirradiated crystals only.

For the examination of the chemical track etching efficiency in each olivine crystal especially in those with ρ_{MIN} values, a series of multiple control etching was performed up to four times by 6 hours in WN-conditions. Before it the crystals were irradiated (with additional surface polishing or without it) by the ^{252}Cf source. The obtained results indicate that the fission-induced track density values in about 90 per sent of all crystals irradiated by this manner fall inside 2σ- statistical interval.

In summary, it can be noticed that the present work suggests that the history of irradiation of the individual olivine grains was started before their incorporation into the micro-porphiritic chondrules, that was possible in the low-temperature accretion processes only [4]. Obviously the individual chondrule matter in their formation processes was experienced a different degree of the main thermal influence that did not smooth out during the whole subsequent meteorite history.

References. [1] Kashkarov L.L., Genaeva L.I., Kalinina G.V., Lavrukhina A.K. Abstr.18th Lunar Planet. Sci. Conf., 1987, 479. [2] Kashkarov L.L.-Izv.AN SSSR, ser.phys., 1988, v.52, N12,2321. [3] Kashkarov L.L., Genaeva L.I., Kalinina G.V., Lavrukhina A.K. -Meteoritika, N47, 1988, 113. [4] Kashkarov L.L., Kalinina G.V.- Abstr. 20th Lunar Planet. Sci. Conf., 1989, 504. [5] Arrhenius G. et al.- Lunar Sci.Conf, 2nd, 1971, 2583. [6] Kashkarov L.L., Fisenko A.V.- Abstr. 23th Lunar Planet. Sci.Conf., 1992, 661. [7] Krishnaswami S. et al.- Science, 1971, v.174, 287.

TRACK AND THERMOLUMINESCENSE STUDIES OF KAIDUN METEORITE GLASSES

Kashkarov L.L., and Korotkova N.N. Vernadsky Institute Geochem. and Analyt. Chem., Russian Acad. of Sci., Moscow Russia

Study of transparent glasses of Kaidun carbonaceous chondrite [1] allowed to get a preliminary information about the characteristics of radiation-thermal environment during the meteorite parent body formation [2,3]. The heating temperatures of carbonaceous substance during this unique breccia formation did not exceed 250-300°C [1]. According to our preliminary data [3] the track densities in the Kaidun glasses do not correlate with total intensity of natural TL (TL_{nat}). Now we present the results of track and TL studies of seven indi dual glass inclusions (GI) picked from Kaidun carbonaceous matrix as well as the results of U concentration (Cu) determination in 40 individual glasses. We have measured the Cu values in order to estimate the contribution of the fragments of spontaneous and induced fission of U and extinct transuranium elements (^{244}Pu, etc.) into observed natural track densities in each of glass samples under study.

Seven coarse- and oval-shaped GI samples were studied. All the samples are the homogeneous isotropic glasses apart from those having the fine-grained structure (8.1 and 8.2) in which tracks could not been seen. The strong difference of track diameter values (D) has been revealed among the GI samples of different chemical compositions under the same etching regime (20% HF, 20°C, 20 s). The examples of some etched GI samples are given in fig.1 a, b, c. Microphotograph "d" shows the artificial ^{252}Cf fission fragment tracks, the same etching. The rather high track densities (ρ) with uniform distributions were found in all GIs (Table 1). The highest ρ value in the GI 10.4.2 may be explained by unequal contributions of tracks due to cosmic ray VH-nuclei and spontaneous and induced fission fragments of U (and possible ^{244}Pu). The latter source contribution may be estimated by means of Cu measurement in the same glass samples.

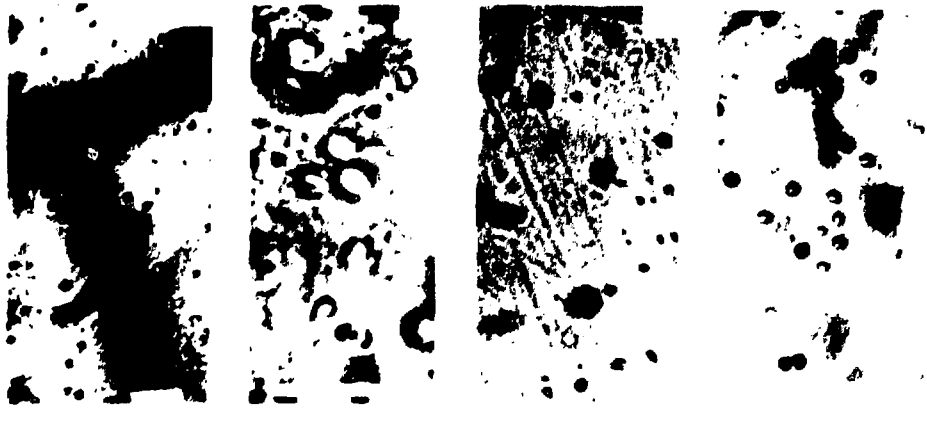

Fig. 1. Photomicrographs of natural tracks (a,b,c) and artificial ^{252}Cf fission fragment tracks (d) in some Kaidun glasses (etching in 20% HF, 20°C, 20 s). Indicated scale 20 μm

Table 1. Track and TL parameters of some Kaidun chondrite glasses

Sample, group*	Mass, mg	Track density¤, x10⁵ sm⁻²	TL - parameters (TL/m), rel. unit. Artificial TL (x10)#				
			TL_{LT}			TL_{HT}	
			TL	T_{peak}°C	$\Delta T_{1/2}$	TL	T_{peak}°C
8.1	0.20	-	6.1	183	101	1.6	314
8.2	0.10	-	36.3	170	76	6.8	340
4.1.I	0.30	6.5	6.6	170	130	1.6	302
4.2.III	0.05	33.0	48.2	170	125	20.4	290
4.3,IV	0.05	9.5	34.2	170	136	8.2	290
4.4,III	0.15	5.4	9.8	183	107	1.6	290
4.5,I	0.20	5.2	55.7	183	142	16.5	290

* Or normative content (mass %): Igr. - 2.0; II - 1.2; III - 2.4; IV - not determ. [2]

¤ Total track density $\Omega = \Omega_{SF} + \Omega_{GCR} + \Omega_{pp.fis.}$

\# TL induced by gamma-radiation dose of 250 krad.

The measurements of TL_{nat} and artificial (TL_{art}) have been carried out by means of our methodic [4]. The peak temperature of glow curve for all GIs is in the narrow range of 170-190°C. On the base of peak width at half-height $\Delta T_{1/2}$ the GIs were divided into three groups with the $\Delta T_{1/2}$ values of 77+-3, 105+-5, 135+-10°C. Taking into account the sensitivity to the TL storage we have revealed the three GI groups for which the TL_{art} differs by a factor of ~5. The isotropic GIs and those with fine-grained structure have the same TL_{art} values. See table 1 and fig. 2.

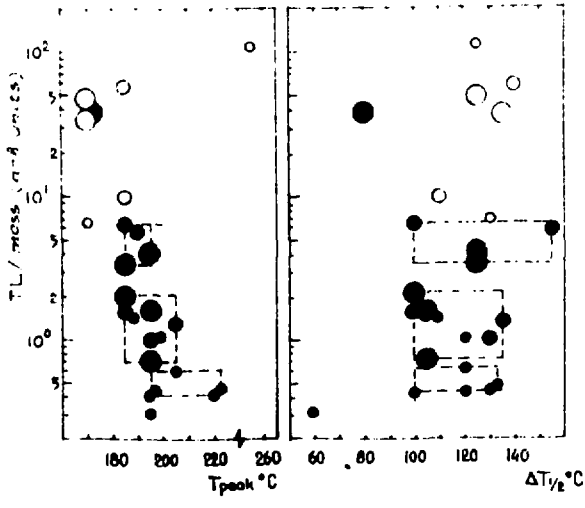

Fig. 2. The TL parameters for the Kaidun glass inclusions

The presence of three GI groups with a great difference of TL_{art} may be explained by their different devitrification degree. There is a hint at the correlation between TL_{art} intensi-

ty and orthoclase content in GIs. The observed various TL parameters indicate the different thermal conditions before or during Kaidun breccia formation.

The values of O_{nat}, O_{ind}, and Cu measured in the same ~40 individual Kaidun glass samples including the seven GIs described above are presented in fig.3. The observed ρ_{nat} value

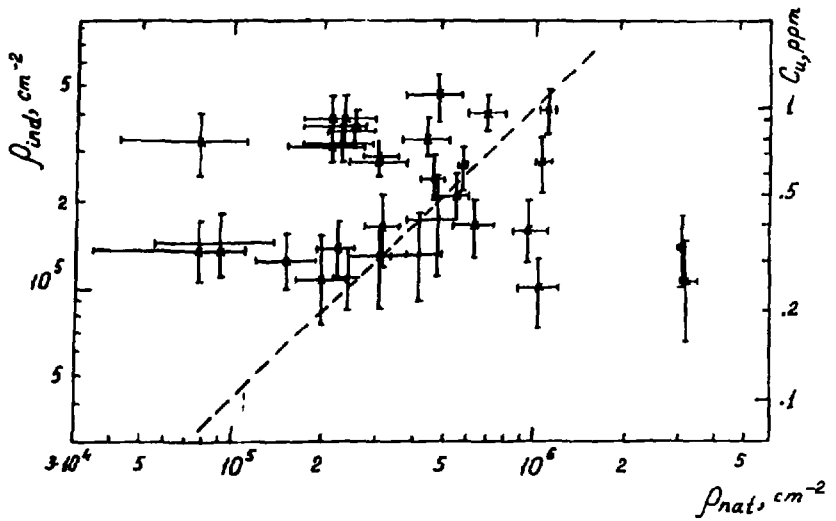

Fig. 3. The induced (ρ_{ind}) and natural (ρ_{nat}) track densities depending on Cu values measured in the same Kaidun glasses

of natural tracks is over the range of ~1.5 order of magnitude at the ~5-times Cu value variation (0.24-1.2 ppm). It is seen that: 1) there is no correlation between ρ_{nat} and Cu; 2) the grains are present with ρ_{nat} excess (the points to the right of dashed line which corresponds to the ρ values stored by the individual glass grains during 4.5 b.y.). These measured track densities ranging from $2 \cdot 10^8$ to $3.5 \cdot 10^8$ cm^{-2} can be attributed both to the early pre-accretion cosmic ray irradiation stage either to the secondary-neutron or fast-proton induced fission as well as to the spontaneous fission of extinct ^{244}Pu. The latter source is the most plausible, and the observed ρ_{Pu}/ρ_U ratio varies from the very small values up to maximal value of ~10 on condition that all track excesses are due to ^{244}Pu.

The comparison of natural track diameter distribution with that of artificial tracks of ^{252}Cf fission fragments (see Table 2) indicates the absence of track annealing in the chemical group I,II,IV glasses under natural conditions and the partial annealing of natural tracks in the group III glass at ~200°C on condition of short-time heating.

Table 2. Track diameter data for Kaidun glasses

Sample group	Natural track		^{252}Cf fission fragment tracks			
			Fresh		Annealed*	
	Track number	D*, μm	Track number	D, μm	Track number	D, μm
I	240	1.5+-0.4	30	1.5+-0.3	-	-
II	66	1.7+-0.2	68	1.8+-0.2	32	1.0+-0.2
III	113	1.4+-0.3	14	2.1+-06	25	1.5+-0.3
IV	79	2.1+-0.2	27	2.1+-0.4	54	1.2+-0.2

* σ- values are the standard deviations.
* Annealing at 200°C for 1 hour.

The substance of different glass inclusions appear to retain the ancient tracks stored at the early stage of Kaidun meteorite parent body formation and almost was not influenced by heating events.

References. 1. Ivanov A.V., Skripnik A.Ya., Ulyanov A.A. et al. Meteoritika (1986),45,3-19. 2. Korotkova N.N., Ruchman G.G. Skripnik A Ya. et al. Meteoritika (1986),45,38-46. 3. Kashkarov L.L., Korotkova N.N., Kashkarova V.G. et al. Lunar and Planet. Sci.Conf.XXI (1990),1013-1021, Houston. 4. Kashkarova V.G., Kashkarov L.L., Baryshnikova G.V. et al. Meteoritika (1988),

TRACK RADIOGRAPHY OF HEAVY ELEMENTS IN MINERALS

I.G.Abdullaev[1], O.G.Belogurov[2], S.F.Vinokurov[2], N.B.Khokhlov[2], V.V.Kushin[2], V.P.Perelygin[1], R.I.Petrova[2], S.G.Stetsenko[2].

1- Joint Institute for Nuclear Research, Dubna

2- Moscow Physical Engineering Institute, Moscow

The problem of low concentration measurements of heavy elements (Pt-Pb) in minerals is connected with searching for a new ore deposits. In many cases it is necessary to measure not only the average content of the element in a sample, but to determine its spatial distribution in mineral with spatial resolution of about 10 μm.

For example, in one of deposits of Middle Asia in carbon rock the high level of Pt concentration was found out. It exceeded the background level of concentration to about 10^2-10^3 times. However, the next accurate mineralogy analysis did not confirm the presence of nugget Pt, which is usually formed at such levels of concentration.

In our work we measured the yields of instant fission fragments and induced α-activity produced at the bombardments of Pt, Au, Pb targets by $^{12}_{6}C$ ions.

The exposure of the samples has been performed at the Laboratory of Nuclear Reactions, JINR in Dubna. The initial ion energy was 9.1 MeV/n, integral ion flux was $3 \cdot 10^{12}$ cm^{-2}. To decrease the ion energy for some patterns, the Al foils were used. Accelerated ion beam bombarded the targets from Pt, Au, Pb with natural isotope content . The thicknesses of the targets exceeded the fragment ranges. On the bombardment surface of the target a thin (15 μm) mica nuclear track detector was placed to register the instant fission fragments. Ion beam vertical dimension was about 25 cm, and beam profile was rather homogeneous.

Induced α-activity was registered by CR-39 nuclear track detector. Exposure time was 1.5 hour and 144 hours to detect short - lived and long - lived components, respectively.

Before etching, the mica detectors were being annealed at 450°C during 4 hours. Such a procedure eliminated the background tracks from recoil nuclei and compound nuclei tracks. To etch the detectors we used the well - known procedure /5/.

In the figure the dependencies of the backward fission fragment creation cross section σ_f of Pt, Au and Pb on the energy of bombardment ions are shown. In finding out the σ_f we took into

account that effective target thickness which the fragments could left was 5 mg/cm^2. The curves in the Figure are in satisfactory agreement with the results of work /6/.

The main data of α-activation of the targets are collected in the Table.

In the last two columns there are evaluations of the experimental effective cross sections of α-particle yields σ_α for exposure durations of 1.5 hour and 144 hours. The cross sections were estimated by formula: $\sigma_\alpha = 2 \cdot M \cdot n / (\rho \cdot R \cdot N_A \cdot J)$ (1), where ρ - target density, R - 5 MeV α-particle range, M - atomic weight, J - ion flux on the target, n - surface density of tracks in detector.

In relation (1) one supposed that α-particles left the thick target in geometry described in /5/, and that registration efficiency was about 1.

It was found out in the experiment that σ_α was practically independent of ion energy in the region of 7-9 MeV/n. For the energy of 6 MeV/n, σ_α was about 0.75 from the previous one.

As one can see from the Figure, the fission fragment cross sections for investigated nuclei are very close each other. For example, for the energy of 9 MeV/nucleon, $\sigma_f^{Pt} : \sigma_f^{Au} : \sigma_f^{Pb} = 1 : 1.15 : 1.18$. Thus, in f-radiography of Pt, Au and Pb with $^{12}_6C$ ion the excitation function proves that the yields of these elements are similar.

Let us evaluate the sensitivity of f-radiography. In the case of diffuse distribution of the element in the sample the relationship between concentration of the element n_x and the surface detector track density n of fragments is: $\sigma_\alpha = 2 \cdot n \cdot \rho_x / (\rho \cdot R \cdot \sigma_f \cdot J)$ (2), where ρR - fragment range in the sample, ρ_x - density of the sample. Let the minimal track density $n = 10^3$ cm^{-2}. Then, supposing for the estimation ρR = 5 mg/cm^2, ρ_x = 10 g/cm^3, σ_f = 0.3 barn, we could estimate the minimal accessible concentrations: $n_x = 4 \cdot 10^{16}$ cm^{-3} for $J = 10^{14}$ cm^{-2}.

Sometimes, it is necessary to measure the local contents of the element in mineral; the number of atoms N in local area on surface of the sample is: $N = n' / (\sigma_f \cdot J)$ (3), where n' - the fission fragment track number, which forms the spot on the autoradiogram. Let minimal track number n' = 100, then: $N_{min} = 3 \cdot 10^{12}$ for $J = 10^{14}$ cm^{-2};

From the Table one could make the next conclusions. The α-particle yields are rather different for all elements. The boundary nucleon, which could be still activated by $^{12}_6C$ is Au. As for

Pt. its activation is practically negligible. Thus, one has the principle possibility to distinguish and to identify close elements (for example: Au - Pt). Obviously, it is necessary to select the bombardment ion for every investigated element.

The sensitivity of α-radiography could be estimated from the assumptions done already. For diffusion distribution of the element, concentration n_x could be determened from equation (2) if to replace σ_f by σ_α. Let ρR = 18 mg/cm^2 and $\sigma_\alpha = 10^{-2}$ barn, then: $n_x = 4 \cdot 10^{17}$ cm^{-3} for $J = 10^{14}$ cm^{-2};

In the case of local content of element, the minimal numbers of atoms are $N_{min} = 10^{14}$; for J $3 \cdot 10^{14}$ cm^{-2};

Thus, the sensitivity of f-radiography exceeds the sensitivity of α-radiography to about one order of magnitude. In real measurements, it is useful to apply both the methods and thus, to combine the high sensitivity of f-radiography and high selectivity of α-radiography.

The spatial resolutions of both the methods depend on the fragment range and α-particle range in the sample and in the detector and are equal to 10 - 20 μm.

Table Element	σ_α (1.5h) barn	σ_α (144h) barn
Pt	$<10^{-5}$	10^{-3}
Au	10^{-4}	$2.5 \cdot 10^{-3}$
Pb	$7 \cdot 10^{-3}$	10^{-2}

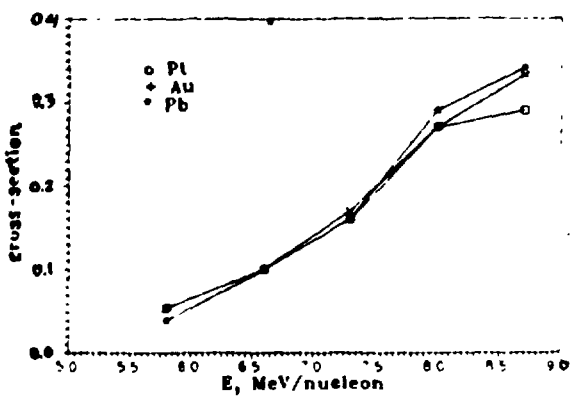

Fig. The backward fission fragment creation cross section σ_f of Pt, Au, Pb versus the energy of bombarding ions

References

1. Ermolaev N.P., Kist A.A., Fleciyan E.S., Khoroshilov V.L. - The Geology of Ore Deposits, v XXV, N 2, 1983, p 68 -91.
2. Flerov G.N., Berzina I.G. Radiography of the Mounting Materials and Ares. Moscow, Atomizdat, 1979.
3. Perelygin V.P., Stetsenko S.G. Abstracts of the3d International Workshop on Solid State Nuclear Track Detectors and Their Application, Odessa, 1991, p 97.
4. Ermolaev A.N., Perelygin V.P., Starodub G.Ya. Stectenko S.G. Soviet Geology, N 7, 1987, p 27 - 33.
5. Durrani S.A., Bull R.K. Solid State Nuclear Detection Principles, Methods and Applications., AERE, Harwell, UK.6. Bazin S.D., Itkis M.G., Muzichka Yu.A., et. al. Preprint JINR R7-12802, Dubna, 1979.

APPLICATION OF SR-39 FOR INVESTIGATION OF (γ,α) REACTIONS

V.A.Vtyurin, *JINR,Dubna*
G.N.Zalesny, *University of Saratov, Russia*

High resistance of SR-39 plastic material to γ-radiation /1/ opens an interesting possibility for its use in investigating p-spectra from (γ,α) reactions on light nuclei near the threshold, where the application of the other types of detectors, e.g. semiconducting ones, is hindered by large pulsed loading and high intensity of γ-background.

This work is devoted to the investigation of spectrometric and background characteristics of SR-39 in real conditions of the experiment on the study of the reaction $^{9}Be(\gamma,\alpha)$ near threshold.

Measurement

The measurements were carried out on a 6.2 MeV, 5 μA electron beam of the microtron of the Saratov University, Russia.

The beam from the accelerating chamber went through a 0.1 mm titanium window and 0.8 mm tantalum converter, in which bremsstrahlung was excited. The beam of photons was hardened by transmitting it through a 50 mm thick graphite absorber, behind which a 150 mm beryllium target and two plastic detectors for forward and backward α-detection were positioned. The target irradiation time was about 3 hours. We used the CR-39 produced in Italy /2/.

The detectors were calibrated using the α-source of natural uranium and samarium-147 source. The energy of α-particles was changed by varying the distance between the α-source and plastic detector.

Analogous measurements were performed with a nonirradiated plastic detector.

Results and discussion

The most convenient range for doing α-spectroscopy is from 0.5 to 2 MeV. The diameter of the track is directly proportional to the α-particle energy /3/.

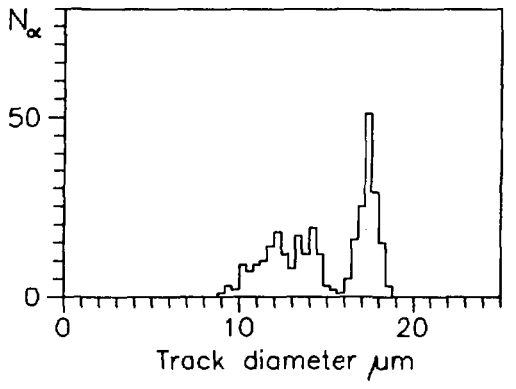

Fig. 1

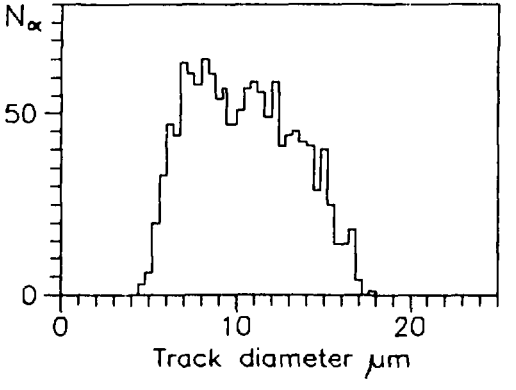

Fig. 2

Fig.1 shows the results of natural uranium α-source measurements at 9h etching time. The distance between the α-source and the plastic detector is 22 mm, Eα = 2.0 and 0.85 MeV. One may see that this method of registration allows one to obtain quite satisfactory energy resolution in the α-energy range up to 2 MeV, when this range is varied by changing the air gap between the sample and the detector.

The comparison of spectra registered by an exposed and not exposed to γ-radiation detector in the conditions of the given experiment did not recall any significant difference in energy resolution.

Figure 2 shows the distribution of track diameters from the thick beryllium sample placed in immediate contact with the detector. The comparison is made with the existence of α-particles of the energy higher than 1MeV. These results are obtained for the α-particles with energy more than 1MeV. The track

density of the $^{9}Be(\gamma,\alpha)$ reaction is 10^{5} cm^{-2} at background track density 10^{2} cm^{-2}.

The authors are grateful to Mr. A.Golovchenko for his help in the preparation of the detectors, to Drs. S.P.Tretyakova and V.P.Perelygin for valuable discussions and Drs. F.V.Rodionov and A.M.Goriachev for access to the Saratov University facilities.

References

1. B.G.Cartwright, E.K.Shirk, P.B.Price Nucl.Instr.& Meth. 153, (1978), 457-460.
2. MACRO Collaboration (1991) Nucl. Tracks Radiat.Meas., Vol.19,Nos 1-4, pp.641-646, 1991.
3. P.F.Green et.al. Nucl.Instr.& Meth. 203, (1982), 551-559.

THE RELATIVISTIC NUCLEI BEAM MONITORING BY MEANS OF HIGH THRESHOLD FISSION CHAMBER

D.Chultem, Ts.Damdinsuren, L.Enkh-Gin, L.Lomova,
V.Perelygin, K.Tolstov

Joint Institute for Nuclear Research
141980 Dubna

We have carried out the study of interaction of 3.65 GeV protons and ^{12}C nuclei at energy of 3.65 GeV/nucleon with lead target in order to find the possibility of relativistic nuclei beam monitoring based on registration of induced fission. The detectors were formed of thick (200μm) Meliuex foil and 100 μm lead layers placed close together. These stacks were exposed perpendicularly to the beam of relativistic nuclei.

Thick (200μm) aluminium foil has been exposed as activation monitor simultaneously with track detectors.

The Figure shows the proton beam profile histogram obtained with Meliuex track detectors at energy 3.65 GeV. The fission cross-section of Pb by 3.65 GeV protons is 140±20 mb. The result of this experiment is in reasonable agreement with[1,2,3].

From our result we conclude that the fission fragment ionisation chamber with electrodes covered by lead may be used as beam monitor of relativistic nuclei, moreover due to rather high fission threshold of lead nuclei it will be not sensitive to the light charged particles and slow secondary nuclei which is very important in the experiments with high intensity beam.

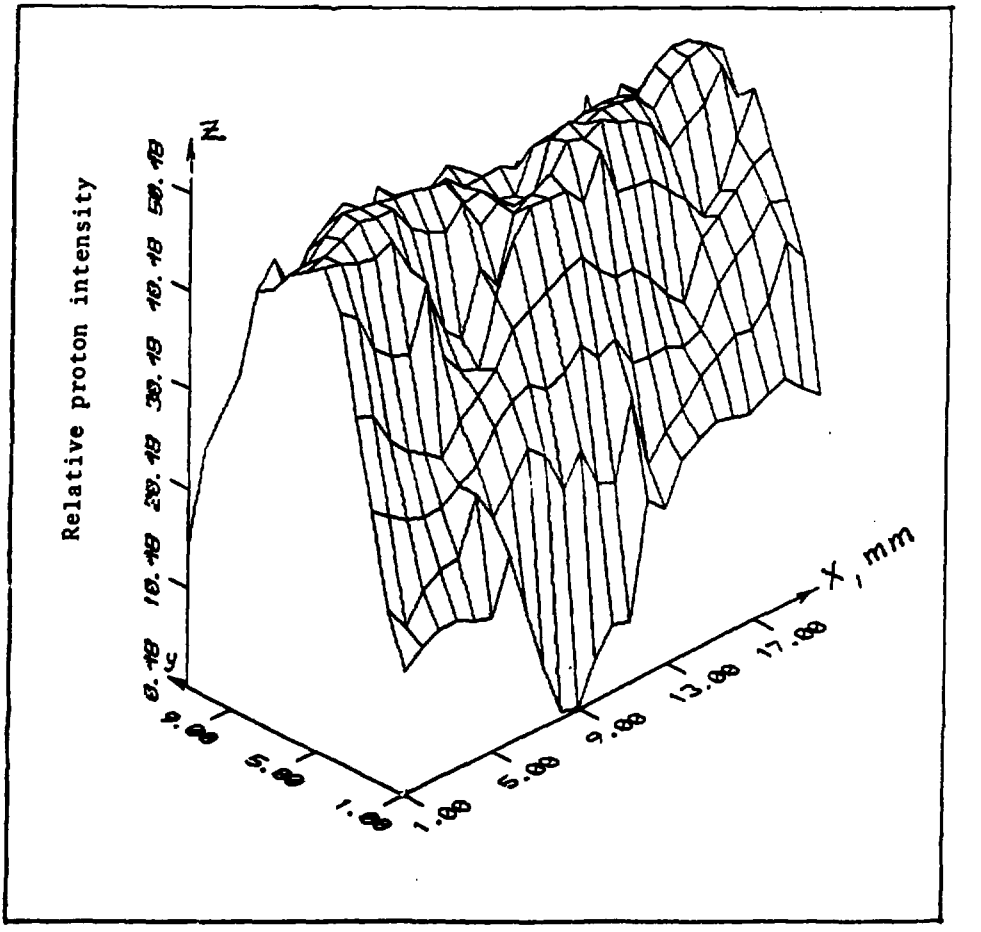

References

1. G.Rémy, J.Ralorosy, R.Stein, M.Debeauvais, J.Tripier. Nucl.Phys. A163(1971), p.583.
2. R.Brandt, F.Carbonara, E.Cieslak, H.Piekarz, J.Piekarz, J.Zakrzevski. CERN Preprint.
3. J.Huidis and S.Katcoff. Phys.Rev. C13, 5,p.1961 (1976).

THE SPACE DISTRIBUTION OF NEUTRONS GENERATED IN MASSIVE LEAD TARGET BY RELATIVISTIC NUCLEAR BEAM

D.Chultem, Ts.Damdinsuren, L.Enkh-Gin, L.Lomova, V.Perelygin, K.Tolstov

Joint Institute for Nuclear Research
141980 Dubna

The investigation of the neutron generation in extended lead target including its space distribution inside the target volume by means of threshold fission chambers KNT-8 and passive activation detectors has been performed in 1990 /1/.

The present paper is devoted to implementation of solid state nuclear track detector in the research of that kind/2/.

Figure 1 presents measured neutron space distribution inside the lead target and intensities of neutrons emitted from the target.

Figure 2 shows the neutron distribution in the thick water degrader. These distributions were obtained by means of thick (200μ)

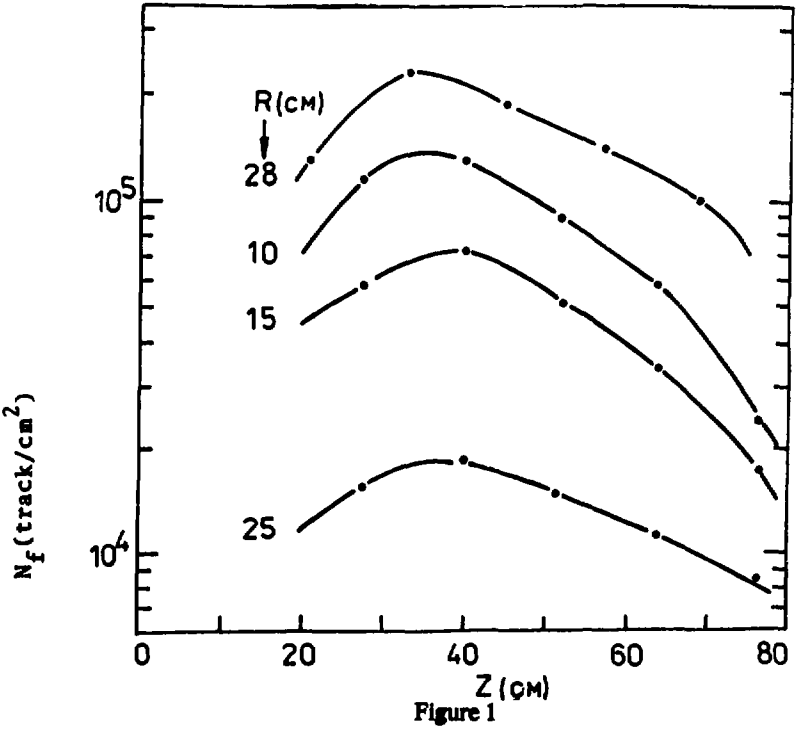

Figure 1

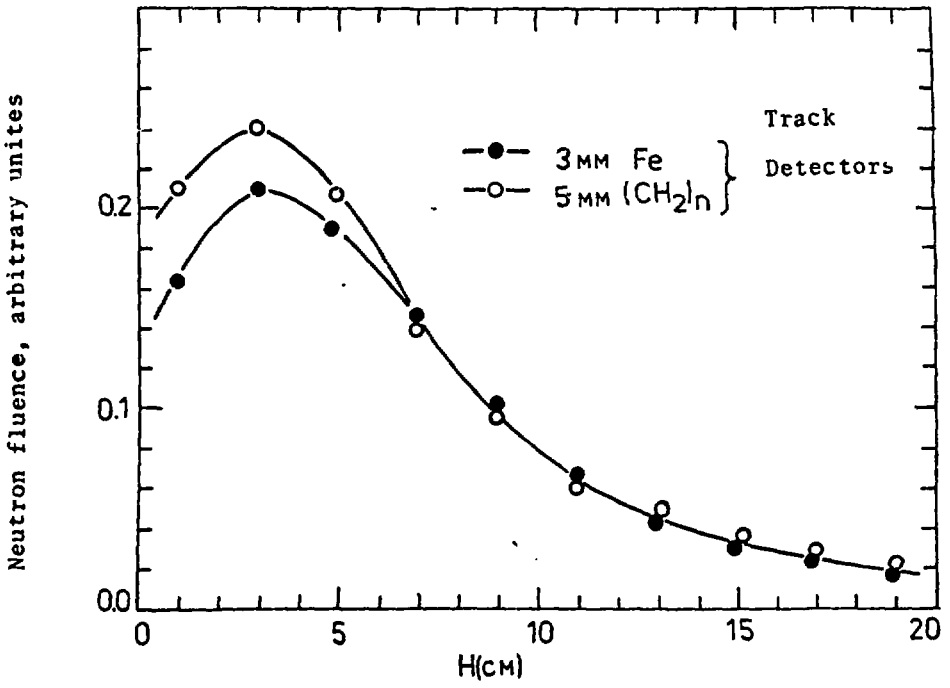

Figure 2

mylar detectors exposed in contact with natural uranium metallic foils. The result of our experiment is in complete agreement with the data[1] and shows that this well-known technique developed for neutron dosimetry[2,3] can be applied successfully in researches carried out at the external beams of accelerated relativistic nuclei.

The data obtained are used now for calculations of numbers of secondary fast neutron generated by fast heavy projectiles in spallation target.

References

1. V.A.Voronko, V.M.Dyachenko, V.M.Kostin, L.G.Levchuk, V.S.Miroshnik, V.Ya.Migalenia, K.D.Tolstov, N.A.Khizhniak. Atomnaya Energia v.68, N°6, p.449, 1990.
2. R.M.Walker, P.B.Price, R.L.Fleischer. Appl.Phys.Lett., v.3,p.28, 1963.
3. S.A.Diurrani, R.Ball. Solid State Nuclear Track Detectors. Principles, Methods and Applications. AERE, Harwell, UK, Pergamon Press, 1987.

APPLICATION OF NUCLEAR TRACKS IN MATERIALS SCIENCE AND MICROTECHNOLOGY

R.Ilić
J.Stefan Institute, University of Ljubljana, POB 100,
61 111 Ljubljana, Slovenia

Abstract

Historical and current activity in application of ion tracks in solids to materials and technology will be assesed. The variety of unique radiographic technique have been developed and are currently explored for: (i) investigation of internal structure of solids, (ii) microstructural research of materials, (iii) analytical investigation, (iv) depth profiling, (v) trace analysis and (vi) non-destructive investigation. The application of ion tracks in polymers, glasses and crystals in micro technology comprises: (i) change of bulk material properties, (ii) influence of local properties, (iii) production of new devices in microtechnology. The possibilities to extend the present radiographic and microtechnological technique will be discussed as the conclusion of the lecture.

Using the Activation Radiography in Geological and Geochemical Studies

E.S. Flitsiyan

Institute of Nuclear Physics, Uzbek Academy of Sciences,
Ulugbek, Tashkent 702132, Republic of Uzbekistan, CIS

To study the spatial distibutions of gold and other elements in the objects of various nature, a method of the neutron-activation radiography has been elaborated which based on irradiating a sample studied with a neutron flux followed by the photoregistration of the induced activity of the element under examination.

Radiographic methods for studying the distributions of more than 30 elements, having the local detection limits within $10^{-3} \div 10^{-8}$ $g \cdot mm^{-2}$ with the resolution of 1 - 100 μm, have been developed.

The application of the methods elaborated to analyze geological and geochemical objects results in obtaining the representative data on the regularities of the element distributions in minerals and samples of ores and holding rocks.

The elaboration of the local analysis methods based on the registration of spontaneous and forced uranium and thorium fission fragments contributed a great deal of the geological knowledge.[1,2]

A considerable practical result achieved in this application of the local methods proved the expedience of developing similar methods for other elements. There has been shown a possibility of using radiography to study the geological samples for boron, lithium, lead and bismuth by irradiating the microsection studied with neutrons and multi-charged ions and registrating the α-particle tracks.[3-7]

However, the radiography making use of the registration of the charged particle and fission fragment tracks has turned out to be developed only for light and fissionable nuclei.

For some other elements such an approach has required special elaborations. Among others, the method of the local, statistically reliable determination of concentrations and spatial distributions of precious elements is undoubtedly of great importance. This is caused by structural features of new types of gold- and silver-bearing ores in the slates, characterized by the non-contrast concentration boundaries between the "dead rock" and industrial deposits. The evaluation of gold and silver little components in any mineral association determines both the success of the geological prognosis

and the possibility to solve the fundamental duestions of ore formation theory. The development of the radiographic analysis of gold and silver components in rocks ensures, just in the case of radioactive metals, a higher standard of ore geological evaluation.

In order to solve the problem under consideration, the method of neutron-activation radiography for gold, silver and some other elements has been elaborated which based on irradiating the sample studied with a netron flux followed by the photoregistration of the element's induced activity.[8] To determine the local element concentration by the method, an activated rock microsection is placed, together with an irradiated standard, on an appropriate photoemulsion that serves as a detector of the induced irradiation. The exposed emulsion's photoblackening density was observed to be related to the amount of an element in the sample region adjacent to the detector and the analytical form of the dependence has been derived.

Justifying the application of the neutron-activation radiography for the element distribution analysis has required the main factors influencing the conditions of obtaining the selective radiograms, such as the resolution, detection limit, optimal irradiation regimes, exposure and photoexposure of sample to be evaluated.[9]

Such factors as the sample exposure duration, photoemulsion development time, distance between the sample and photomaterial, as well as photoemulsion type (the size of silver halogenide grains and emulsion layer thickness), have been observed to influence the radiography resolution at a certain irradiation energy.

Fig. 1 shows the changes of photoimage size versus the size of radionuclide sources presented as various flat discs (0.5; 0.6; 1.0; 3 mm) in dependence on the exposure time, all the sources having had the same specific activity. If the exposure time varies from 50 to 300 sec, there is practically no distortion in the original size of irradiation source (curve 1). The gradual increase in the exposure time within 600 + 4000 sec results in a considerable distortion of the original source size (curves 2, 3, 4, and 5), and further increase brings a distortion stabilization (curve 6).

Let us consider now the possible reasons of such a distortion. In the case of short exposure, the probability of a β-particle, emerging from a source reacting the crystal situated directly above it, is much higher compared with that for a crystal neighbouring in several microns aside. However, the probability of a β-particle double hit is also higher for the crystal above a source. If the exposure time is

relatively small, the number of crystals with a high probability of double hit is small, and the grain density distribution above a source is characterized by a sharp peak (the best resolution). If the exposure time is so great that the probability of double hit in the crystal above a source becomes significant, the grain density above it does not increase in proportion to the number of interactions with β-particles, which results in the grain density distribution curve widening and flattening, and, consequently, the resolution worsening. Finally, all the crystals above a source are activated and a further increase in the exposure time will cause the increase in the number of developed grains only in the low grain density region far from the source. Probably due to the reason, the low grain density radiograms obtained by using low specific activity irradiation sources have often, in contrast to the advantages expected from the statistical point of view, the better resolution than on the radiograms from the sources being several times more intensive.

Fig. 2 shows the change in photoblackening versus the distance between a sample and photomaterial for three various emulsions: the X-rays films PM-1 (the average diameter of non-developed grains, d_g, of silver halogenide is 1.3 μm, the emulsion thickness, l_{em}, is 15-16 μm), and PT-1 (d_g = 0.5 μm, l_{em} = 15 μm) and a "Micrat" film (d_g = 0.5 μm, l_{em} = 5-7 μm). As seen from Fig. 2, the greatest image distortion with increasing distance from the source (resolution worsening) takes place if one uses the films with a thick emulsion layer.

Compared with the emulsion thickness, the decrease in the average crystal diameter produces not such a strong effect (curves 2 and 3). These results give evidence for existing point of view, according to which the emulsion blackening density depends on the number of exposed crystals per an emulsion area unit rather than their total number. For the FT-1 films the change in the distance between a sample and emulsion from 10 to 100 μm has been found to lead to the resolution worsening from 50 to 60 μm (see Fig. 3).

Thus, if a close contact between the source and photomaterial is impossible (e.g. if the emitting microinclusion is not on the sample surface, or if it is necessary to put a thin gasket of inert material to prevent a chemical interaction between a sample and emulsion), the separating distance should be as small as possible, with a thin emulsion being preferable.

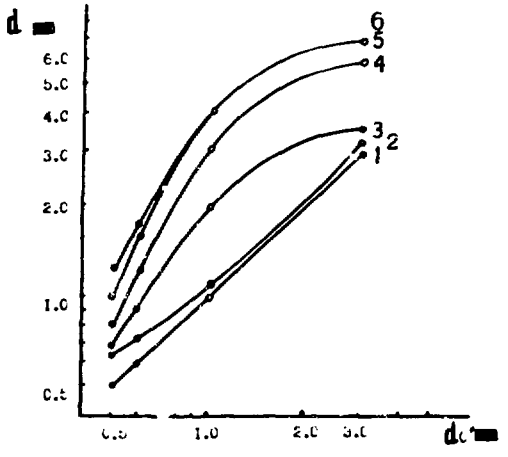

Figure 1

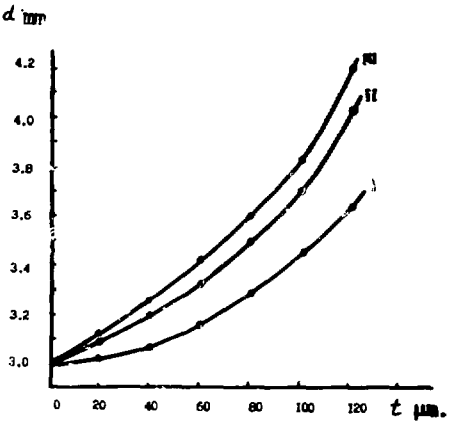

Figure 2

Figure 1. Dependence of changing the photoblackening size, caused by the radioactive sources of various diameters (0.5; 0.6; 1.0; 3.0 mm) versus the exposure time: 1 - t_{exp} = 60 ÷ 300", 2 - t_{exp} = 600", 3 - t_{exp} = 1000", 4 - t_{exp} = 2000", 5 - t_{exp} = 4000", 6 - t_{exp} = 5000".

Figure 2. Dependence of the distortion in the radioactive source image versus its distance from a photomaterial of a "Microat" film (I) and the X-ray films RT-1 (II) and RM-1 (III).

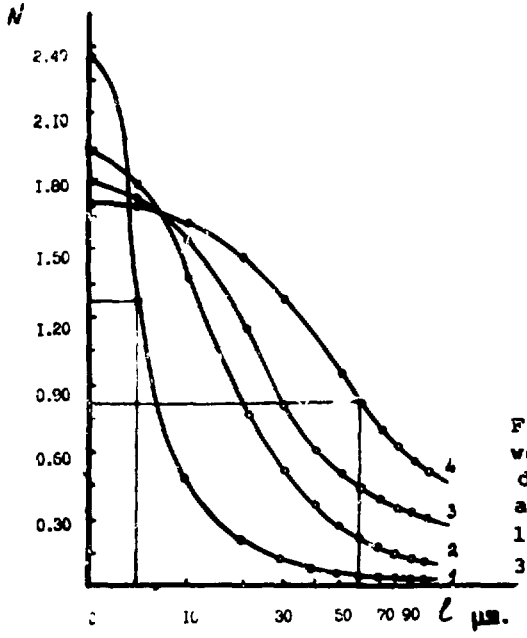

Figure 3. Resolution worsening with the increasing distance (ℓ) between a sample and a FT-30 film: 1 - ℓ = 0 μm, 2 - ℓ = 20 μm, 3 - ℓ = 60 μm, 4 - ℓ = 100 μm

The data obtained allow one to find an optimal set of conditions, such as the choice of photomaterial, sample preparation for the analysis, exposure parameters suitable for each case under study.[10]

Further analysis of the radiographic images was devoted to studying of the optical density distribution of an exposed and treated photoemulsion. By analyzing the optical density distribution obtained by photometering a radiogram, one can, in principle, determine the size, shape and location of the element inclusion of interest.[11]

Microphotometering the radiograms obtained, as well as comparing the extinction values with standards, allows a quantitative characterization of the element distribution in a microsection. Fig.4 illustrates the data on the radiographic study of gold distribution under neutron irradiation. In the case of point gold concentrations one should study the profiles including these points. The gold distribution in every microsection is evaluated by hundreds of measurements.

The intensity of photoemulsion blackening above the visible gold with known standard may serve as an internal standard. Besides, the special comparison standards have been developed which model the matrix composition and structure.

The irradiation time for a sample, being given in dependence on the problem under consideration, is determined by the neutron flux density permitting one to detect the separate gold contours or disperse gold microinclusions, as well as gold itself, in an inclusion.[12] The sensitivity of the technique considered as a modification of the neutron-activation analysis is $1 \cdot 10^{-6}$ g·mm^{-2} with the relative standard deviation of 8 - 10%.

The technique elaborated for studying the microgold distributions in powder-like samples was used to find the representative conditions of gold analyses.

The neutron-activation technique as applied to study a silver distribution makes use of the nuclear reaction

$$^{109}Ag(n,\gamma)^{110m}Ag \quad ,$$

with the ^{110m}Ag radionuclide formed having a half-life of 253 days. The technique of Ag determination turns out to be worse than that of gold, although the silver photoregistration is higher due to the number of "interfering" radionuclides decreasing. The Ag determination sensitivity is $5 \cdot 10^{-6}$ g·mm^{-2} with the relative standard deviation of 5 - 8%.[13]

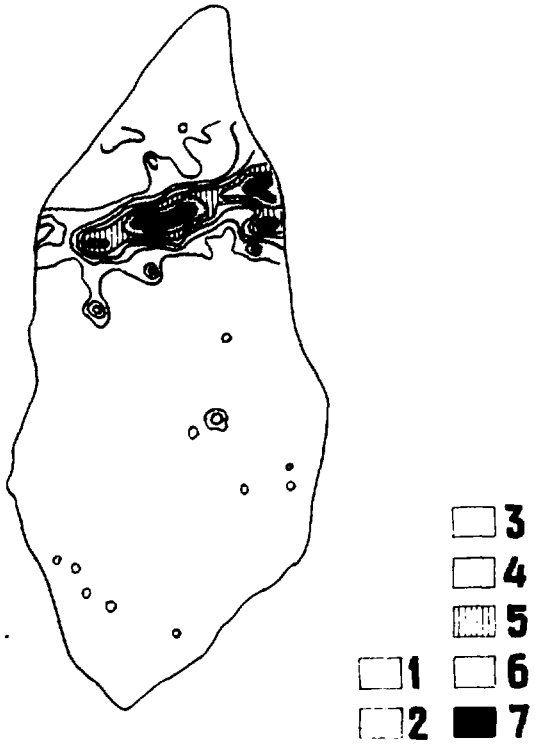

Figure 4. Gold distribution concentration profiles obtained by photometering a quartz section over 0.15 mm^2 square (the gold content is given): 1 - less than $1 \cdot 10^{-6}$ g, 2 - $(1+2.6) \cdot 10^{-6}$ g, 3 - $(2.6+4.6) \cdot 10^{-6}$ g, 4 - $(4.6+7.5) \cdot 10^{-6}$ g, 5 - $(7.5+11.0) \cdot 10^{-6}$ g, 6 - $(11.0+16.6) \cdot 10^{-6}$ g, 7 - $(16.6+25.1) \cdot 10^{-6}$ g

Figure 5. A radiogram of the silver distribution in a quartz section from the clevage zone

Fig. 5 presents a neutron-activation radiogram of silver distribution in a quartz microsection from the clevage zone obtained by irradiation with the fission spectrum of $6 \cdot 10^{17}$ $n \cdot cm^{-2}$ and exposed for 6 months for the short-lived nuclides to decay. Studying the spatial distribution of the little components of gold and other elements in sulphide-impregnated ores of black slates has required a special elaboration.[14] Using a special aluminium filter in obtaining the radiograms with subsequent comparison of the radiograms obtained with the filter and without it allows one to reveal two gold forms in the ores: sulphide-impreganated and free ones.

The results achieved by applying the methods proposed to study gold and silver distributions were used in working out a geochemical model of precious element ore formation in the black slates.[15]

The above-described investigation has been carried out with using simultaneously the methods different in their sensitivity and resolution, which has allowed us to supplement and enlarge their possibilities.

The number of techniques presented does not cover the possibilities of the nuclear physical approaches to local analysis to solve numerous problems in geological and geochemical studies, but speaks for the large prospects of their application.

REFERENCES

1. G.N. Flerov, I.G. Berzina, Radiography of Minerals, Rocks and Ores (in Russian), Atomizdat, Moscow, 1979.
2. R.L. Fleisher, P.B. Price, R.W. Walker, Nuclear Tracks in Solids, Univ. of California Press, 1975.
3. G.N. Flerov, I.G. Berzina, J. Radioanal. Chem., 16 (1973) 461-472.
4. I.G. Berzina, I.B. Rerman, A.SD. Nazarova, Dokl. AN SSSR, 201 (1971) 686-689 (in Russian).
5. A.A. Berezina et al., Geokhimiya, No.1 (1977) 141-147 (in Russian).
6. A.N. Ermolaev, V.P. Perelygin, S.G. Stetsenko, E.S. Flitsiyan, Geokhimiya, No.2 (1990) 195-206 (in Russian).
7. B.P. Zverev, L.E. Krasivina, O.G. Murtazin et al., Atomnaya Energiya, 41 (1976) 351-352 (in Russian).
8. A.A. Kist, G. Sattarov, E.S. Flytsiyan, Geokhimiya, No.11 (1984) 1699-1710 (in Russian).

9. E.S. Flitsiyan, A.V. Romanovsky, L.G. Gurvich, A.A. Kist, Atomnaya Energiya, 61 (1986) 133-136 (in Russian).
10. E.S. Flitisyan, Development of a Complex of Nuclear Physical Methods of Local Analysis in Geology and Geochemistry (in Russian), in: Activation Analysis, Fan, Tashkent, 1990, p.140-148.
11. N.P. Ermolaev, A.A. Kist, E.S. Flitsiyan, Geologiya Rudnykh Mestor., No.2 (1983) 86-91 (in Russian).
12. V.L. Khoroshilov, E.S. Flitsiyan, N.P. Ermolaev, V.A. Chimenov, Geologiya Rudnykh Mestor., No.1 (1984) 52-60 (in Russian).
13. N.P. Ermolaev, M.I. Ilyin, L.G. Pal'mova, E.S. Flitisyan, Geologiya Rudnykh Mestor., No.1 (1986) 48-57 (in Russian).
14. V.S. Shatsky, O.A. Koz'menko, E.S. Flitisyan, N.V. Sobolev, Dokl. AN SSSR, 315 (1990) 477-480 (in Rissian).
15. V.P. Loshchinin, E.S. Flitisyan, Zapiski Vsesoyuznogo Mineral. Obshchestva, Issue 43 (1990) 156-161 (in Russian).

THE STUDY OF URANIUM DISTRIBUTION IN MATERIALS FOR MICROELECTRONICS WITH TRACK DETECTORS

A.G.Dutov, S.V.Shiryaev, K.E.Lobanova, L.A.Smakhtin
Institute of Solid State Physics and Semiconductors, Minsk
Science Institute of Physical Chemistry, Obninsk

At present, the application of integrated circuits in high fidelity systems is hampered by numerous errors and failures.
90% of errors, according to the experimental evidence[1,2], are caused by charge generation in the device active range comparable in value with the charge of information unit.
Therefore there arises a need for determination of sufficiently low (parts per ten, hundred of ppb) U and Th content in semiconductor materials, microcircuit enclosures, etc. This problem has been given considerable attention in the literature, for instance in [3,4,5].
At the same time, the distribution of the U,Th atoms and other α-active elements is practically unstudied.
In this paper the studies on uranium distribution in plastic samples and metallic aluminium used in fabrication of enclosures and electrical connections for microcircuits by means of the f-autoradiography[6] techniques are reported.
Plastics are complex composites containing polymers, filling agents: silicon or aluminium dioxide, stibium and bromine additions.
The total uranium and thorium content in samples was determined by activation analysis, some results are summarized in Table 1.

Table 1.

Average uranium and thorium content in samples from the NAA data

samples	U content in ppm	Th content in ppm	corresponding α-particles flow $cm^{-2}h^{-1}$
aluminium 1	0.315	0.188	1.82
aluminium 2	3.04	0.0043	15.41
aluminium 3	0.0081	0.0023	0.044
plastic 1	0.015	0.006	0.80
plastic 2	0.0038	0.019	0.021
filling agent OS	0.021	0.0041	0.11
filling agent OSSF	0.0085	0.0027	0.046
filling agent Ch	0.26	0.014	1.34

Samples of no less than $1cm^2$ were polished at two sides with a diamond paste, raised in a box, dried and packed into a container. The fission fragments were detected with lavsan as the most radiation resistive polymer[6]. The irradation was carried out in the horizontal channel of 10-13 Mw WWR-C reactor by employing neutron beams with total fluence ($5 \cdot 10^{16}$ cm^{-2}) and a cadmium filter.
The detectors were etched in a standard fashion - 40% KOH, 6 min at 60°C. With a 100x microscope lens dozer of traces and some accumulations were revealed, in this case the uranium content in the sample did not exceed 10 ppb.

The detection limit of uranium was no worse than 0.2 ppb, that of thorium - 0.1 ppm and limited by the lavsan film defects.
The uranium content upon neutron irradiation with full fluence was calculated using the expression:

$$C_u = (2p/R)(m_{us}/p_{us})$$

, where p -the tracks density of sample, η_{us} - weight of standard, R - the fission fragments run in the sample, could with sufficient accuracy be evaluated using the values for the air. For the fission fragments $R = 7 \cdot 10^{-4}\sqrt{A}/d$,where d - the density and A - the average mass number for the sample.

Fig.1 shows the distribution of the uranium fission fragments tracks of a part of sample aluminium 1. The "A" range is 44 mcm^2 with U concentration of 6.1 ppm and the "B" range - 1.9 mcm^2 at C_u =46.8 ppm. Uranium atoms accumulations are characteristic not only to aluminium but also to plastics where their content is lower. Nevertheless, the 1-2 accumulations of the B- type for 10 cm^2 of the sample surface were revealed.

In calculations of the uranium concentration for the B- type accumulations a correction for the effect of traces enhancement in a detector by estimating the probability[7] of the fragment emission from the spherical accumulation with the 2r diameter is:

$$P = 1/2(3(R/2r)-(R/2r)^3) .$$

It is clear that the formation of accumulations in a plastic or aluminium occurs due to various reasons. For plastic it is possibly deficient mixing and grinding of filling agents, since the uranium content in natural quartz sand could reach 100 ppm.
In aluminium the uranium atoms are deposited at dislocations. The diffusion processes at the grain and twins boundaries under repeated high temperature treatments of aluminium ingot in the process of fabrication are prominent in the emergence of uneven impurity content.

As is known[8] the diffusion coefficient at the grain boundaries increases by several orders of magnitude as compared to that of equilibrium one, and at the same time, there are channels in them with relatively low atom packing densities of the basic substance, the boundaries thickness does not exceed some interatomic distances. Thus, one observes perfect ranges of large impurity elements accumulations in a polycrystal.

Fig.2 illustrating the uranium distribution in aluminium obtained with lower magnification, may, to some extent, serve as a confirmation.

Periodicity is observed in the distribution of accumulations due to the dislocations distribution and large angle grain boundaries.

In this case the A-type range (fig.1) can be treated as the onset of the B-type inclusion formation.

Thus, at the average uranium content in microelectronic materials at the ppb level its concentration up to the ppm level is highly probable causing not only errors but also failures of memory cells after a while.

The most hazardous in this respect is aluminium where periodic uranium accumulations could occur with the uranium content of a few tens of ppm within 100-200 mcm from each other.

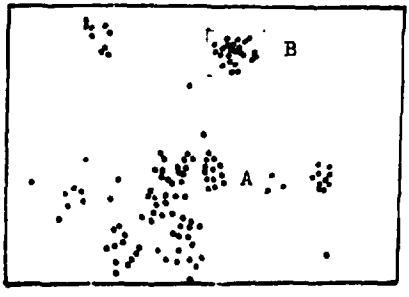

Fig.1 A part of the f-autoradiogram of distribution of U in Al (100x)

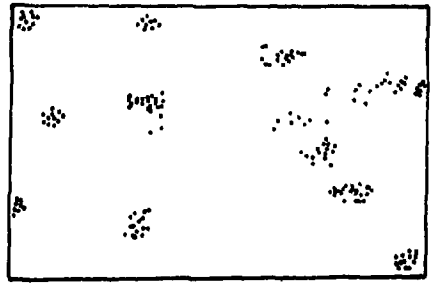

Fig.2 Distribution of U in Al (30x)

References

1. K.Takeuchi, M.Aoki, Y.Watanabe, K.Itoh. Sol.St.Electr. 1990,33, No.11,p.1477-1483.

2. A.A.Chernishev , A.S.Chenigenko, Yu.A. Borisov et al . ,Z.Electr. Techn., 1986, 7, 157p.
3. E.W.Haas, R.Hofman. Sol. St. Electr., 1987, 30, No.3, p.329-337.
4. F.F.Dyer,J.F.Emery, L.C.Bate. J.Rad. Nucl. Chem., 1987,110,No.1, p.221-226.
5. K.P.Egger, V.Krivan. Fresenius Z.Anal. Chem.,1987, 327,No.2,p.119
6. G.N.Flerov,I.G.Berzina.The autoradiography of minerals, mountain rocks and ores.,M.,A.I.,1979, 223p.
7. V.A.Stupin.,Communication of the S.I.A.R.,1986, 18, 699.
8. I.Kaur, W.Gust, Fundamentals of grain and interphase boundary diffusion.,Z.P.,St., 1989, 445p.

Application of CR-39-Type Plastic Track Detectors and Thin-Layer Inorganic Sorbents for Determination of Alpha-Active Radionuclides Microconcentrations in Water

A.A.Djakov, V.Yu.Rostovtsev
Research and Development Institute of Power Engineering, Sverdlovsk branch, Ekaterinburg

A.V.Voronov
Chlopin Radium Institute (St. Petersburg).

N.D.Betenekov, E.G.Ipatova
Ural Polytechnical Institute, Ekaterinburg

In nuclear power engineering an important radiation safety aspect is a control of activity accumulation in a primary circuit and radioecological condition of reactor off-sites. Both require a fission materials control, including alpha-irradiators in a primary coolant and off-site pools, when fission materials concentration in these waters is 10^{-12} -10^{-10} g cm^{-3}.

A requiried highly sensitive method of control was developed based on plastic track detectors and thin-layer inorganic sorbents (method PTD-TIS).

CR-39 Fabrication Process

The CR-39 detector, based on diethyleneglycolbisalylcarbonate (DEGBAC) monomer, was produced by the Ukrainian R & D Institute of Plastic Materials (Donetsk). Its fabrication process was developed in the Chlopin Radium Institute (St.-Petersburg).

To meet the requirements of alpha-dosimetry the optimal polymer is one of the content: 96% of DEGBAC and 4% of benzol peroxide (BP) [1].

Background characteristics perfection is obtained by the combination of initiators: 4% of BP and 0.5% of tetrabutylperbenzoate (TBPB). Within the frames of this work four batches of CR-39 were fabricated.

Etching Regimes Optimization and CR-39 Selection for Quantity Production

Detector specimens from all four batches were irradiated by Pu-239 alpha-particles (E = 5.155; 5.143; 5.105 MeV) from the "ОСИАН"-set; the geometry being "close adjacent to" and at 1 cm -distance in air. Irradiated and nonirradiated specimens of CR-39 were etched electrochemically (ECE) simultaneously.

Literature data on etching regimes for CR-39 of various brands and companies - PATRAS, Germany [2]; American Acrilics, Inc., USA [3]; Persore Moulding, Ltd. Works,U.K. [4,5], TASTRAK [6], - were analysed and ECE regime variants were selected to registrate 5 MeV alpha-particles:

- preliminary chemical etching (pre-CE):
  - a) 4N KOH, 80° C, 5h;
  - b) 7.25N NaOH, 70° C, 5h;
  - c) 5.35N KOH, 70° C, 2-5h;

- electrochemical etching (ECE):
12-20 kV_{eff}/cm, 3 kHz, 25° C; 4-8 h;

d) 80 vol.% of 7.8 N KOH + 20 vol.% of C_2H_5OH;
e) 30 % of KOH.

The specimens of all four detector batches were etched at these conditions. The most alpha-particle registration efficiency and the least background density of discharge spots in all etching regimes belong to CR-39 from batch N4 (DEBAC N1, initiators: BP-4%, TBPB-0.5%). This CR-39 modification was reproduced in a sufficient quantity and all the following experiments were performed on it.

The ECE conditions for "quantity-production" CR-39 were optimized to reach a maximum signal-to-background ratio (including conditions of the best count of discharge spots). Pre-CE (variant "C", 5h) followed by ECE (composition "d" and "e", electric field voltage: 14.6; 16.7; 19.4 keV/cm, during 6, 7 and 9 h). The following data proved to be optimal: ECE composition - variant "d", alcohol-bearing, electric field voltage - 16.7 kV_{eff}/cm

For these conditions the background discharge spot density was 30 ± 3 cm^{-2} and practically did not increase with ECE stage extension from 6 to 9 h. However, it increased to 100 ± 20 cm^{-2} with the voltage increase to 19.4 kV_{eff}/cm. The discharge spot diameter was from 50 to 100 μm. A high quality of detector surface was kept stable.

U-and Pu-Concentration Technique with TIS Application

The literature data and TIS operation experience lead to the following conclusion: to concentrate microquantities of U and Pu from a water solution in order to define acceptable TIS is based on Ti hydroxides [7].

It was experimentally stated that the dependences of U-233 sorption on water solutions acidity has a form of a curve with the maximum in the range of pH-values from 4.5 to 5.5 for titaniumdioxide and pH 6-7 for cerium dioxide.

In the experiment on Pu-239 sorption by thin-layer titanium hydroxide from various solutions the acidity dependence of microcomponent concentration in the sorbing layer (in the pH-range from 2 to 8) was not found.

An assessement of sorbent specificity in respect to the component extracted is the distribution coefficient, characterising the element amount, absorbed by a sorbent mass unit in specific conditions. The distribution coefficient "k" is defined from the relationship:

$$k = C_T/C, \ cm^3.g^{-1}, \qquad (1)$$

where C_T - concentration of U or Pu in a solid phase (sorbent), gU(Pu)/gTi(Ce);
C - concentration of U or Pu in a solution, $g.cm^{-3}$;
and does not depend on U or Pu concentration in a solution. Sorption experiments were carried out to define U and Pu distribution coefficients. There were used water solutions with different initial content of U-233 and Pu-239 and thin-layer hydroxides of Ti and Ce, 2-20 μg Ti(Ce)/cm^2. TIS was precipitated on polyetheleneterephthalat (lavsan) and CR-39 by thermal hydrolysis of the solution, containing

$TiCl_4$ and carbamide. The results of the experiments are shown in Fig.1.

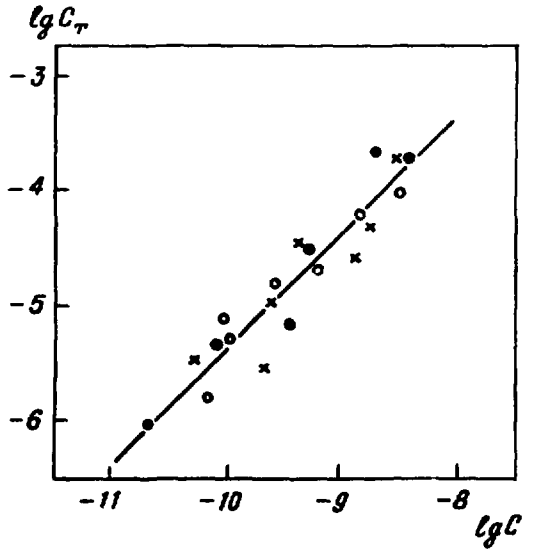

● – U-233 in distillate and ABP,
o – Pu-239 in distillate at pH = 3.4;
× – Pu-239 in APB at pH = 3.5

Fig.1. Isotherm of U and Pu sorption by thin-layer titanium hydroxide from solutions

It is stated, that the distribution coefficients of U-233 and Pu-239 in the definition error limit (at the confidence coefficient 0.95) are numerically equal and constitute:

$$K_{min} = 6.8 \times 10^3 cm^3 g^{-1},$$
$$K_{max} = 2.2 \times 10^5 cm^3 g^{-1},$$

being independent of a solution type (distillate, ABP) and sorbent (TiO_2, CeO_2).

When U-concentration exceeded 10^{-8} g·cm^{-3} the isotherm deviation from linearity was observed. It was caused by the saturation of most active sorption collector centers by the microcomponent, the centers capacity can be estimated by the value not less than 2 mgU/g Ti.

The static exchange capacity of these most active sorption centers relative to Pu is not less than 100 μgPu/g Ti. Thus, the obtained diffusion coefficient proved high thin-layer titanium hydroxide specificity to U and Pu.

Main Characteristics of PTD-TIS Method

The main characteristics of PTD-TIS Method: sensitivity and detection limit should be considered in comparison with "wet" method, when PTD is exposed directly in a solution.

Pu determination

Track density on detectors, irradiated by alpha-particles from a thin target, T, and irradiated in a solution, d_T, are defined by the expressions:

$$T = (1/2)\cdot K^{\alpha}_{dry}\cdot a\cdot W\cdot t, \quad cm^{-2}, \tag{2}$$

$$d_T = K^{\alpha}_{wet}\cdot a\cdot C\cdot t, \quad cm^{-2}, \tag{3}$$

where K^{α}_{dry} - efficiency of alpha-particle registration by the detector in case of the thin target, rel. units;

K^{α}_{wet} - proportionality coefficient for registration of alpha-particles in a solution, cm;

a - Pu specific activity, alpha decay/(g s);

W - Pu density on the target (TIS), g/cm^2;

C - Pu concentration in a solution, g/cm^3;

t - detector irradiation duration, s.

PTD-TIS Method sensitivity gain is defined by the ratio:

$$T/d_T = (1/2)\cdot(K^{\alpha}_{dry}/K^{\alpha}_{wet})\cdot W/C. \tag{4}$$

Based on the distribution coefficient definition, k,(eq.1) and consideration of the evident relationship

$$W = C_T\cdot w, \tag{5}$$

where w-TIS thickness, gTi/cm^2,

we obtain: $$T/d_T = (1/2)\cdot(K^{\alpha}_{dry}/K^{\alpha}_{wet})\cdot k\cdot w. \tag{6}$$

There were experimentally defined the coefficients:

$$K^{\alpha}_{dry} = 0.4;$$

$$K^{\alpha}_{wet} = 9.0 \times 10^{-4} \text{ cm}$$

for electrochemically etched CR-39.

We obtain $T/d_T = 170$ for TIS of the thickness 20 $\mu gTi/cm^2$ using mean logarithmic value $k_{lg} = 3.9 \times 10^4\ cm^3g^{-1}$.

Detection limit for Pu^{lg} in water media is determined by background density of tracks on CR-39. Assuming $3\sqrt{T_{bgr}}$ as a detection limit criterion, we obtain (from eq.2) minimal detectable activity of thin target (TIS) during exposure time(t):

$$A_{min}^{TIS} = a\cdot W_{min} = 6\sqrt{T_{bgr}}/(K^{\alpha}_{dry}\cdot t), \ Bq\cdot cm^{-2}. \tag{7}$$

At t = 1day

$A_{min}^{TIS} = 1.2 \times 10^{-3}\ Bq\cdot cm^{-2}$ ($3.3\times10^{-14}\ Ci\cdot cm^{-2}$)

or

$W_{min}(Pu\text{-}239) = 5.3\times10^{-13}\ g\cdot cm^{-2}$.

Assuming TIS background contamination by alpha-irradiators does not exceed these values and taking into consideration (1),(5) and (7) we obtain a detection limit for Pu in water:

$$A_{min} = A_{min}^{TIS}/(k \cdot w), \quad Bq \cdot cm^{-3}. \qquad (8)$$

For irradiation exposure being one day and TIS thickness 20 $\mu gTi/cm^2$:

$$A_{min}\ (Pu) = 1.5 \times 10^{-3}\ Bq \cdot cm^{-3} (4 \times 10^{-11}\ Ci/l),$$
$$C_{min}\ (Pu\text{-}239) = 7 \times 10^{-13}\ g \cdot cm^{-3}.$$

Uranium determination

A lavsan PTD having a covering TIS layer was exposed to the solution studied and then irradiated by thermal neutrons in a reactor or other source.

Sensitivity gain compared to the "wet" method is defined by the expression:

$$T/d_T = (K_{dry}/K_{wet})W/C = (K_{dry}/K_{wet}) \cdot k \cdot w. \qquad (9)$$

Using the data K_{dry} and K_{wet} for lavsan [7] and data on k_{tg} from eq.2, we obtain $T/d_T = 790$ for TIS of the thickness 20^{tg} $\mu gTi \cdot cm^{-2}$.

Uranium determination sensitivity gain is realized by the corresponding lower necessary neutron fluences.

Its detection limit is connected with natural contamination of TIS by uranium ($C_{Tbgr} = 10^{-7}$ gU/gTi) and when the distribution coefficient is considered (eq.1) it equals :

$$C_{min} = C_{Tbgr}/k \simeq 3 \times 10^{-12}\ g \cdot cm^{-3}.$$

Thus, a limit of U detection in solutions does not depend on a TIS thickness and two orders lower than a detection limit of "wet" method, where the limiting factor is the natural contamination of lavsan PTD by uranium (10^{-10} $g \cdot cm^{-3}$).

Conclusion

The performed experiments resulted in the development of PTD-TIS method to define microconcentrations of U and Pu in water media.

The method is based on the developed techniques of CR-39 type detector and thin-layer inorganic sorbents based on titanium hydroxide, the experimental results on optimization of CR-39 electrochemical etching and Pu-239 irradiated by alpha-particles, and the results of U and Pu behaviour study in the system water solution - TIS.

Application simplicity, high sensitivity and the low limit of U and Pu detection - are pronouncing characteristics of the PTD-TIS method, providing its applicability to solve the problem of nuclear reactor safety, radioecology and other fields of research.

References

1. А.В.Воронов, Н.П.Кочеров, Щ.Е.Шигаев, Н.Н.Алексеев, В.С.Никифоренко. Опыт изготовления и свойства детекторов заряженных частиц на основе диэтиленгликольбисаллилкарбоната //Препринт РИ-195. М., 1986. 17 с.
2. A.Guhr, O.Sarenio, A.Rimpler, R.Lehmann. An Improved CR-39 Detector Material with Low Background and It's Use in National Radiation Protection Monitoring Programmes // Рабочее совещание "Твердотельные трековые детекторы ядер и их применения" (сборник докладов). Дубна, 1990. Д13-90-479. С. 37-40.
3. L.Tommasino, G.Zapparoli, R.V.Grifith and A. Mattei. Electrochemical Etching – II. Methods,Apparatus, Results //Solid State Nuclear Track Detectors. – Proc. 10th Int. Conf.Lyon, 1979. Oxford e.a., 1980. P.425 – 433.
4 S.A.R.Al-Najjar, R.K.Bull and S.A.Durrani. Some Chemical and Electrochemical Etching Properties of CR-39 Plastic //Ibid. P. 323-327.
5. G.Espinoza, A.Moreno and J.I.Golzarri. Uranium Determination in Water using Solid State Nuclear Track Detectors //Solid State Nuclear track detectors.-Proc. 11th Int. conf. Bristol, 7-12 Sept., 1981. Oxford e.a., 1982. P.591-595.
6. M.Humar, T.Šutej, J.Skvarč, L.Mljač, M.Radež, R.Ilič. Indoor and Outdoor Radon Survey in Slovenia by Etched Track Detectors //Preprint Submitted to: Radiation Protection Dosimetry (5 th Int. Symp. on Natural Radiation Environment. Salzburg, 1991). 21 p.
7. Дьяков А.А., Ростовцев В.Ю., Бетенеков Н.Д., Ипатова Е.Г. Разработка высокочувствительного метода определения делящихся материалов в водных средах с использованием тонкослойных неорганических сорбентов и пластиковых трековых детекторов. // Материалы 3 Всес. школы-семинара по ТТД и АРГ. Одесса, 5-10 сент. 1991. – 6 с.

DETERMINATION OF URANIUM IN SOME LIQUIDS BY USING SSNTD

Z. En, N. Jumaev and M. M. Usmanova
Institute of Nuclear Physics of the Uzbek Academy of Sciences
Tashkent

To determine some impurities in liquids different "dry" methods of analysis are known to be developed to a great extent. However, when a dry residue obtained, contamination of a sample to be studied and uncontrolled losses of determined elements are possible. For this reason the "wet" techniques of analysis are of practical interest. At present there are a few publications devoted to a "wet" approach to determine some impurities by SSNTD. Among them due attention should be paid to the survey article by A. A. Djakov (Radiochimiya, N. 4, 1987), in which various information on determining uranium by the "wet" techniques with the use of the plastic track detectors has been systematized.

It is known that in a neutral solution the uranium particles are of high sorption activity on a detector surface and tend to formation of the clusters causing the stars of tracks to occur. This occurrence leads to a non-uniform distribution of tracks and, as a consequense, to a high distortion of results. Our experiments show that in distilled water because of high sorption of the uranium particles on the lavsan surface the density of tracks is approximately three times higher than that to be expected. One of the ways to avoid the formation of the clusters is the addition of some acid to the neutral solution.

In this work a possibility of uranium concentration to determine by a "wet" technique in water and aqueous solutions of alkali and salts by means of fission fragment registration using a lavsan detector has been studied. A lavsan film to be placed into analysed liquid was set to a reactor for thermal neutron irradiation ($\Phi \leq 10^{16}$ cm^{-2}).

All the experiments were based on the "input - determine" principle. Amounts of uranyl nitrate [$UO_2(NO_3).6H_2O$] were being added into alkali solutions (0 - 6.0 N KOH) available until its concentration riched $1.10.10^{-5}$ $g.cm^{-2}$. The irradiation times were from 2 to 15 hours. It has been found that when the KOH concentration was lower than 0.5N the stars of tracks took place. When the KOH concentration was higher than 0.5N the distribution of tracks was uniform.

Table.

Comparison of the concentrations of uranium introduced into KOH solutions with these obtained experimentally

irradiation time, h	concentration of KOH, N	uranium concentration, $\times 10^{-6}$ g.sm^{-3} input	determined
2	0	5.79	5.89 ± 0.30
	0.5	- " -	5.63 ± 0.26
	1.0	- " -	6.18 ± 0.30
	2.0	- " -	5.47 ± 0.36
	4.0	- " -	5.26 ± 0.40
	6.0	- " -	5.71 ± 0.50
5	0	5.79	5.69 ± 0.32
	0.5	- " -	5.39 ± 0.32
	1.0	- " -	5.36 ± 0.28
15	0	5.79	6.20 ± 0.50
	0.5	- " -	5.66 ± 0.44
	1.0	- " -	5.82 ± 0.25

In the table given above a comparison of the concentrations of uranium introduced into the KOH solutions and these determined in our experiments are shown.

The relative root-mean-square deviation of the measurements is $S_r \leq 9$ % for P = 95 %.

The determination limit of uranium depends on its content in the detector used. The content of uranium in the lavsan films is of approximately 10^{-8}%. So its determination limit is of n.10^{-10}g/g.

The experiments on the registration of the fission fragments in a NaCl solution have been carried out as well. The concentration of NaCl was equal approximately to that of sea water. Two cases were considered: the NaCl solutions with and without addition of some nitric acid. In both the cases the results of the measurements coincide.

Thus in this work the possibility to determine uranium concentration in some liquids, such as aqueous alkali and salt solutions, by using SSNTD has been studied. It is shown that for the concentration of these solutions higher than a certain "critical" value, the distribution of tracks is uniform. This case allows, in accounting the number of tracks, one to scan the surface of a detector and to increase the number of observation points, thus improving the accuracy of analysis. The possibility to obtain such a uniform track distribution is one of the advantages of "wet" analysis approach.

THE USE OF SSNTD FOR SOLVING ECOLOGICAL PROBLEMS ARISING AT NPP OPERATION

A.V.Zvonarev, V.G. Liforov, E.Ja. Smetanin

Institute of Physics and Power Engineering.

Obninsk.

Two examples of using the SSNTD method for solving the problems arising at NPP operation are considered:

1) Cross-section measurements of transactinides with large half-lives for solving the problem of their transmutation.

2) Detection and determination of concentration of fissile isotopes penetrating into the ground as a result of releases, accidents at NPPs and reprocessing plants.

1. The problem of transactinide burning out in fast reactors calls for providing reliable data on fission cross-section for these nuclides on neutron spectra characteristic of fast reactors. Verification of neutron constants was performed at the critical assemblies CBR [1] and BR-1 [2] by means of measuring the ratios of ^{237}Np, ^{238}Pu, ^{240}Pu, ^{241}Pu, ^{242}Pu, ^{241}Am, ^{243}Am, ^{244}Cm to ^{235}U fission cross- section at neutron spectra close to that in the BN-600 reactor core and "harder" one (E_{av}=1MeV). For the measurements the SSNTD method was used with calibrated layers of the above nuclides 10^{13}-10^{14} 1/cm^{2}thick. The thicknesses chosen make unnecessary the corrections for the effects of cross-section selfscreening, as well as do not call for special measures for ensuring work safety, because layer activities do not exceed MSA (minimum significant activity). The SSNTD method in this case has substantial advantages over other ones, e.g., the activation detectors method or fission chambers. A possibility to use microgram quantities of the materials under investigation, reduces considerably the expenses for their purchasing.

In the experiments at the CBR and BR-1 rigs a common track detector design with a calibrated layer was used comprising a fission fragments detector, a calibrated layer of a nuclide investigated and a collimator placed between them. Sodium silicate glass was used as the track detector. Track counting was carried out at the microcomputer-controlled scanning microscope. Track density reached 10^5 1/cm^2.

In Table 1 the results of measurements of some cross-section ratios and their comparison with calculated data are presented. In the upper line of the table the spectral index of the uranium-238 fission rate to uranium- 235 is given characterizing neutron spectrum "hardness".

Table 1.

	BR-1(plutonium core)		CBR-18 (thorium core)	
	Experiment	Calculation / Experiment	Experiment	Calculation / Experiment
^{238}U	0.165 ± 0.005	0.99 ± 0.04	0.0261 ± 0.0011	1.057
^{237}Np	0.771 ± 0.023	1.04 ± 0.04	0.232 ± 0.011	1.184
^{240}Pu	0.877 ± 0.026	0.91 ± 0.03	0.272 ± 0.07	1.035
^{241}Pu	1.29 ± 0.04	1.02 ± 0.03	1.332 ± 0.035	0.983
^{242}Pu	0.658 ± 0.02	0.98 ± 0.03	0.191 ± 0.07	1.00
^{241}Am	0.825 ± 0.025	1.00 ± 0.04	0.201 ± 0.07	1.04

2. Work on studying ground samples was a logical extension of work on using SSNTD in the BN-350 reactor coolant samples studies for their fissile nuclides content [3]. The point was to solve the problems of preparing the samples to be examined and the reference samples. Work on studying the dependence of the fission fragments recording efficiency on ground grains size, on fissile nuclides quantity, on the reference sample preparation method was carried out. The ground samples from the regions exposed to effects from the accidents at the Chernobyl NPP and the "Mayak" IP (Chelyabinsk region) were investigated. The samples were in the form of powder with a definite grain size, that was placed into a container with the SSNTD (quartz glass) mounted in it. The containers were placed into the BR-1 reactor thermal column and the central channel of the BR-1 core. The method allowed one to determine both the fissile nuclides absolute value (g/g) and the isotopic ratio of these nuclides (uranium-235 + plutonium-239 and uranium-238). Sensitivity of the method is determined by natural uranium content in the grounds (uranium-238 10^{-6} g/g, uranium-235 10^{-8} g/g) unless any steps on chemical separation of uranium and plutonium from the grounds analyzed are undertaken.

Table 2 presents some results of ground analysis taken in the "Mayak" IP area and, for comparision, in the Kaluga region.

Table 2.

Chelyabinsk region		Kaluga region
Sample N1	Sample N2	Sample N3
$1.3*10^{-6}$ ± 20% g/g natural uranium	$4.0*10^{-6}$ ± 20% g/g isotope ratio (0.8 ± 0.15)% uranium-235/uranium-238	$1.0*10^{-6}$ ± 20% g/g natural uranium

The above examples of the SSNTD use confirm large potentialities of this method for solving the problems related to environmental control.

REFERENCES

1. Golubev V.I., Dolgov E.V., Efremov A.I. et al. Calculational and experimental validation Studies of Irradiation Devices for Cobalt-60 Buildup. Voprosy atomnoy nauki i tekhniki. Ser.Nuclear Constants, 1991, issue 4, pp. 56-70.

2. Zvonarev A.V., Kolyzhenkov V.A., Liforov V.I. et al. Experimental and Calculation Studies of Cross-Section Ratios for a Wide Set of Nuclides at the BR-1 Reactor. Voprosy atomnoy nauki i tekhniki. Ser.Nuclear Constants, 1990, issue 3, pp. 67-79.

3. Zvonarev A.V., Liforov V.G. The Use of the SSNTD Method in Studies at Power and Research Reactors. Proc, of the Working Meeting on "Solid-Stak Nuclear Track Detectors and Their Applications". Dubna, 1990, pp. 113-116.

THE APPLICATION OF TRACK METHODS FOR ALPHA-EMITTERS STUDIED IN ZONES AFFECTED ON NUCLEAR TESTING AND TECHNOGENIC ACTIVITIES IN KAZAKHSTAN.

IVAN CHASNIKOV

High Energy Physics Institute of
Academy of Sciences of Republic of Kazakhstan

It is no secret nowadays that the mining and processing of uranium and the production of nuclear fuel and nuclear weapons components are carried out in many regions of Kazakhstan. Testing of nuclear, hydrogen, neutron and other weapons of mass destruction took place in the eastern, western and other parts of Kazakhstan for 40 years. Many towns of our republic can be considered as zones of ecological disaster, where large-scale industrial enterprises throw millions of tons of harmful substances into atmosphere. If we recall additionally the Aral sea and other problem areas, it will be difficult to find a pure ecological zone in Kazakhstan. There is no other country or republic where all the problems are closely connected as in Kazakhstan. Unfortunately the levels of radiation and their negative influence on human health and environment were not studied well enough. Practically speaking, there is no information on the complex influence of different harmful factors on people and nature.

The specific regularity of the course of deceases and infant mortality which are the indicators of society health levels and environment safety were found in some regions of Kazakhstan. It should be noted that such effect was not observed in republics and countries situated far from the nuclear test sites. Some publications pointed out that the maximum of infant mortality was observed 22 - 25 years after the period of the most intensive nuclear weapons testing (1953-1956) and that these facts are connected with symptoms of irradiation of Kazakhstan citizens in the second generation.

Different programs for the rehabilitation of irradiation victims are being worked out by the state and public organizations among them the Republican program "Ecology" and the program "The revival of the Earth and Human Being" suggested by the International anti-nuclear movement "Nevada-Semipalatinsk". These programs include studies of alpha-emitters in the zones of ecological disaster with the help of nuclear track detectors. In the Institute of High Energy Physics there is a well equipped group of scientists studying nuclear interactions at high energies. These people are able without any difficulties to carry out the investigation of alpha-emitter characteristics.

Such work is necessary to determine the exposition dose power at the expense of the inner irradiation of a person and to define ecological disaster zones. There will be received the data concerning the concentration of radio-nuclids in the organism of a human being in different years as a dependence on a concrete place and mode of life.

It is planned to use in work different track detectors. Taking into account that Kazakhstan has suffered not only from nuclear explosions at its territory but from the China test-site "Lop-Nor", it is important to study the concentration of Plutonium and other alpha-irradiators influencing the objects of the environment.

I have been charged to invite the participants of this meeting and everyone who wants to take part in the work of the Republic Conference on the programme "The revival of the Earth and Human Being" and as far as possible make some contribution to the realization of the presented Programme.

DETERMINATION OF THE ENVIRONMENTAL RADIOACTIVE CONTAMINATION BY USING RADIOGRAPHY

I.G. Berzina

Institute of Railways Transport, Moscow, Russia, CIS

Technological activity of man has led to complicated ecological problems caused by the activity and found in the contamination of environment. One of the sources of such a contamination is the radioactive pollution.

In carrying out the measurements to determine the radioactive environmental contamination, it is necessary, in addition to evaluation of the concentration of the radioactive elements, to determine their local and spatial distribution.

The method giving such possibilities is a radiography one (Flerov and Berzina, 1979; Recommendations, 1991).

The sensitivity of the (n,f) radiography technique to evaluate the concentration of the fission elements (in absence of the interfering ones) is,for example, of 10^{-10}% for uranium under natural conditions. The spatial resolution of the technique is of several microns, which exceeds considerably the possibilities of other techniques of elemental analysis.

In general, a detector reveals a set of different track densities corresponding to the places of the fission element inclusions in an object under study, the image form permitting the evaluation of the fission element concentration and true inclusion's sizes.

In nature there can be many accumulators of radioactive elements, such as rocks, soils, waters and plants. Radioactive elements may be found in environment either in natural or thechnologically processed form. In the first case, the most distributed element is uranium,

whereas, in the second one, either uranium, plutonium, or both the elements are present in dependence on the processing technology.

In field work the determination of concentration and the identification of fission elements can be carried out by a prolonged exposure of a detector in a definite air volume. In this case the plants' leaves can serve as the accumulators of information about the radioactive environmental contamination.

Accumulation of microelements by plants takes place during a full biological cycle consisting of absorbing the elements together with the nutrients from soil by the root system, processing these elements and polluting them in the form of an assimilate onto the surface plant parts. After that the microelements return into soil with fallen leaves, accumulate in the humus and may penetrate once more into plants during the next vegetation period. If there is a technogenic source of the environmental radioactive contamination, the income of the radioactive elements into a productive soil layer may be due to the surface water streams, rain falls, dust sediments from atmosphere, etc. The dust settles down on plants' leaves by gluing to the adhesive parts of plants, and accumulates in them during a vegetation period. This fact is of great importance, since it enables one to reveal the radioactive contamination in agricultural plants and identifies the ways of getting the radioactive contamination into plants.

The dust which settles down after a nuclear accident can contain various fission elements in the different concentration rates. In such a case there is the problem of evaluating the concentartions and determining the spatial distributions of uranium and plutonium in soils and so-called ' hot particles'. As it has been found, the correlation between these elements' concentrations in 'hot particles' is not a constant factor. However, the raiography is khown to enable one to evaluate the concentration and determine the spatial distribution for each element under study. By using a double exposure of the object investigated with changing a detector, one

determines firstly the total distribution of all alpha-sources of uranium and plutonium and searches afterwards for the alpha-radiation from plutonium nuclei. To evaluate the concentration and determine the spatial distribution of plutonium during the secondary exposure, the screen of a definite thickness, for instance, made from lavsan, is placed between the object and detector, to absorb the α-particles emitted by the uranium nuclei. The α-particles have the energy less that these emitted by plutonium which are only registered by the detector in such a case. Then, the two elements can be separated by using the substraction method.

The investigations carried out have showed that, from the group of the fission elements, only uranium has been found in the plants growing near uranium deposits. As examples, in Figures 1 and 2 the distributions of uranium over the leaves of poplar trees and wormwood growing near a uranium deposit are shown. In these figures one can see the dispersed uranium distributions throughout the green mass of the leaves and their manifestations with the increasing concentrations in both veinlets and assimilate secretions. Besides, the uranium-containing inclusions having settled down from air are seen there. If uranium is absent in soil and gets onto a plant in the form of dust, its distribution over a leaf's surface does not follow the leaf's macrostructure. Such a distribution of uranium over a leaf of a poplar tree growing about 20 km from a uranium deposit is given in Figure 3.

The radioactive dust has also been found on the plants and in the soils after Chernobyl accident. In this case uranium and plutonium have been determined in the form of 'hot particles' alloyed with other components of the reactor materials. As it has been established, neither uranium nor plutonium does not penetrate into the plants, growing in the region, through the roots. The 'hot particles' either keep being in the soil, are gone up with wind as dust and reach the plants from outside, or are carried by the water streams. The fission elements on the leaves, in the roots and in the soils manifest themselves

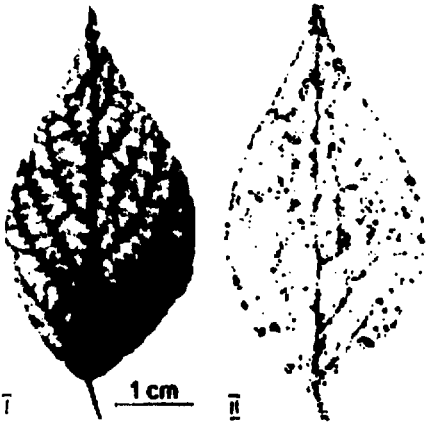

Figure 1. A uranium distribution over a leaf of a poplar tree growing near a uranium deposit: I - a poplar leaf; II - a detector

Figure 2. A uranium distribution over a leaf of wormwood growing near a uranium deposit: I - a wormwood leaf; II - a general detector's view; III - a part of the detector under high magnification

in the form of 'hot particles'. Figure 4 presents characteristic total distributions of uranium and plutonium in the 'hot particles' in the soils and on the plant surfaces in the Chernobyl accident region. One can see the particles' parts not containing radioactivity, alloyed with the radioactive ones.

By using (n,f)-radiography, the total concentration measurements of fission elements in the soils in Chernobyl zone have been carried out. The data obtained exhibit satisfactory agreement with the data due to neutron-activation analysis (NAA) to determine the uranium concentration, C_U, measured at the same places of the plant sampling. According to the data available by both the methods, the average concentration of fission elements in soil is 10^{-5} %. Table 1 represents the data on the determination of the fission element concentration, C_{fe}, obtained by (n,f)-radiography and the ones on the uranium concentration C_U measured by using NAA.

Together with the concentration of fission elements, that of cesium has been measured in the rock under study. In determining the cesium concentration, as well as evaluating the background which was of 25 imp/h, the exposure time was 1000 s for all samples.

Table 1

The concentration of uranium, plutonium and cesium in the samples from Chernobyl zone

Number	$C_{fe} \cdot 10^{-5}$ %	$C_U \cdot 10^{-5}$ %, NAA	C_{Cs}, imp/h
1	1.06	0.99	390
2	2.38	0.95	107
3	2.64	1.00	766
4	0.53	0.85	background
5	0.66	0.81	256
6	4.23	1.21	background
7	1.32	1.89	background
8	0.53	1.00	32

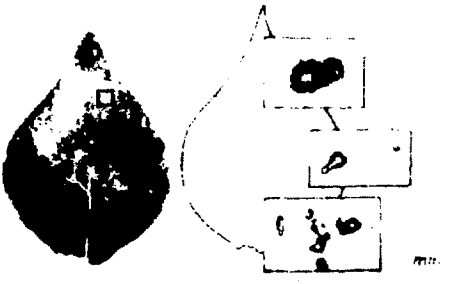

Figure 3. A uranium distribution over a leaf of a poplar tree growing ~20 km from a uranium deposit: I - a poplar leaf; II - a detector

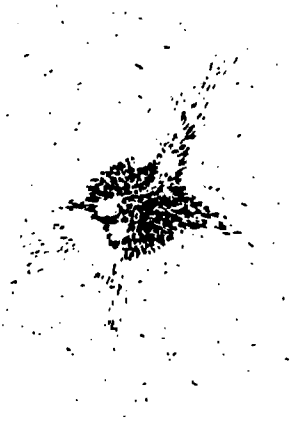

Figure 4. A characteristic distribution of uranium and plutonium in the 'hot particles' found in the soils of Chernobyl zone

The data presented in Table 1 makes it clear that at present a higher cesium concentration does not correspond to a higher uranium one. It seems to give evidence in favour of different migration ability of uranium, plutonium and cesium when they are present in soil.

Determination of spatial distributions of radioactive elements in the plant leaves after Chernobyl accident in 1986 and 1991 has shown that in due course a redistribution of the radioactive elements, in particular, of cesium, occurs. So, in Figure 5 is presented the cesium distributions in leaves,obtained in 1986 and 1991. If immediately after the accident the gamma-active elements were in dust settling down on the plants' leaves, in 1991 the elements penetrated into the plants through the root system during the biological cycles as described above. The indentification of the radioactive radiation was carried out by means of the lead screens of different thickness, placed between the object studied and an X-rays detector. By evaluating the absorbed energy, dE, over the lead screen thickness, dE/dX, it was established that in 1991 the main gamma-source is cesium.

Variuos plants turn out to absorb cesium through the roots in different manners. In some cases the leaf's macrostructure is revealed, in other ones cesium can only be found in peripheral parts of leaves and at their bottom, in other cases cesium does not penetrate into leaves during the same time. The latter cases are of great

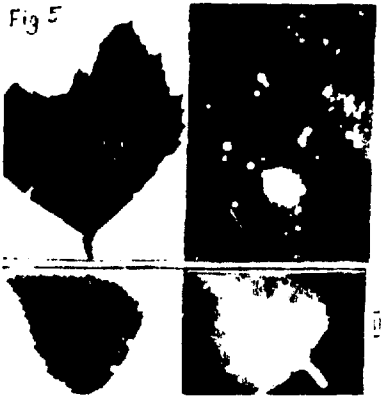

Figure 5. A distribution of the gamma sources in the plant leaves in Chernobyl zone: I in 1986; II in 1991

practical value, for the agricultural plants not accumulating cesium in the productive parts can be selected.

As is shown above, the spatial distribution of environmental radioactive contamination may change in due course. In order to determine the territories safe for men living, it is necessary periodically to carry out a combined high-sensitive control of environment. Existing methods applied nowadays to evaluate environmental radioactivity do not provide complete information about availability of the local α-sources. It is the radiography method that allows one to determine the ecological environmental radioactive contamination with a high sensitivity, accuracy and visuality. The plant leaves can serve as the accumulators and adequate markers of the radioactive contamination of an area with α-radiation sources, there being a real possibility to evaluate the linear sizes of the sources.

References

Flerov, G.N. and Berzina I.G. (1979) Radiography of Minerals, Rocks and Ores. Atomizdat, Moscow. (in Russian)

The GSI Recommendations. Uranium Content and Spatial Distribution in Samples: An MI 2172-91 Measurement Technique. (1991). Gosstandart, Moscow. (in Russian)

DETERMINATION MICROQUANTITIES OF Pu WITH THERMAL NEUTRONS AND GAMMA-RAYS

V.P.Perelygin, Yu.T.Chuburkov, Yu.S.Korotkin, I.Zvara, Z.Szeglowski and Yu.Ts.Oganessian

Joint Institute for Nuclear Research, 141980 Dubna, Russian Federation

Man-made plutonium, in particular the ^{239}Pu isotope due to atmospheric nuclear explosions, atomic power and atomic engine reactor accidents, failures in the processes of chemical treatment of nuclear reactor fuel and other reasons provides dangerous local and significant global level of *Pu* content in the environment. In accordance with our estimations the averaged concentration of *Pu* at the Earth surface now is about 10^{-13} g/g. This value much exceeds the concentration of natural *Pu* as determined in 1991 by authors [1,2] at the level $(2\ 5)\cdot10^{-16}$ g/g for deep underground rocks and hot spring water from Salton Sea. In routine analysis of surface specimens these authors [1,2] obtained the typical value of *Pu* concentration at the level of $\approx10^{-13}$ gram per gram [3].

Now the daugerous level of *Pu* concentration is estimated to be about $(1\text{-}2)\cdot10^{-12}$ g/g. Our work was stimulated by the Chernobyl event which produced the fallout of dangerous amount of radionuclides, in particular, *Pu*, in large regions of Ukraine, Belorussia and also Russian Federation. The man made *Pu* widely distributes and redistributes at the Earth's surface, now it starts to take part in the soil cycle, surface water cycle and biological cycle. Now due to these processes one can't exclude the formation of dangerous secondary locations of *Pu* at the level $1\text{-}2\cdot10^{-12}$ g/g as compared with "normal" level $\sim10^{-13}$ g/g.

The most widely applied technique of *Pu* exploration for Chernobyl samples is based on direct registration of α particles due to *Pu*, *Am* nuclei α decay with the nuclear emulsions, plastic track detectors (4-7). It allows one to find α-active "hot particles" with diameters of 0.01 0.8 μm, but does not provide the sensitivity of *Pu* exploration at the level higher than 10^{-8} g/g [4 7]. To provide the sensitivity level up to 10^{-12} g/g of *Pu* one must use about 10^3 grams of soil specimens for chemical treatment and further many hour registration of α decay of *Pu* isotopes by means of semiconductor detectors. One can see that such method could not provide quick and effective analysis of many hundreds of specimens from Chernobyl fallout area, or other damaged regions. For radical increase in productivity of *Pu* exploration in environmental samples we choose another experimental approach, based on the separation of plutonium from the specimens, but due to much higher sensitivity, we use only few grams of specimens being investigated. Our method also includes the procedure of chemical separation of plutonium from the specimens controlled with short-lived ^{236}Pu α active tracer but due to much higher sensitivity as compared with α-decay registration technique, only few grams of representative specimens are necessary. In fig. 1 the dependence of a number of registered fission fragment tracks on the number of ^{239}Pu nuclei at the preparation for the thermal neutron flux 1.3×10^{15} is presented. As one can see from fig.1, the sensitivity of our method is much higher than for α-decay registration during 10 hours with semiconductor detectors for the same specimens.

In Table 1 the results of Pu determination for some Chernobyl fallout area soil specimens from North Ukraine are presented. As one can see from Table 1 the Pu concentrations varies from 10^{-13} to $5.7 \cdot 10^{-12}$ g/g.

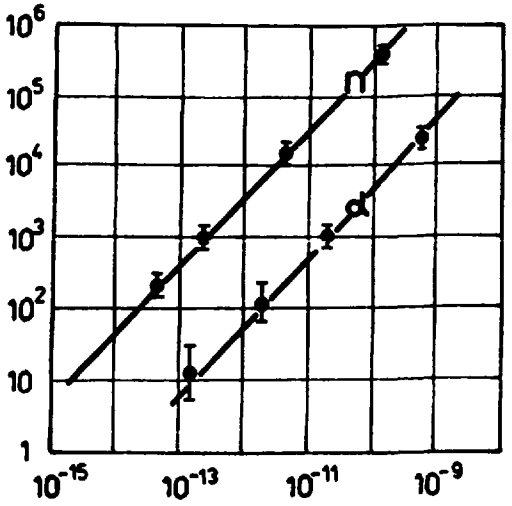

Fig. 1. The dependences of number of tracks due to thermal neutron-induced fission of ^{239}Pu on polytherephtalate detector and number of α-particle counts due to ^{239}Pu α-decay on semiconductor detector on plutonium content in thin homogeneous layers. The thermal neutron fluence was 1.3 10^{15} cm^{-2}, α-decay of ^{239}Pu was registered during 10 hours at semiconductor detector with efficiency 30%

The control on the possible minor admixtures of U and also Th nuclei was performed with intense beams of γ-rays ($E_\gamma \geq 20$ MeV) at MT-25 microtron of JINR.

The total flux of γ-rays was about 10^{19} cm^{-2} [9]. One can see that the experimental dependences of fission fragment yields for neutron-induced fission of ^{239}Pu, ^{235}U and γ-ray induced fission of ^{239}Pu,^{238}U,^{232}Th provide one unambiguous check of minor content of Th and U nuclei in extracted Pu specimens at the level 10^9–10^{10} nuclei. The present-day level of ^{239}Pu exploration sensitivity is about 10^{-13} g/g. But one can easily reach the level of sensitivity up to 10^{-15} g/g - by using higher neutron fluences - 10^{18}–10^{20} cm^{-2}, some non-organic glasses, crystals - with a very low content $\geq 10^{-14}$ g/g of natural uranium admixtures.

The technique being developed is based on the JINR experience in nuclear chemistry and dielectric track detector study. We used the unique combination of the Joint Institute for Nuclear Research basic experimental installations, pulsed reactor facilities (IBR-1, IBR-2), microtron MT-25 and cyclotron U-200.

In conclusion the authors wish to express their deep gratitude to S.P.Shtaniko, A.G.Belov, G.V.Buklanov, G.G.Bankova for their assistance and support.

Table 1. The results of Chernobyl samples analysis

NN	sample	^{239}Pu concentr., g/g	nn	sample	^{239}Pu concentr., g/g
1.	I-1a	$4 \cdot 10^{-13}$	21.	L-2/10	$1.1 \cdot 10^{-12}$
2.	I-1	$5.0 \cdot 10^{-13}$	22.	B-3-26	$1.8 \cdot 10^{-12}$
3.	L-17/2	$4.4 \cdot 10^{-12}$	23.	A2-8	$1.1 \cdot 10^{-12}$
4.	A1-17	$5.0 \cdot 10^{-13}$	24.	L-18/2	$8.0 \cdot 10^{-13}$
5.	B1-27	$9.4 \cdot 10^{-13}$	25.	V-1/7	$5.0 \cdot 10^{-13}$
6.	B3-20	$1.6 \cdot 10^{-12}$	26.	G-1	$6.0 \cdot 10^{-13}$
7.	B3-14	$5.7 \cdot 10^{-12}$	27.	B3-43	$4.0 \cdot 10^{-13}$
8.	L-13/1	$1.5 \cdot 10^{-12}$	28.	G2-9	$5.0 \cdot 10^{-13}$
9.	L-12/2	$2.0 \cdot 10^{-13}$	29.	E2-59	$2.3 \cdot 10^{-12}$
10.	L-10/1	$1.3 \cdot 10^{-12}$	30.	A4-95	$4.0 \cdot 10^{-13}$
11.	D-6/1	$2.0 \cdot 10^{-12}$	31.	V1-5	$7.0 \cdot 10^{-13}$
12.	L-5/2	$4.0 \cdot 10^{-13}$	32.	D-7/2	$1.8 \cdot 10^{-12}$
13.	L-10/2	$4.0 \cdot 10^{-13}$	33.	L20-2	$5.0 \cdot 10^{-13}$
14.	L-2/1	$8.4 \cdot 10^{-13}$	34.	L22-1	$4.0 \cdot 10^{-13}$
15.	D-16/1	$5.0 \cdot 10^{-13}$	35.	L-11/2	$6.0 \cdot 10^{-13}$
16.	D-19/1	$1.1 \cdot 10^{-12}$	36.	D-9/2	$2.3 \cdot 10^{-12}$
17.	L-1/1	$7.0 \cdot 10^{-13}$	37.	L-4/2	$3.2 \cdot 10^{-12}$
18.	L-14/1	$1.2 \cdot 10^{-12}$	38.	L-21/1	$6.0 \cdot 10^{-13}$
19.	L-13/2	$1.3 \cdot 10^{-12}$	39.	H_2O	$\leq 10^{-15}$
20.	L-11/1	$7.2 \cdot 10^{-13}$			

References

1. M.Ganz, H.Barth, M.Fuest, D.Molzan, R.Brandt "Natural Pu-Tracks within the Continental Crust", Radiochimica Acta (1991) v.52/33, p.403.
2. M.Ganz. Diplomarbeit, Marburg, FRG (1986) p.24-57.
3. R.Brandt, private Communication, 27 March 1992.
4. R.Broda, B.Kubica, Z.Szeglowski, K.Zuber "Alpha Emitters in Chernobyl Hot Particles". Radioch.Acta (1989) v.48, p.89.
5. E.I.Knizhnik, S.G.Stetsenko, V.V.Tokarevsky "Assessment of Alpha-Activity and Alpha-Contamination of Soil Surface using Polymer Track Detectors. Abstr. of Papers of 15th Int. Conf. on Particle Tracks in Solids, ed. by P.Vater, Marburg, 3-7 Sept., 1990, p.271.
6. A.B.Akopova, N.V.Victorova, J.V.Magradze, A.A.Moiseenko, K.M.Ovtanyan, K.I.Tumanyan "Autoradiographic Study of Radionuclides in the Samples of Plants and Soils from the Area of Chernobyl Power Station", ibid, p.23.
7. V.A.Nikolaev, T.S.Potapova "Applications of Cellulose Nitrate Track Detectors for the α-activity measurements in natural water". Radiochimija (1990) N3, p.145.
8. Yu.P.Gangrsky, B.N.Markov, V.P.Perelygin "Registration and Spectrometry of Fission Fragments", M., Energoizdat, 1981.
9. Otgonsuren, L.Enchjin, Sh.Gerbish, V.P.Perelygin, R.I.Petrova "The Determination of Th Content in Specimens by means of γ-rays and α-particles", JINR Communication (1991) Dubna, P14-91-503.

USAGE OF THE SOLID-STATE NUCLEAR DETECTORS FOR STUDY OF THE DISPERSITY COMPOSITION AND FUEL FALLOUT ALPHA-ACTIVITY IN THE WATER-SOIL MEDIUMS AFTER THE CHERNOBYL ACCIDENT

N.V.Victorova*, V.V.Demchuk*, S. .Tretyakova**

*Ukrainian Hydrometeorological Research Institute, Kiev, Ukraine
**Joint Institite for Nuclear Research, Dubna

Unique character of the Chernobyl accident, in particular, a relatively long high-temperature period of the accident development caused forming of different specific fine-dispersive radioactive particles, which were heterogenous by morphology, composition and physical-chemical properties, therefore methods [1-3], that were applied for the study of global fallouts formerly, are not sufficient to examine particles described in this work. Side by side with traditional radiochemical and radio-spectroscopy methods, which allow one to obtain the integrai estimation of pollution, it is necessary to intensify the control for individual radioactive carriers - nuclear particles behavlour in the environment. In particular, the present paper deals with the main study results of the fuel fallouts radioactive particles by means of some nontraditional research methods.

It is well known, the principal advantages of methods, based on radiography, are:

- possibility for nondestructive analysis of sample;
- simultaneous determination of the radioactivity value and its localization in object;
- high sensitivity, allows one to characterize individual "hot" particles.

Proceeding from the above-stated, we've made an attempt to apply the nuclear emulsion [4] solid-state nuclear track detectors for dispersity analysis and alpha-active "hot" particles identification with example of the Pripyat River flood-plain soil, located in the Chernobyl Fallouts Near Zone.

EXPERIMENT

Thin specimens were prepared in a such way. Soil portions were dried up to the normal-dry state and the dry soil quota was sifted through the sieve onto the plate, covered with gelatine or emulsion layer. Soil was uniformly put on the all area up to forming of the thin layer, controlled visually.

Exposure duration was chosen experimentally by means of the visual observation of the hot particles alpha-activity autographs.

Dielectric detectors of CR-39 type (polyallilcarbonate) and LR-115-11 (cellulose nitrate) are widely used in alpha-radiography. As all dielectric detectors, they are characterizing by threshold sensitivity. According to Bragg's curve (energy loss in the matter dependence on particles energy), they have upper and lower limits of registered energy: minimal one corresponds to the situation when α-particles run is too small to produce the observable track after etching, and maximal one - energy at which the track etching rate (V_t) is small and it is comparable with detector material etching rate (V_t). For CR-39 this interval is equal to 0.1 - 85 MeV, and for LR-15-11 - from 0.1 to 4-5 MeV. Note, the detectors registration ability depends on critical angle (θ_{cr}), which for CR-39 is equal to 10°, and for LR-115-11 - to about 20°. Angle value can be varied according to the work regime and practically depends on the etched layer parameters.

The irradiation geometry was 2π. Registration efficiency yielded by a "thin" source is defined as $E_f = 1-\sin(\theta_{cr})$; (1)
and for a "thick" source as $E_f = \cos^2(\theta_{cr})$; (2)
("thick" source- is that one with thickness, exceeding alpha -particles range).

Detector LR-115-11 was used for preliminary registration of the alpha-irradiating particles, and CR-39 for determination of the dispersity structure, dose dependence and radionuclide composition.

There were used lavsan absorbers with 23 and 27 μm thickness for isotope separation according to alpha-particles energy. The former cuts off energies of E < 4.5 MeV, and the latter - E < 5.0 MeV.

The critical registration angle for absorbers with 23 μm thickness was equal to 52°, and for 27 μm thickness - 60°.

The detectors were etched by 20% NaOH solution at 75°C to the track diameter ~6.5 μm. The particle size with spherical track distribution in projection towards detector plane (fig.1) was determined either by maximum vertical tracks eliminated from each other or by equally directed parallel ones. Size by vertical (height) was determined by maximum spot size taking into account the minimal registered critical angle. Particle activity was determined by a number of registered events taking into account the critical registration angle.

$$h = R \cdot \operatorname{tg} \alpha, \quad (3)$$

where h - the particle height, R - the whole spot radius, α -the critical rigistration angle.

Figure 1 shows the particle image photographs, detected by CR-39. Investigated particles activity was determined by the method of total alpha-particle tracks number counting in the autograph. Since exact particles do not exist in practice, every particle was measured 16 times with different microscope table turns approximately by 30° around particles autography image

center. The mean value was accepted to be equal to an effective particle diameter. "Hot" particle diameter determination in such way was estimated by the mean-square deviation and was equal to not less than 85%.

Fig. 1. Image of the fuel particle from the river Pripyat flood-plain soils on CR-39: a. without absorber; b. with 23 μm Melinex absorber; c. with 26 μm Melinex absorber. Exposure duration was equal to 30 hours. The irradiation angle was 2π

Reliability of conducted measurements was checked by the direct control of individual particles with usage of microscope MPE-2. Results of indirect particles size determination and direct measurements are shown in table 1.

Investigated particles activity was determined by the method of total alpha-particle track number counting in the autograph.

Table 1.

Estimation of particle diameters by direct and indirect methods

Hot particle number	Particle diameter (μm)	
	Method of the parallel tracks on autograph	Direct method
1	171.0	176,5
2	78.9	73.0
3	77.3	76.6
4	71.2	70.4
5	63.3	58.8
6	56.1	55.7
7	48.9	49.5
8	41.6	38.0
9	36.9	36.7
10	31.0	29.2

RESULTS

Soil and bottom sediments sampling to explore dispersive and radionuclide characteristics was carried out in the bench-mark river Pripyat flood-plain areas. Sampling was conducted by means of the pipe sampler with diameter equal to 50 and 25 mm. It is implied that "hot" particles are subdivided into 2 particle classes:

1) particles of condensation origin, formed on the condensation aerosol nuclei and secondary particles, formed on the soil complex particles in consequence of exchangeable radionuclide forms sorption mechanism;

2) fuel containing particles, consist of disparaged fuel materials, fuel-nonactive carrier complexes (graphite, concrete, etc.).

According to their nuclide composition, purely Cs particles belong to the first class. Nuclide structure of the second class corresponds to the radionuclide content of irradiated fuel. In consequence of nonactive carriers presence in the second class particles, their real size exceeds calculated size in some times (calculation of Ce-144, Eu-155, and total Pu). Condensation particles has surface activity distribution: $A \sim f(R^2)$; fuel containing (especially within ultra dispersion region - <3-5 μm) volume $A \sim f(R^3)$.

The 1st class particles number to the 2nd class number ratio for Pripyat near flood-plain zone is equal to 10-25 and 75-90% respectively.

Hot particles size distribution corresponds to the logarithmic normal one. The cumulative distribution is fitted on the straight line in the log-log scale.

Note should be taken that hot particles in fine-dispersive region are presented mainly by condensation beta-irradiated particles <2-5 μm and particles with size > 5 μm mainly correspond to fuel composition of 10-20% fuel content.

REFERENCES

1. Bychovsky A.V., Zaraev O.M. Gorachiye aerozolnye chastitsy pri tekhnicheskom isspolzovaniyi atomnoi energiyi. - M.: Atomizdat, 1974, 230 p (In Russian).
2. Styro B.I., Gharbalauskas Ch.A. et al. Atomnaya Energiya, 1963, v.15, N.3, p.262-270 (In Russian).
3. Styro B.I., Vebra E.Yu., Shopauskas K.K. Atomnaya Energiya, 1964, 19, N 6, p.528-536 (In Russian).
4. Akopova A.B. et al., Nucl. Tracks and Rad. Measur., 1991, v.19, N 1-4, p 733-738.

ON STUDY OF DISPERSE AND RADIONUCLIDE CHARACTERISTICS OF CHERNOBYL FALL-OUT PARTICLES BY MEANS OF MACRO-RADIOGRAPHY

V. V. Demchuk,* N. V. Victorova,* V. V. Morozov,* E. B. Ganja,*
*Ukrainian Hydro-Meteorological Research Institute

The character of contamination of close-in Chernobyl NPP zone is mainly determined by dispersion of fuel materials from 4-th block reactor. At the same time considerable quantity of gas and volatile radionuclides was released and distributed separately due to high temperature during the accident and some days after April 26, 1986.

Radioactive particles including dispersed fuel particles, condensed and secondary sorbed ones are potential secondary source of contamination of biotic and abiotic environmental systems in NPP zone. The mechanical and physic-chemical stability of these particles in environmental conditions together with ion exchange processes in soil complexes determines the dynamics of radionuclides transformation and therefore a number of essential parameters for radionuclides migration modeling.

A proper description of secondary source of water-soil system contamination and process of radionuclides transport outside 30-km zone require detailed study of structure, forms and density of environment contamination by aerosol solid state fall-out. The investigations of dispersive, radionuclide and physic-chemical properties of radioactive particles which have been carried out by number of institutions were of qualitative and estimative character. Only some individual particles of 10-20 μm size were examined because of difficulties in separation and identification of ultra-dispersed ones (less than 5-10 μm).

But according to preliminary estimations the share of the fraction <10 μm in total storage of hot particles in soil varies from 40% to 70% depending on the site under investigation. Hence, to assess migration parameters and stability of solid fall-out in environmental conditions one should study the whole range of dispersed particles.

An assessment of dispersive and radionuclide characteristics by means of contact radiography allows to identify the particles in range of ≥0.1 μm with activity of ≥0.01 Bq/particle. An UkrHI research team in collaboration with scientists from NRI (Kiev), JINR (Dubna) and Erevan Institute of Physics developed the methods of ultra-dispersed particles identification by means of contact radiography and registration by solid state track detectors.

The X-ray films RT-5, RT-6, RM-V were used as detectors. The method under consideration is based on ability of nuclear radiation to form an invisible image on X-ray film, which becomes visible after film is developed. That

invisible image is formed mainly by β-radiation of fission products contained in fuel particles. α-radiation practically doesn't contribute to formation of image due to self-absorption in thick sample layer and comparatively low (3-4 orders lower) specific activity respective to γ and β-radiation of such fission products as ^{137}Cs, ^{90}Sr-^{90}Y, ^{144}Ce-R, ^{106}Ru-Rh,etc.

An isotopic content of fuel particles from nearby Chernobyl NPP zone and contribution of each nuclide to total β-activity are presented in table 1. An isotopic content was calculated out of 4-th NPP block loading on April 26, 1986. As one can see in table 1 two isotopes are mainly responsible for image on X-ray film: ^{137}Cs - 47.9%, ^{90}Sr-Y - 39.0%.

Taking into account that efficiency of registration of β-particles of energy $E_{max} > 2.8$ MeV 2.5 times less than in case of ^{137}Cs-particles (E_{max}>550 MeV), one can easily neglect registration of high-energy particles of Ce-Pr and Ru-Rh chains which totally contribute some 17%. The contribution of two main radiances therefore can be estimated as 55% for ^{137}Cs and 45% for ^{90}Sr-Y.

In brief the procedure of contact macro-radiography is as follows. The specimen i.e. environmental sample quota with fuel particles be exposed in close contact with X-ray film and after film is developed the image (i.e. macro-radiogram) is ready. To get good radiograms which fit the standards of resolution, sensitiveness and reproduction of results one should not only to choose photo materials properly, but to pay special attention to specimen preparation technology. The sample should be dispersed as a very thin layer (if possible of thickness comparable with hot particles size) and fixed rather firmly on the substratum. Preliminary preparation of soil or bottom sediment samples is as follows: the sample is dried in paper envelope at normal temperature and then finely powdered and homogenized.

One must take into account that practically all the fuel particles are positively charged (some dozens or hundreds elementary charges) due to presence of α and β-active nuclides [1]. For this reason they are in close contact with non-active soil particles. The fuel particles couldn't be destroyed by powdering and homogenizing of specimen. One can place the specimen on the substratum in two ways: by dry dispersion through the sieve (with cells of 50x50 μm or 100x100 μm) or suspending it in water before it's placed on the substratum. The second way is more safe (especially when activity of specimen is high), but using the first, one can ensure uniform placement of the sample as a very thin layer. The optimal sample to be placed on the substratum of 18x24 cm is about 0.1-0.2 g. In this case 100-200 particles per 1 square cm can be identified using RT-S X-ray film and 50-100 particles per 1 scm by use of RM-V X-ray film with EUI-4 amplifying screen. The calculated gain of RM-V by EUI-4 respective to RT-S (without screen) equals 2.71±0.36.

The largest possible portion, which provides an identification with estimation error not greater than 20% respective to ideal case is some 1-1.5 g for 18x27 cm square.

The usage of X-ray film as a substratum gives a number of advantages because the sensitive photo-layers and protecting screen are manufactured on the base of gelatine and glycerine. The thickness of the photo- layer and protecting screen is 8-10 μm and up to 3 μm, respectively. After gelatine is moistened the specimen is placed on the substratum and when gelatine is dry again specimen is fixed firmly on the surface. The substratum with the specimen placed on it should be screened by lavsan 2.5-8 μm thick.

The resolution of RT-5 X-ray film is 2.7 times higher than that of RM-V, so it can be used for more active samples of 10^5 Bq/g on ^{137}Cs. RM-V film with EUI-4 amplifying screen has greater registration efficiency and fits low and medium active samples (less than 10^3 Bq/g) and exclusively qualitative assessment of the specimen.

To separate a particle first of all the substratum and macro-radiograph should be overlapped by 3-4 bench-marks made in advance. The particle can be whether cut off with piece of substratum or extracted by the needle and placed on specially prepared substratum.

An exposure time is one of the essential parameters of radiographic method. Some difficulties in its determination usually arise because a number of factors should be taken into account: radiation energy, source radioactivity, type of film, optical density of the material, specimen thickness, etc.

Dependence of spot optical density D on the value of exposure H can be represented graphically as a characteristic curve [2] at fixed source activity.

A straightforward segment of characteristic curve is of great importance for here an optical density value increases proportionally to radiation quantity logarithm. So it's called a normal exposure domain. Therefore it's necessary to provide conditions of exposure so that black spot density remains within this domain.

In case of fuel-content material the characteristic curve will represent dependence of spot diameter on exposure time T_o at fixed source activity (see fig.1). An exposure time intervals were taken as 3, 6, 15, 24, 48, 96 and 163 hours. The black spot diameter increase was traced for 23 particles of ^{137}Cs activity ranged from 0.04 Bq/part to 20 Bq/part. In double logarithmic scale the experimental points can be placed on the straight line with error not greater than 10% for activities greater than 1 Bq/part. The equation for approximating curve is as follows:

$$\mathrm{Ln}\ D = A \times \mathrm{Ln}\ T_o + B,$$

$$D = kT_o^A,$$

where D is the black spot diameter,

T_o - exposure time, A - the slope of the straight line in double logarithmic scale, and k - the coefficient for type of film and conditions of its development.

For all the particles of activity greater than 0.4 Bq/part the slope is almost the same and is about 0.39±0.05.

In fig.2 experimental points and approximating curve for spot diameter vs hot particle ^{137}Cs activity are shown. This dependence was determined for RM-V X-ray film with EU1-4, T_o=4 days. The particles were sampled from flood plain soils near Pripyat River on May 30, 1991. The equation of the curve is of the form:

$$D_{spot}[mm] = k_1 A^c,$$

where A is a particle activity in Bq ,

C - the slope of the straight line in double logarithmic scale,

k_1 - the coefficient for the type of film and development conditions.

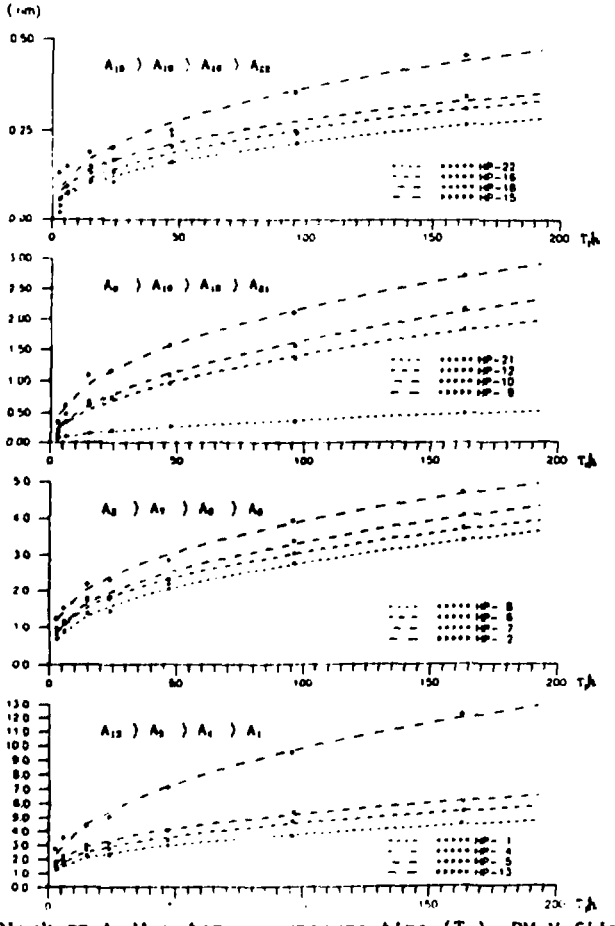

Fig.1. Black spot diameter vs exposure time (T_0), RM-V film, linear scale

If k_1 and C are in hand, an activity of particles associated with concrete black spots on RM-V film can be ascertained. For this type of particles

$$C = 0.47 \pm 0.05$$

$$k_1 = 0.98 \pm 0.02 \ .$$

Having a number of functional dependencies of spot diameter on exposure time and particle activity available one can easily draw the characteristic

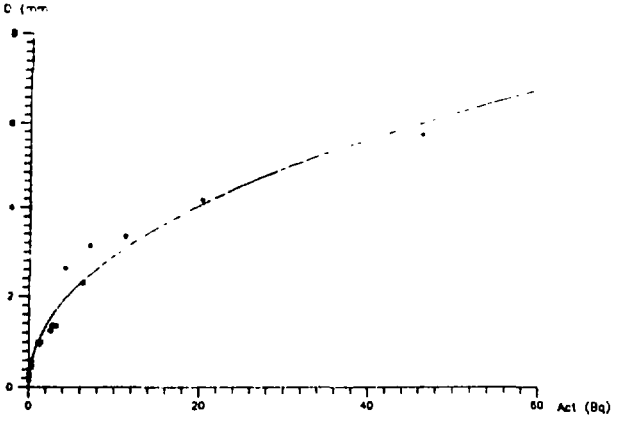

Fig.2. Black spot diameter vs hot particle activity, RM-V film, T_0=96 hours

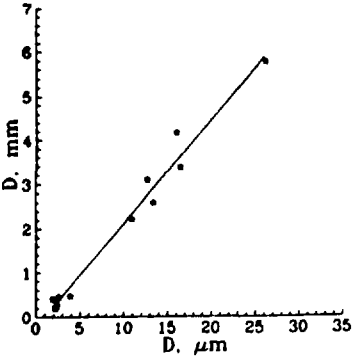

Fig.3. Black spot diameter vs hot particles size in the sample, RM-V film with EUI-4 screen

curve for RM-V X-ray film with EUI-4 amplifying screen. It demonstrates the dependence of spot diameter (mm) on irradiation dose $I \times T_o$ (see fig.1).

According to definition [2,3] the sensitiveness is ability of photo material to turn black when being irradiated. The less exposure is needed for certain degree of blacking (at the same source activity) the higher is the sensitiveness of material.

An optical density which exceeds the density of the veil D_o by x can be taken as sensitiveness criterion (so $D = D_o + x$). For the RM-V X-ray film the optical density x was taken 0.5. So using this type of film with amplifying screen one can obtain the visible spot diameter of optical density by 0.5 higher than veil after 20-25 hours of exposure. The lower limit of particles activity was taken 0.01-0.05 Bq/part. So to obtain a representative image of the particle of mean ^{137}Cs activity 0.03 Bq not less than 40 hours of exposure was needed (in 1991).

In fig.3 the dependence of black spot diameter (RM-V film with EUI-4 screen) on hot particle size is shown. Experimental values of fuel particles size were ascertained by means of registration by solid state track detectors CR-39. The approximation was performed by least squares method.

Thus the methods described here make it possible to use macro-radiography for particles size estimation and study of transformation and destruction of them in environment as well.

REFERENCES

1. Bykhovsky A.V., Zarayev O.M. Hot Aerosol Particles and Technical Use of Nuclear Power. Atomizdat, 1974, 230 p. (in Russian)

2. Korobkov V.I. The Methods of Macro-Autoradiography. Vyscshaya Shkola, 1967, 185 p. (in Russian)

3. James T.H. The Theory of Photography. Himiya, 19809, 458p. (in Russian).

4. Borovoy A.A. et al. The Fuel of Chernobyl NPP's Fourth Block. Manual. IAE, Chernobyl, 1988, 147 p. (in Russian)

5. Belyayev S.T., Borovoy A.A. et al. - The Chernobyl Source Term. In Proc. Seminar "Comparative Assessment of the Environmental Impact of Radionuclides Released during Three Major Nuclear Accidents: Kyshtym, Windscale, Chernobyl", Luxemburg, October 1-5, 1990. Brussels, CEC, 1991, p.71-92.

SOLID STATE TRACK DETECTOR (SSTD) INVESTIGATION OF AERIAL "HOT" PARTICLES IN RADIOACTIVE CONTAMINANT ZONES OF THE REPUBLIC BELARUS

Zhuk I.V.[1], Lomonosova E.M.[1], Boulyga S.F.[2], Tzekhanovich I.A.[2], Drugachenok M.A.[3], Kudryashov V.P.[3], Mironov V.P.[3]

The most toxic radionuclides released into environment as a result of an accident on Chernobyl NPP are the nuclei of transactinides. They penetrate into human body mainly by inhaling and resultant irradiation dose depends upon disperse composition of aerosol particles, as well as physical and chemical properties of radioactive nuclei.

The aim of the paper is to estimate dimensions of aerosol particles trapped in air using aerosol filters for different villages of Belarus and to make a conclusion about the structure of them.

The particles dispersed composition was investigated by autoradiography and SSTD methods. First of all X-ray PT-1 film was exposed with the 50 CM aerosol filter surface during 3 - 14 days. After film developing 0.5 - 2 cm film spots with black patches were cut out and radiometric, gamma-spectrometric and radiochemical analysis was carried out.

Several of these peaces of filters in contact with SSTD (artificial fluorine flogopit mica) were then irradiated by thermal neutron fluency with $F = 10^{14}$ n/cm. After chemical etching SSTD were looked through using optical microscope, and photos of "hot" particles were made on "Micram-200" film.

As a rule the black patch is a crowded particle accumulation of different sizes (often more than ten) on a small area. For example, a black patch cut out by radiography in an air filter taken from the village Novshchina (Khoinic's district) actually was produced by fifteen "hot" particles of 5 - 200 10^{-6} m dimensions on a spot 0.016 cm and the main activity caused by 12 particles from 0.00013 cm.

1 - The Institute of Problems of Energetics, 2 - The Institute of Radiation Physics and Chemistry Problems, 3 - The Institute of Radiational Biology, Academy of Sciences of Republic Belarus

In the following table dimensions of these "hot" particles are listed.

TABLE.1 "Hot" particle dimensions revealed on the air filter of village Borisovshchina

Particle number	1	2	3	4	5	6	7	8	9	10	11	12	13	14	15
Dimension 10^{-6} m	220	40	9	6	6	6	6	8	6	6	6	6	20	80	9

A 0.0022 cm^2 black patch, developed on an aerosol filter taken from the village Krasnosel'e (Khoinic's district) was produced by three identical particles (about 60 10^{-6} m dimensions) and a number of smaller particles of much less radioactivity.

Another black patch of the same filter was produced by a single very radioactive "hot" particle of about 110 10^{-6} m diameter.

The SSTD method line resolution is limited by the value 1 - 3 10^{-6} m (dimension of a fission fragment track as it could be seen through an optical microscope after chemical etching) and it should be taken into account in "hot" particle minimum dimension determination.

Track piling on SSTD (up to ten tracks in a pile) indicates that smaller "hot" particles are in presence in black patches, but the main transactinide activity is caused by the activity of large particles.

On the 20 x 20 mm filter area (the filter had been placed in the village Borisovshchina, Khoinic's district) after thermal neutron irradiation of that area, five "hot" particles were found out.

The particles number 1 (diameter d = 250 10^{-6} m) and number 2 (d = 120 10^{-6} m) were found on a distance 1.05 mm from each other.

The group of particles number 3 (d = 50 10^{-6} m) and number 4(d = 170 10^{-6} m) were found on a filter area 0.17 x 0.25 mm .

On the filter one very large "hot" particle number 5 (370 10^{-6}m) was found.

Let's consider particles number 1 and 5. Their fission fragment tracks resolution is quite good on photographies. Density of fission fragment tracks after irradiation of these particles with thermal neutrons ($10^{14} n/cm^2 \pm 10\%$) was $2\ 10^{-6} cm^{-2}$ and $1.5\ 10^{-6} cm^{-2}$, correspondingly.

Having compared expected density of tracks and the one obtained experimentally, one can make a few conclusions about the composition of "hot" particles.

1. Let "hot" particle be a particle of RBMC-reactor fuel with diameter $250\ 10^{-6} m$ (N 1) and $370\ 10^{-6} m$ (N 5). Material composition of fuel is available from [1] taking into account time corrections. Using the relationship between fission fragment track density and neutron fluency [2] and taking into account that the diameter of"hot"particle $d >> R_o$ (fission fragment mean free path), we got the expected density of tracks:

$$n = 5\ 10^{-9} cm-2$$

That value exceeds by more than three orders of magnitude experimental values. Thus, the conclusion is : revealed "hot" particles are not the particles of reactor fuel.

2. Let's suppose that the "hot" particle is a soil particle, not contaminated with radionuclides and it contains uranium isotope of natural origin. According to [3] average activity of uranium in soil is approximately 22.2 Bk/kg. In that case expected track density is about $2.5\ 10^{3} cm-1$. That density is about three orders of magnitude lower than experimentally obtained one. Thus, revealed "hot" particles are not the particles of soil, which contain natural uranium.

3. Let "hot"particles be dispersed ($d << R_o$) particles of reactor fuel, adhered onto inert carrier-particle of reactor structural or ballast materials. In that case, relationship between neutron fluency and track density gives the thickness of fissile layer about $4\ 10^{-9}$ and $3\ 10^{-9} m$ and the volume of this layer $820\ 10^{-6}$ and $1270\ 10^{-6} m^3$ for particles number 1 and 5, correspondingly. According to reference [1], fine fuel particles formed as a result of Chernobyl NPP accident have the sizes distributed in accordance with logarithmic normal low with median value $5\ 10^{-6} m$.

Having in mind the volume and average size of particles we got , that the quantity of adhered particles should be several dozens.

Conclusions are the following:

1. "Hot" particles dimension range is 5 - 370 10^{-6} m.
2. The main part of transactinides' activity is caused by the large 'hot' particles.
3. To our mind, "hot" particles, revealed on aerosol filters are fine dispersed fuel particles, adhered on inert carrier-particle.
4. There is no straight dependence between activity of particles and their dimensions.

Further investigation of "hot" particles will be devoted to identification of particles smaller than described here, using irradiation of filter patches with high fluency of neutrons and decreasing of etching time up to zero as well as to investigation of dispersed composition of particles.

References

1. Geometry and characteristics of particles of fuel release as a result of Chernobyl NPP accident / S.A.Bogatov, A.A.Borovoj, Yu.V.Dubasov, V.V.Lomonosov / Atomic Energy - 1990.- v.69, iss.1.-p.36-40. (In Russian).
2. Fission density distribution measurements on critical assemblies using track detectors. / A.P.Malykhin, L.P.Roginetz, V.A.Levadnyj, O.I.Yaroshevich / News of the Academy of Science of BSSR, Ser. Physics-Energetics Sci..- 1970.-n.2.-p.16-23. (In Russian).
3. Reference book on nuclear energy technology: Translation from English / Run F., Adamantiades A., Kentok J., Brown Ch.-M.-Energoatomizdat, 1898.-p.32. (In Russian).

RADON LEVELS IN DWELLINGS OF UKRAINE

A.V.Zelensky, I.P.Los, T.A.Pavlenko, V.V.Grigorash, M.G.Buzinny

The Ukrainian Scientific Center of Radiation Medicine of the Academy of Sciences and Ministry of Public Health

Introduction

Chernobyl accident drew attention of public and scientific community to all sources of ionizing radiation including natural ones, among which ^{222}Rn is the nuclide that produces main part of the dose. Considerable part of Ukraine (30-40%) covers the Ukrainian Crystal Massive (UCM) that emits relatively high concentrations of natural radionuclides into the environment. Since 1988 we have been providing measurements of ^{222}Rn levels in houses on the territory of Ukraine. To date we obtained about 1500 measurements in regions which are either partially or completely situated above the UCM.

Methods

Here we report the results obtained only with the help of passive diffusive cells with cellulose nitrate detector LR115 II (Kodak, France), and cellulose nitrate detector (CND) (State Research Institute of Photochemical Industry, Pereslavl Branch, Russia).

Standard chemical etching in NaOH solution was carried out prior to clamps were counted on exposed detectors with the help of "AIST" spark counter (Radium Institute, Saint-Petersburg, Russia). Minimum detection limit for a 30-day exposition with 30% error stands at 8 $Bq \cdot m^{-3}$ for LR-115 and 13 $Bq \cdot m^{-3}$ for CND. The cells were exposed in dwellings of different types taking into account number of floors, type of building materials and scheme of the apartments. The exposure time was 1.5 to 2 months. To receive detailed information about the dwellings where measurements were carried out we used specially developed forms, fully compatible with data base created in dBase IV and running on IBM PS/2, models 30, 60. That information helped to determine levels of ^{222}Rn concentrations in relation to: geological, meteorological conditions, construction of dwellings etc. Later on data received will help to create system for ^{222}Rn concentrations prediction for separate districts and populated areas. In means of simplicity of comparing indoor ^{222}Rn concentration measurements data was recalculated

into equilibrium equivalent concentration (EEC) using an equilibrium factor of 0.45 as suggested by the ICRP Report N50 [1].

Results and discussion

Preliminary statistic analysis of data showed that it was reasonable to divide data into three groups depending on the type of dwellings: I - single-story houses, II - first floor in multi-story houses, III - other floors in multistory houses. Data for these groups of dwellings is presented in table 1. The highest indoor ^{222}Rn concentrations were found in single-story houses and first floor of multistory houses. It seems it's due to underground ^{222}Rn emission. Another special feature is its high concentrations in adobe and pise-walled houses. Usually, this type of dwellings do not have foundation and ceiling. Stove heating and ventilation type used are driving force for ^{222}Rn flow (thermal stack effect). Brick houses usually do not have hermetic isolation from the basement, while air-vents are usually closed to prevent rodents penetration. Average EECs for dwellings made of different building materials are given in table 2. Difference of concentrations between brick and panel multistory buildings might be explained by different types of ventilation and high velocity of ^{222}Rn emission from porous bricks constructions. Talking about first floors of multistory buildings, ^{222}Rn concentrations depend on the types of ceiling.

Significant source of ^{222}Rn in the air of any room can be water. This is proven by high average EECs in multistory buildings of Cherkassyi region, where high levels of ^{222}Rn in underground water were found (figures reaching thousands Bq $\cdot l^{-1}$). Frequency distribution of indoor ^{222}Rn concentrations for above mentioned three types of dwellings has a good fitting with lognormal distribution (Fig. 1).

Average concentrations of ^{222}Rn for:countryside houses - 85 Bq $\cdot m^{-3}$; for first floor of multistory houses - 48 Bq $\cdot m^{-3}$; for other floors of multistory houses - 32 Bq $\cdot m^{-3}$. The probability of finding houses where EEC levels exceed 1500 Bq $\cdot m^{-3}$ is less than 0.1%, corresponding to the radon frequency distribution parameter in countryside houses; exceeding - 500 Bq $\cdot m^{-3}$ - 2%; exceeding 200 Bq $\cdot m^{-3}$ - 8%; exceeding 100 Bq $\cdot m^{-3}$ (existing hygienic limit for dwellings) - 28%.

Analysis on different regions (tables 1) shows that the highest concentrations are found in Cherkassyi, Zaporozhye, Dnepropetrovsk and Donetsk regions - the ones that are situated in abnormal areas on the UCM. Minimal concentrations are found in Poltava and Chernigov regions, which are situated outside the UCM. Average EECs for different regions presented in tables 1 differ from the average EECs shown on fig. 1, due to different number of measurements carried out in the regions.

Finally, the annual effective dose equivalent for Ukrainian population due to ^{222}Rn irradiation was estimated to be 3.4 mSv [2], that is 76% of total dose cased by natural radiation (Fig.2).

Table 1

Equivalent equilibrium concentrations of radon-222 in dwellings of Ukraine

Region	Number of meas.	Max.	Average	Standard deviation	Geometr. mean	Geometric deviations		% measurements exceeding levels (Bq per m^3)		
						(-)	(+)	50	100	200
Single-story houses										
Poltava	67	255	48	49	33	19	45	31	12	3
Zhitomir	84	437	47	61	29	19	50	29	7	4
Zaporozhye	93	633	130	107	97	53	115	83	47	17
Vinnitsa	49	263	91	48	78	34	61	80	43	2
Kiev	118	331	82	62	61	34	75	61	30	5
Kirovograd	21	506	93	112	56	35	92	62	24	10
Ivano-Frankovsk	73	241	55	40	45	22	41	45	5	1
Cherkassyi	84	648	136	99	107	55	112	83	62	17
Chernigov	32	74	28	17	24	11	19	13	0	0
Dnepropetrovsk	10	386	160	130	97	66	206	70	60	40
Donetsk	15	197	102	46	92	35	58	93	47	0
AVERAGE:			88	66	62			56	28	8
SUM	646									
The first floor of multistory houses										
Vinnitsa	12	108	34	26	27	13	25	25	8	0
Kiev	39	190	47	42	34	19	41	31	10	0
Kirovograd	4	67	33	25	20	14	46	25	0	0
Ivano-Frankovsk	36	74	37	18	32	14	25	25	0	0
Chernigov	3	40	28	10	26	9	13	0	0	0
Cherkassyi	26	290	101	63	81	41	83	77	42	8
Poltava	135	176	30	24	23	12	27	16	2	0
Dnepropetrovsk	15	228	90	67	64	38	92	60	40	13
Zhitomir	7	53	30	17	23	13	32	23	0	0
Zaporozhye	23	232	55	55	38	22	50	38	13	4
Donetsk	23	164	89	44	74	37	73	71	38	0
AVERAGE:			52	36	33			35	14	2
SUM	323									
Multistory houses, > 1st floors										
Poltava	141	131	26	23	19	11	24	13	2	0
Dnepropetrovsk	13	130	23	33	15	8	17	8	8	0
Zhitomir	33	158	25	26	19	10	19	6	3	0
Zaporozhye	38	75	28	15	24	10	18	8	0	0
Kiev	68	150	28	26	20	11	24	15	1	0
Vinnitsa	35	133	29	26	22	11	23	11	6	0
Ivano-Frankovsk	3	33	19	11	15	7	15	0	0	0
Kirovograd	13	31	19	7	18	5	8	0	0	0
Cherkassyi	55	349	64	63	45	26	60	49	15	4
Donetsk	9	82	34	18	30	11	17	11	0	0
AVERAGE:			30	25	23			12	4	0
SUM	407									

Table 2

Types of r aterials	Number of measurements	Average EECs of ^{222}Rn Bq $\cdot m^{-3}$
Single-storey houses		
Brick	386	87
Wood	122	47
Slag concrete	22	86
Adobe	65	104
Stone	3	78
Shell rock	10	213
Multistory houses, first floors:		
Brick	115	57
Panel	166	32
First floors above:		
Brick	176	28
Panel	218	24

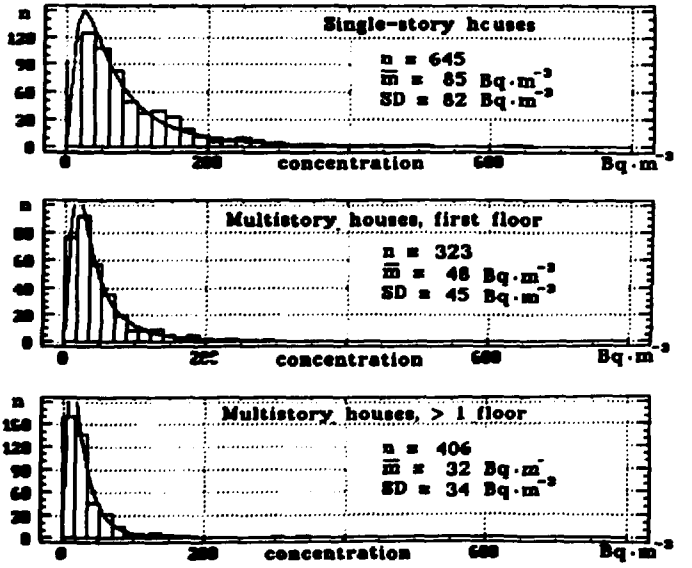

Fig.1 Frequency distribution of radon indoors concentrations under types of houses in Ukraine

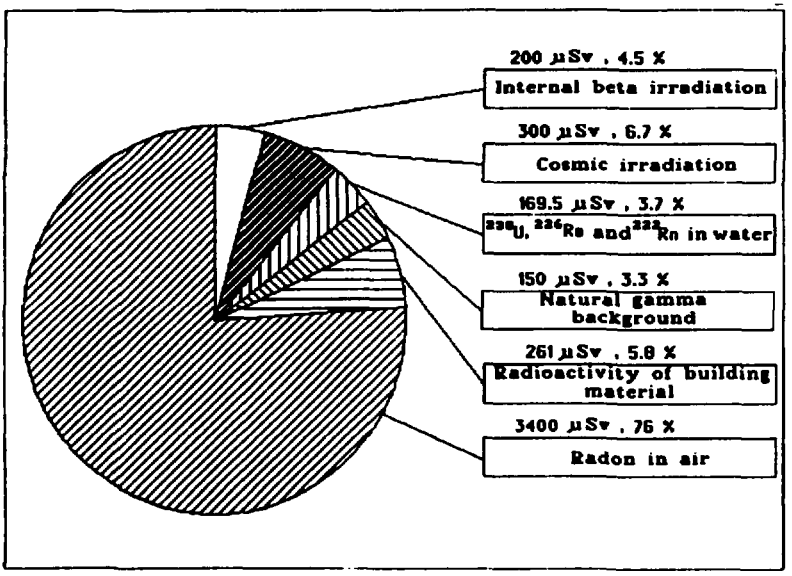

Fig. 2. Dose pie of main sources of natural radiation

REFERENCES

1. Lung Cancer Risk from Indoor Exposures to Radon Daughters: ICRP Report N. 50. - New York, 1988. - V.17 - N1, - 60 p.

2. Exposure levels on Ukrainian population due to natural radiation. // I.P. Los, A.V.Zelensky, M.G.Buzinny, T.A.Pavlenko, oth./ Actual problem of radiation medicine, 1992. (In press).

SSNTD-technique for radon measurements indoors and in the soil in Sweden

Gilbert Jönsson
Physics Department, Lund University
Box 118, S-221 00 Lund, Sweden

Introduction

The presence of radon gas in the indoor air is a current subject in the Swedish environmental debate. The gas is supposed to be the reason for about one third of the additional lung cancer cases each year in Sweden (1). There are also ideas about other cancers caused by radon daughter exposures (2). Measurements of radon/radon daughter levels were performed in more than 100 000 dwellings in Sweden during the last two decades (3). A great part of these indoor measurements is based on SSNTD-technique.

The soil and bedrock, the building material and the household water are the three main sources of the indoor radon. The first source is found to give the highest radon levels indoors. The local authorities, which are responsible for the local environment and the building permit of the community, use soil radon maps to find houses with high radon levels and to prevent high radon levels in future buildings. Measurements of the radon levels in the ground contribute to the basic knowledge needed for the construction of these radon maps. SSNTD-technique is useful also for these type of measurements.

The use of plastic film, Kodak LR 115-II, in radon detection from technical point of view, is discussed in this report. The film is a tool in large scale investigation of radon levels indoors and in the soil in south Sweden. The measured radon levels in the ground combined with a geological survey including geochemical and gamma-radiation maps give the basis for soil radon maps covering a community. The indoor radon measurements are a sort of a test of the maps (4).

The Kodak LR 115-II-film – technical details

Etching and some consequences

The film, with its 12 μm thick alpha sensitive layer, is non-strippable. Alpha particles, having energies between about 1,3 MeV and 4,1 MeV, will be registered depending on the angle of incidence, A in fig. 1, of the particle (5) if the etching conditions are:Etching time = 2 h; NaOH-solution = 10%; Etching temperature =59°C.

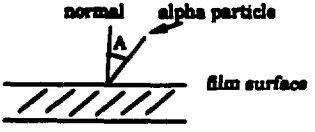

Figure 1. Angle of incidence of an alpha particle is A

If the etching does not always give the same residual thickness of the sensitive layer there must be a correction of the found number of holes to a reference thickness.

Alpha particles from disintegrating radon daughters, plated out on the surface of the film. will not be registered.

A careful washing of the film in water (temperature around 60 °C) after the etching and in softened water at the end means that the holes in the film will be free from etch residua . The reading in microscope of the etched film is, manual or by means of a CCD-camera, is facilitated if the holes are distinct.

Storing

The storing of the film should have its own chapter. In order to minimize the background level the boxes with sheets of film should be kept in sealed plastic bags. Film from boxes stored in room temperature (about 20 °C), dry and in shadow may still be intact after ten years although the etching time should be shortened.

Clean handling

It is important to have no or low background exposure of the film:

1. Foils of aluminum or other materials in close contact with the film may cause an enhanced background exposure to the film. One reason for this is maybe the presence of alpha radioaktive nuclei in the aluminum or material.
2. When the film is cut for use in a radon detector the tools and instruments used as well as the surface of the used table should be clean.
3. The room, where the film is stored or treated, should be at a low radon level.

The detection of indoor radon daughter levels

Radon - radon daughters

The LR 115-II-film will, without cover or with low-density thin cover, register alpha particles from both radon and radon daughter disintegrations.

If the film is placed in a closed box with radon gas leaking into the box the exposure is a measure of the radon level outside the box. The dimension of the box is critical from the point of view of the plate out of the radon daughter nuclei on the surfaces inside the box.

The reference levels of indoor radon in Sweden are given as radon daughter levels in Bq/m^3 (EER) using the equilibrium factor F which is defined as (6)

$F = EER/C_{Rn}$ where $EER = 0.104 \times C_1 + 0.514 \times C_2 + 0.382 \times C_3$, with C_1, C_2 and C_3 as the activity concentrations of the individual Rn daughters ^{218}Po, ^{214}Pb and ^{214}Bi and C_{Rn} as the radon concentration. The F-value is supposed to be 0.5 in the mean in Swedish dwellings. As an example, the radon level 100 Bq/m^3 means 50 Bq/m^3 as radon daughter level (EER).

It is necessary to calibrate the detectors in air with known concentration of radon and its daughters. These calibrations are made at the Swedish Radiation Protection Institute in Stockholm.

Statistics

The sensitivity of the LR 115-II-film is somewhat lower than that for CR 39 (5). The Kodak film has a smaller sensitive solid angle and a narrower energy interval of the alpha particles. The used etching conditions give a sensitivity of the Kodak film of around 1 hole mm^{-2} per $kBq \cdot d \cdot m^{-3}$ radon daughter level (EER) (7).

The counting statistics is essential for the error of radon daughter level, found in a room. In principal, the error of one detector is given by

$$\Delta_{det} = \left(\Delta^2_{stat} + \Delta^2_{read}\right)^{1/2}$$

where Δ_{stat} is the pure statistic error,e.g. standard deviation of the Poisson distribution and where Δ_{read} is a contribution from varying etching and readout conditions. Δ_{read} is expected to be 10-15% of Δ_{stat}. The longer the time of exposure the lower the relative statistical error.

Another essential contribution to the error of the measured radon daughter level is the number of detectors. Minimum two detectors should be used in each dwelling. The arithmetic mean of the radon levels, given by the detectors, is taken. In Sweden, the limitation schemes say that the radon daughter level must be below 200 Bq/m^3 in a building older than about one year. The figure is an annual mean. The measured mean value of the radon daughter level of the dwelling is adopted as an annual mean value in Sweden if the time of exposure is over 1 month. The error of the annual mean value is given by the formula (8)

$$\Delta_{total} = \left(\Delta^2_{det1} + \Delta^2_{det2} + \Delta^2_{year}\right)^{1/2}$$

where Δ_{year} is an error given by

$$\Delta_{year} = 22\% - 0.3 \cdot t + v \, .$$

The letter t is the exposure time in weeks. The letter v is a ventilation factor which is equal to 20% if the dwelling is self-ventilated.

The detection of soil radon concentrations

The detector

The radon levels of the air in the soil is detected by LR115-II-films placed in cups at a depth of 70 cm if possible. One or two pieces of film must be put in the cup in such a way that the exposure from thoron and the effects of moisture are minimized, at least if no filter is used. The time of exposure must be at least 10

days. Then the "build up" effect of radon gas inside the cup on the total radon concentration is reduced and the amount of gas is equilibrated.

The volume of the cup must be large enough in order to avoid uneven exposure of the piece of film from radon daughters plated out inside the cup. Also, the distance of the film to the open end of the cup must be considered if no filter is used.

The cup is put in digged or drilled holes in the ground and the soil is refilled according to figure 2. The cup may also be put in a tube. The tube should be closed in order to avoid convection.

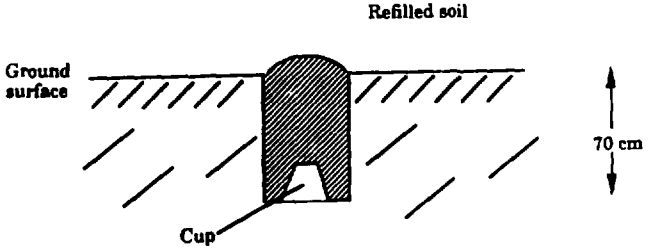

Figure 2. The cup with the films is placed at the depth of 70 cm below the ground surface

The cups are often dirty after the exposure and digging, which gives rise to a washing of the film in the cup as soon as possible in order to avoid a further exposure of the film, scratches on the film or "hot spots" in the film.

Droplets of water on the film during the exposure often give zones in the film with reduced number of holes. This effect must be "by-passed" at the counting of the holes.

Recommended limitations

The Swedish authority of physical planning and building(1) recommends a classification of the ground, which means three different intervals of radon concentrations in soil air: less than 10 kBq/m^3, 10-50 kBq/m^3, more than 50 kBq/m^3. The constructors and designers of a building are recommended to put radon-safe buildings on the high risk ground. The radon concentrations refer to a depth of 1 m below the surface of the ground.

Depth dependence

Although the recommended limits of the radon concentrations in the soil air in Sweden refer to the depth of 1 m below the ground surface this depth is unpractical and sometimes impossible to achieve. It is then important to pay attention to the fact that the radon concentration in the soil normally increases with increasing depth at least in the depth interval 0-2 m (9). A typical dependence is given by the formula $C(t)=K\,(1-e^{-t\ \ t})$ where $C(t)$ is the concentration at the depth t and

where K and k are constants defined by calibrations. At depths shallower than about 25 cm it is normally no sense to talk about a depth dependence.

Radon measurements in the soil and indoors – examples

Soil radon measurements

At the construction of a soil radon map the measurements of the radon levels in the ground give important information together with a geological survey of the soil and the bedrock. The map in fig.3 from the community of Lund is based on 260 soil radon measurements. The distribution of these measurements is given in fig.4.

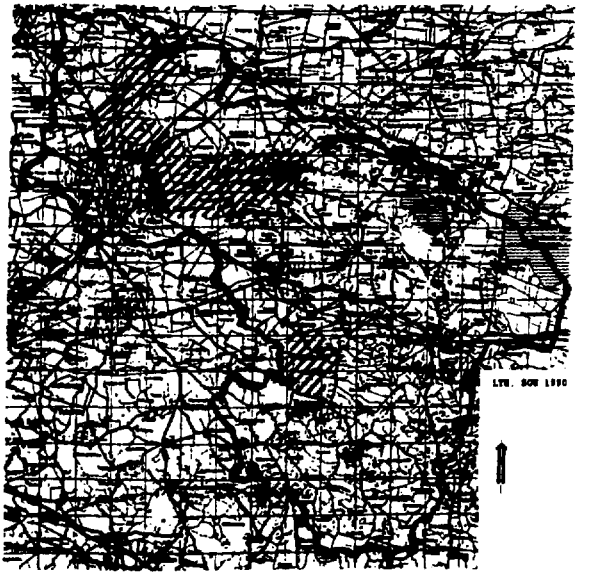

Figure 3. An example of a soil radon map. The shadowed parts are areas where the soil radon levels normally are between 25 and 50 kBq / m^3. The rest of the community normally has radon concentrations in the soil between 10 and 25 kBq / m^3. The area of the community is about 450 km^2

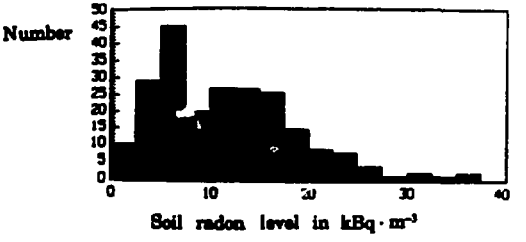

Figure 4. The distribution of the measured radon concentrations in the community of Lund

Indoor radon measurements

Normally, two detectors are exposed in a dwelling. The inhabitants themselves of the dwelling make the exposure following an instruction which is included in the parcel together with the two detectors. The parcel is sent as a regular letter to the inhabitants,who send the letter back to the laboratory after the exposure. The inhabitants enclose data about the dwelling/house and the exposure time. Fig.5 shows a distribution from a community where the radon source is not only the ground but also the building material (light weight concrete).

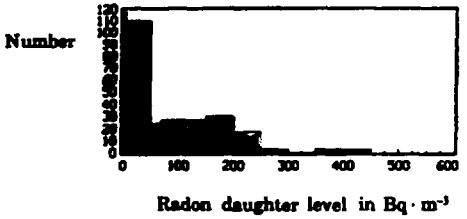

Figure 5. The distribution of indoor radon daughter levels typical for a community in south Sweden

References

(1) G. A. Swedjemark, H. Wahren, A. Mäkitalo, W. Tell: Experience from indoor radon daughter limitation schemes in Sweden. Environment International 15, pp 253-260 (1989).

(2) D. Henshaw, J.P. Eatough, R.B. Richardson: Radon as a causative factor in induction of myeloid leukaemia and other cancers. The Lancet 335, pp 1008-12 (1990).

(3) G.A. Swedjemark, A. Mäkitalo: Distributions of radon in houses as a basis for radiological protection – Swedish expericence. Rad. Prot. Dos. 36, pp 125-128 (1991).

(4) G. Jönsson: Solid state nuclear track detectors in radon measurements indoors and in the soil. Nucl. Tracks Radiat. Meas. 19, pp 335-338 (1991).

(5) G. Jönsson, R. Hellborg: The exposure of plastic films and their response to 1,3–5,5 MeV helium ions. Nucl. Instr. & Meth. B63 , pp 399-406 (1992).

(6) G. Jönsson: Indoor ^{222}Rn measurements in Sweden with the solid-state nuclear track detector technique. Health Physics 54, pp 271-281 (1988).

(7) G.Jönsson: Indoor radon gas and its detection with Kodak plastic film. Nucl.-Tracks Radiat. Meas. 13, pp 85-91 (1987).

(8) From national regulations of indoor radon measurements in Sweden. Swedish Radiation Protection Institute, Stockholm.

(9) K. Kristiansson, L. Malmqvist: Evidence for non-diffusive transport of Rn-222 in the ground and a physical model for transport. Geophysics 47, pp 1444-1452 (1982).

DETERMINING THE SPATIAL SCALE OF VARIATION IN SOIL RADON VALUES USING A NESTED SURVEY AND ANALYSIS

S.A.Durrani, I.Badr, G.L.Hendry* and M.A.Oliver**

School of Physics and Space Research
University of Birmingham,
Birmingham B15 2TT. England

* Department of Earth Sciences/ ** Department of Geography
University of Birmingham

Abstract

The statistical method of 'unbalanced nested sampling' has been applied to radon measurements in the field in order to determine the scale and pattern of spatial variation in radon soil-gas concentrations. This technique allows these parameters to be economically determined over several orders of magnitude by incorporating a spatial scale in the nested analysis.

By sampling the radon concentrations in soil at 108 individual points over a 225 km^2 area in the Hereford and Worcester county of the English Midlands, it was shown that 95 % of the total variation in the activity concentrations occurred over a scale of less than 10 m - the distance between the closest sampling points used.

The soil-gas concentrations were determined using the 'can technique' - a simple passive detection system employing solid state nuclear track detectors. This technique allows radon gas to diffuse through a filter into a can buried at a depth of 50 cm containing a 2 cm x 2 cm piece of CR-39 plastic, the can unit being placed at the bottom of a 70 cm long PVC tube. Alpha tracks from the decay of radon gas were then etched electrochemically.

The results of the nested analysis, if confirmed by further measurements at other locations, would imply that there is little evidence of spatial correlation of the measurements: i.e. that the radon seems to behave erratically over small distances and that the surrounding radon values are thus unsuitable for estimation by interpolation.

OPTICAL PROPERTIES OF NUCLEAR TRACK FILTERS

A.V.Mitrofanov
Lebedev Physical Institute, Academy of Sciences of Russia, Moscow, Russia
P.Yu.Apel
Joint Institute for Nuclear Research, Dubna, Russia

A track-etch filter (TEF) or nuclear track filter (NTF) can be considered as inhomogeneous medium. The optical properties of this medium depend upon the type of material and pore size, number density N as well as upon orientation of pores in the filter. The optical transmittance of the holes in such filter is highly sensitive to the pore size and geometry if the wavelength λ is comparable with pore diameter and the filter material (or the material of coating) is not transparent for the radiation in a given spectral range. The design of porous diffraction filters are based on this fact. The idea to use TEF as diffraction filters and filtering in the spectral IR band using TEF have been discussed in [1-2]. Interesting suggestion have been reported in [3-4]. The first experiments devoted to the measurements of the TEF transmittance in UV, VUV and X-ray spectral bands have been carried out in [5]. This problem has been investigated in some details in [6-8].

Let us note here the main previous and recent results.

Consider nuclear track filter with identical through cylindrical pores oriented normally to the sample surface. Pores are randomly distributed on the surface. As a first approximation the VUV or the soft X-ray transmission of the samples with low pore density N is determined as the sum of the contributions of individual channels to the filter transmittance:

$$T = T_p * \pi D^2/4 * N, \text{ where } T_p = T_p(\lambda, D, L) \text{ is}$$

the transmission of an individual pore, D is the pore diameter, L is the filters thickness, and $\pi D^2/4 * N$ is the porosity of a filter. Single pore transmission T_p at λ=120 nm as a function of pore diameter D is shown in Fig.1 for polyethylene terephthalate (PETP) filters with several different thicknesses. Solid curves are plotted through experimental points [7]. In the measurements of T_p the direction of a weakly divergent beam of VUV radiation coincided with the normal to the surface of the samples. In this case the transmissions T_p in the soft X-ray spectral region (λ≈1-10

nm), as it might have been expected, were comparable with unity. Thus, these track-etch polymer films can be considered as cut-off filters (VUV and soft X-ray radiation filters with excellent edge characteristics).

The mechanism by which radiation is transmitted through a TEF may be as follows. The pores in the film are the hollow dielectric waveguides which, in most cases, are not coupled to one another. These microwaveguides have walls with large attenuation factors for radiation with the wavelength shorter than the UV transparency limit of the polymer.

The penetration of UV and VUV radiation through a pore is then largely governed by two phenomena: 1) diffraction at the entrance and exit openings of the pores; and 2) the losses due to the propagation of the radiation in the waveguides. For small pore diameters the incident radiation is scattered at large angles, so that the diffraction angle λ/D becomes comparable or even greater than the aperture angle D/L of the pore channels, i.e. Fresnel number $F = D(2/\lambda L)^{1/2}$ is approximately one. Also, since the VUV or the soft X-ray radiation is effectively reflected from the absorbing walls only in the case of glancing angles of incidence, a comparatively small reduction in the pore diameter leads to a considerable reduction in the filter transparency. As can be seen from Fig. 1 the result differs from the case of the transmission of microwaves in metal waveguide with a diameter greater than the critical values $D > D_{cr} = 0.586\lambda$ (for H_{11} mode), when the wave propagates almost without loss, being reflected from the walls of waveguide (see ref. [1]). It should be noted that at present there are no proper theoretical calculations of T_p, even for such a simple porous filter geometry as considered here.

Fig. 2 illustrates the cut-off spectral characteristics of the 10 μm thick PETP NTF without coating and with 0.2 μm thick Ni layers deposited on both sides. Curve 3' corresponds to the filter with 0.64 μm pore diameter (see Fig.3) which was coated by Ni (sputter deposition). Original value of the pore diameter (before deposition) of this sample was equal to 0.75 μm. As the result the transmittance decreases, the slope of $T(\lambda)$ lines changes and the UV transparency limit of the filters disappears after the metallization of the filter.

In the spectral range of 0.1 to 0.3 μm the dotted lines 1' - 3' can be approximated by exponents (or by the straight lines on the scale chosen [8]). These curves were found to decrease inclination in the visible and near IR range.

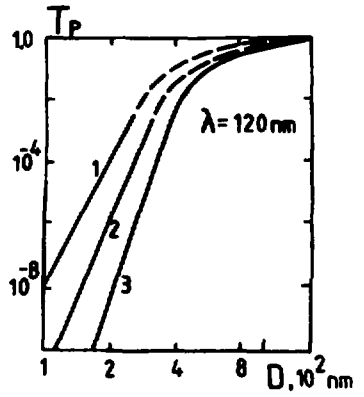

Fig. 1. Single pore transmission T_p at λ=120 nm vs pore diameter D of PETP filters with thickness L=2.5 μm (1), 5 μm (2) and 10 μm (3) [7]

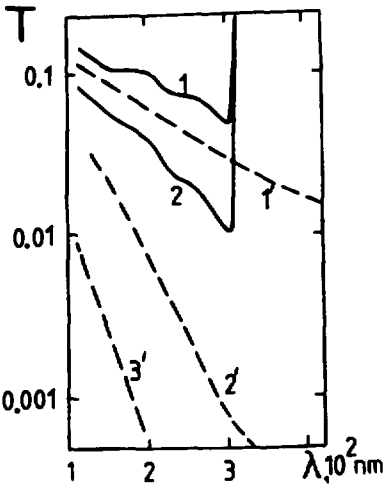

Fig. 2. Measurements of transmission T vs λ of uncoated PETP NTF with D_1=1,2 μm and D_2=1,0 μm (solid curves 1 and 2 respectively) and T vs λ for the same filters but with 0.2 μm thick Ni metallization (dotted lines 1', 2' and 3'). L=10 μm, N=2,5•10^7 pore/cm^2, D_3=0.75 μm (before Ni deposition)

Slightly undulating shape of curves 1 and 2 is explained by the strong nonmonotonic dependence of the optical constants in VUV and UV range [9], where polyethylene terephthalate has absorption bands near 143 nm, 195 nm and 245 nm. As a consequence reflection from the pore walls changes with λ. These reflections give a certain λ-variable addition to the value of T_p and T.

In some cases other type of small-amplitude oscillations on the T(λ) curves are observed for the NTF with large size pores (Fig. 4, a and b). These oscillations are similar to maxima and minima of transition or reflectance of thin transparent smooth films. However the distance $\Delta\lambda$ between neighbouring maxima or minima of T vs λ curve for porous films is about 2n times greater than the same $\Delta\lambda$ for continuous film with the refraction index n.

Fig. 3. Scanning electron micrograph of a sample 3' with Ni layer. The tilt angle is equal to 0°

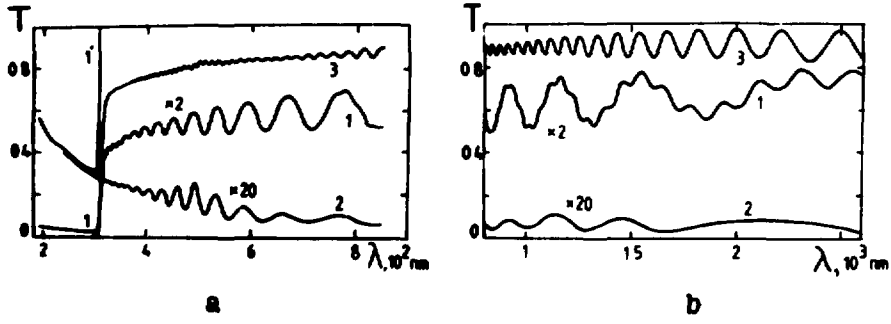

Fig. 4 a,b. Transmission T as a function of λ. 1: Uncoated 7.8 μm thick PETP porous film with D = 2.5 μm, N = $2*10^6$ pores/cm^2. 2: The same sample with Au (~0.1 μm) thick sputtered films on each filter's side. 3: 6.7 μm thick PETP film without pores. T vs λ curves were measured by Hitachi spectrometer, model 340.

T vs λ oscillations are due to relative by small value of power loss of the visible or near IR radiation propagated along the pores and in part reflected from pores outlets. If the sample is uncoated then such oscillations are observed together with close maxima and minima in interference pattern of polymer film (see curve 1 in Fig. 4a and b).

It is worth noting that presented optical characteristics are interesting from the point of view of the fabrication of highpass diffraction filters. Other optical properties such as polarization and transparency, angular anisotropy, scattering, etc. will be considered elsewhere.

References

1. G.N.Flerov and V.S.Barashenkov, Usp. Fiz. Nauk 114 (1974), pp.351-373.
2. G.N.Flerov, Vestnik Akad. Nauk SSSR 4 (1974), pp. 35-48.
3. M.A.Gruntman and V.B.Leonas, Preprint 925. Space Research Institute, Moscow (1983).
4. M.A.Gruntman. SPIE Vol. 1549 (1991), pp. 385-394.
5. A.V.Mitrofanov, Prib. Tekh. Eksp. N°3 (1983), 226. See translation in Instr. Exp. Tech. vol. 26, N°4, part II (Plenum, USA, 1984), pp. 971-974.
6. A.V.Mitrofanov, Preprint 240, P.N.Lebedev Phys. Inst., Moscow (1985).
7. A.V.Mitrofanov and P.Yu.Apel, Nucl.Instr. and Meth. A282 (1989), pp. 542-545.
8. A.V.Mitrofanov, F.A.Pudonin, P.Yu.Apel and T.I.Gromova, Nucl.Instr. and Meth. A308 (1991), pp. 347-351.
9. S.Larate et al., Appl. Phys. Lett. 50 (1987), p. 624.

PETP TRACK MEMBRANES MODIFIED BY RADIATION GRAFTING

N.I.Zhitariuk

Laboratory of Nuclear Reactions, Joint Institute for Nuclear Research, Dubna, P.O.Box 79, 101000 Moscow, Russia

One of the promising trends in composite membrane technology is radiation-induced graft polymerization. Using a proper polymeric substrate of definite pore size with high mechanical strength and sufficient chemical resistance one can obtain a membrane characterized by selectivity and mass transfer rate which depend on the grafted polymer nature and its distribution between the pores. This method can be used to obtain asymmetric membrane whose selective layer consists of polymer which is not able to form a suitable film by means of cooling from the melt or pouring from the solution.

The track membranes which in our work serve as a substrate for preparing graft membranes are made of poly(ethylene terephthalate) (PETP) film. They have high strength at a low thickness (10 μm), low dispersion of pore size, low adhesion of particles to the surface of membrane, etc. Besides these advantages, they also have some bottlenecks: low resistance to concentrated alkaline solutions, poor retention in the pores of extragent solutions which, as a rule, have low overall solubility parameter. The latter follows from hydrophilization of membrane surface as a result of etching. As was pointed out[1,2], such shortcomings can be eliminated by means of grafting a suitable polymer onto track membranes made of PETP. However, it is necessary to take into account that their pore size can be changed during grafting and this can affect the flow rate of modified membranes.

The aim of the work is to investigate some properties of track membranes modified by grafted polystyrene (PS) and poly(methylvinyl pyridine) (PMVP) as a function of porosity and pore size (in figures they are marked "F" with pore size in μm). For comparison the monomers are also grafted onto PETP film (in figures it is marked "L" with thickness in μm).

Biaxially oriented PETP film of 10 μm thick manufactured in Russia (marked as L-10) is used (lavsan™ film prepared in accordance with SU State Standard 24234-80). The film was filled with 0.2 % wt. of kaolin. Track membranes were prepared by irradiation of PETP film with ions of $^{132}Xe^{+8}$ accelerated at the cyclotron U-300 at JINR[3]. Graft polymerization on membranes and film was carried out by the

methods of preirradiation in air and vacuum[4]. An irradiated matrix was placed into liquid monomer which was bubbled by argon or evacuated and thermostated at 70 °C during different periods of time. After the completion of polymerization the grafted samples were washed by boiling benzene (when styrene is grafted) or boiling ethanol (when MVP is grafted) during 24 hr. Grafting yield was calculated as the percentage weight gain of membrane or film. Gas permeability through PETP track membranes and graft membranes were determined at a differential pressure up to 0.2 bar by means of a gas flow into the atmosphere. Knowing the gas permeability of original membrane (U_0) and of graft one (U_{gr}) their ratio (U_{gr}/U_0) has been calculated. Swelling of polymeric substrate was investigated with a gravimetric method.

Relative gas permeability of graft membranes. During graft polymerization the size of membrane pores is expected to change. The effect of pore clogging was investigated for membranes both with different pore sizes and between pore distances under the condition of constant porosity (from 8 to 9 %) (Fig. 1), and with different porosity, that is when membranes have constant pore density ($6 \cdot 10^6$ cm^{-2}) but different pore diameter (Fig. 2).

In the first case (Fig. 1) the relative gas permeability changes negligibly at low grafting yields. This range of grafting yields depends on the pore size of membrane substrate and expands with pore size. Subsequently, as the grafting yield increases, there is a sharp drop of gas permeability (with the exception of membrane 1-F-gr-PS for which a drop of gas permeability takes place

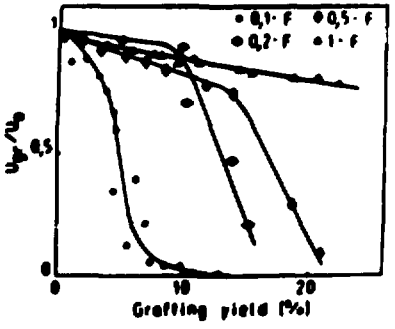

Fig. 1. Relative gas permeability for graft membranes with constant porosity as compared with that for original ones vs. grafting yield of PS

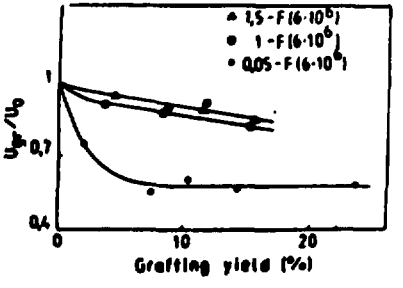

Fig. 2. Relative gas permeability for graft membranes with constant pore density as compared with that for original ones vs. grafting yield of PS

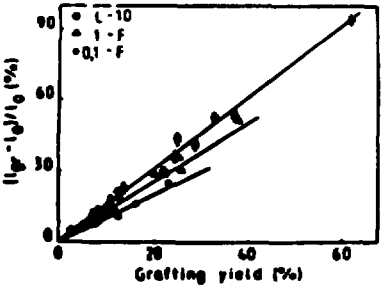

Fig. 3. Relative thickness of film (L-10) and track membranes 1-F and 0.1-F vs. grafting yield of PS

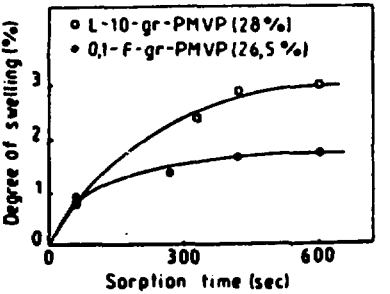

Fig. 4. Swelling curves of track membrane and film grafted with PMVP followed by quaternization with methyl iodide

at a higher grafting yield, i.e. more than ~ 60 %). Since there is a linear change of membrane thickness during grafting (Fig. 3) it may be supposed that a sharp drop of gas permeability occurs because of decreasing pore size. The obtained dependences suggest that at a low grafting yield the effect of membrane surface modification can be reached without pronounced reduction in pore size. As follows from Fig. 2 the character of pore clogging is approximately identical for membranes with large pores [1-F($6\cdot10^6$) and 1.5-F($6\cdot10^6$)]. But when we compare the curves of gas permeability change for membranes with close pore size, i.e. 0.1-F (Fig. 1) and 0.05-F($6\cdot10^6$) (Fig.2) it can be seen that the character of gas permeability reduction changes depending on the average distance between the pores: for low L (0.6 μm against 4.8 μm) clogging of pores intensifies as the grafting yield reaches ~ 7 %.

Swelling of graft membranes. Swelling of composite membrane in liquid can show the change in its structure as a result of grafting. The swelling, on the other hand, can affect both the pore size and the critical surface tension and thus the flow rate through membrane[5,6]. In the case of hydrophilic polymer grafting the graft material quickly swells in water (Fig. 4). The degree of swelling reaches the equilibrium value in a few minutes at room temperature. Such a high rate of swelling seems to be affected by more hydrophilic and less dense structure of grafted polymer as compared with original matrix. Thus, grafting of various monomers leads to the growth of composite membrane swelling in the solvents which have the overall solubility parameter near to that of graft polymer.

Thus, during grafting of PS the pores of track membranes are clogged by grafted polymer to a greater degree when their original diameter is smaller and their number per unit surface area is larger. As can be seen, the change of the relative thickness gain of the sample during accumulation of grafted PS decreases in the range: L-10, 1-F, 0.1-F, that is as *L* decreases and hence because of increasing surface area.

References

[1] V.M.Kochkodan, M.T.Brik, B.V.Mchedlishvili, and N.I.Zhitariuk, *Ukr. Khim. Zh.* 53, 100 (1987) (in Russian)

[2] P. Yu. Apel et al., *"Proc. intern. symp. membranes and membrane separation processes"*, Sept. 11-15, 1989, Torun, Poland, 1989, p. 341

[3] G. N. Flerov, *Vestn. Akad. Nauk SSSR*, No 4, 35 (1984) (in Russian)

[4] N.I.Zhitariuk, P.A.Zagorets, and V.I.Kuznetsov, *J. Appl. Polym. Sci.* 40, 1971 (1990)

[5] N. I. Zhitariuk, V. I. Kuznetsov, and N. I. Shtanko, *Preprint JINR 18-88-537*, Dubna, JINR, 1988 (in Russian)

[6] F. Harjanto, H. Mendjel, J. Sledz, and F. Schue, *Makromol. Chem.* 186, 559 (1985)

A method to determine the statistics of pore formation in polymers

M. Danziger
Dresden University of Technology
J. Krüger and A. Schulz
Institut für Reine und Angewandte Kernphysik, Univer[illegible]at Kiel

1 Introduction

It is now more than 30 years since Young (1958) and Silk and Barnes (1959) published the first results on nuclear tracks in solids. These investigations were only the beginning of the development of new track detectors in nuclear physics. At present a wide spectrum of problems exist, concerning the etching techique of material irradiated by heavy ions.
The explanation of the interactions of heavy ions with solids along their trail, especially the so called core of the track, is now as ever an actual problem. The core is the range where the ion generates a primary disturbance. By the recent publications a new model is introduced [1]. This model bases on the theory that the incident ion is causing a disturbed structure directly around its trajectory, described by vitreous properties [2].
The irradiation originates local regions, where charged particles or dipoles are not compensated completely. Though the solid is electrically neutral, i.e., the sum of all charges is zero, the separate regions can have charges causing polarization.
The separate regions are interconnected and if there is a change of polarity in one of them the others will "feel" it
The change of the solids structure along the latent trail expresses the energy loss of the ion on its travel through the matter.
During the etching process the deposited energy is transferred to the whole solid. The influence of etching reactions can effect a change of polarization in a separate region by the transition of a free charge or dipole from one state of equilibrium into another.
The energy barrier between these states of equilibrium is very small and so a transition from one into the other is possible. These are so called two level systems. But a transition of a charge or dipole into another state of equilibrium is connected with a change in polarization in the surrounding. The neighbouring regions react to this change and this response can be compared with an oscillation of the regional units. These are low-energy excitations.
That's why the model is called the Model of Low Energy Excitations.
A response function [3], describing the reaction of the solids of the external disturbance, i.e. the penetrating ion, released by the etching process,

$$\psi(r) = \frac{a_0^2}{k_B T\, e^{n\gamma}\, l_0\, k_c^n}\, r^{-n} \cdot exp\Big(-\frac{r^{1-n}}{(1-n)e^{n\gamma}\, l_0\, k_c^n}\Big) \qquad (1)$$

can be calculated by the model. Thereby r is the pore radius, k_c the maximal wave number of the low energy excitations, l_0 is the distance between two states of equilibrium if no correlations occure, a_0 the polarization density, n the so called interaction parameter, k_B the Boltzmann constant. T the absolute temperature and γ the Euler constant.
The response function is proportional to radial etching rate in the case of only one pore in the investigated solid

In the case of high pore density in the solid the radial etching rate is proportional to the imaginary part of the Fourier-transformation of the response function

$$\chi'' = \int dr\psi(r)sin(kr) \tag{2}$$

with

$$k = \frac{1}{\bar{r}} \quad .$$

The value $\bar{r}$ is the effective radius.
Since for instance in irradiated polymers the radius of the core is smaller than 10 nm, a high quality technique of measure is necessary to reach out measurements in a range smaller than 1 nm radius of pore.
For calculating the effective radius

$$\bar{r}(t) = \sqrt{\frac{1}{\kappa(R(t) - R_L)} \frac{d}{NS\pi}} \tag{3}$$

with $\bar{r}$ effective pore radius at the time t, κ conductivity of the etchant, R(t) electrical resistance of the conductance cell with membrane at the time t, R_L resistance of the conductance cell without membrane. d thickness of the solid film, N track density, and S area of the sample in the case of high track density, some important assumptions are provided:

- cylindrical shapes of the pores
- very thin films of solids (polymer films).

If it is possible to measure the time development of these small radii it is given a new question namely the statistics of the opening process of the pores.
The time dependence of the pore opening can be developed by applying the model of low energy excitations.
This paper will present an experimental setup connected with a method which allows one to determine the statistics of the pore origin and to modulate the etching process for values of radii smaller than 5 nm.

2 Experiment

Within the etching cell filled with electrolytical solution the investigated matter is fixed between two electrodes. The cell and a reference resistance are switched in series whereas a generator provides this circuit with alternating voltage.
During the etching process the values of the voltages, measured directly at the reference resistance as well as at the exit of the generator, are transferred to a computer for evaluating these data.

Fig. 1 shows the principle of the experimental set-up.
By inset of a thermostat water of constant temperature can rinse through

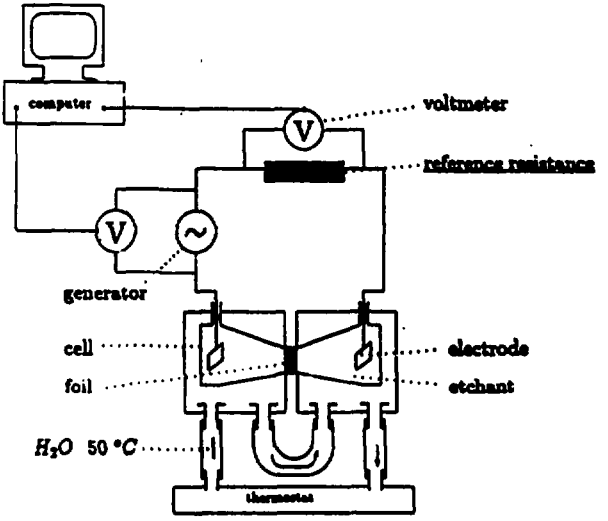

Fig. 1 Schematical representation of the experimental setup

the double wall of the etching cell, providing for unchanged etching conditions during the whole measurement. In the case of vitreous solids irradiated by heavy ions, for example thin polymer films, the etching means penetrate along the trajectories with track etching rate v_S, that is considerably higher than the bulk etching rate v_B.

Soon the first channel-like micropores are originated within the sample and its small current, following the alternating voltage, can run through the matter.

An ohm resistance can be assigned to the polymer film and the time development of its value while the etching process forms the basis for the calculation of the origination of the radius of the pore. According to Fig. 2 the value of the resistance, dependent on the time, is computed by evaluating the data both of the reference voltage and the voltage of the generator: The calculation of the resistance of the polymer film is based on the following equation:

$$\frac{U_{ref}}{U_0} = \frac{|Z_{ref}|}{|Z_{ref} + Z_f|} \tag{4}$$

U_{ref} and U_0 are the corresponding effective voltages.

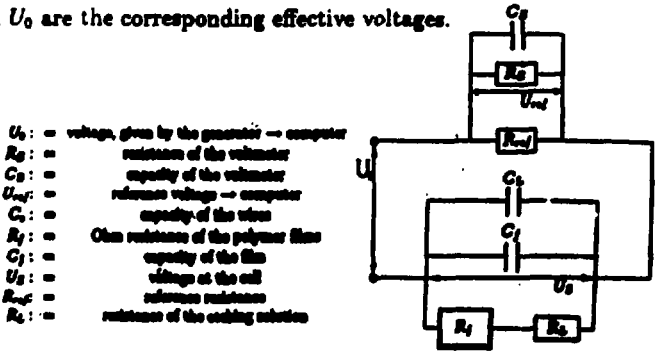

Fig. 2. Equivalent circuit of the experimental setup

Z_{ref} and Z_z describe complex resistances, with $Z_{ref} = R_{ref}||R_E||X_{CE}$ and $Z_Z = R_f||X_C$. X_{CE} and X_C name the capacity resistance. Two other quantities R, C are defined:

$$R = R_{ref} + R_L \,,$$

$$C = C_L||C_f = C_L + C_f \,. \tag{5}$$

The next equation shows the relation between R and U_0 as well as U_{ref}:

$$R = -\frac{1}{k}\, Re(Z_{ref}) + \sqrt{\frac{1}{k^2} \cdot R_e^2(Z_{ref}) + |Z_{ref}|^2 \cdot \left(\frac{U_0^2}{U_{ref}^2} - 1\right)} \,, \tag{6}$$

$$k = 2 \cdot Im(Z_{ref}) \cdot \omega \cdot C + 1 - \omega^2 C^2 |Z_{ref}|^2 \left(\frac{U_0^2}{U_{ref}^2} - 1\right) \,,$$

$$\omega = 2 \cdot \pi \cdot f \qquad \text{(f... frequency)}$$

As long as no micropore has still broken through the resistance R_f of the thin film can be set as an infinite high value (∞).
During this phase of the etching process the illustrated circuit in Fig. 2 can be taken.

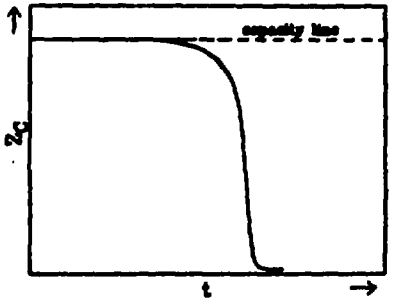

Fig 3. Time dependence of Z_C

$$(R_f = \infty). \tag{7}$$

For the determination of the capacity C the next equation is assumed:

$$Z_C := \frac{1}{\omega C} = \sqrt{\left(\frac{U_0^2}{U_{ref}^2} - 1\right)} \quad (R_{ref}||R_E). \tag{8}$$

In Fig. 3 the time dependence of Z_C is shown.
The curve possesses an approximate horizontal curve in the range of the time of the beginning of the measurement to about 1000 s.
This range of constant Z can be fitted by a movable line, the so called capacity line and make it possible to determine an exact capacity for every moment.
Then this uncertain value is substituted in (8) for calculating the time dependence of R(t), presented in Fig. 4.

For measuring the time dependence of the radial etching rate, corresponding to the reaction of the solid on the etching process connected with the influence of the irradiation, it is necessary to aim cylindrical shapes of etching microchannels, especially in the range of very small radii of pores. Therefore

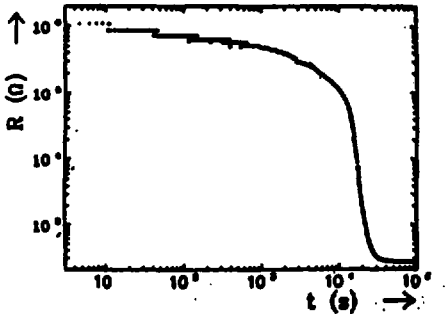

Fig. 4. Time dependence of the foil resistance

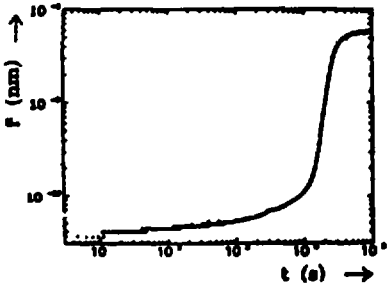

Fig 5. Effective pore radius versus time

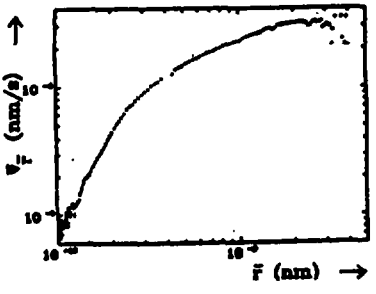

Fig. 6. Etching rate versus the effective radius of etched pores

polymer films smaller than 10 μm thickness are used. Furthermore to reach out a highest desintegration of time during the measurement extremely dilute etching solutions are inserted. Using (3) and the relation R(t) a time function of the pore radius can be illustrated by graph (Fig. 5).

In the case of films with high track density, r(t) has to be interpreted as an effective radius $\bar{r}$. The differentiation of the curve $\bar{r}(t)$, executed by the program, leads to the radial etching rate of the pore, of course this is an effective rate too (Fig. 6).

These experimental results accord to the outputs calculated by the model of the low-energy excitations.

3 Experimental results in connection with the model of low-energy excitations

In Fig. 6 the radial pore etch rate is shown obtained by the experiment (stars) and a

theoretically calculated curve with the help of the model of low-energy excitations. Fitting the theoretical dependence $\chi''(\bar{r})$ (see eq.(2)) to the experimental curve total group of model parameters n. k_c, l_0 and a_0 are computed by a parameter adaption by means of the computer program MINUITS (Cern-Library).
For the parameter optimization only values of $\bar{r}$ lower than r_p are taken. In addition to this fact only this part of the curve was taken, whose shape in a double logarithmic manner is like a straight line. As has been shown in Fig. 6, for $\bar{r} \leq 0,1$ nm a deviation exists between the experimental and the theoretical curve. What's the cause of this difference ?
By the assumption that all pores are opened over the whole range of $\bar{r}$ the model calculates the fitting function $\chi''(\bar{r})$. So it is not taken into account that the pores don't open simultaneously. But this asynchronous process of the opening of the pores has to be considered for values of $\bar{r} \leq 0,1$ nm. It is now possible to derive a time distribution of the number of opening pores N_{esp} by including the mentioned difference between experimental and theoretical curve:

$$\frac{\bar{r}(t)}{\bar{r}_{lee}(t)} = \sqrt{\frac{N_{const}}{N_{esp}}}\ , \tag{9}$$

the time dependence of N_{esp} can be calculated

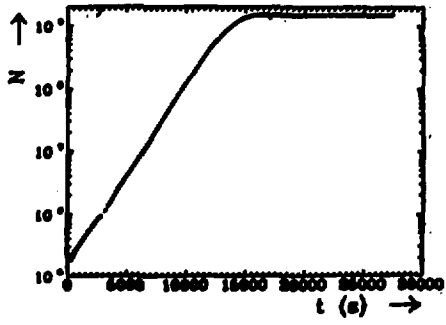

Fig. 7. Number of opened pores in dependence of the time

$$N_{esp} = N(t) = N_{const} \cdot \frac{\bar{r}^2_{lee}(t)}{\bar{r}^2_{esp}(t)} \tag{10}$$

where $\bar{r}_{esp}(t)$ the time dependent experimental values of the pore radius, $\bar{r}_{lee}(t)$ the values of pore radius, calculated by the model of low-energy excitations and N_{esp} the time dependent number of already opened pores.
In Fig. 7 the calculated curves for N(t) are shown.

4 Conclusion

It was shown that it is in principle possible to determine the statistic of the pore generation, represented in Fig. 6. For calculating the time distribution N(t) the model of

low-energy excitations, describing the etching rate in dependence of the effective radius $\bar{r}(t)$, is used.

Optimal measuring conditions are required for achieving exact statements about the pore opening process by applying the method performed in this paper. The represented results were accomplished by an experimental set-up, that must be still improved for the future.

References

[1] Danziger M. and Andrássy G.: Experimental and Theoretical Study of Heavy Ion Irradiation Processes in Polymer Materials.
phys. stat. sol. (b) **161**, 223 (1990)

[2] Andrássy G. and Danziger M.: The Model of Low-Energy Excitations and the Process of Pore Formation in Polymers.
Communication of the Joint Institute for Nuclear Research. Dubna
E7-91-89 (1991)

[3] Danziger M.: Description of the Universal Vitreous Behaviour of Solids with Low-Energy Excitations and its Application to the Processes in Polymer Materials Irradiated with Heavy Ions
Nucl. Tracks Radiat. Meas., Vol. 19, Nos 1-4, pp. 55-60 (1991)

Theoretical Estimations of Nuclear Track Membranes Sterilization Ability

Kuznetsov L.V.
Laboratory of Neutron Physics, Joint Institute for Nuclear Research, Dubna, Russia 141980

Abstract. Influence of multiple holes on sterilization ability of track membrane is studied in terms of effective pore radius, provided circular form of single track holes (channels). It is shown that when effective radius is not very large the triple pores are the most important, their distribution over effective radius is calculated. For large pores we present a statistical approach, based on concept of critical local porosity. The results can be used in designing of track membranes with optimum parameters.

1 Introduction

Nuclear track membrane technology now became a well-established commercially exploited process, the membranes being used in a great number of applications [1]. One of the most important questions concerning nuclear track membrane production is how to find a compromise between selectivity and permeability of filters. Permeability grows with membrane porosity, provided etched track size is fixed, but selectivity decreases monotonically due to the channel overlap [3]. The latter effect was studied from different points of view [2],[3],[4] for structures with different channel shapes. In the paper of Riedel and Spohr [3] it was pointed out that the ability to select microscopical particles of given size by nuclear track membrane is not determined by the number of multiple holes. And we want to add that even the simplest stochastical pattern formed by identical parallel channels uniformly dispersed on film surface has enormous number of various statistical characteristics, so it is very important to choose those, that are relevant to the problem under consideration. For instance if you are to investigate disk-shaped particles filtration you must estimate one type of average values, and in case of spherical particles — some other averages. Still in both cases, if you want to get a representative characteristic related to the particular filtration process, you can't avoid the analysis of pore shape, and it is harder than only to count pore multiplicity.

2 Effective pore radius

In the following we will consider filtration of identical rigid spherical particles through the membrane with uniform channel density n_0, assuming channels to be parallel. All the channels are identical, their radius is R_0, their diameter — $d = R_0/2$. Following [3],[4] we define:

- $S_0 = \pi R_0^2$ — area of single channel,
- $p = n_0 S_0$ — nominal porosity, further referred to as porosity,
- P_m = probability that a channel is involved in a grouping of channels (pore) of multiplicity m (geometrical figure formed by intersection of such grouping with film surface will be referred to as m-cluster).

Now for any given pore we define its effective radius R^* as radius of maximum rigid spherical particle which can still penetrate through it. Thus defined R^* equals the radius of the maximum circle inscribed into the cluster. Now we can split P_m defining:

- P_m^0 = probability that a channel belongs to m-cluster with $R^* = R_0$,
- $P_m(R)$ = probability that a channel belongs to m-cluster with $R^* < R$.

The values defined allow to construct distribution function of clusters over R^*. Since each m-cluster must be counted only once [3], for the distribution function we obtain

$$P(R) = \sum_m \frac{1}{m} P_m(R)$$

and corresponding distribution density

$$n(R) = \sum_m \frac{1}{m} \frac{d}{dR} P_m(R).$$

The probabilities P_m, P_m^0 and $P_m(R)$ must be calculated numerically. We use the formulas [5]:

$$P_m = \frac{n_0^{m-1}}{(m-1)!} \int_{\Omega_m} d^2\vec{r}_2 \dots, d^2\vec{r}_m e^{-n_0 S_{tot}(\vec{r}_2 \dots \vec{r}_m)}, \qquad (1)$$

$$\Omega_m \subset R^{2m-2} : \forall i = 2, \dots, m \; \exists j_1 \dots j_k : |\vec{r}_1 - \vec{r}_{j_1}|, \dots, |\vec{r}_{j_k} - \vec{r}_m| < d,$$

$$S_{tot}(\vec{r}_2 \dots \vec{r}_m) = mes\{O(\vec{r}_1, d) \cup \dots \cup O(\vec{r}_m, d)\},$$

where $O(\vec{r}, d)$ is a circle of radius $2R_0$ with its center in $\vec{r}$. The integral in this formula is weighted volume of Ω_m — region in R^{2m-2} corresponding to bound clusters. Weight function $e^{-n_0 S_{tot}(\vec{r}_2 \dots \vec{r}_m)}$ is a probability for particular cluster to survive, i.e. not to get another circle intersecting with it.

Now we note that Ω_m can be divided in two parts: $\Omega_m^0 \subset \Omega_m : R^*(\vec{r}_1 \dots \vec{r}_m) = R_0$ and $\Omega \backslash \Omega_m^0$, where the first part corresponds to "secure" clusters with effective radius $R^* = R_0$, and second part corresponds to "leaking" clusters with effective radius larger than R_0. Analogously to (1) the probability of secure clusters is:

$$P_m^0 = \frac{n_0^{m-1}}{(m-1)!} \int_{\Omega_m^0} d^2\vec{r}_2 \dots d^2\vec{r}_m e^{-n_0 S_{ext}(\vec{r}_2 \dots \vec{r}_m)} \tag{2}$$

and distribution function of leaking clusters is:

$$P_m(R) = \frac{n_0^{m-1}}{(m-1)!} \int_{\Omega_m(R)} d^2\vec{r}_2 \dots d^2\vec{r}_m e^{-n_0 S_{ext}(\vec{r}_2 \dots \vec{r}_m)}. \tag{3}$$

3 Results for m=3

As could be seen from (2), to calculate pore distribution function over R^* one have to sum up over all multiplicities. But P_m, P_m^0 drop drastically with increase of m in the range of porosities we are considering ($p < 20\%$), so we can take only several first terms. The same holds true for $P(R)$, but in this case the summation begins from $m_{min}(R) = [\pi(arcsin(R_0/R))^{-1}] + 1$ (see [5]). It means that for obtaining $P(R)$ in the region where R/R_0 is not much bigger than unity it will be sufficient to study clusters with $m = 3, 4$, and even only 3-clusters are enough for estimations, while for $R/R_0 > 1.5$ one has to deal with $m = 5, 6, \dots$

We restrict ourselves by the first region, which corresponds to filtration of particles through the membrane with channel diameter only slightly less than particle size. This is the case when one is interested in achieving as high permeability as possible. Clusters with $m = 3$ are especially important here. Figure 1 shows the dependence of P_3, P_3^0 and $P_3^{leak} = P_3 - P_3^0$ on porosity. Our results for the probability for a channel to be involved in 3-cluster are in good correspondence with results of Riedel and Spohr [4] for square channels, though our values are somewhat bigger and the difference grows with p.

Comparing P_3^{leak} with P_3 we see that percentage of leaking clusters increases with growth of p, but not considerably — from 20% at p=1% to 25% at p=20%. It could be concluded that leaking clusters are more compact than secure ones , though effect is not crucial. Figure 2 shows distribution density of 3-clusters $n_3^*(R)$ over effective radius. The average value of effective radius of 3-cluster is about $1.05R_0$.

We used Monte-Carlo technique for calculating integrals in 1- 3, our runs took about an hour of PC/AT-386 computer time. We had no opportunity to perform longer runs, but if one would require more precise figures, they can be easily obtained, providing the appropriate computer is available.

Fig.1 Probabilities that a channel belongs to: triple pore — P_3, secure triple pore — P_3^0, leaking triple pore — P_3^{leak}, as functions of porosity

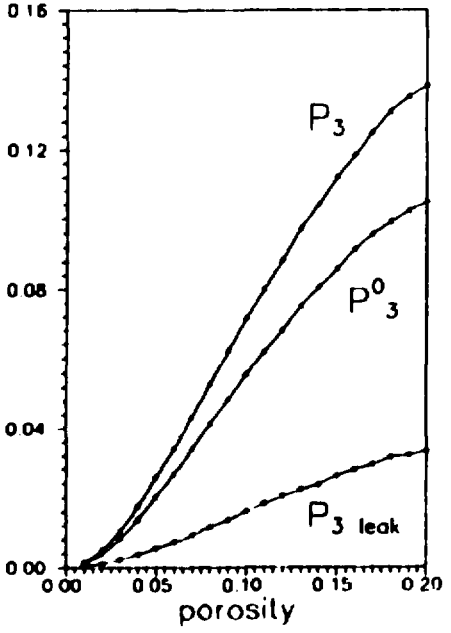

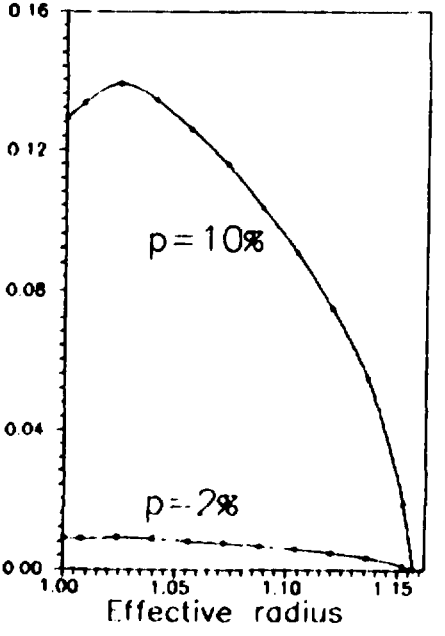

Fig.2 Distribution density of triple pores over effective radius (the latter measured in units of R_0)

4 Problem of complete sterilization

The described approach, based on the shape analysis of every possible configuration, loses its applicability when we are interested in filtration of particles which size is more than two-three times bigger than d. It occurs due to two reasons — impossibility of carrying out calculations because of drastic increase in required computer time for large multiplicities and principal ambiguities in definition of R^* for some configurations (for instance, what effective radius we should ascribe to hoof-shaped chain of channels if the internal area is linked with outside by very thin bridge, liable to break under the slightest pressure?)

It's true that pores with character size from $2d$ and bigger are very rare, but how can we judge whether we needn't consider them? If we take $d = 0.2\mu$m, $p = 10\%$, then $n_0 = 3 \cdot 10^6$, and if the probability for a channel to be involved in a pore with R^* is P^*, there will be about $N = n_0 P^*$ such pores on a square centimeter of membrane. Restrictions on N vary according to the problem under consideration. We choose the criterion $N = 1 \iff P^* = 1/n_0$ for dividing pores in those which must be accounted for ($P^* > 1/n_0$), and those which really rare and irrelevant ($P^* < 1/n_0$). It could be seen that we still must deal with pores with very low values of P^* which can't be treated by exact method anyway.

So we propose a semi-phenomenological approach for estimation of P^* for large pores. Our central assumption is — if on a square with side l the local porosity $r = N_{hole} \cdot S_0/l^2$ reaches some critical value r^* the pore is formed at this place with character size l. Critical porosity depends on l and on film thickness and can be fitted from experimental data. But we will assume for $l/d \in [2, 5]$ the values $r = 1 \div 1.2$, and won't discuss now its dependence on film thickness.

Now, based on this assumption, we can estimate density of pores with size l as

$$n(l) = \frac{1}{l^2} P(\alpha; p, r) \tag{4}$$

where $\alpha = l/d$, and $P(\alpha; p, r)$ is probability to find on a square $l \times l$ the value of local porosity more than r, while the overall porosity is p. Using Poisson distribution we find

$$P(\alpha, p, r) = \sum_{m=[\alpha^2 r]} \frac{(\alpha^2 r)^m}{m!} e^{-\alpha^2 r} n(l; d, p, r) = \frac{1}{l^2} \sum_{m=[\alpha^2 r]} \frac{(\alpha^2 p)^m}{m!} e^{-\alpha^2 p} \tag{5}$$

Figure 3 shows dependence of $n(l)$ for three values of r, while the overall porosity is fixed $p = 0.1$. Figure 4 shows $n(p)$ for $r = 1$ and two values of α. Channel diameter was chosen to be $d = 0.2\mu$m.

Fig.3 Number of holes of character size l on $1cm^2$ of a film with $p = 0.1$, $d = 0.2\mu m$ for three values of critical local porosity

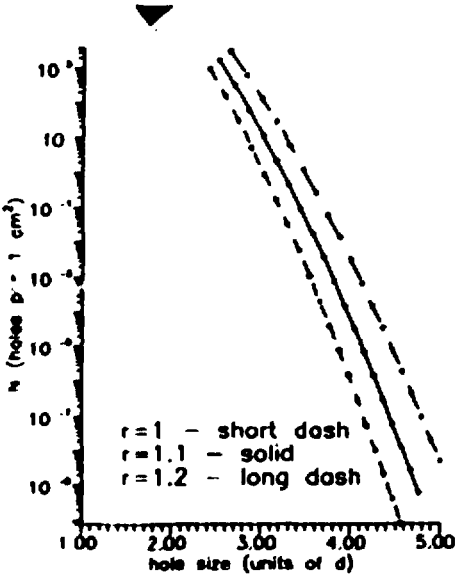

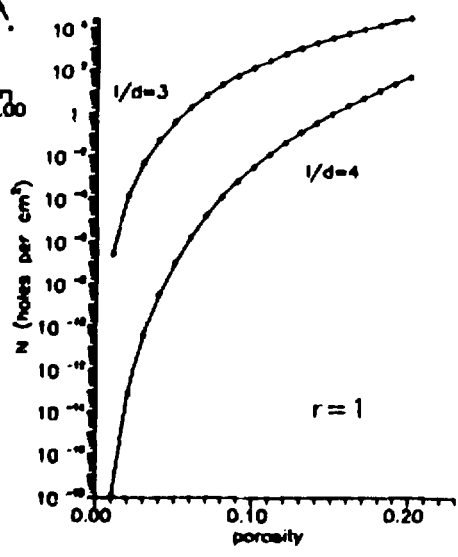

Fig.4 Number of holes with $l/d = 3, 4$ on $1cm^2$ of a film as function of porosity

5 Conclusion

As it was pointed out before, we believe that correct problem statement is one of the critical points in investigation of statistical pattern of nuclear track membranes. In the first part of our report we restricted ourselves to consideration of spherical-shaped particle filtration, but the technique described can be applied to has great variety of similar problems. One only has to figure out what pore parameter is relevant to the problem, and change the algorithm calculating R^* for new algorithm, calculating required value. The latter could be the maximum length of interval, inscribed into the pore for studying disk-particle filtration, the ratio of pore perimeter to pore area for modeling membrane behavior under the bubble test, etc.

The channels in most of industrial track membranes are not parallel, and to describe them we must account for channel angle distribution. In the statistical approach this will lead to dependence of r on this distribution, but the exact method needs some modification.

The author is grateful to Professor Perelygin for his stimulating interest in this work.

References

[1] Spohr R., *Ion tracks and Microtechnology*, (Vieweg, Braunschweig, 1990)

[2] Bereshenkov B.S., *Dispersion of pores of nuclear membranes*, Preprint JINR P14-10532 (in Russian)

[3] Riedel C., R. Spohr, *Radiat. Eff.*, 42, p.69 (1979)

[4] Riedel C., R. Spohr, *Nucl. Tracks*, 5, p.265 (1981)

[5] Kuznetsov L.V., to be published

MESO-OPTICAL FOURIER TRANSFORM MICROSCOPE WITH DOUBLE FOCUSING

Yu.A.Batusov, L.M.Soroko, V.V.Tereshchenko

Laboratory of Nuclear Problems
Joint Institute for Nuclear Research, Dubna, Russia

The meso-optical Fourier transform microscope (MFTM) described in the earlier papers |1,2,3| is designed for fast searching for particle tracks in nuclear emulsion with known orientation and dip angles. In the system |1| the meso-optical mirror with ring response produces two meso-optical images of the particle track which are on the opposite sides of the focal ring. The focusing of the diffracted light is taking place only in the meridional section along the radial coordinate. In the sagittal section of the MFTM there is no focusing at all and as was explained in |4| MFTM in the sagittal section can be considered as one dimensional "pin-hole" camera. It was also shown in |4| that the length of the meso-optical images in the sagittal section of the system |1| is equal to the diameter of the field of view of the MFTM. This property of the MFTM with single focusing enables one to localize spatially the end of the straight line particle track in the field of view of the MFTM.

The first prototype of the MFTM with double focusing which has been studied in |5| contains a single cylindrical lens to accomplish the focusing along the radial coordinate. The focusing along the angular coordinate in the sagittal section of the MFTM is produced by the Fourier transform lens. The meso-optical images of the particle tracks have the form of blurred spots. The double focusing gives the amelioration of the signal-to-noise ratio but needs one sacrifice - the observation could now be accomplished only in a small part of the orientation angles. The main drawback of the first prototype of the MFTM with double focusing |5| was very small aperture of the single cylindrical lens used in these experiments: 1:30. Due to this the expected resolution along the radial coordinate was only 15 μm. The main obstacle for increasing of this feature of the system were spherical and coma aberrations of the single cylindrical lens.

To remove this drawback of the first prototype of the MFTM with double focusing we made a special cylindrical objective with two cylindrical lenses to suppress the spherical and coma aberrations.

In this paper we describe in detail the MFTM with double focusing. It is shown experimentally that this device enables one to get extremely high concentration of information about the position of the particle track in the nuclear emulsion layer and thus to increase the signal-to-noise ratio .

Schematic diagram of the meso-optical Fourier transform microscope (MFTM) with double focusing is shown in Fig. 1. The convergent light beam has an astigmatic structure: the focus in the meridional section is in the median plane of the nuclear emulsion layer 1, and the focus in the sagittal section is in the plane where the pick up matrix of the read-out CCD TV-camera is mounted. The distance between the center of the CCD matrix and the optical axis of the system is R. The distance between nuclear emulsion layer and Fourier transform plane is H. The width of the illuminated region was equal to d = 36 μm, and the length D = 3.0 mm.

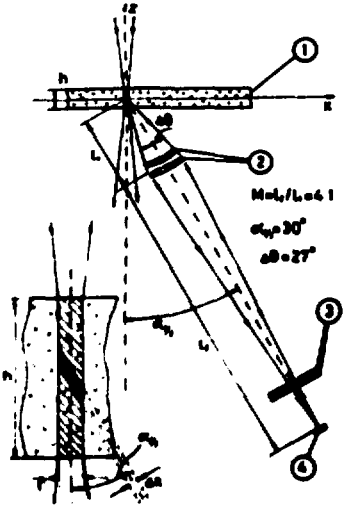

Fig. 1. Schematic diagram of the meso-optical Fourier transform microscope (MFTM) with double focusing: 1 - nuclear emulsion layer, 2 - cylindrical objective, 3 - neutral absorber of the light, 4 - CCD-matrix of the TV-camera. Below to the left section of the nuclear emulsion layer: single hatched region is the illuminated volume, double hatched region is the part of the illuminated volume which sees one pixel

The diffracted light is transformed by the cylindrical objective 2 into the meso-optical image which is picked up by CCD TV camera 4. The concentration of the diffracted light into images spots was so high that we use neutral absorber filter 3.

The cylindrical objective of our device was constructed as a projected system of two components with fixed distance to the object l_1 = 32 mm, and to the pick up matrix of the CCD TV-camera, l_2 = 128 mm. The linear magnification of this system was M = 4:1. The calculations were made according to the recommendations [7] to suppress the spherical and coma aberrations. The expected resolution of the system is equal to 2 μm.

The test experiments with one arm MFTM of double focusing were accomplished for particle tracks of neon nuclei from "1" to "8" and of shower particle tracks which are lying to the right from the particle track "8". The positions of these particle tracks, the orientation angle θ_{xy} and the dip angle θ_z measured by the manual system with ordinary microscope are given in Fig. 2.

The results of the measurements of Z-coordinate of these particle tracks made by MFTM with double focusing are shown in Fig. 3. The depth of the nuclear emulsion layer h = 200 μm can be decomposed into 33 pixels of CCD-matrix. We see the non-horizontal position of the nuclear emulsion layer which produces an angle 1°G with horizontal plane of the system.

The results of the measurements accomplished automatically by the computer are presented in Fig. 4 in the form of 3D-plot with four parameters: effective orientation angle θ_{xy}^{ef}, transversal (radial) coordinate X, effective depth coordinate Z and the intensity of the meso-optical signal I. The measure of the latter was a diameter of the ball on the top of the Z-segment. We must conclude from Fig. 4 that the c'c"-doublet of the parallel particle tracks is not resolved into two components. The cause of this is the computer program which can distinguish two spots on the screen of the computer monitor when they have large mutual distances.

Meanwhile the c'c"-doublet is indeed a resolved one on the screen of the computer monitor with horizontal axis as a Z-coordinate and with vertical axis as an θ_{xy}^{ef}-coordinate. The comparator level was equal to 200 when the noise corresponded to comparator level 150.

The two resolved peaks of c'c"-doublet are shown in Fig. 5 in another scale for the same axes X and θ_{xy}^{ef} .

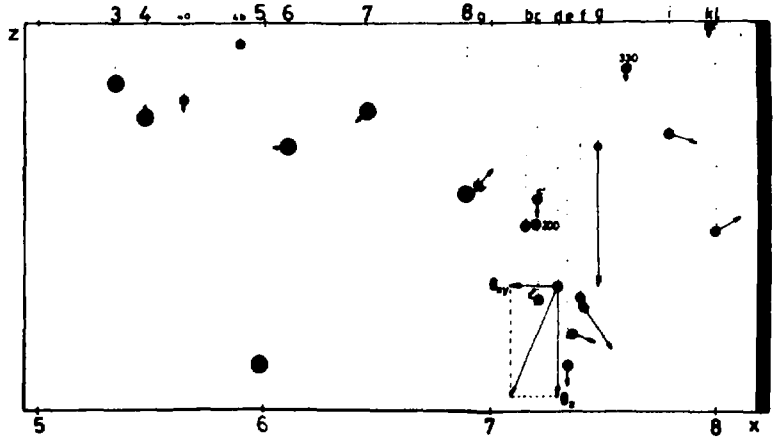

Fig. 2. The object of the test measurements: particle tracks of high ionization level (neon nuclei) "3" - "8" and the shower particles tracks a, b, ... Four parameters of each particle track are depicted: transversal coordinate X, depth coordinate Z, orientation angle θ_{xy} and dip angle θ_z

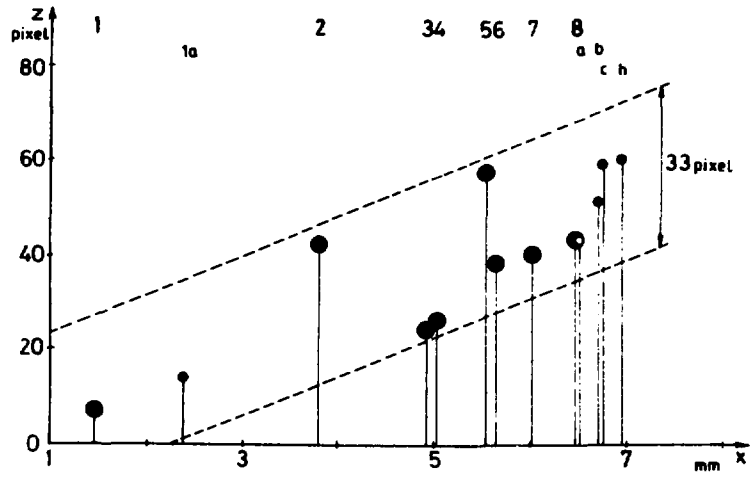

Fig. 3. The results of the measurements of the depth coordinate Z of the object particle tracks: 1 pixel corresponds to 6 μm of Z-axis

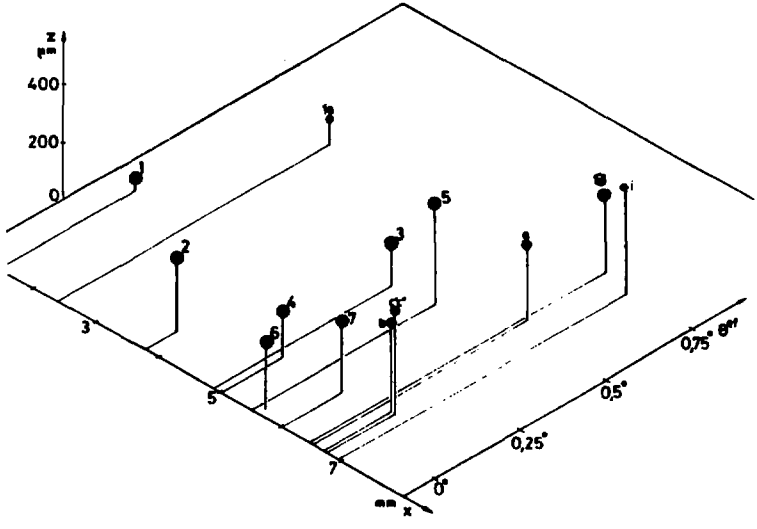

Fig. 4. 3D-plot with four parameters (see text)

The cross section of the c'c"-doublet along Z-axis is shown in Fig. 6. We see that two peaks c' and c" are well resolved for mutual depth distance δZ = 60 μm. The resolution of the system can be estimated as $\Delta Z = \pm 15$ μm. One pixel of CCD-matrix corresponds to 10 μm along Z-axis.

To make the equivalent comparison of the MFTM with double focusing and the Fourier transform microscope of the direct observation we accomplish the control experiment with inverse position of the cylindrical objective. The linear magnification of the cylindrical objective was equal in this configuration to M_2 = 0.25 instead of M_1 = 4.0 in the main experiments. The resolution along Z-coordinate was equal to $\Delta Z \approx 150$ μm and we cannot discriminate the particle tracks with different Z-coordinates. The results of these measurements with inverse geometry can be presented now in the form of 2D-plot.

* * *

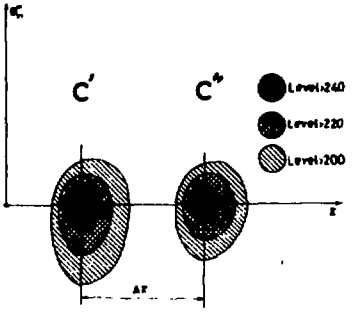

Fig. 5. The resolved peaks of c'c"-doublet in the coordinate frame Z, θ^{ef}_{xy}

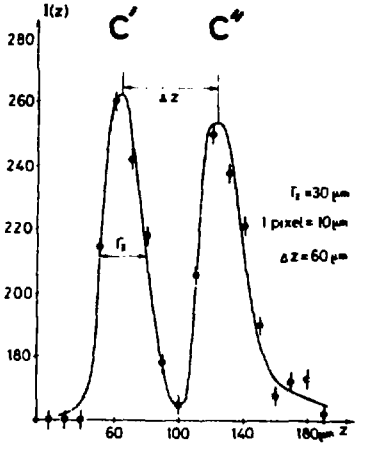

Fig. 6. The cross section of the c'c"-doublet along Z-coordinate (see text)

The properties of the MFTM with double focusing were tested experimentally. It was proved that the information about the particle track in nuclear emulsion can be concentrated in one spot in the plane of the CCD-matrix of the TV-camera. The dimensions of this spot are of the order of 2x3 pixels.

The analogous concentration of the information were observed in the MFTM with single focusing [1] but the dimension of the corresponding spot along angular coordinate was equal to the length of the field of view of the MFTM.

In our system with double focusing the corresponding dimension of the spot has been changed from 2.7 mm to 40 μm or 60 times smaller than in the previous system |1|.

The angular resolution of the MFTM with double focusing can be estimated as $\delta\theta = 1.3'$ and the resolution along the depth coordinate Z as $\delta Z = 10$ μm. This gives 20 additional degrees of freedom along Z-coordinate in comparison to the Fourier transform microscope of the direct observation. The noise is suppressed in the same proportion. The system with two arms will have $\delta Z \simeq 7$ μm and $\delta X \simeq 3$ μm.

References

1. Astakhov, A.Ya. et al. Nucl. Instr. and Meth., A283 (1989) 13-23.
2. Soroko, L.M., Nucl. Tracks Radiat. Meas. 19 (1991) 267-700.
3. Soroko, L.M., Nucl. Tracks Radiat. Meas. 18 (1991) 391-402.
4. Soroko, L.M. Commun. JINR, P13-87-527, Dubna, 1987, in Russian.
5. Soroko, L.M. Commun. JINR, P13-87-460, Dubna, 1987, in Russian.
5. Soroko, L.M. Commun. JINR, P13-87-468, Dubna, 1987, in Russian.
6. Batusov, Yu.A. et al. Commun. JINR, E-13-91-427, Dubna, 1991.
6. Slyusarev, G.G. Metody rascheta opticheskikh system, Mashinostroenie, Leningrad, 1969, p. 350, Equations VI.21 and VI.22.

JUMPING SPARK COUNTERS OF RADIUM INSTITUTE

V. A. Nikolaev, V. E. Kopchenov, A. V. Kozunov
S. M. Krivonogov, N. B. Plastinin

Khlopin Radium Institute, Roentgen str. 1,
Saint-Petersburg 197022, USSR

INTRODUCTION

For realizing the spark jumping technique, proposed by Cross and Tommasino, 1970, various designs of the spark counters are used (Monnin, 1980). From 1976 till 1991 our institute developed many types of spark counters with different complexity degree for exploitation in various conditions. Fig. 1 shows an external view of these counters and Table 1 gives their main technical characteristics.

TABLE 1. Spark counters technical characteristics

FEATURES	COUNTER MODEL				
	AIST, MAK	MSK	AIST-3	ISTRA	HECTOR
Automation type	-	-	control	device	computer
Pressure device type	manual	manual	motor	magnit	motor
Maximum detector square, cm^2	20	1,5	1,5	1,5	1,5
Reproducibility of count, %	2	4	2	2	2
Linear range fluence, cm^{-2}	4000	4000	4000	2000	3000
Number of package detectors	1	1	1	1	100
Weight of instrument, kg	5	0,3	4,5	3	7
Counting time for 1000 tracks/cm^2, min	4	4	3	3	3

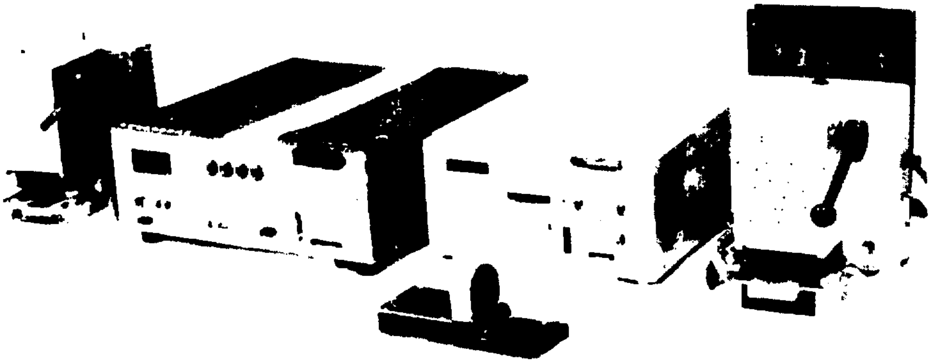

Fig. 1. Jumping spark counters of Radium Institute

It has been shown (Somogyi et al., 1977; Nikolaev et al., 19[illegible]) [illegible] results are obtained if only an optimum pressure [illegible] on the active area of the sparking counter. It can be seen from fig. 2 that insufficient pressure causes a little length and a big slope of the plateau. But too high pressure gives a great probability of short circuit beetwin electrodes. Thereby for all our counters the most attention is given to mechanism for pressing and pulling the aluminized foil.

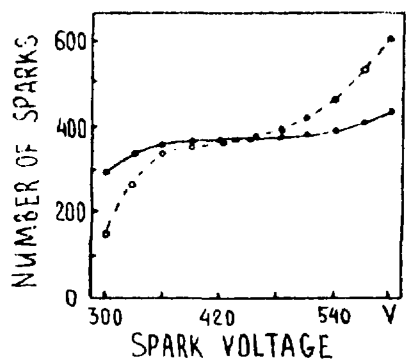

Fig. 2. Number of sparks versus the voltage applied at an [illegible] ([illegible]) and insufficient ([illegible] line) pressure.

SPARK COUNTERS WITH MANUAL PRESSING DEVICE: AIST, LAK, LSK

AIST (Nikolaev et al., 1978) is the most simple and widespread in our country counter which operates with an external serial high-voltage and scaling blocks. It features high reliability and possibility of pressure adjustment the value of which has a high reproduction from cycle to cycle. This counter is equipped with set of interchangeable cassettes with electrodes of different shape and size which allows operation with different track detectors (Fig. 3).

LAK (Kopchenov, 1991) has similar to AIST mechanical block which incorporates high-voltage block, voltmeter and scaler. It has little sizes and power consumption from an accumulator about 4W, which makes it convenient for operations in car laboratory.

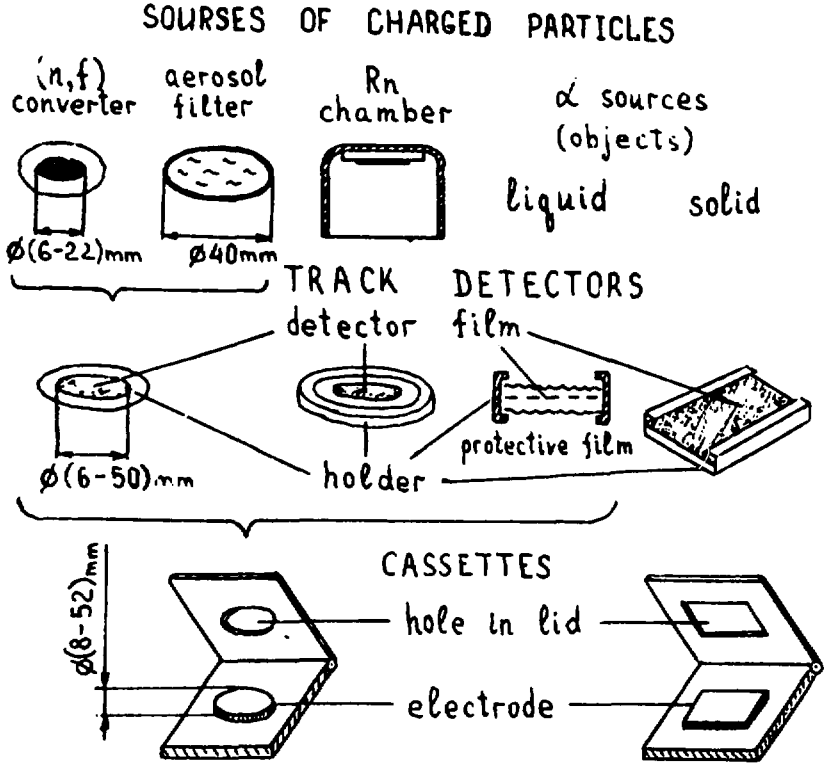

Fig. 3. Additional equipment for spark counters

MSK (Fig. 4) is the smallest one of our counters ("pocket" variant) It was designed for operation with detectors of one size and has possibility of pressure adjustment. Due to small weight and size it's portable and suitable for business trips. Etching procedure may be performed in commonly used every-day vacuum flask, so the total weight of kit for chemical and breakdown processing doesn't exceed 2 kg. The counter operates with external scaling and high-voltage blocks.

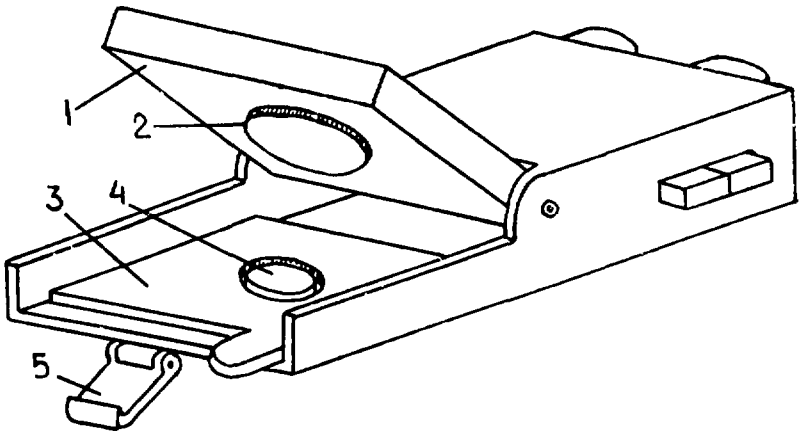

Fig. 4. Small-sized spark counter MSK:
1, cover; 2, buffer; 3, cassette;
4, electrode; 5, high voltage input

Circuit diagrams of this counter are shown in fig. 5. The distinctive characteristic of this diagram is a part for track short-circuit elimination (Evdokimov et al., 1988). In the case of short-circuit, defined like an absence of sparks during (1-2)S, an operator may produce a powerful electrical discharge of capacitor C by means of switch S1 for evaporation of aluminium from the track and so short-circuit elimination. Another feature of this circuit (Fig. 5b) is the absence of parallel to the detector capacitor which connected as a rule for elimination of secondary break-downs through the track. Special measurements (Evdokimov et al., 1986) have shown practical absence of such break-downs in our counters at an optimum pressure. Owing to minimum (spurious) capacitance of spark

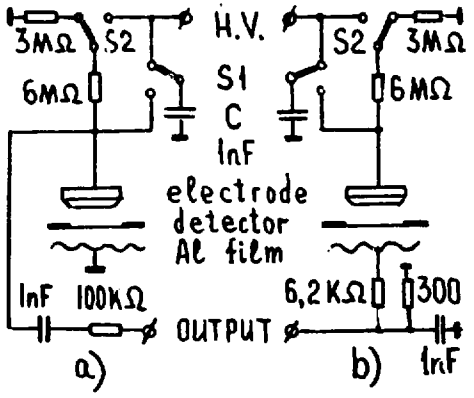

Fig. 5. Circuit diagrams of counters
a) parallel
b) consequent

discharge chain the diameter of zone evaporated in Al layer is minimal too, so we have a linear measured range of the traversing track density up to 4000 cm^{-2} (fluence 8000 cm^{-2}).

AUTOMATED SPARK COUNTERS: AIST-3, ISTRA

In order to design the counter for common use with minimum service operations control device has been developed which assures the counter operation for one detector automatically according to a preset program.

The first counter of such type was AIST-3 (Evdokimov et al., 1987) in which the end of breakdown process was determined by the absence of pulses for 2 s. This counter was equipped with unique pressing mechanism which comprises an electromotor drive of elastic spherical segment with a radius of 5 cm. By this geometry the detector is pressed from the center to the periphery and thereby additionally smoothed and prevented the formation of insulated zones on detector at high tracks density.

Spark counter ISTRA (Kopchenov et al., 1989) is the further development of our automatic devices. It was intended in prospect for serial production and has more simple design in comparison with

AIST-3. For example, this counter has decreased weight-size indices, electromagnetic press drive and device for track short-circuit elimination. In the absence of sparks during 1 s, this device produces a powerful electrical discharge. The absence of breakdowns during the next second determines an end of count (Evdokimov et al., 1988).

MULTICHARGED SPARK COUNTER-HECTOR

Automated counters AIST-3 and ISTRA facilitate the work of operator but practically don't free him because he must recharge the detector every (2-4) minutes. For regular processing of many detectors, as, for example, during dosimetric examination of great collective, a multicharged spark counter has been developed. It has container for 100 detectors, which are equipped with a readable code. Operation control of the apparatus is performed by standard serial minicomputer. Mechanisms for pressing and pulling the aluminized foil are similar to those of apparatus AIST-3, ISTRA and are carried out with electromotors. Information from scaling circuit can be read out through output device in minicomputer. The block diagram of the apparatus is shown in Fig. 6.

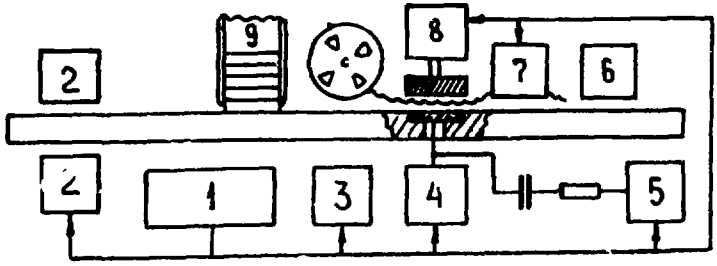

Fig. 6. Block diagram of the device HECTOR: 1, computer; 2, photocode reductor; 3, disk rotator; 4, high voltage block; 5, scaling circuit; 6, detector output mechanism; 7, mechanism for pulling aluminized foil; 8, pressing mechanism; 9, detectors container

CONCLUSION

All spark counters developed by us (except HECTOR which is now under test) are widely used both in our institute and in others for track count from alpha and fission fragment detectors (Evdokimov et al., 1986) in nuclear physics (Vorob'ev et al., 1986), neutron dosimetry (Borodin et al., 1990), radon volume activity measurements (Vorob'ev et al., 1990), alpha-dosimetry of solid and liquid samples (Nikolaev and Potapova, 1990).

REFERENCES

Borodin V. E., I. B. Vorob'ev, E. P. Korshunova, A. S. Krivokhatskiy, V. I. Lebedev, V. A. Nikolaev, T. S. Potapova and A. V. Sannikov (1990). *Dosimetric characteristic of neutron track detectors for high-energy accelerators.* At. Energy, 69, 167-171.

Cross W. G. and L. Tommasino (1970). A rapid reading technique for nuclear particle damage tracks in thin foils. Rad. Effects, 5, 85-89.

Evdokimov A. V., V. E. Kopchenov, A. S. Krivokhatskiy, V. A. Nikolaev and A. I. Shipunov (1986). Fission fragments and alpha particles radiometry with plastic films and spark counter AIST. Radiochemistry, 6, 816-819.

Evdokimov A. V., V. E. Kopchenov and V. A. Nikolaev (1987). Automated spark counter AIST-3. Instrum. Exper. Techniques, 4, 239-240.

Evdokimov A. V., V. E. Kopchenov and V. A. Nikolaev (1988). Avt. svid. no. 14315180, prior. ot 09.02.87.

Kopchenov V. E., A. V. Kozunov, A. S. Krivokhatskiy and U. A. Nikolaev (1989). Automated spark counter, ISTRA. Nucl. Tracks Radiat. Meas., 16, 69-70.

Kopchenov V. E. (1991) Jumping spark counter. Instrum. Exper. Techniques, 3, 238.

Monnin M. M. (1980) Methods of automatic scanning of SSNTD's. Nucl. Instr. Meth., 173, 63-72.

Nikolaev V. A., B. M. Aleksandrov, V. S. Vedeneev and A. S. Krivokhatskiy (1978). Automatic counter of tracks. Instrum. Exper. Techniques, 4, 57-59.

Nikolaev V. A. and T. S. Potapova (1990). Application of cellulose nitrate track detectors for alpha activity measurements in water samples. Radiochemistry, 3, 145-150.

Vorobjev I. B., A. V. Kozunov, V. E. Kopchenov, A. S. Krivokhatskiy, V. A. Nikolaev and S. M. Solovjev (1986). The use of spark count method for neutron investigations. At. Energy, 61, 35-40.

Vorobjev I. B., A. S. Voronin, V. A. Nikolaev, S. M. Solovjev, V. I.Yurevich and R. M.Yakovlev (1990). The use of threshold detector method in investigations of neutron fields with hard energy spectrum. Preprint RI-218, Atominform, 17 p.

Vorobjev I. B., A. S. Krivokhatskiy, V. A. Nikolaev, V. G. Potapov and M. V. Terentjev (1990) Method and equipment for radon volume activity measurements in air of radon laboratories and hospitals. Hygiene and Sanitary, 3, 71-72.

APPLICATION OF AUTOMATIC SPARK-OVER TRACK COUNTER FOR FISSION DENSITY DISTRIBUTION MEASUREMENT IN A CRITICAL ASSEMBLY

Zhuk I.V.[1], Lomonosova E.M.[1], Gloubokij N.N.[1], Edchik I.A.[1]
Ridiko L.I.[1], Yaroshevich O.I.[1], Boulyga S.F.[2], Tzekhanovich I.A.[2]

Recently an automatic spark-over track counters (ASTC) are widely being brought into action to count number of tracks on a surface of alpha- and fission track fragment detectors as part of the study on nuclear physics, neutron and reactor dosimetry [1].

Authors used in experiments on nuclear zero power reactors (critical assemblies) ASTC, visual counting technique and thin film breakdown counters (TBC) [2]. The results of the experiments are compared and analyzed.

In this paper the axial distribution of U-235 and U-238 fission fragments density in fast-thermal assembly FTA-5 is studied. The critical assembly consists of fast core, imitating composition of a fast resonance spectrum core of advanced steam-cooled reactor, safety zone (belt), filter and converter zone, thermal zone [3]. The critical assembly is surrounded with radial polyethylene reflector.

As a detector for registration of fission fragments emerged from the target plastic film of 6 mk thickness was used. To get optimal etching and conditions for counting as well as to carry out experiment correctly the following registration characteristics of film were investigated:

- dependence of registration effectiveness on duration of etching,
- temperature of etching solution, density of etching reactive, fission fragment track density;
- dependence of ASTS counting rate on voltage.

The measurements were carried out under the following conditions:

---

1 - The Institute of Problems of Energetics,

2 - The Institute of Radiation Physics and Chemistry Problems, Academy of Sciences of Republic Belarus

- etching in the KOH-solution (density of solution 1.25g/cc, corresponding to 20 C, at 60 C,
- etching duration was 45 minutes,
- while track counting with ASTS four preliminary breakdowns under voltage 600 V and six operating breakdowns at voltage 390 V of solid track detector were produced.

Axial distributions of U-235 and U-238 fission density were measured in the centre of the fast core and in the polyethylene reflector of the thermal zone. Targets were manufactured by coating with fission substance (0.2 mg/sc for U-235 and 2 mg/sc for U-238) of an aluminum background (diameter 19 mm, 0.2 mm thickness).

Fission layer diameter of the background coincided with the diameter of solid track detector (STD).STDs in close contact with corresponding radiators were located on a special holder, one STD from another being spaced with 27 mm. Six measurements for each distribution were conducted under constant exposition time and assembly power.

At the center of critical assembly axial distributions of U-235 and U-238 fission density were measured.U-235 fission density distribution was measured in the lateral reflector of thermal zone.

Precision of axial fission density distributions includes (for confidential interval 0.95) the following components:

- statistical error of measurements ; for the fast core measurements it does not exceed 3 and 5 percent for U-235 and U-238, correspondingly;
- systematical error of impulse number in the mode of counting;for the track density range of 1000 - 3000 tracks/cm^2 it is about 2 percent;
- systematical error due to uncertainty in the content of U-235,U-238 is about 0.5 percent for fissile targets;
- systematical error due to uncertainty in the content of fissile material is about 3 percent for each separate target;
- systematical error due to uncertainty due to presence of background tracks; for spark-over counting it does not exceed 10 tracks/cm^2 (about 0.5 percent);
- systematical errors connected to etching reagent concentration uncertainty, its temperature, so on were eliminated by simultaneous etching of the whole set of detectors.

So, the total error in axial fission density distributions with ASTS technique of counting of fission fragments is 4-5 percent in the central part of core and 6-7 percent for regions of minimal neutron flux density. The resulting error of measurements in TBS method and visual counting of tracks does not exceed 4 %.

However, taking into account that ASTS technique eliminates the limitations (absence of electronics and time consuming visual counting), and at the same time it has high efficiency and low disturbance for visual counting technique as well as fast getting of result (TBS- method), it should be concluded that application of ASTS counters for measurements on critical assemblies is reasonable.

References

1. An application of track detectors for measurements of alpha activity of soil and water in the 30 kilometer zone around Chernobyl NPP / A.B.Gromov, V.E.Kopchenov, V.A.Nikolaev, S.B.Stolyarov, V.V.Tokarevskij // The Third All-Union Workshop on Solid Track Detectors and Self-Radiography. - Odessa, 1991, - p.52 (In Russian).
2. An Application of Thin-Film Break-Down Counters in the Experiments on Reactor Physics on Critical Assemblies / S.I.Gulnik, I.V.Zhuk, E.M.Lomonosova, S.E.Chigrinov // The Fifth All-Union Meeting on Metrology of Neutron Irradiation on Reactors and Accelerators. - Moscow : VNIIPTRI. - p.77-79 (In Russian).
3. Simulation of the Core Conditions of a Light Water Power Reactor with the Fast-Resonance Neutron Spectrum in a Fast-Thermal Critical Assembly BTS-5 / P.N.Alekseev, A.G.Morozov, I.S.Slesarev, et al. // International Conference on the Physics of Reactors: Operation, Design and Computation. April 23-27, 1990, Marsell, -France.-S.III-3 - S.III-11.

THE METHODS OF TRACK MEASUREMENT IN NUCLEAR EMULSION BY THE TEMP DEVICE

ALESHIN Y.D., KOLESNIKOV B.B., MAKSIMOV A.I., MELNICHENKO I.A., SILAEV V.I.

Institute of Theoretical and Experimental Physics, Moscow

In the paper we present the first results obtained with a new TEMP device for search and measurement of events in the nuclear emulsion.

Three-coordinate measuring TEMP device was made on the basis of two-coordinate DIP device [1], for search for events in nuclear emulsion. The main details of TEMP device are:

1) a motion of stage has accuracy 0.5 mkm in all three coordinates,
2) a stage is equipped with electrical drives for X, Y and Z digitizers,
3) an optical system of device projects a nuclear emulsion picture on the television chamber,
4) an accuracy of the counter-registrating system is 0.5 mkm,
5) an operator table,
6) electronic circuits and power blocks,
7) TV monitor WK4060,
8) the maximum of emulsion plate is 100 × 200 mm.

The detailed description of the function blocks of TEMP device is considered in our early papers [2,3].

The device consists of an optical-mechanical part of a counter read-out system and TV system. The nuclear emulsion to be measured is placed on a stage which can measure with an accuracy about 0.5 mkm. By means of optical system an image is projected into a TV screen. The total magnification on a projection screen is optical magnification and television magnification equals 100 times. Specially for this device a universal algorithm of an operator for various emulsion chamber was created. For example, operator on the TEMP device followed along the g tracks in chamber of similar experiment [4] from layer to layer during one minute.

References

1. Aleshin Y.D., et al., preprint ITEP, 7-92, 1992.
2. Aleshin Y.D., et al., preprint ITEP, 4-87, 1987.
3. Aleshin Y.D., et al., preprint ITEP, 30-89, 1989.
4. Aoki S., et al., Nucl. Tracks and Radiat. Meas. 12, 1986, 249.

DEVELOPMENT OF A NATIONAL PERSONNEL NEUTRON DOSIMETRY PROGRAM IN THE ISLAMIC REPUBLIC OF IRAN

M. Sohrabi and M. Katouzi

National Radiation Protection Department
Atomic Energy Organization of Iran
P. O. Box 14155-4494, Tehran
Islamic Republic of Iran

ABSTRACT

A neutron personnel dosimetry program has been recently put into operation at the National Radiation Protection Department (NRPD) of the Atomic Energy Organization of Iran (AEOI) to provide services to some AEOI workers as well as to those working with neutrons in different applications. The dosimetry program applies the Neutriran Albedo Neutron Personnel Dosimeter (NANPD) (1). It is based on the detection of fast neutrons by direct interactions in polycarbonete and by the detection of albedo neutrons and direct thermal neutrons by the interaction $^{10}B(n,\alpha)^{7}Li$ applying electrochemical etching (ECE) of recoil and alpha-induced tracks in polycarbonate. The principle, the dosimetric parameters and the design characteristics of the dosimeter as well as its response on 18 different phantom configurations were previously studied in detail (2-4). To provide more reliablity of neutron dose evaluation at low and high doses and to further assure safety of exposed foils during handling and ECE operations, a new foil combination with an additional ^{10}B convertor and two polycarbonate foils was also designed and incorporated into the dosimeter for a service on trial. Based on this design, the service went experimentally into operation covering only 30 neutron workers at this preliminary stage. In this paper, some relevant parametric and dosimetric characteristics and calibration of the dosimeter as well as monitoring experiences are presented and discussed.

1. M. Sohrabi, Nucl. Instrum. and Meth. 165, 135 (1979).
2. M. Sohrabi and M. Katouzi, Radiat. Prot. Dosim. 34, 149 (1990).
3. M. Sohrabi and M. Katouzi, Nucl. Tracks Radiat. Meas. 19, 537 (1991).
4. M. Sohrabi and M. Katouzi, Radiat. Prot. Dosim. in press (1992).

Рукопись поступила в издательский отдел
1 марта 1993 года.

Редакторы Э.В.Ивашкевич, Е.И.Хижняк
Макет Р.Д.Фоминой

Подписано в печать 13.09.93
Формат 60x90/16. Офсетная печать. Уч.-изд. листов 15,03
Тираж 250. Заказ 46649. Цена 210 р.

Издательский отдел Объединенного института ядерных исследований
Дубна Московской области